University of Nottingham
School of Mechanical, Materials, Manufacturing, Engineering and Management

Abrasive Water-jet – Controlled Depth Milling of Titanium Alloys.

By

Gary Fowler.

Thesis submitted to The University of Nottingham
For the degree of Doctor of Philosophy

July 2003

Contents

Abstract

Abrasive waterjet (AWJ) technology is used in a routine manner in manufacturing industry to cut materials that are difficult to cut by other methods. Whilst the technology for through cutting of materials is mature, the process is also being developed for controlled depth milling (CDM) of materials.

The aerospace industry have a requirement to remove redundant material from components manufactured from difficult to machine Ti6Al4V and titanium aluminide alloys and thus reduce component weight. The two main processes available to facilitate this are chemical milling and AWJ-CDM. The two processes have the advantage that they impose negligible forces, thus allowing flexible structures to be processed. However, the process of chemical milling is under threat due to the high costs associated with the disposal of the spent acids. *Thus, this research seeks to evaluate the AWJ-CDM process as a replacement for chemical milling for Ti6Al4V and titanium aluminide alloys.* The magnitude and effect of the process characteristics of chemical milling on fatigue life are well established; however, this is not the case for AJW-CDM. The aerospace industry considers the characteristics of surface roughness, grit embedment and surface morphology to be significant parameters in determining the fatigue life of components manufactured using AJW-CDM. Therefore, before AJW-CDM can be considered a viable alternative, the effect of the process variables on the workpiece characteristics have first to be established.

The current research has determined the role of a number of process parameters on the material removal rate, roughness and waviness, grit embedment and surface morphology in the AJW-CDM of Ti6Al4V and titanium aluminide. Nozzle traverse speed and jet impingement angle are shown to govern the operative mechanism of material removal and thus the material removal rate. It is also shown that the surface waviness can be reduced as the traverse speed is increased and as the jet impingement angle is decreased, but it should be noted that waviness increases with number of passes of the jet over the workpiece. The surface roughness is not strongly dependent on traverse speed. Surface waviness and roughness are strongly dependent on jet impingement angle; significant reductions are possible by employing low angle milling techniques. Smaller sized grit leads to a reduction in material removal rate but also to a decrease in both waviness and roughness.

It has been demonstrated that grit embedment can be minimised either by milling with a high jet traverse speed at low impingement angles or by low speed milling at jet impingement angles up to 45° in the backward direction only. However, even in the best

cases, 5% of the area of a milled surface comprised of embedded grit. Surface morphology can either exhibit directional grooving or cratering, depending upon complex interactions of the various processing parameters.

The understanding of the role of various process parameters on the workpiece characteristics will allow the process parameters to be optimised for given requirements. Future work needs to examine the fatigue performance of the AJW-CDM structures, and again optimisation of the processing parameters to maximise fatigue life can be performed. Masking has been employed to provide an economic manufacturing solution for the AJW-CDM process for a specific component. Thus, AJW-CDM has been established as a potential replacement process for chemical milling.

Publications

This doctoral thesis is contains work that has been submitted for publication elsewhere:

Paper 1:

Fowler G.; Shipway P. H.; Pashby I. R.; "Abrasive water-jet controlled depth milling of Ti6Al4V alloy – an investigation of the role of jet-workpiece traverse speed and abrasive grit size on the characteristics of the milled material." Submitted for publication in Journal of Materials Processing Technology, Feb 2003

Paper 2:

Fowler G.; Shipway P. H.; Pashby I. R.; "Work piece grit embedment when AWJ milling titanium alloy" Submitted for publication in Journal of Materials Processing Technology, April 2003

Paper 3:

Fowler G.; Shipway P. H.; Pashby I. R.; "Abrasive water-jet controlled depth milling of Ti6Al4V alloy – an investigation of the role of jet angle on the characteristics of the milled material." Submitted for publication in Journal of Materials Processing Technology, June 2003

Acknowledgements

The Author is indebted to a great number of people for their help and encouragement during this work. Special thanks are extended to:-

Philip Shipway,

Ian Pashby

who provided guidance, technical and moral support through out the project.

The Author is also grateful for the technical support provided by Rolls-Royce plc and assistance provided by Nottingham University laboratory technicians Mr Stuart Branston and Mr Barry Holdsworth.

The Author would like to thank, the Engineering and Physical Sciences Research Council (EPSRC), Rolls-Royce plc, Institution of Mechanical Engineers (I.Mech.E) and the Institution of Electrical Engineers (I.E.E) for providing financial support in the form of Grants, Sponsorship and Scholarships for PhD research.

Glossary

AJW	Abrasive Water Jet
AJW-CDM	Abrasive Water Jet-Controlled Depth Milling
CFD	Computional Fluid Dynamics
FEA	Finite Element Analysis
CAD	Computer Aided Design
CAM	Computer Aided Manufacture
CNC	Computer Numerical Control
MMC	Metal Matrix Composite
EDX	Energy Dispersive X ray Analysis

Chapter 1

1 Introduction.

Abrasive waterjet (AWJ) is a technology for removal of material. Abrasive particles are entrained into a jet of water which has been accelerated to high velocities by the use of pressures in excess of 130 MPa. The particle laden jet impinges onto the surface of the workpiece and material is removed by an erosion process.

Abrasive waterjet (AWJ) technology is used in a routine manner in industry to cut materials that are difficult to cut by other methods. Whilst the technology for through-cutting of materials is mature, the process is also being developed for controlled depth milling (CDM) of materials but the technology is less mature.

AWJ cutting is a mature technology and was implemented in the aerospace industry in the 1980's, when AWJ machine tools first became available. AWJ cutting has particularly good capability at cutting thick sections (e.g. 50 mm aluminium or thicker depending on machine capability and material) with the minimal application of force to the workpiece. As such, in certain areas AWJ cutting has been employed as it is the cheapest method at present available to produce the required features.

At present, aerospace manufacturing companies have a number of components that require material to be selectively removed from their surfaces to meet component shape requirements or to reduce weight where material is not required to provide strength or stiffness. Material can be removed by:

- *Traditional machining methods.* This is costly on difficult-to-machine materials such as titanium. Significant forces are applied to the workpiece which makes machining of thin, flexible structures difficult.
- *Electro discharge machining.* The component to be machined has to be electrically conductive and is subjected to an electric discharge (spark) which erodes by melting the material, the molten material being flushed away from the target component. The melting and solidification process of the material creates a 'recast layer' of material, which can reduce fatigue life [Fordham et al. 1997].

- *Laser Machining.* A beam of light of sufficient energy is focussed on the component to melt and remove the target material. The process produces low machining forces and although it can be utilised for manufacturing thin flexible structures, the high heat input of the process can lead to component distortion and the development of a heat affected zone which can reduce fatigue life [Fordham et al. 1997].

- *Chemical Machining (Chemi-milling).* Here the component is masked and submerged in a tank of acid for a set period of time. As material is removed chemically, negligible forces are exerted on the component during processing and it can thus be employed for machining of thin flexible structures. This process is mature and currently employed by a number of aerospace equipment manufacturers [Hashish, 1987], [Hashish, 1998a], [Harris, 1976] in a number of applications but is under threat due to environmental constraints. The acids need to be treated before disposal and the equipment to do this is expensive to both procure and maintain.

- *Spray etching.* Here the acid is sprayed onto the surface of the component rather than the component being submerged in acid. Like Chemi-milling, it is a process which exerts very low forces on the component and can thus be employed for machining of thin flexible structures. This method has been investigated as a replacement for chemi-milling. Again, there are environmental constraints surrounding disposal of the effluent from the process.

- *AWJ Controlled depth milling (AWJ-CDM).* AWJ-CDM employs an abrasive laden water jet to remove material from the surface of a component with no through-cutting. The process of material removal is in essence the same as in AWJ cutting and thus it has been shown to be suitable for the processing of difficult-to-machine materials. The process exerts low machining forces making it suitable for the manufacture of thin flexible components. However, it has been found that if similar parameters to those used for AWJ cutting are employed for CDM, the surface waviness of the component is very high (of the order of millimetres). There has however been some success reported in the literature in achieving a depth tolerance of $\pm$ 0.03 mm using AWJ-CDM [Hashish, 1987].

The processes described can be employed to machine materials that are considered difficult to machine by traditional methods, or to machine thin flexible structural components that require the use of low machining forces in manufacture in order to eliminate distortion. Moreover, the described processes have been categorised as roughing and/or finishing processes in relation to their manufacturing capability as so can be given due consideration when selecting a manufacturing strategy for a process for the manufacture of components. Although AWJ has been similarly categorised for through-cutting [Kovavevic, 1995], there is some doubt as to where AWJ-CDM sits as a manufacturing technique for finishing operations due to the lack of information on the waviness and roughness capabilities.

Chemical milling is a mature process, is widely used, and has been employed for many years. However, increased legislation on the disposal of chemical substances has resulted in an increase in the environmental disposal cost for chemical milling and etching processes. Such costs have prompted research to find an alternative suitably environmentally friendly solution. Abrasive water jet machining is considered in this context. The main problem to be solved in use of AWJ as a CDM technique is that of tolerances on depth, surface waviness and surface roughness of the milled area.

1.1 Aims and objectives of the work.

Thus, this project seeks to define a robust methodology for AWJ-CDM for a component manufactured from titanium alloy that is currently chemically milled. It will begin with a parametric study to identify key process variables to determine their effect on the magnitude of material removal rate, roughness and waviness, grit embedment and morphology.

The ability of the process to replicate the desired geometry will then be assessed and the improvements made if required. Finally, the two processes will be compared in terms of technological capability and economic viability.

The processing of titanium aluminide by this route will also be considered.

Chapter 2

2 Literature Review.

2.1 Description of AWJ process and mechanisms of material removal.

The mechanism of AWJ removal of material is erosion. An abrasive medium is entrained into a rapidly moving water jet, accelerated along a tube and impinges upon the workpiece resulting in material removal.

Erosion models were developed prior to the inception of AWJ technology. Early models were developed by Bitter [1963a, 1963b] and Finnie [1960] in the 1960's for the prediction of erosion due to particle laden fluid streams. These erosion models have formed the basis of many of the depth-of-cut models employed in the AWJ area. The erosion models are generally concerned with rate of material removal and not the spatial distribution of material removal.

Bitter sub-divided the mechanisms of erosion into (a) deformation wear [Bitter, 1963a] and (b) cutting wear [Bitter, 1963b]. He indicated that deformation wear takes place at high impingement angles whereas cutting wear takes place at low impingement angles.

Bitter's erosion models are based on the energy expended by impacting spherical particles. Bitter [1963a, 1963b] stated that in deformation wear, provided the elastic limit of the target material is not exceeded, then the material will not be destroyed. When the elastic limit is exceed then plastic deformation occurs to the point where material is removed when it reaches its strain to failure. He also investigated the rebounding of particles from the surface and included this effect in a coefficient *K*, termed the wear coefficient.

Bitter accounted for particle shape using apparent particle size and an apparent increase in density/mass. He further proposed different equations dependent on the angle of impingement as the erosion mechanism changed from deformation wear to cutting wear. For brittle substrate materials, impingement angles of 90° result in the maximum erosion, and for ductile materials, impingement angles of 30° result in maximum erosion [Bitter, 1963a].

2.1.1 The erosion process.

In erosion, a particle is pressed against the surface with a force due to the deceleration of the particle and the surface responds by undergoing elastic or plastic deformation, which may subsequently lead to cracking depending upon the material type.

2.1.1.1 Description of particles.

2.1.1.1.1 Hardness.

If particles are harder than the surface that is being worn, then the influence of hardness is low. However, if the hardness (H_v) of the surface to be eroded is similar in value to that of the particle (or harder than the particle itself), the ratio of the hardnesses becomes very significant. The wear rates become very low if the surface is considerably harder than the particle. This may be rationalised as follows: if the particle is harder than the surface, it will act as a rigid indentor and will result in the plastic strain being taken up by the surface. If the particle is soft in comparison with the surface, the particle will deform or fracture (Fig. 2.1). In the case of AWJ machining of titanium, most abrasive particles will be significantly harder than the material. Table 2.1 shows the hardnesses of a number of abrasives and materials.

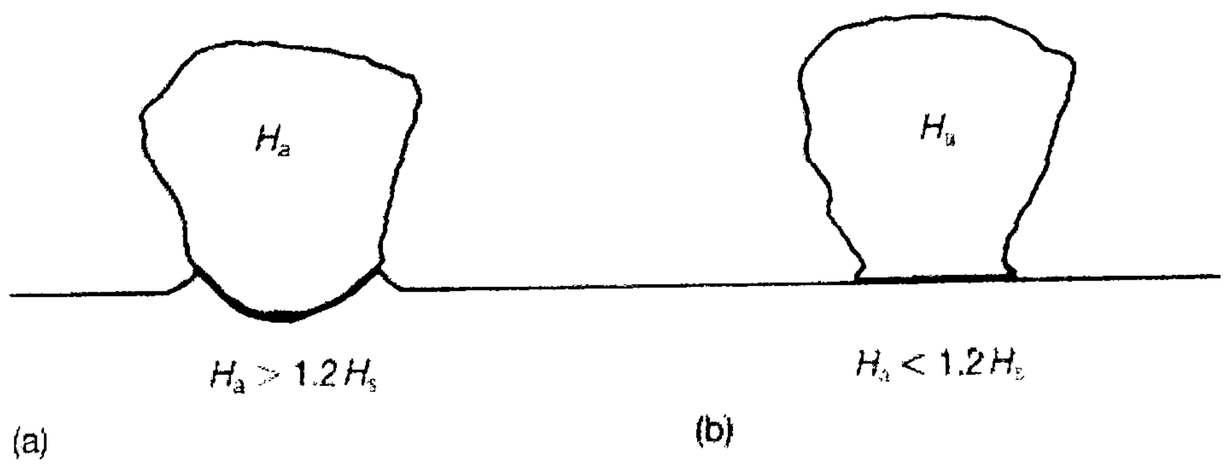

Figure 2.1 Illustration of the contact between a grit particle under normal load and a plane surface showing (a) surface deformation and (b) deformation of the abrasive particle [Hutchings, 1992].

	Hardness (HV) / kgf mm^{-2}
Abrasives	
Diamond	6000 – 10000
Silicon carbide	2100 – 2600
Alumina	1800 – 2000
Silica	750 – 1200
Garnet	600 – 1000
Fluorite	180 – 190
Materials	
Titanium and alloys	200 – 330
Martensitic steels	400 – 1000

Table 2.1 Hardnesses of common abrasives and materials [Hutchings, 1992].

2.1.1.1.2 Particle shape.

It is generally found that the greater the angularity of a particle, the greater the resulting material removal rate. The angularity of an abrasive differs greatly with its source. Differences between rounded sand and angular sand are often clearly visible under an optical microscope.

Fig. 2.2 shows two batches of silica particles of different angularity. Such differences in angularity often result in a difference in material removal rate of a factor of ten or more. However, it is difficult to define angularity in a meaningful quantity; one measure is the roundness factor of a particle. This is determined by producing a two dimensional projection of a particle (e.g. by transmitted light microscopy). The roundness factor, F, can be defined as the ratio of the area *A* of the projection and the area of a circle with the same perimeter *P* as the projection. In terms of these quantities:

$$F = \frac{4\pi A}{P^2} \qquad \text{Eq. 2.1}$$

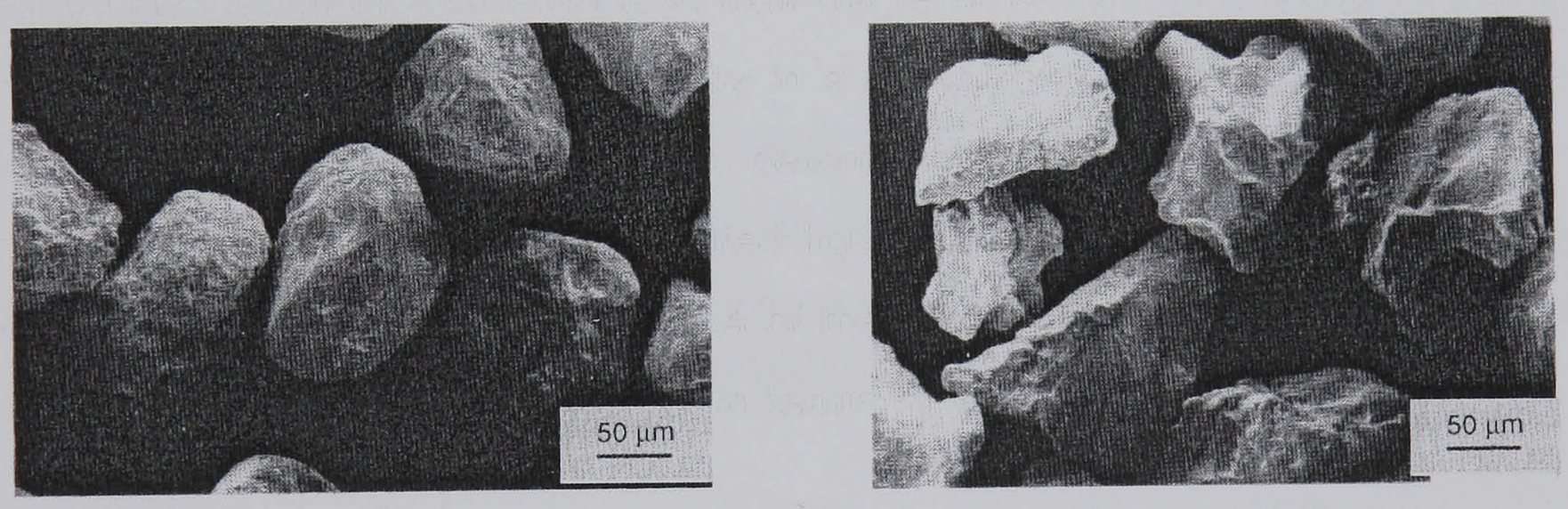

(a) **(b)**

Figure 2.2 SEM micrographs of silica particles: (a) rounded and (b) angular morphology [Hutchings, 1992].

Whilst this factor does give some idea of particle shape, it is the local sharpness that may be more important. For instance, a square and an oblong may both be seen to have similar angularities but very different roundness factors. Recent work by Stachiowiak and Stachiowiak [2000] has attempted to describe local angularities by the *spike parameter*; which represents the particle boundary by a set of triangles constructed at different scales to describe the sharpness and size of the particle boundary.

2.1.1.1.3 Particle size.

Abrasive particles may vary in size from sub-micrometre to many millimetres, although most of those commonly utilised for material removal lie in the size range 5 - 500 μm. In laboratory erosion experiments, it is found that there exists a *size effect*. If particles of all sizes were equally effective, the material removal rates (in the form expressed in Fig. 2.3) should be constant. This is generally found to be true for particles greater than about 100 μm in diameter. However, below this threshold, material removal rates do decrease dramatically. The reasons for this are complex, but may involve the difficulty of nucleating dislocations in small volumes of material under stress (with these volumes getting smaller as the particle size is decreased) [Hutchings, 1992].

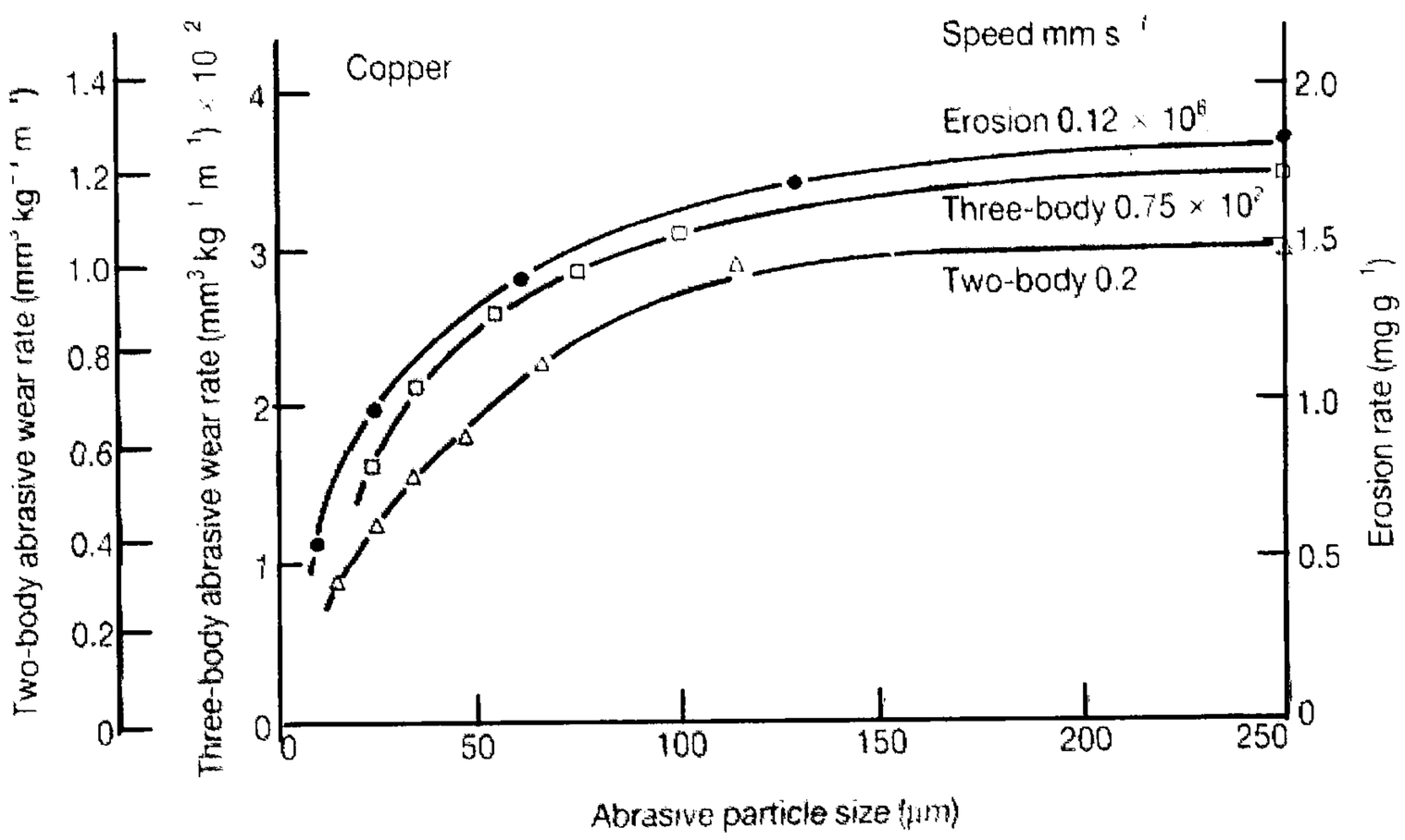

Figure 2.3 Material removal rates of copper under conditions of two-body abrasion, three-body abrasion and erosion with to silicon carbide particles of different sizes [Hutchings, 1992].

2.1.1.2 Mechanisms of material removal.

In erosive removal of material, particles carried in a fluid stream impinge upon a surface. If the particles are travelling with enough energy, they will cause a permanent indentation into the solid surface. In a simple manner, we can assume that the work done in creating an indentation of volume V in a material of hardness H is simply $V \times H$. This work can be equated to the energy of the incoming particle. Thus,

$$V = \frac{m U^2}{2 H} \qquad \text{Eq. 2.2}$$

where m is the mass of the particle travelling with a velocity U [Hutchings, 1992]. This can be converted to a mass of material removed. Material removal rate is normally expressed as the mass of material removed from a surface per unit mass of abrasive

particles striking the surface. However, erosion is more complex than this, and in fact the mechanism of erosion depends upon the angle of impact of the particles as well as upon the material characteristics [Hutchings, 1992],[Bitter, 1963],[Finnie, 1960].

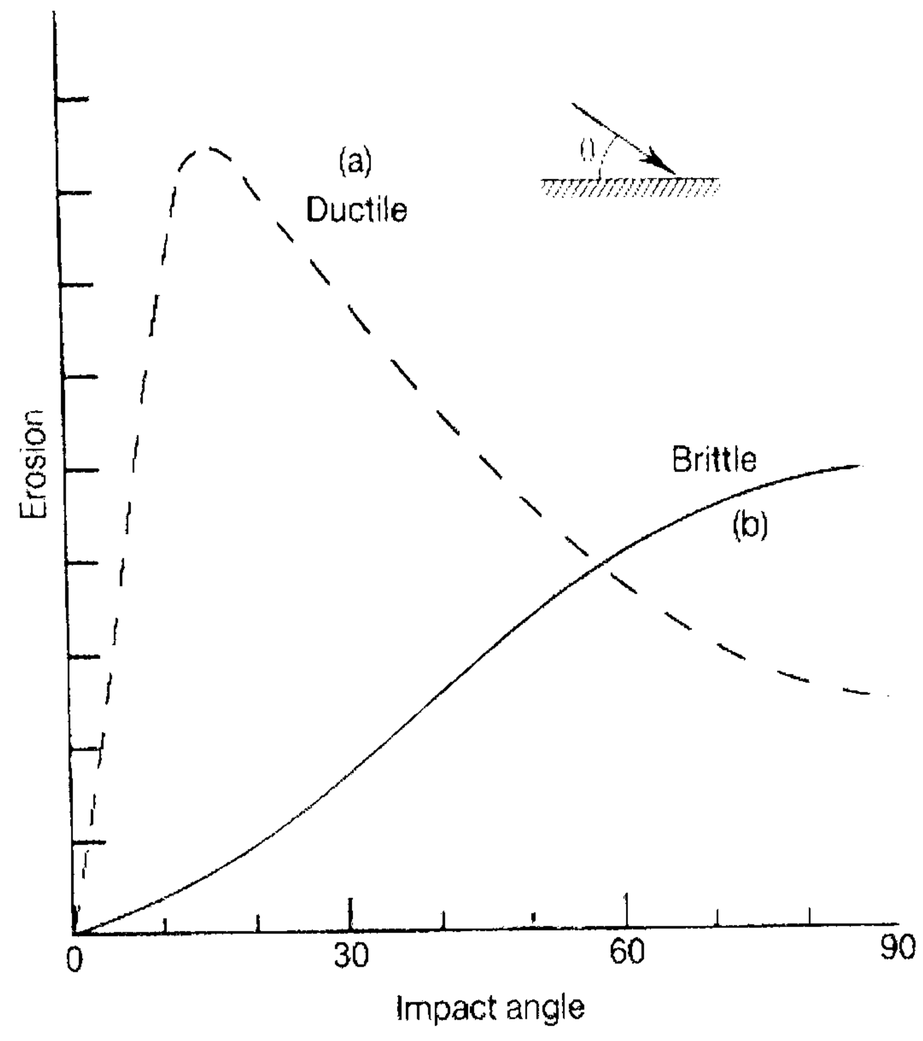

Figure 2.4 The angular dependence of erosion for (a) ductile and (b) brittle materials [Hutchings, 1992].

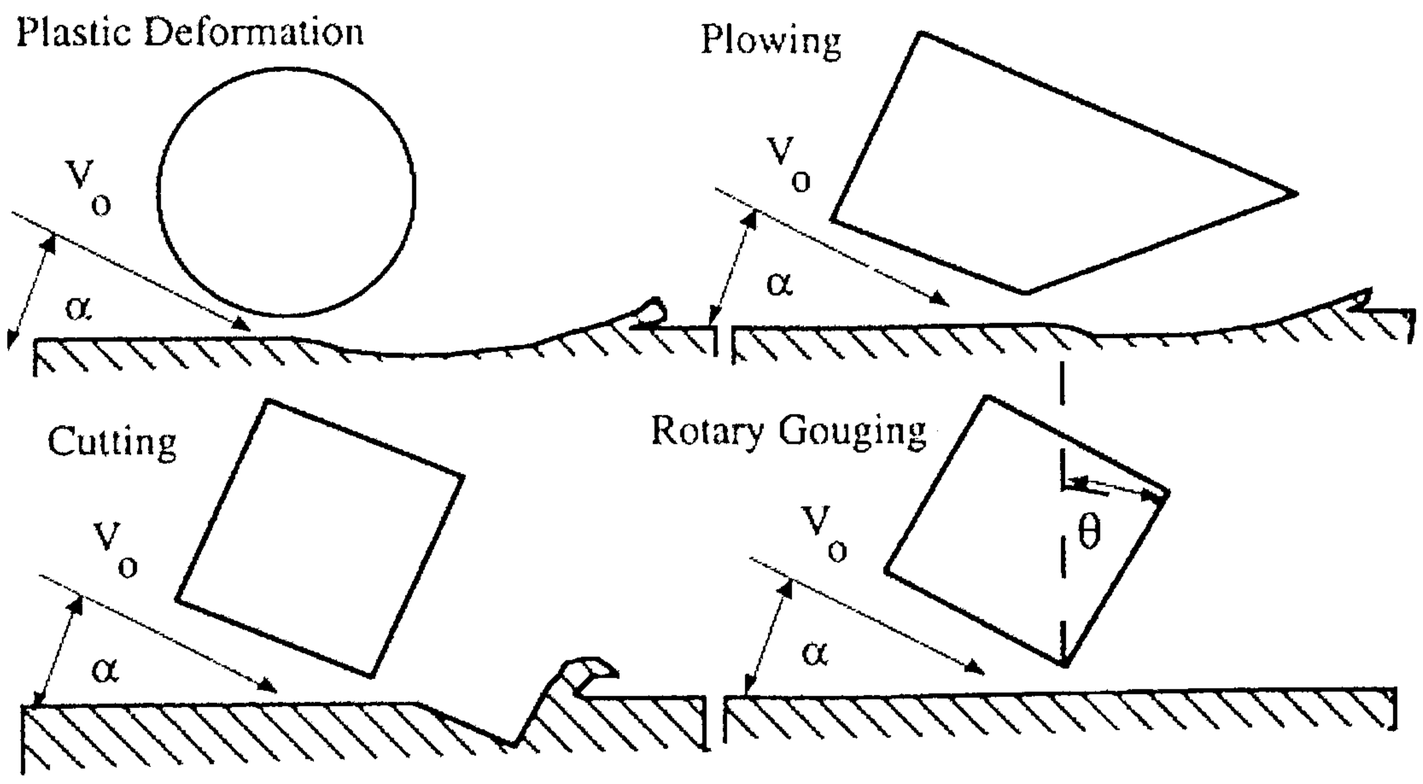

Figure 2.5: Illustration of micro cutting erosion mechanism for ductile material [Summers, 1995].

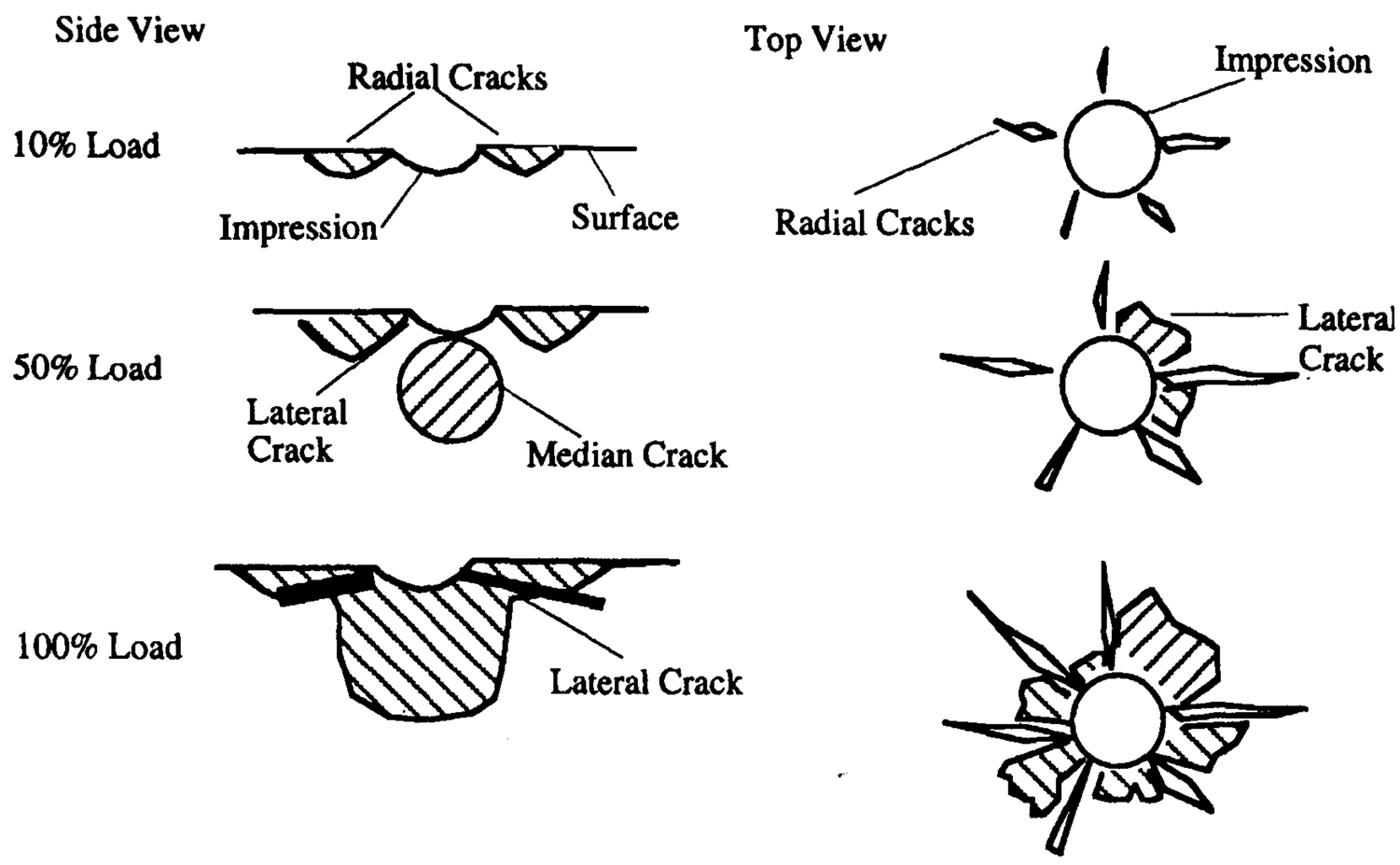

Figure 2.6 Schematic representation of the growth of damage in a brittle target under increasing impact pressures [Summers, 1995].

Ductile materials tend to be most efficiently removed by a cutting and ploughing action. At low impingement angles, θ, (Fig. 2.5) there is little force to press them against the surface and thus little indentation. At high impact angles, there is little tangential motion to cause a groove. Thus, at intermediate angles, erosion is highest. A model for the erosion of metals suggests that:

$$E = \frac{K \rho U^n}{H} f(\theta) \qquad \text{Eq. 2.3}$$

where ρ is the density of the material being eroded. In practice, the velocity exponent n is normally than observed to be between 2.3 and 3.0 indicating a stronger dependence on velocity than predicted in the simple models. This higher value may be associated with an increase in the number of particles needed to remove each fragment of wear debris, and to a consequent change in the mechanism from one dominated by single impacts events to one better described as fatigue or accumulation of plastic strain. The dependence of material removal rate on the hardness of the material is often not as predicted in Eq. 2.3 [Hutchings, 1992]. There are many possible reasons for this:

- The material that is being removed has already been subject to damage resulting from the removal of the material immediately above it. Thus, it will be strain hardened. Strains of up to eight have been recorded.
- The strains are imposed at very high rates involving heating etc. To give an impression of the strain rates involved, we can consider the normal impact of a sphere onto a rigid-plastic surface. In this situation it can be shown that [Hutchings, 1992]:

$$\dot{\varepsilon} = \frac{2^{1.5}\, U^{0.5}}{5\,\pi\, r}\left(\frac{3\,H}{2\,\sigma}\right)^{0.25} \qquad \text{Eq. 2.4}$$

where $\dot{\varepsilon}$ is the mean plastic strain rate, σ is the density of the sphere and r is its radius. The strain rates associated with AWJ processes will typically be between 10^5 and 10^7 per second.

In brittle erosion, the processes by which material is removed are primarily associated with subsurface cracking leading to lateral cracking etc (Fig. 2.6). The erosion damage depends primarily on the depth of indentation (since ploughing and cutting are small factors in such a process) and thus the process shows an angular dependence that some have described as $(U \sin \theta)^n$. One equation for the volume erosion of materials is as follows [Wiederhorn and Hockey, 1983]:

$$\frac{E}{\rho} = r^{0.7}\, U^{3.2}\, \frac{\sigma^{0.3}}{K_c^{1.3}\, H^{0.25}} \qquad \text{Eq. 2.5}$$

where σ is the density of the eroding particles. Fig. 2.7 illustrates the erosion rate of a number of ceramics plotted in this way.

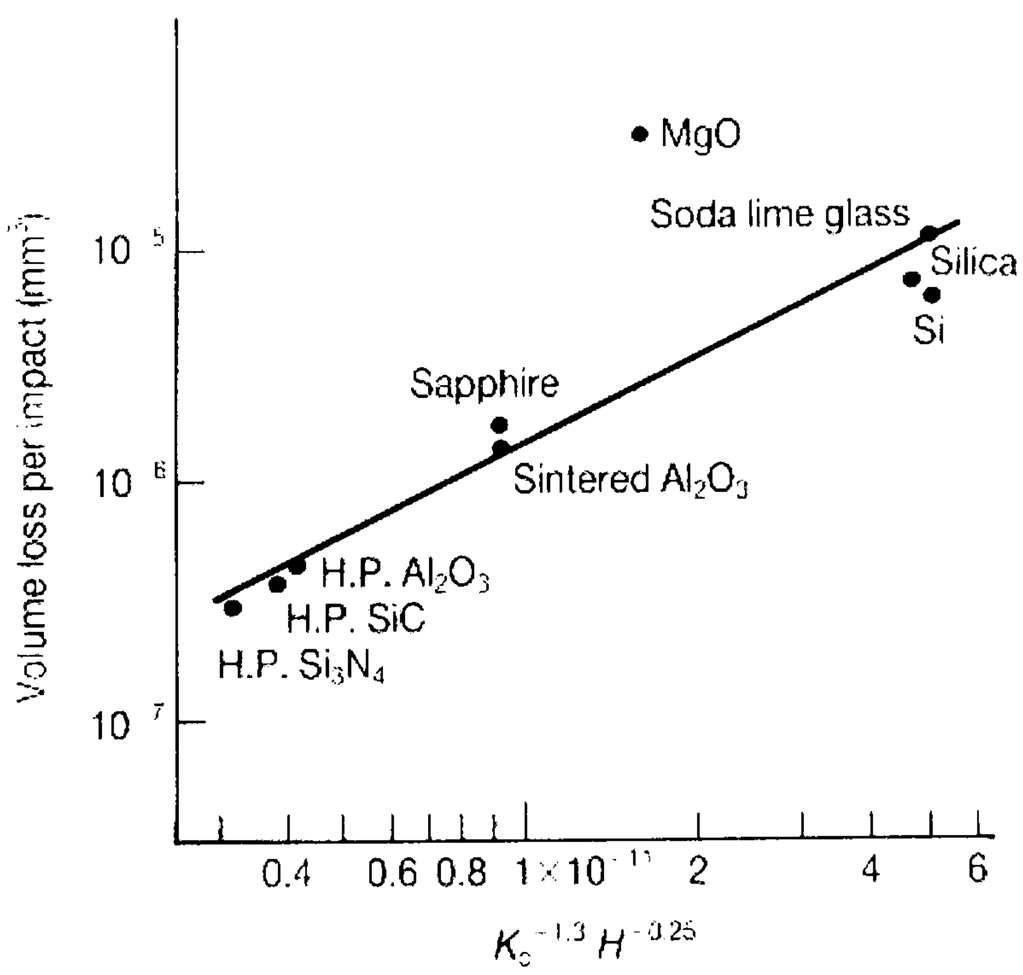

Figure 2.7 Comparison of the dynamic model for erosion with the experimentally measured values for a range of ceramics eroded at normal incidence by 150 μm SiC particles at 63 m s^{-1} [Wiederhorn and Hockey, 1983].

2.2 Manufacturing processes using AWJ technology.

2.2.1 AWJ cutting.

AWJ technology has been used to cut a variety of materials for a number of years. Manufacturing industry has used AJW technology since the 1980's. However, it has mainly been used for through-cutting with the majority of research directed at cutting greater depths, cutting different materials and optimizing grit type and sizes. From 1988 the research expanded into turning, drilling, milling, and the development of models to describe the processes.

In the area of AWJ cutting, much of the research addresses the parameters of stand off distance, grit size, type of grit, abrasive mass flow rate, water jet pressure, nozzle diameter, number of nozzles etc investigating their effects on the depth of cut, kerf geometry or surface finish. The research covers materials such as aluminium and alloys thereof, polymer composites, tungsten carbide, ceramics, steel, stainless steel, titanium and alloys thereof.

2.2.1.1 New developments in AWJ cutting.

Significant recent developments in AWJ cutting fall in to two categories; these are high pressure water jet and cryogenic jets. Research has been conducted in these two areas to improve cutting efficiency or reduce environmental impact.

2.2.1.1.1 High pressure abrasive water jet.

Conventional abrasive water jet machines employ pressure of nominally 68.9 MPa (10 000 psi) to 413 MPa (60 000 psi). Hashish [1999] has conducted research into high pressure AWJ and has utilised pressures in the region of 650 MPa (94 250 psi) with the resulting benefit of using less water and grit when compared to conventional abrasive water jet machining.

2.2.1.1.2 Cryogenic jets.

The adoption of cryogenic jets and ice abrasive water jets is a more recent innovation. Ice abrasive water jet cutting employs ice particles to replace the abrasive grit that is entrained into the water jet. Ice jet machining generates better quality of kerf geometry than abrasive water jet cutting [Li et al. 1996a, Kovacevic et al. 1997]. Cryogenic jet cutting is where liquid nitrogen reduces the temperature of the material to be cut, it becomes more brittle and is more easily removed. This has been employed in the

cutting of steel, titanium, polycarbonate and glass. Liquid carbon dioxide and liquid ammonia jets have also been employed in cryogenic jetting with some success [Kovacevic et al. 1997]. The development in cryogenic jetting was driven by a need for a more environmentally friendly process to eliminate or reduce the production of process waste in nuclear applications. A further development is to entrain abrasive grit such as garnet into the liquid nitrogen jet, [Dunsky and Hashish, 1996] to improve the process further for more conventional applications. The process is termed Abrasive Cryogenic Jet Cutting [Hashish and Dunsky, 1998b].

2.2.2 AWJ slotting/turning.

A number of researchers have investigated the adoption of AJW for turning and slotting, mounting the workpiece on a rotational table in a pseudo lathe, [Hunt et al. 1988]; [Hashish, 1992b, 1995a]. Hashish's research investigated surface roughness and material removal rates of a variety of materials using different type and size of grits mass flow rates, pressures and stand off distances. Dimensional tolerances of ± 0.025 mm for turning titanium, with surface roughness values of Ra 1.0 μm have been achieved when utilising slow traverse speeds [Hashish and Stewart, 2000].

2.2.3 AWJ drilling.

Drilling using rotating jets has been used since the 1970's [Savanick et al. 1975] in the mining and quarrying industry for drilling shot blasting holes. Savanick and Krawza [1989] employed a rotating collimating nozzle with carbide deflector plates for focussing the abrasive jet to drill holes and slots in rock. When this apparatus was traversed linearly a straight kerf of good quality was produced. Hashish [1989b] in his research into the drilling of rock employed a system of a high pressure jet with offset/multiple stationary jets that were rotated. Hashish [1992b, 1996b] employed the techniques normally used for drilling rock to drill metals by rotating the workpiece around a stationary water jet to drill high quality holes in rods to a depth of 3m.

Other drilling techniques tend to involve piercing where the abrasive water jet is held stationary in one place until the water jet eventually pierces through the material. A further technique is to oscillate the abrasive water jet about a fixed position where the hole is to occur. Such a technique is utilised to improve piercing time [Summers, 1995].

2.2.4 AWJ milling.

AWJ milling is significantly different to AWJ cutting. In the case of milling, the AWJ process is used to remove material to a limited depth from the component and thus the fluid conditions are different from the case of through-cutting where the jet stream passes through the material. In milling, much of the abrasive impacts with the workpiece at angles close to 90° [Hashish, 1987].

In his investigation of multiple pass milling, Hashish [1987] found that depth uniformity control should be considered at the beginning of the process as irregularities in one pass are not corrected by the subsequent passes but instead are exaggerated. This was also found to be the case by Liu [1998] who employed abrasive water jet milling to near-net-shape process concave glass lenses. In this process, each subsequent pass had to be mechanically reworked to correct any irregularity. Ojmertz [1996] suggested the use of glass beads as a finishing medium instead of garnet to reduce the irregularities formed during milling with multiple passes of the jet. He found that the surface roughness was reduced by 40 % by using glass beads as a post treatment to the milling process.

2.3 Process variables in AWJ machining.

There are a large number of variable parameters which must be considered when seeking to understand and optimise AWJ cutting or milling processes. These are grouped and tabulated below.

Parameter type	Specific variables
Cutting Parameters	Traverse speed Stand off distance Angle of attack (impingement)
Hydraulic Parameters	Water jet pressure Nozzle diameter (focus) Nozzle length Orifice diameter Polymer additives Nozzle wear Nozzle alignment Venturi or direct injection mixing of abrasive
Abrasive Parameters	Grit material Grit size Grit particle shape Density of grit material Particle size distribution Particle hardness Abrasive condition Abrasive flow rate
Material parameters	Ductile or brittle behaviour of the material Fracture strength Material hardness/heat treatment Machinabilty
Machining Strategy	No of passes of the jet Masks Nozzle rotation Lateral (jet) Increment
Process Methodologies	Smart Nozzles

Table 2.2 Table of Parameters involved in Abrasive Water Jet Machining [Momber and Kovacevic, 1998].

Only some of these parameters in AWJ milling have been examined in detail in the literature.

Table 2.3 lists the parameters that have been the subject of research, and indicates also the process characteristics influenced by each parameter which have been investigated. [N.B. A cross in table 2.3 does not indicate that there is no influence of that parameter on that characteristic, but simply that there are no reports in the literature on that interaction].

Parameter	Material removal rate	Waviness	Roughness	Grit embedment
Water pressure	✓ [Hashish,1989b]	✓ [Ojmertz, 1993]	✗	✗
Lateral increment	✓ [Ojmertz, 1993]	✓ [Ojmertz, 1993]	✗	✗
Jet impingement angle	✓ [Hashish,1989c]	✗	✓ [Li, 1996b]	✗
Number of passes	✓ [Hashish,1998a]	✓ [Hashish,1987]	✗	✗
Traverse speed	✓ [Hashish,1998a]	✓ [Hashish,1987]	✗	✗
Stand off distance	✓ [Hashish,1987]	✗	✗	✗
Nozzle design	✓ [Momber and Kovacevic, 1998]	✗	✗	✗
Abrasive characteristics -particle size	✓ [Hashish,1998a]	✗	✓ [Li, 1996b]	✗
Abrasive flow rate	✓ [Kulekci, 2002]	✗	✗	✗
Masks	✓ [Hashish,1998a]	✗	✗	✗

✓ = information available. ✗ = information not available.

Table 2.3 Roles of parameters known to affect material removal rate, roughness and waviness and grit embedment in AWJ milling.

The effect of the parameters tabulated in table 2.3 on process and workpiece characteristics are discussed in more detail in the following sections.

2.3.1 Water jet pressure.

Fig. 2.8 shows that both the depth of cut and the variation in depth (tolerance) increases as the water pressure increases in the AWJ milling of steel. The increase in water jet pressure results in an increase water jet and thus particle velocity, and thus an increase in material removed per impact.

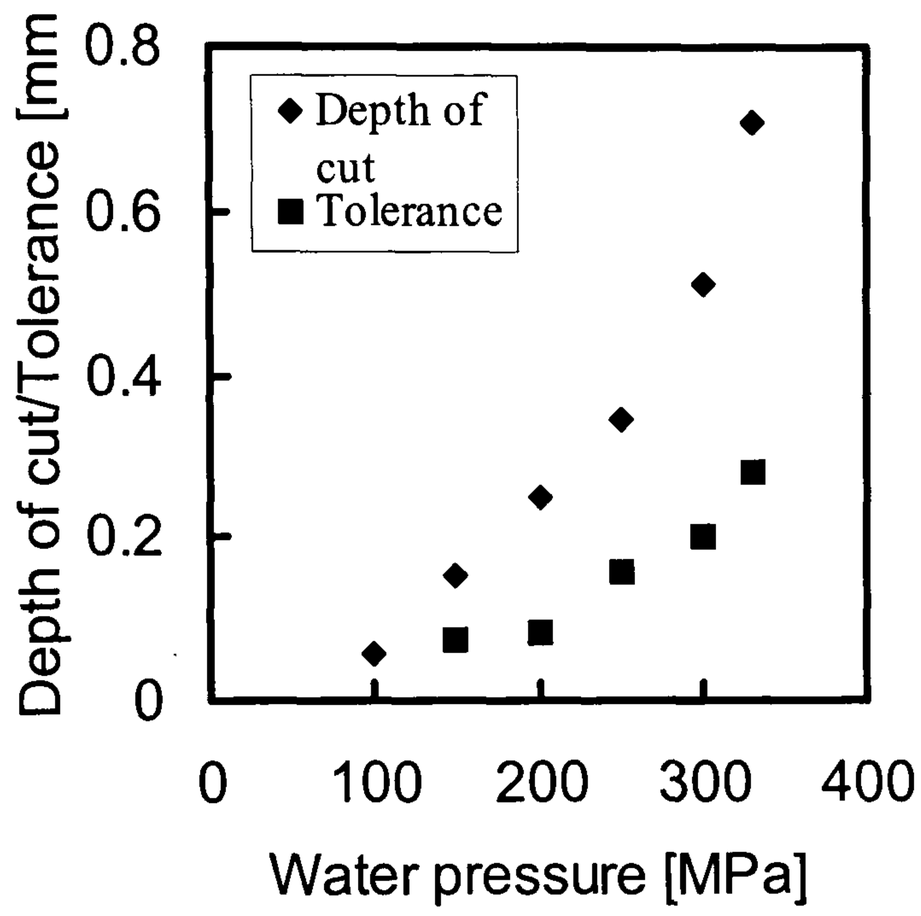

Figure 2.8 Depth of cut and tolerance vs. water pressure. [from Ojmertz, 1997a].

2.3.2 Lateral (jet) increment.

Lateral increments of the jet are used to mill areas larger than the width of the jet. An example of its use would be in milling of pockets. Fig. 2.9 shows that depth of cut decreases as the lateral feed increases. Ojmertz [1997a] suggests that the part of the water jet impinges onto the previously cut surface material and results in an accelerated rate of penetration.

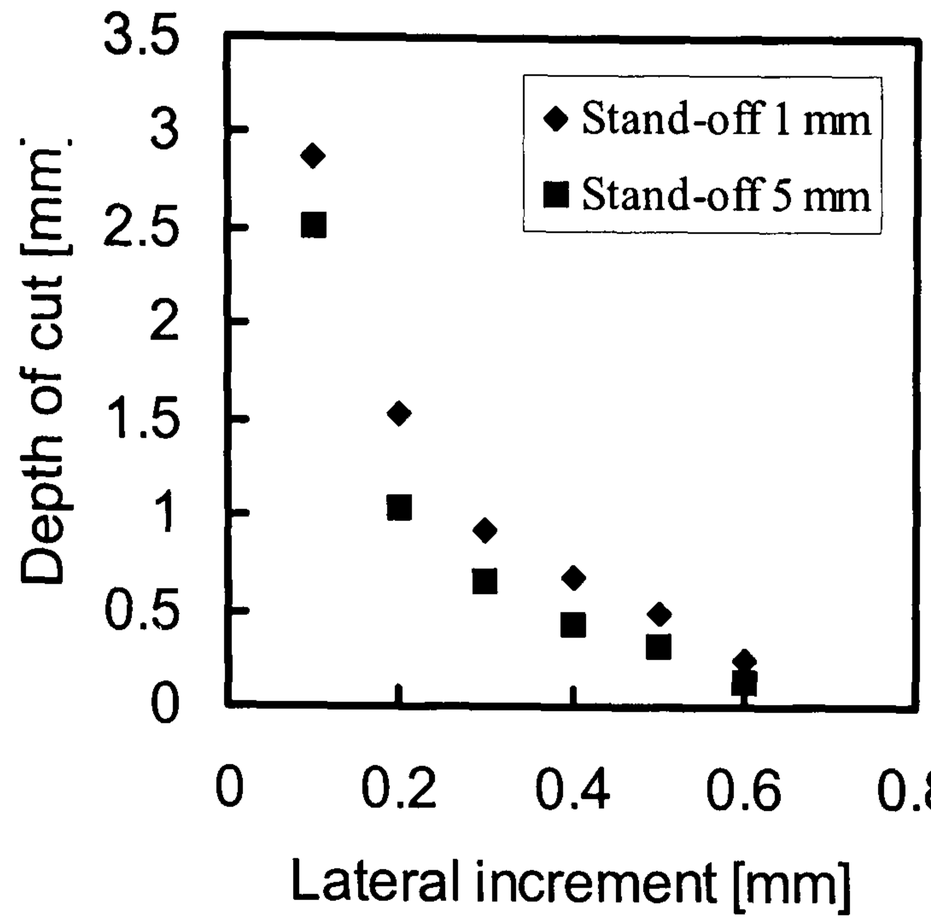

Figure 2.9 Depth of cut vs. lateral feed increment [from Ojmertz, 1997a].

2.3.3 Impingement angle.

Fig. 2.4 and Fig. 2.10 shows that erosion of ductile materials is affected by the impingement angle of the particles. In AWJ milling, impingement angles of 2 - 5° have been used for polishing operations and can be used to control depth. [Li et al. 1996a].

Finnie [1960] in his erosion research, employed a stationary air blast laden with silicon carbide particles to erode various materials at various impingement angles. Soft ductile materials such as copper, annealed steel and aluminium experienced a higher mass loss at low impingement angles, typically 20°. However, brittle materials experienced the highest mass loss at high impingement angles (hardened steel at an impingement angle of 90° and glass 75° to 80°) (Fig. 2.10).

Research into the angular dependence of erosion using abrasive water jets was conducted by Hashish. In AWJ cutting, particle velocities are much higher, the fluid involved is denser than that in air blast erosion. The use of traversing high pressure particle laden fluid streams as those in experienced in AWJ cutting, may result in differing erosion conditions to that observed in stationary low pressure particle laden fluid streams (air blast erosion) by Finnie and Bitter. However, the research on air blast erosion may provide an initial insight into the behaviour of erosion in AWJ-CDM.

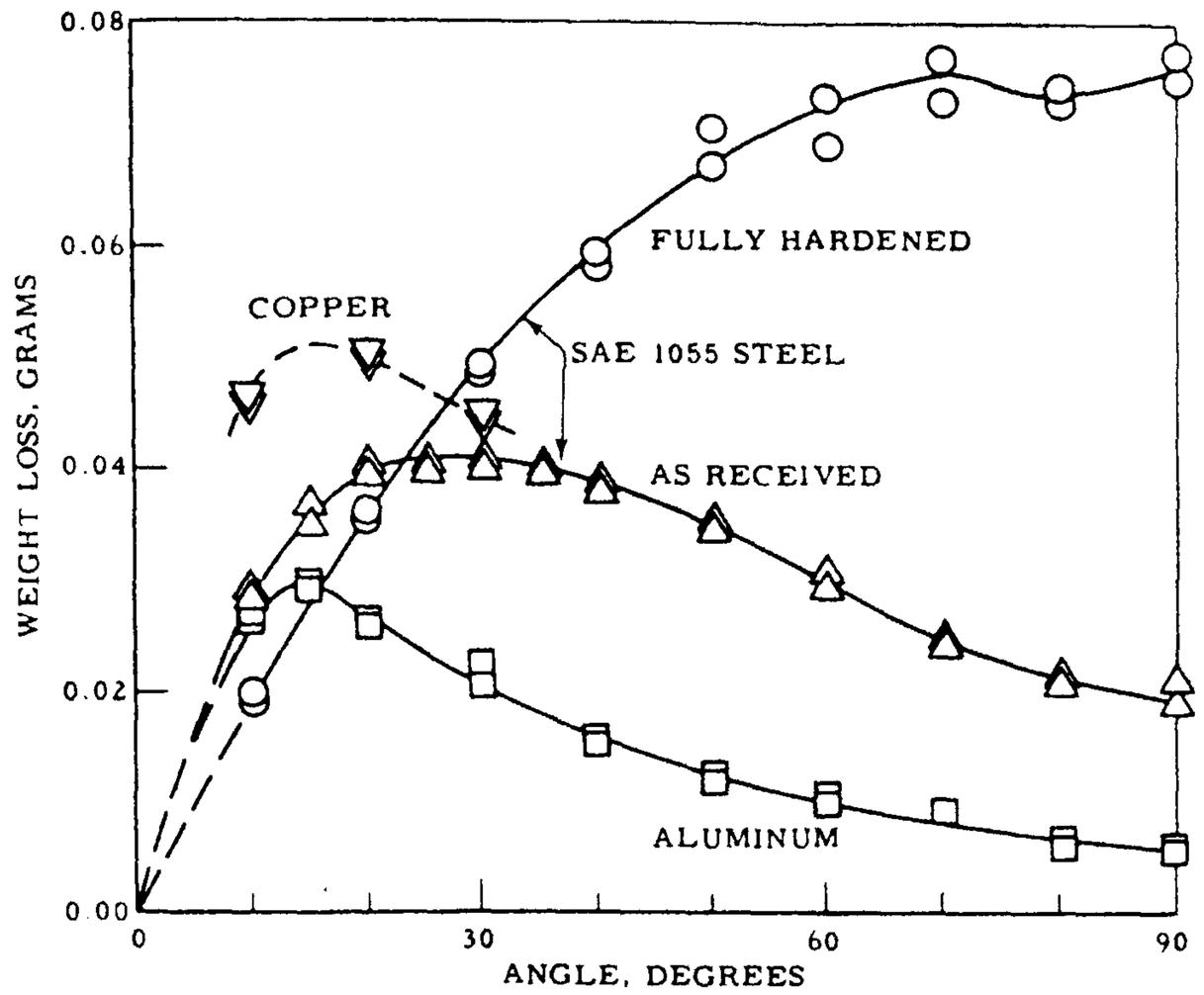

Figure 2.10 The rate of erosion vs. impingement angle [Finnie, 1960].

Hashish [1989c] investigated the effect of impingement angle of abrasive water jets, and employed polymethyl-methacrylate (PMMA) to demonstrate the effect of angle on kerf depth, where the kerf is defined as the geometry of a cut generated by the AWJ process. He demonstrated that backward cutting ($\alpha > 90°$ in Fig. 2.11) produced a shallower depth of cut than cutting at 90°, whilst cutting forwards ($\alpha < 90°$ in Fig. 2.11) at 70° produced the deepest depth of cut (Fig. 2.11).

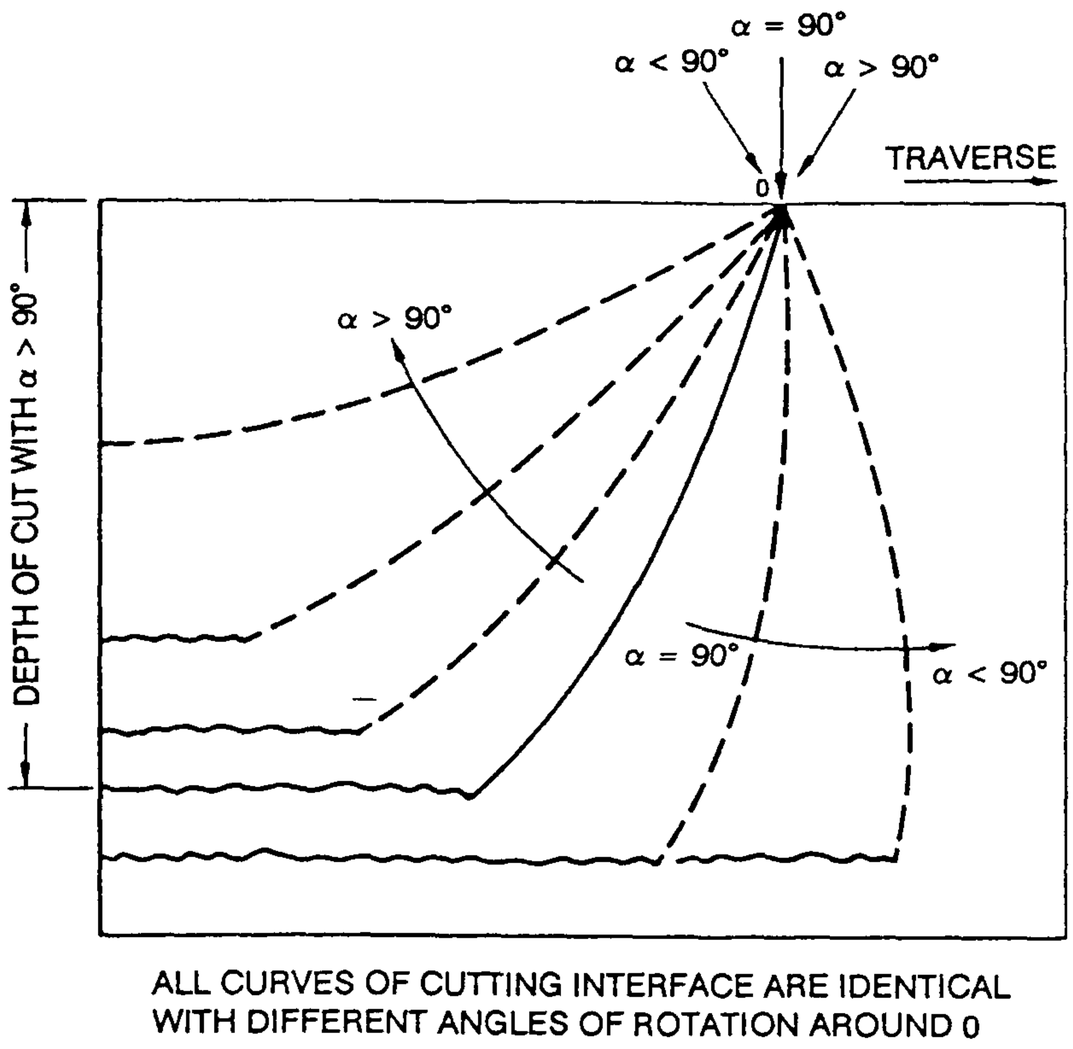

Figure 2.11 Illustration of kerf cut at angles of 60° - 110°. Traverse in the direction of the arrow. Note change in depth and kerf front [Hashish, 1989c].

The change in angle also affected the kerf front geometry. Whilst the research apparatus and erosion conditions are very different from those in the work of Bitter, Finnie, the impingement angles for maximum erosion by AJW of Ti6Al4V [Hashish, 1989c were similar to those observed by Yerramareddy and Bahadur [1993] in their research into air blast erosion of Ti6Al4V.

Hashish [1989c] suggested that the cutting with water jet impingement angles can increase the volume removal by factor of three or four times over that observed when cutting with normal jet impingement angles.

2.3.4 Number of passes of the jet.

Ojmertz [1996] in his study of abrasive water jet milling used multiple passes of the jet as a milling technique with defined milling patterns. The pattern configuration only had a small effect on surface waviness. He employed a Taguchi methodology and demonstrated that many interdependent variables affect the ability to achieve a consistent depth of cut in the milling process [Ojmertz, 1993]. His research also showed that eight passes of the AWJ over the workpiece are optimal for industrialised slot milling with multiple passes of the jet [Ojmertz, 1996]. Hocheng et al. [1997] used six passes in his experiments, and Hashish used up to one hundred. Therefore, we may conclude that the optimum number of passes is dependent on the surface waviness, the cumulative depth and depth tolerance requirement as well the abrasive machining parameters selected. Fig. 2.12 shows the progression of milling depth as the number of passes increases for milling of aluminium.

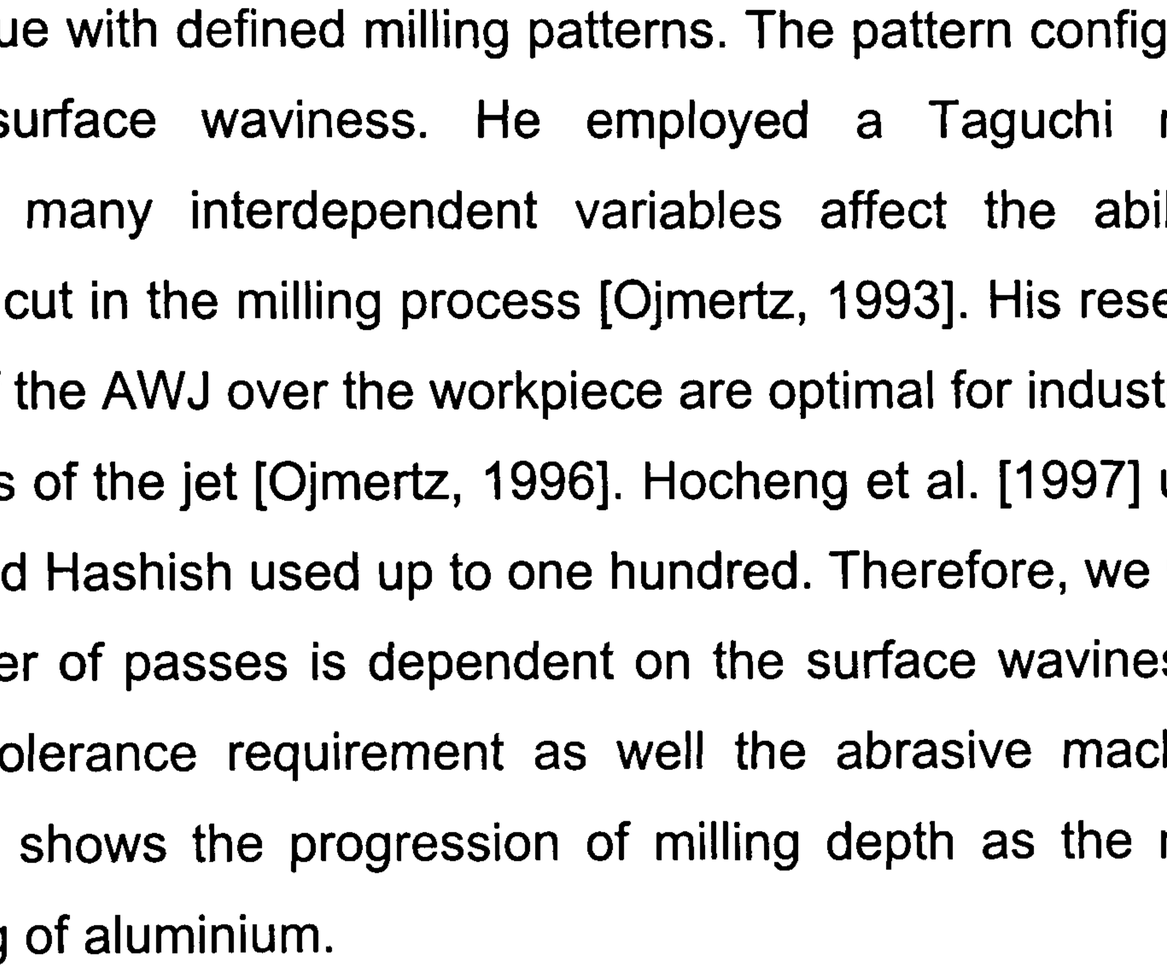

Figure 2.12 Progression of milling depth and depth per pass in AWJ of aluminium with garnet grit [Hashish, 1998a].

2.3.5 Jet traverse speed.

Another key feature for optimized through-cutting is that of the jet traverse speed. If the speed is too slow, the production capacity is reduced; however, if it too fast, through-cutting is not achieved or the surface roughness and waviness of the through-cut kerf is poor with a large number of striation marks present.

However, in milling, the surface roughness and waviness are strongly dependent on the traverse speed. Hashish [1987] performed a preliminary investigation of milling with abrasive water jets. He determined that high traverse speed reduced the depth of cut and changed the geometry of the kerf. At higher traverse speeds it was found that the depth of cut was more controllable, and more consistent when compared to using lower traverse speeds at the same parameter settings.

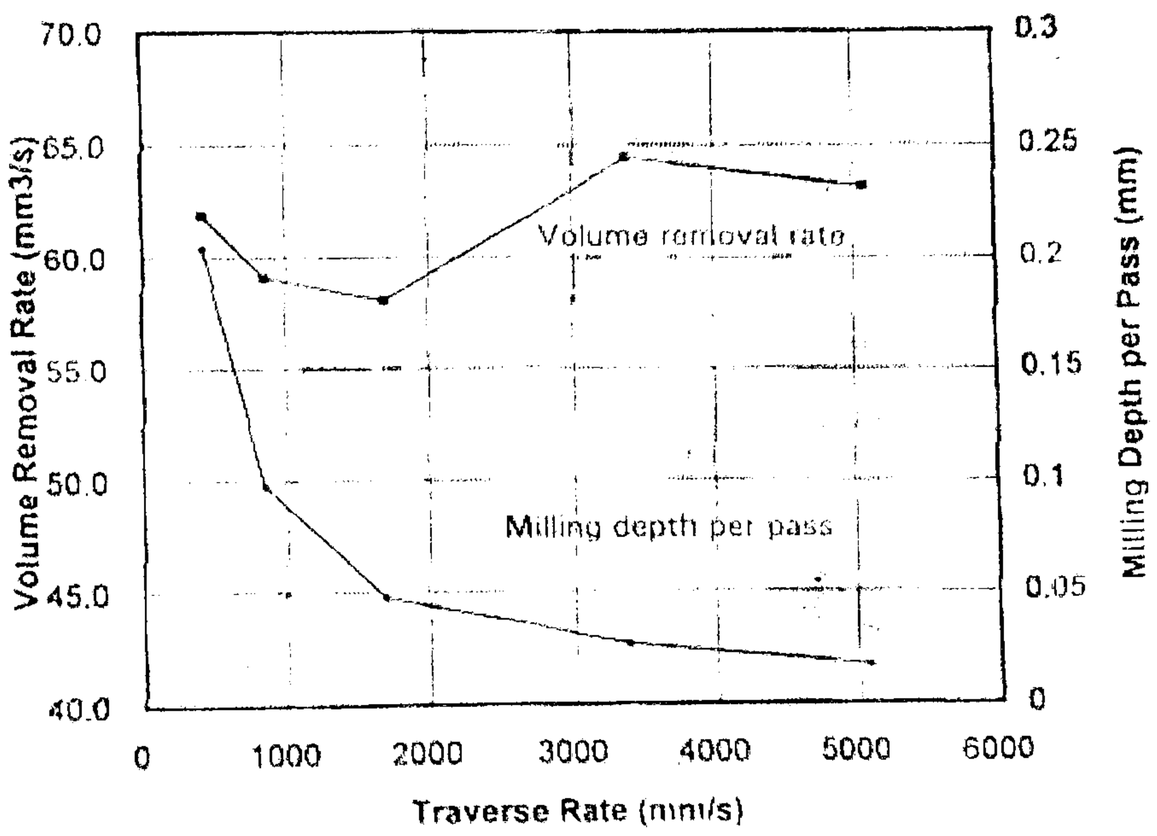

Figure 2.13 Effect of traverse rate on volume removal rate and milling depth per pass in AWJ of aluminium with garnet grit [Hashish, 1998a].

Fig. 2.13 shows that the depth of cut is reduced as the traverse speed increases, whilst the volume removal rate remains at an approximately constant value. However, at lower traverse speeds, there is seen to be a significant increase in the material removal rate as the traverse speed is reduced (Fig. 2.14). The actual traverse speed at which this occurs is dependent upon nozzle stand off distance.

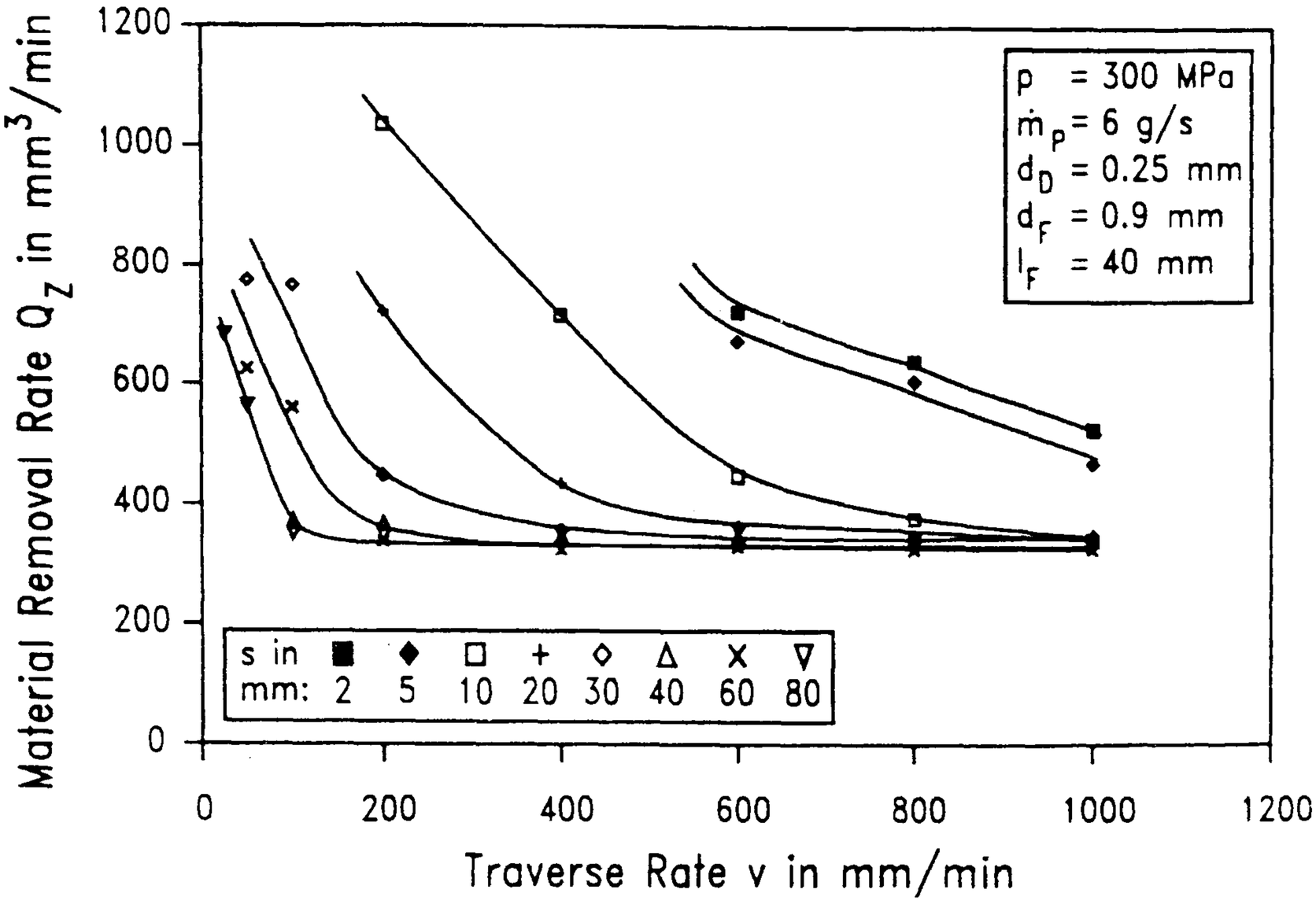

Figure 2.14 Material removal rates in relation to traverse rates at different stand off distances. Where p = water jet pressure, $\dot{m}_p$ = abrasive flow rate, d_D = nozzle diameter, d_F = focus diameter, l_F = focus length, s = stand off distance [Laurinat et al. 1993].

2.3.6 Nozzle stand off distance.

Laurinat et al. [1993] observed that as stand off distance increased, the material removal rate decreased; the influence of stand off distance on material removal rate was less strong at stand off distances between 2 - 5 mm (Fig. 2.14). Hashish [1987] also found that for through-cutting, changes in stand off distance from an optimal value are detrimental to the cutting performance. However, for milling techniques use of a non-optimal stand off distance may be beneficial in controlling the geometry of the kerf. Fig. 2.15 shows how the kerf geometry changes as the traverse speed and stand off distance are increased. An increase in traverse speed reduced kerf depth, whilst an increase in stand off distance produced a wider kerf cross-sectional profile.

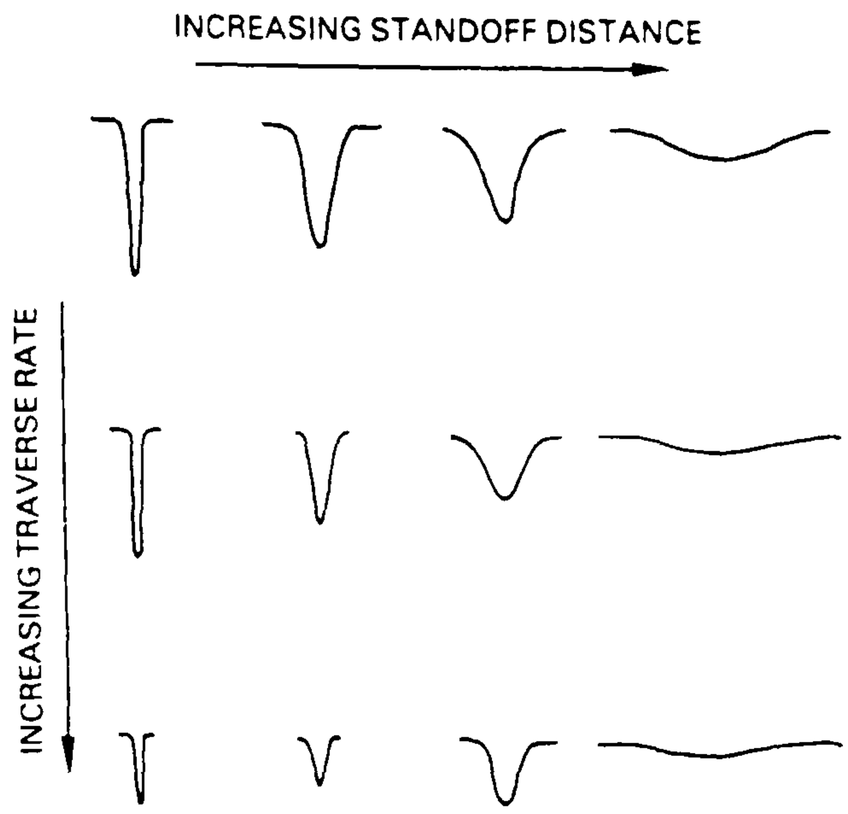

Figure 2.15 Cut shape geometry variation with stand off distance and traverse rate [Hashish, 1987].

2.3.7 Nozzle design.

Hydraulic monitors used for mining and fire fighting generally have a nozzle that has a short entrance cone, with a plain bore reducing in size to form a choked exit diameter [Summers, 1995]. These nozzles are expensive to manufacture, but are considered to be the best for plain water jets. However, they are susceptible to excessive wear when used for abrasive water jet cutting as the abrasive impinges on the reduced diameter of the exit.

Therefore, the nozzles generally used for abrasive water jet cutting have a short entrance cone to aid abrasive grit entry with a plain bore nozzle the same size as the exit diameter and are less susceptible to abrasive wear. Some have a short entrance cone with a diverging section to fan the jet outwards.

The longer the focal length of the nozzle the higher the velocity of the abrasive particles. The optimal length for highest velocity increases with increases in [Momber and Kovacevic, 1998]:

(a) water jet pressure;

(b) abrasive material density;

(c) abrasive particle size;

(d) abrasive particle roundness.

The optimal focal length is also affected by the frictional losses, which reduce the particle velocity, such that the depth of cut is reduced.

Ye and Kovacevic [1999] used computational fluid dynamics (CFD) and Finite Element Analysis (FEA) to model the flow of abrasive laden flow through a nozzle. They concluded that the geometric design of the nozzle affected the transportation and acceleration of the abrasive particles and the rate of wear the nozzle experienced. CFD shows that an optimised tapered inlet, nozzle diameter, and nozzle length will lead to better energy utilisation and less abrasive erosion in the nozzle.

In the early development of AWJ technology, nozzles in general have been axisymmetric; the most common shape is round since this cross section has been the easiest to produce using conventional machining processes. However, this cross section may not be the optimal shape for metal removal or control of tolerance, surface roughness and waviness nor for producing features such triangular thread forms. Yong and Kovacevic [1996] investigated rectangular, triangular, annular and elliptical nozzle shapes by modelling and experimentation. They employed an off line simulation technique to evaluate different cross sections before committing to expensive experimentation and evaluation. Simulation suggested that the cross section had a significant influence on the value of surface waviness. They concluded that the optimal nozzle shape was elliptical with a designated orientation for best surface quality and depth of cut. They suggested that the curvature of the water jet developed by the focussing action of the nozzle played an important role in the formation of surface waviness.

From their simulations, they concluded that a controllable depth of cut is possible by rotating and moving an elliptical jet and other non-circular jets. Their cutting and drilling experiments with non-circular jets showed a good correlation with the modelling.

2.3.7.1 Spiral jets.

Horri has patented a number of applications using spiral jet nozzles from spray grinding, spray coating, pure spiral jets and abrasive spiral jet, [Horri, 1987, 1990, Horri et al. 1991a, 1991b, 1992]. He discussed the development of the spiral nozzle, by employing a hydrocyclone to demonstrate the coanda spiral effect using air and water at low pressure. The velocity distribution of the jet is better than that in conventional jet, and yields a higher velocity [Horri, 1990]. The spiral jet is said to entrain abrasive into the centre of the jet more efficiently, and so it is suggested that wear in the nozzle will be eliminated. The spiral jet produced a better quality kerf geometry, a smaller kerf width and a deeper cut than that created by conventional AWJ nozzles. It was also suggested

that the surface roughness is improved although the evidence presented seems to suggest the contrary.

Another methodology in the development of spiral jets was reported by Dickenson et al. [1987], where a vane is implanted in the nozzle to rotate the water jet within the nozzle. The disadvantage of the vane system is that the vane is eroded during the operation of the system.

2.3.8 Abrasive characteristics.

Whilst silica sand and olivine are low cost abrasives, it has also been shown that they result in lower material removal rates than the more expensive abrasives, such as garnet, thus making the more expensive abrasives more economic to use [Faber and Oweinah, 1991]. In fact, it appears that garnet is often the most economic to use. Aluminium oxide resulted in higher material removal rates but is expensive. Copper slag also resulted in high material removal rates but was expensive and produced inconsistent results. Iron grit produced higher material removal rates than aluminium oxide but again is much more expensive although it can be recycled [Summers, 1995]. Some common attributes found during the course of the research were that the denser the grit and the larger the particle size, the higher the ensuing material removal rate. However, smaller grit sizes resulted in reduction in the surface roughness and an improvement in the kerf geometry [Faber and Oweinah, 1991]. There is compromise between cost, power consumption, performance, and environmental considerations. Garnet mesh size 80 (180 μm) appears to offer good all-round performance for through-cutting. It is readily available and widely used in industry [Summers, 1995].

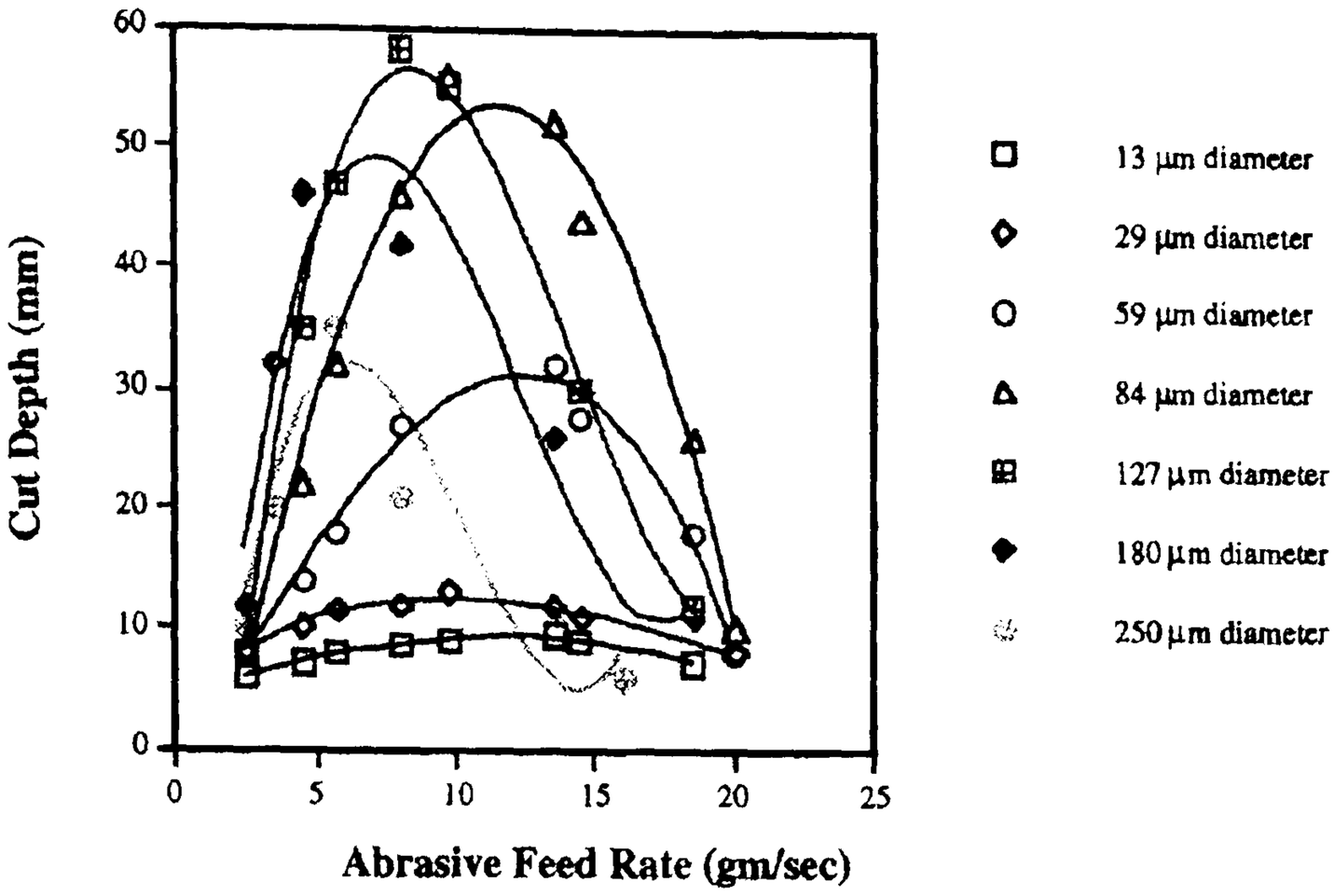

Figure 2.16 The depth of cut as a function of the grain size of the abrasive, when using corrundum particles to cut aluminium at 400 MPa at a traverse speed of 0.83 mm s^{-1} (50 mm min^{-1}) [Summers, 1995].

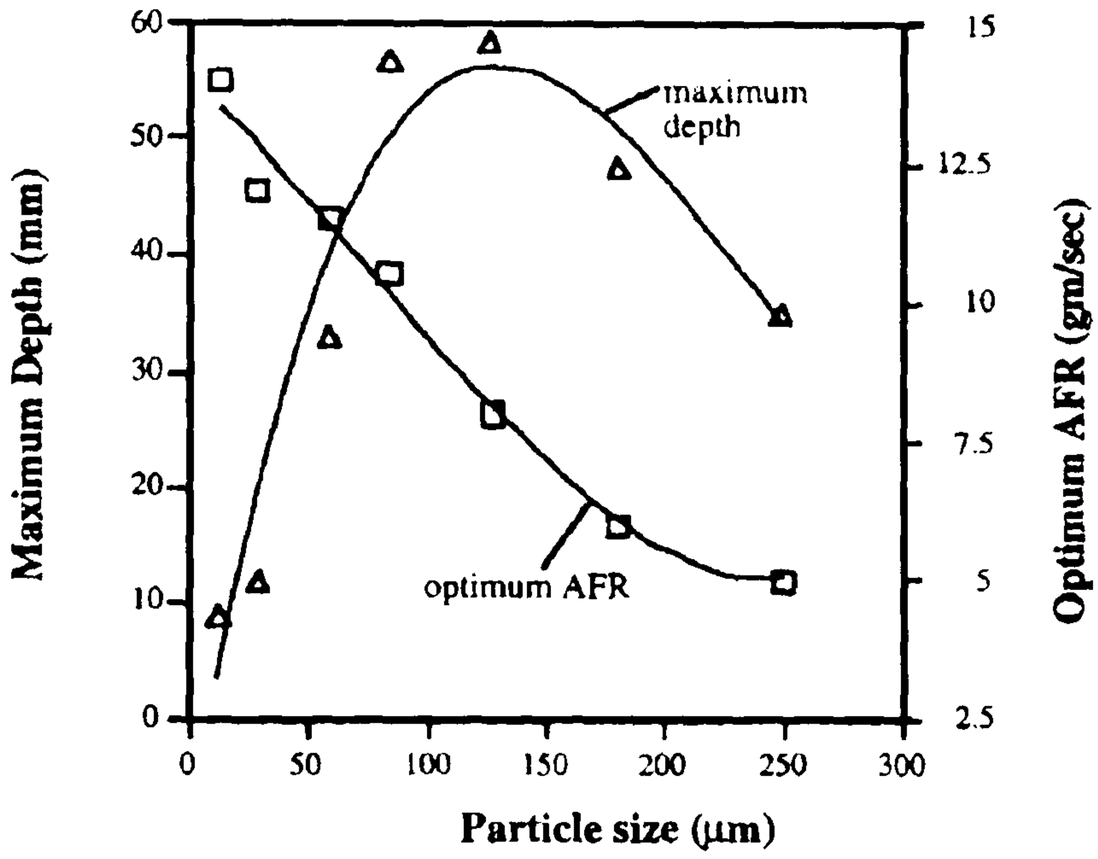

Figure 2.17 Optimum Abrasive flow rate and maximum depth of cut as a function of particle size [Summers, 1995].

Although the choice of abrasive is often made on economic grounds, the entrainment of the chosen abrasive particle into the water jet, its physical size and its distribution, affect the cutting performance of the abrasive water jet [Faber and Oweinah, 1991].

A particle distribution that is well controlled and consistent will produce a consistent cutting performance [Bennett, 1996]. This suggests that the quality and consistency of the supplied abrasive should be checked regularly as a part of the quality control procedure for the process. Fig. 2.16 shows that depth of cut is highest for an intermediate particle size with lower values for both the larger and smaller sizes of the abrasive. Fig. 2.17 show that where the Abrasive flow rate (AFR) is optimised, there is

an optimum particle size that achieves the maximum depth of cut for the stipulated conditions [Summers, 1995], [Faber and Oweinah, 1991], [Kulekci, 2002].

In AJW-CDM research, Hashish [1998a] suggested that the use of smaller grit reduced the volumetric removal rate. His research indicates that the 250 μm (60#), 150 μm (100#) and 180 μm (80#) garnet grit, result in similar volumetric removal rates of about 60 $mm^3\ s^{-1}$, whilst the smaller 100 μm (150#) garnet grit resulted in a volumetric removal rate of about 40 $mm^3\ s^{-1}$.

2.4 Abrasive flow rate.

Both Fig. 2.16 and 2.17 show that for the abrasive particle sizes and AWJ conditions stipulated [Summers, 1995], the depth of cut is dependent on both the particle size and abrasive flow rate. The depth of cut for a chosen particle size increases to a maximum as the abrasive flow rate increases, whilst further increases in abrasive flow rate reduce the depth of cut. The employment of non-optimised abrasive flow rates could result in low depth of cut and inefficient employment of abrasive (Fig. 2.16). However, an increase in abrasive flow rate can result in a reduction in the waviness of through-cut surfaces (Fig. 2.23).

2.5 Masking for AWJ milling.

A cut mask is a piece of material with a cut profile to match the cavity shape to be milled in a component (Fig. 2.18). It is used in AWJ milling to shield the area around the section where milling is desired. The mask is prepared and mounted on the work piece and aligned to the area where the cavity is to be milled.

Hashish [1994b, 1998a], in his investigation into milling isogrid profiles in aluminium to depths of 0.25 - 6 mm utilised masks of steel of thickness equal to the depth of cut and tungsten carbide masks a ¼ of thickness of the depth of cut.

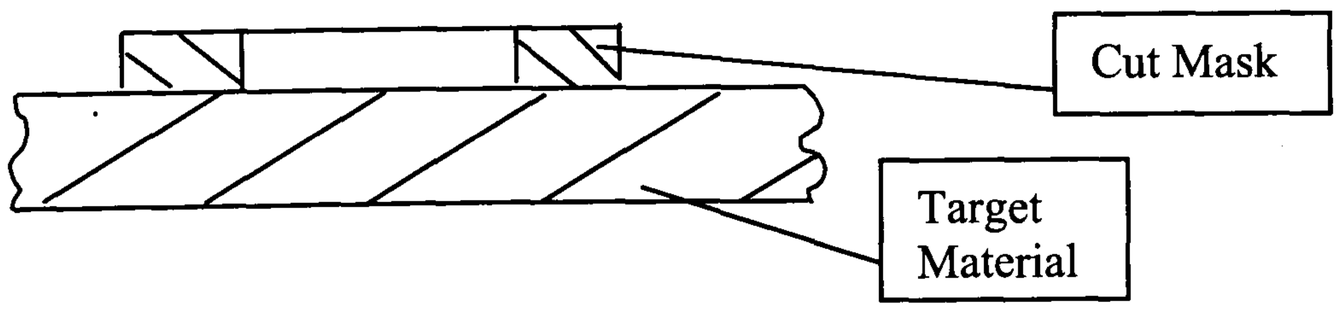

Figure 2.18 Schematic diagram of a cut mask.

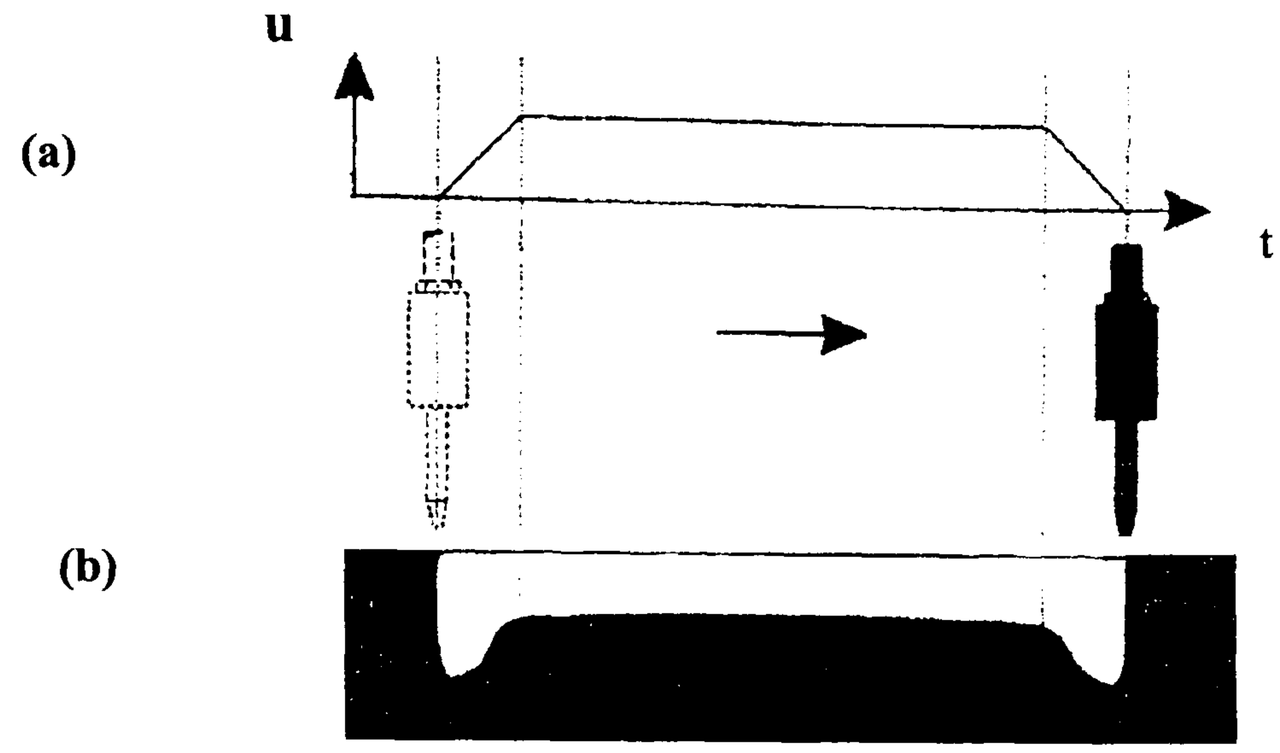

Figure 2.19 (a) Velocity (u) - time (t) diagram indicating the traverse motion with acceleration, stationary velocity, and deceleration. (b) Material removal response to traverse speed [Ojmertz, 1997a].

Fig. 2.19 shows the necessity of utilising a cut mask, and the areas that need protecting from the abrasive water jet, when the abrasive water jet is stationary, decelerating or accelerating [Ojmertz, 1997a]. In the research of Ojmertz on slot milling [1997b], which industrialises the abrasive water jet process to a specific application, the effect of splash damage from the start/stop dwells on traversing and of cutting/milling of geometries on different levels is significant unless the workpiece is masked. It can be inferred that prediction of splash zones and protection of these from damage will need to be considered when industrialising abrasive water jet milling to complex cavities. Ojmertz [1996], also noticed that secondary machining also occurs from splash from the mask itself (Fig. 2.20). This manifests itself as higher surface roughness values and larger depths of material removed in localised areas where the secondary machining has occurred.

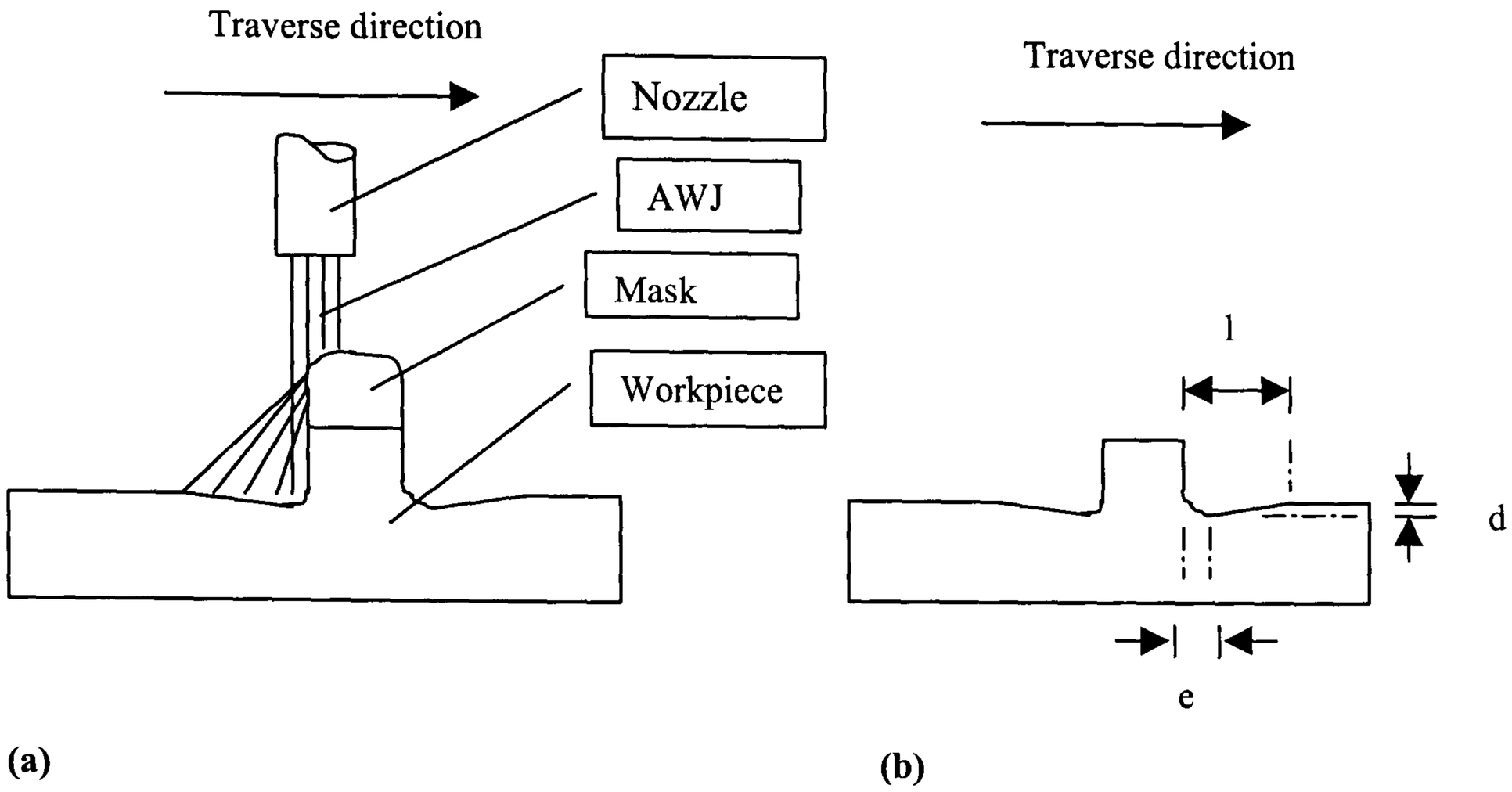

Figure 2.20 Secondary machining effects when AJW-CDM with masks. (a) The wear process of mask and work piece during a masked milling operation. (b) l, d, and e, indicates dimensions of form errors caused by secondary machining due to jet deflections [Ojmertz, 1996].

Both Hashish [1987] and Ojmertz [1996] argue that the mask should be the same thickness as the depth of the cavity to by cut. The abrasive water jet therefore, will not reach the parent material beneath the mask when the abrasive water jet cuts into the mask. In this way the mask is destroyed but leaves the parent material intact.

The literature review on cut masks has indicated that there is very little published research on selection of cut mask materials. There is also very little published research on the cut mask material and geometry requirements needed to produce component geometry to a required a specification. For example, if an AJW-CDM aluminium component required a chamfered edge in a pocket, a steel mask with a 45° chamfer may produce a different angled chamfer since it will have a material removal different to that of the target material. Hashish [1996c] suggested that cut masks can be used to produce the radius of bosses, but reports no detail on the mask radii dimensions required to create the required radii on the eroded boss. Further, cut masks are sacrificial by nature and so they are an additional manufacturing cost. Hashish [1998a] provides an economic analysis of the costs for manufacturing cut masks for the manufacture of AJW-CDM isogrid pattern pockets in aluminium. Further, the latest five axis AWJ machine tools employ pressure ramping [Hashish, 1994a] where the water pressure is applied gradually during the acceleration and deceleration stage of the traversing water jet, possibly eliminating the need for masking and avoidance of secondary machining.

Ojmertz [1997c] addresses the problems of jet head dwell by a process termed 'discreet milling'. Discrete milling consists of eroding the surface of the material by introducing small packets of abrasive grit discontinuously into a steady water jet to create a small pocket or hole. The water jet is moved to a new location the process is repeated. Fig. 2.21 shows the resulting pock marked surface of a cavity created by discrete milling.

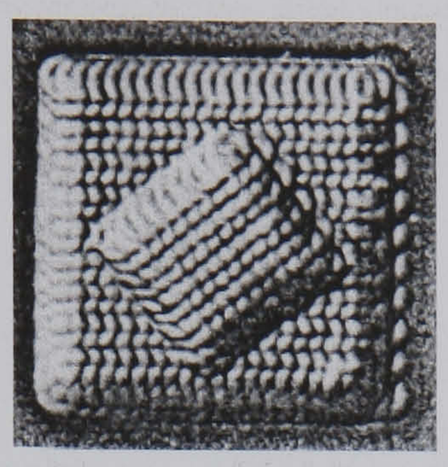

Figure 2.21 Discrete milled pocket level one: 400 cavities, level 2: 100 cavities (level 1 approximately 20 x 20 mm; level 2 10 x 10 mm with a 1mm diameter nozzle). Note: Pock marked surface [Ojmertz, 1997a, 1997c].

Clearly cut masks are of benefit in the manufacture of discrete features but increase manufacturing costs; a further disadvantage is that masks may induce secondary machining.

2.6 On-line process sensing and control.

Sensors have been employed in AWJ processes to initially measure forces on the workpiece for analysis and gather information on kerf geometry and depth, but research suggested that the data capture methodology can be utilised for 'On line process sensing'. However, process sensing can be categorised into three areas: (i) 'Online Process Sensing' where the process signals from sensors are monitored to ensure process is running smoothly, with corrective action being taken manually; (ii) 'Machine monitoring' where the signals from sensors monitor changes in the machine equipment that set process parameters. Such changes are often due to wear and tear in components; (iii) 'Adaptive Control' where the output signal from a sensor monitoring a process parameter is compared to a known reference signal generated by a known process value. Any difference in value between the reference and the input signal is calculated and corrected by an increase or decrease in the process parameter value using a control loop. The control loop adjusts the process parameter automatically until the input signal is equal to the output signal.

2.6.1 On-line process sensing.

Hunt et al. [1988] employed a force sensor attached to tapered and stepped work pieces, to correlate cutting force and surface roughness. They suggested that the traverse speed could be decreased to ensure through-cutting and control the quality of surface roughness by monitoring the signals produced from the sensor whilst the machine was cutting.

Kovacevic et al. [1995] also employed a force sensor and a dynamometer to compare force profiles against surface roughness and waviness profiles, and suggested that the normal cutting force could be used for monitoring surface roughness. The force could be characterised on a scale of surface roughness values and the feedback loop employed to control the adjustments of the selected parameters required to maintain the selected force to achieve the required surface roughness. They suggested that traverse speed and water pressure are the most important parameters to be monitored for quality of surface finish. Kovacevic stated that, up to 1995, only controller feedback loops had been implemented on new cutting systems to control the stand off distance and traverse speed parameters [Kovacevic et al. 1995]. However, he envisaged that the four parameters of water pressure, abrasive flow rate, traverse speed and stand off distance will all be controlled with feedback control loops, at some point in the future. Kovacevic [1992] utilised a force transducer to monitor the depth of penetration of an abrasive water jet. He suggested that the force could be measured and a feedback loop employed to increase the pressure to maintain the depth of cut when a nozzle is worn. The problem here is that the increase in water pressure will increase nozzle wear and will exaggerate the problem. The model of predicted force and the predicted depth of cut had a correlation of about 0.94 and 0.975 when compared to the experimental results.

Westkampfer et al. [1998] suggested the use of feedback and process control to the water jet path to compensate for geometric errors in the geometric form of the component in three dimensional machining. They also suggested the use of CAD/CAM incorporating this feedback as a form of off line machining simulation, presented in the form of integrated manufacturing as a possible way forward for future development.

2.6.2 On-line sensing - machine monitoring.

The elimination of process variation due to system wear has been suggested as a solution to improve the consistency of the depth of cut, surface roughness and improve productivity. Kishkat [1996] suggested the employment of feedback loops for the elimination of down time in the production process. In this case, the sensors are

targeted at malfunctions in the abrasive feed system with possible use for detecting wear in nozzles and prompting the operator to change the nozzle at the next component change over. Kovacevic et al. [1993] utilised an acoustic signal released by flow of the particle laden water jet through the nozzle to monitor the wear on the nozzle. They concluded that the acoustic signal was highly sensitive to small variations in the inside diameter of the nozzle caused by wear and could be employed for on - line monitoring of nozzle wear. They also suggested an indirect measure of nozzle wear which employed a force transducer to monitor the depth of penetration of an abrasive water jet.

A further development by Hashish et al. [1993, 1996a] is the orifice health monitor, which uses a pressure based approach to monitor the edge wear on the orifice and indicates to the operator when nozzle wear becomes unacceptable. No feedback from the orifice to control the pressure to accommodate for the orifice wear was suggested although this may prolong orifice life. The main driver for such instrumentation is to reduce machine down time in changing over worn nozzles and re-aligning the new nozzle with the orifice. Incorrect alignment causes premature nozzle wear and affects the performance of the water jet by perturbing the water flow between jet orifice and the nozzle.

Hashish [1996a] also investigated the control of the abrasive flow rate and employed sensors on the abrasive feed rate system to monitor the abrasive flow rate automatically. The feedback control is used to control the abrasive flow to an accuracy of ± 5%. A consistent abrasive flow rate results in a more consistent depth of cut and surface roughness.

2.6.3 Adaptive control.

Groppetti et al. [1996] proposed an adaptive control model for through-cutting and demonstrated that his adaptive control algorithms will detect an increase in material thickness and automatically change the traverse speed to achieve through-cutting. He employed a biaxial force transducer based on a load cell to provide the sensing capability. Groppetti et al. suggested the utilisation of the vertical and horizontal cutting forces developed by the abrasive water jet to monitor the depth of cut. They noted that the vertical force is more important to control depth and side-kerf surface finish than the horizontal force. The feedback control loop decreases the traverse speed to ensure through-cutting of the workpiece.

2.6.3.1 Acoustic monitoring.

Research on the acoustic monitoring of depth when drilling with abrasive water jets was performed by Kwak et al. [1996] who suggested that acoustic emission is a good indicator of drilling depth and could be used for on line monitoring. They suggested that the sensors could be set to a prescribed depth of cut; when the sensors receive the corresponding acoustic signal, the cutting process is stopped. Mohan et al. [1995] used the acoustic emission technique to detect the depth of cutting. Water jet pressure and traverse speed were varied and the actual depth of cut compared to that of the absorbed jet energy. The investigation showed that the acoustic emission signals can be manipulated so that they could be used to predict depth of cut. This could be used in a feedback loop to develop the process into adaptive control system.

2.7 Workpiece characteristics developed in AWJ processes.

Abrasive water jet machining has been considered a machining process that does not induce any heat affected zone in the cutting region. It is also considered to produce low cutting forces such that only light clamping of work components is required, and as such there is little distortion of the work or residual stress developed during the manufacturing process. However, experiments conducted by Mohan et al. [1996] suggest that a high temperature zone is induced into the cutting region by the process. The high temperature zone was measured using infra red techniques and compared against embedded thermocouples. The temperature rise in the workpiece material for both aluminium and titanium was only about 60°C and thus is unlikely to induce a heat affected zone in material with a recrystalisation temperature above the induced temperature.

Arola and Ramulu [1996] showed that AWJ machining induces localised residual stresses at the free surface similar in nature to those induced by shot peening. These are considered to be beneficial since they are compressive in nature and thus improve fatigue life. It was noted that since there was no strain hardening and little change in the microstructure, the deformation was insignificant. There appeared to be a trend that the resulting residual stresses increased as the melting point of the material substrate increased.

2.7.1 Surface roughness and waviness.

The roughness and waviness are quantitative measures of a surface profile. There are a number of techniques employed to measure surface roughness. The method employed to measure the surface roughness during this investigation was Ra (the Arithmetric Mean of the departures of the profile from the mean line, throughout a prescribed sampling length). It is the most widely used international parameter as a measure of roughness. [Rank Taylor Hobson, 1985a, 1985b, 1994]. Waviness is the undulation of a surface. It can be measured using a number of techniques, the most common being Wt (i.e. total height of the undulation over the sampling length) which is the sum of the height of the largest profile peak height (top of undulation) and the deepest valley depth (bottom of undulation) within the sampling length (Fig. 3.9) [Rank Taylor Hobson, 1985a, 1985b, 1994]. An identifiable feature of through-cut surfaces is that of striation which changes as cutting enters the deformation zone where waviness increases and the striations become more curved (Fig. 2.22). For milling, waviness at the bottom of the kerf are undulations in the milled surface, while the kerf walls exhibit a similar waviness and striation to that observed in Fig. 2.22.

Research into AWJ cutting suggests that the parameters of abrasive flow rate, grit size, multiple passes of the jet, and traverse speed affect the surface roughness and waviness. However, the parameters have different effects when employed for milling as opposed to cutting.

2.7.1.1 Through-cutting.

The surface roughness in through-cutting has two distinct values, relating to the two cutting zones. In the top zone, material is removed by cutting wear, and in the lower zone, material is removed by deformation wear. In the cutting zone surface finish is of a better quality than that of the lower deformation wear zone, which contains curved striations (Fig. 2.22). This is because the abrasive grit in the cutting zone has high energy and erodes the material by micro-cutting. The deformation wear zone has a poor surface finish because as the abrasive grit loses energy the material can no longer be cut and is removed by mechanical deformation. Further, Hashish [1987] suggests that for through-cutting, decreasing traverse speeds and increasing water pressure and abrasive flow rates will reduce surface roughness and waviness. Summers [1995] also concurs with the research conducted by Hashish. He found that the surface waviness of a through-cut surface decreases if the abrasive flow rates are increased and the traverse speed is decreased. Fig. 2.23 shows the increase in surface waviness for a

through-cut surface as the traverse speed increases, whilst the surface waviness decreases as the abrasive flow rate increases. Cappelo et al. [1996] have derived surface finish equations for both the cutting and deformation wear zones.

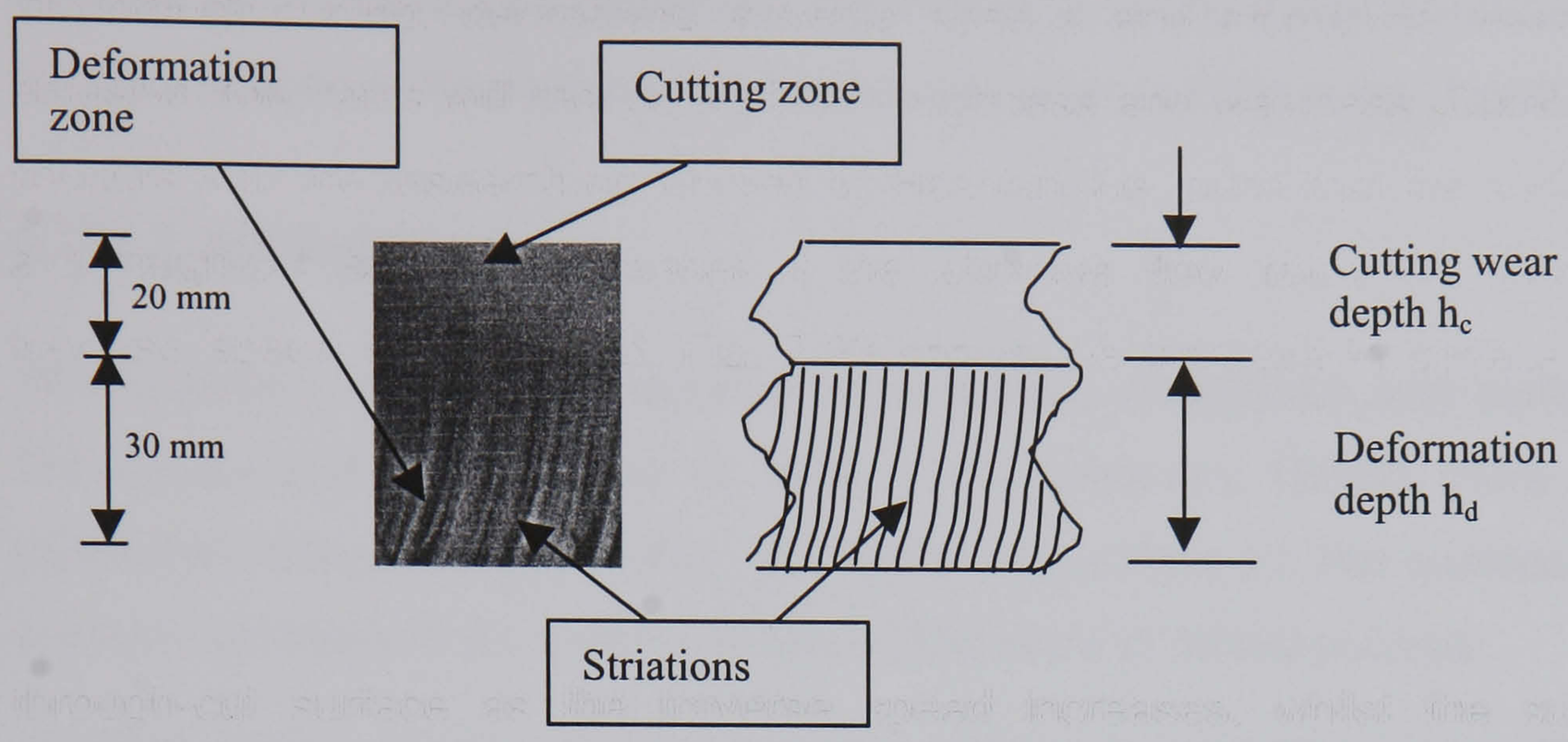

Figure 2.22 Image and schematic diagram of a side wall of a through-cut component showing cutting wear (smooth area) and deformation wear (wavy area) regions as defined by Hashish. The waviness marks are also known as striation marks [Hashish, 1992a].

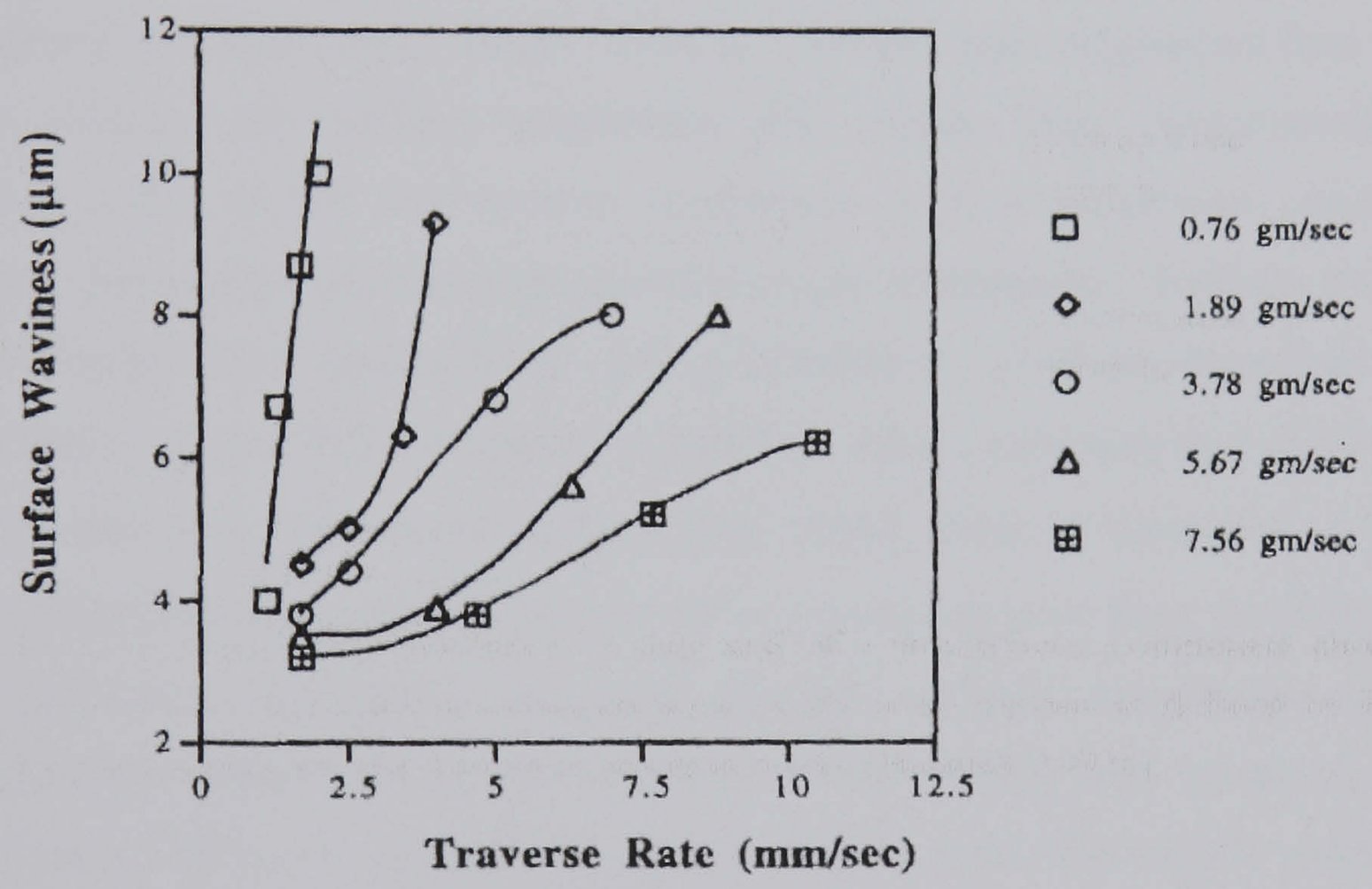

Figure 2.23 Change in traverse speed and Abrasive flow rate on the waviness of a 240 MPa cut on inconel using 180 μm (80 #) garnet [Summers, 1995].

However, some researchers [Chao et al. 1995] suggest that some AWJ machines produced better surface roughness and waviness due to the robustness of the machine itself. The variation is influenced by the machine design, its vibration damping mechanism, the design of the drives and the machine tool slides in the various axes. The wear in these drives and the machines slides also influence the quality and capability of the machine tool to produce geometrically accurate workpieces. Statistical process control and range charts are used to reduce this problem by matching

component tolerances to machine process capability. Chao et al. [1995] measured machine vibrations and compared the machine vibrations in the X and Y axes to those seen in the kerf geometry. He suggested that the surface roughness and waviness was affected by the vibrations caused by the motors, and that these vibrations are the source for the variation in the surface finish produced when cutting in the X and Y directions.

2.7.1.2 Milling.

Whilst some research has examined the surface roughness and surface waviness of through-cut surfaces [Chao et al. 1992, 1995], [Hashish, 1992a], there is relatively little published research on the effect of milling parameters on the surface roughness and surface waviness of the bottom of AWJ-CDM kerfs or milled pockets.

Hashish [1991, 1987] indicated that the milling of aluminium alloy with 180 μm (80#) garnet grit resulted in a surface roughness of 20 μm, whilst milling with 100 μm (150#) grit resulted in a surface roughness of only 13 μm. Ojmertz [1996] also saw similar surface roughness values when milling aluminium alloy. The larger grit also resulted in larger variations in actual cavity depth. Li et al. [1996b] also suggested that the use of smaller grit reduced the surface roughness (Ra) value. They demonstrated that at impingement angles of 90° the surface roughness is at a maximum value for most materials and decreases as the impingement angle decreases. Surface roughness is also material dependent. Under fixed milling conditions, Li et al. observed a surface roughness (Ra) value of 4.0 μm on an aluminium alloy, whereas that developed in a titanium alloy was only 3.0 μm. Ojmertz [1993, 1996] demonstrated that once surface waviness has developed, it cannot be eliminated by subsequent passes of the jet, but is instead exaggerated. Moreover, he observed that surface roughness and surface waviness were not dependent on the depth to which milling was conducted [Ojmertz 1996]. Hashish [1987] and Liu [1998] concur, and stress that depth uniformity and surface control must be considered at the beginning of the milling process. Liu [1998] examined AJW milling of optical glass and found that a secondary mechanical grinding process had to be introduced to reduce surface waviness to acceptable levels between AJW milling steps.

Hashish [1987] suggested that the use of small sized grit also produced less variation in depth or surface waviness. Cavities in aluminium were AWJ milled using 180 μm (80#) garnet grit followed by a milling using a 100 μm (150#) garnet grit with one depth pass being conducted for each grit size. This resulted in a total depth variation of 0.203 mm, whilst a much larger total depth variation of 0.51 mm was achieved when a cavity was

AWJ milled only using 180 μm (80#) garnet grit with 2 passes of the jet. However, there are no details reported for a cavity AWJ milled using 100 μm (150#) garnet grit with two depth passes.

The traverse speed of the jet over the workpiece also has a strong influence of its surface finish. Ojmertz [1993] has shown that low traverse speeds result in an irregular surface morphology of the milled area but that despite this, *lower* surface roughness values are observed. He suggested that low surface roughness values require a high number of particle impacts per unit area; such conditions result from lower traverse speeds, higher abrasive flow rates or by use of a smaller mixing tube to orifice ratio. He also demonstrated that surface waviness improves significantly (i.e. is reduced) by increase of traverse speed up to 0.01 m s^{-1} (600 mm min^{-1}) but that further increases in traverse speed yield only small improvements. However, Hashish [1987] suggested that the traverse speed must exceed a critical value (0.016 m s^{-1} (960 mm min^{-1})) to achieve surface uniformity (i.e. a low surface waviness).

Ojmertz [1993] demonstrated that whilst lower traverse speeds resulted in high surface waviness they also resulted in significantly increased material removal rates. He concluded that the high traverse speeds required for controlling the depth and waviness resulted in low volumetric removal rates.

During AWJ-CDM, there is a desire to minimise the surface roughness and waviness whilst maximising the material removal rate. There are a number of inter-related processing parameters which affect these, one of which is the angle at which the waterjet impinges onto the workpiece surface. Li et al. [1996b] demonstrated that normal jet impingement results in maximum surface roughness for most materials which then decreases as the impingement angle decreases. For example, impingement of a jet at 90° onto an aluminium alloy resulted in a surface roughness (Ra) of 4.0 μm which was reduced to 2.5 μm upon milling with a jet impingement angle of 3° (Fig. 2.24). They indicated that the most significant reduction in roughness was observed as the jet impingement angle fell below 20°. Hashish [1989c] also concluded that milling at low jet impingement angles reduced the surface roughness and waviness. Similarly, Ojmertz [1993] found that when AWJ milling aluminium and steel with different abrasives, a reduction in waviness and roughness of approximately 50% resulted if milling was conducted at low jet impingement angles of 30°. In contrast, Armada et al. [1999] indicated that the angle of jet impingement during grit blasting had no significant effect on roughness. Li et al. [1996b] proposed that the change in morphology was responsible for the reduction in roughness as the impingement angle is decreased. He suggested

that abrasive grit cuts the surface at impingement angles of 0 - 5° ploughs at angles of 5 - 20° and craters or micro-fractures the material at angles of greater than 30°. Preece [1979] also makes a similar observation, namely that the resulting surface roughness increases as the impingement angle increases. Li et al. [1996b] achieved a surface roughness of Ra 1.0 μm at cutting angles of 5° when AWJ polishing aluminium. They indicated that high quality polished surface finishes can be achieved but require the employment of abrasive water jet at low angles of impingement.

AWJ-CDM shows some promise as a method for shaping materials that are difficult to machine by conventional processes. However, as seen, the rate of material removal and the surface finish and tolerances of the machined component depend critically on a number of processing variables, amongst them jet traverse speed jet, grit size, jet impingement angle.

2.7.2 Surface morphology.

The surface morphology of a component is a qualitative description of micro features and is important in component manufacture. If the surface is rough, and irregular it may provide unwanted crack initiation sites and reduce fatigue life or the surface morphology may be such that it results in poor adhesion of coatings.

Stachowiak and Stachowiak [2000] suggested that the morphology of the worn surface is dependent on the shape of the abrasive particles. Rounded particles generated round craters, while angular particles produced sharp indents and narrow cutting grooves.

The surface morphology is also affected by the impingement angle. Griffiths et al. [1999] conducted angled grit blasting research on carbon steel showed that grit blasting at impingement angle of 45° produces furrows with a saw tooth profile which assist adhesion which may be as a result of micro cutting.

Ives and Ruff [1977] also provide further evidence that at impingement angles of 20°, a surface cutting process is evident from their Scanning Electron Microscope (SEM) analysis, whilst at impingement angles of 90° deformation damage is evident.

Research conducted by Ramulu and Raju [1993] on abrasive water jet cutting of aluminium, similarly found that at low impingement angles, material removal was due to micro cutting and increasing the impingement angle resulted in more damage and surface cracking, with deep craters. Li et al. [1996a] concluded that the surface morphology was striated from micro cutting at very low impingement angles using abrasive water jet machining with long stand off distances and pressures of 76 MPa (10

000 psi). The surface roughness also improved as the impingement angle was decreased (Fig. 2.24). The improvement in surface roughness was seen to be due to a change in surface morphology as the impingement angle decreases.

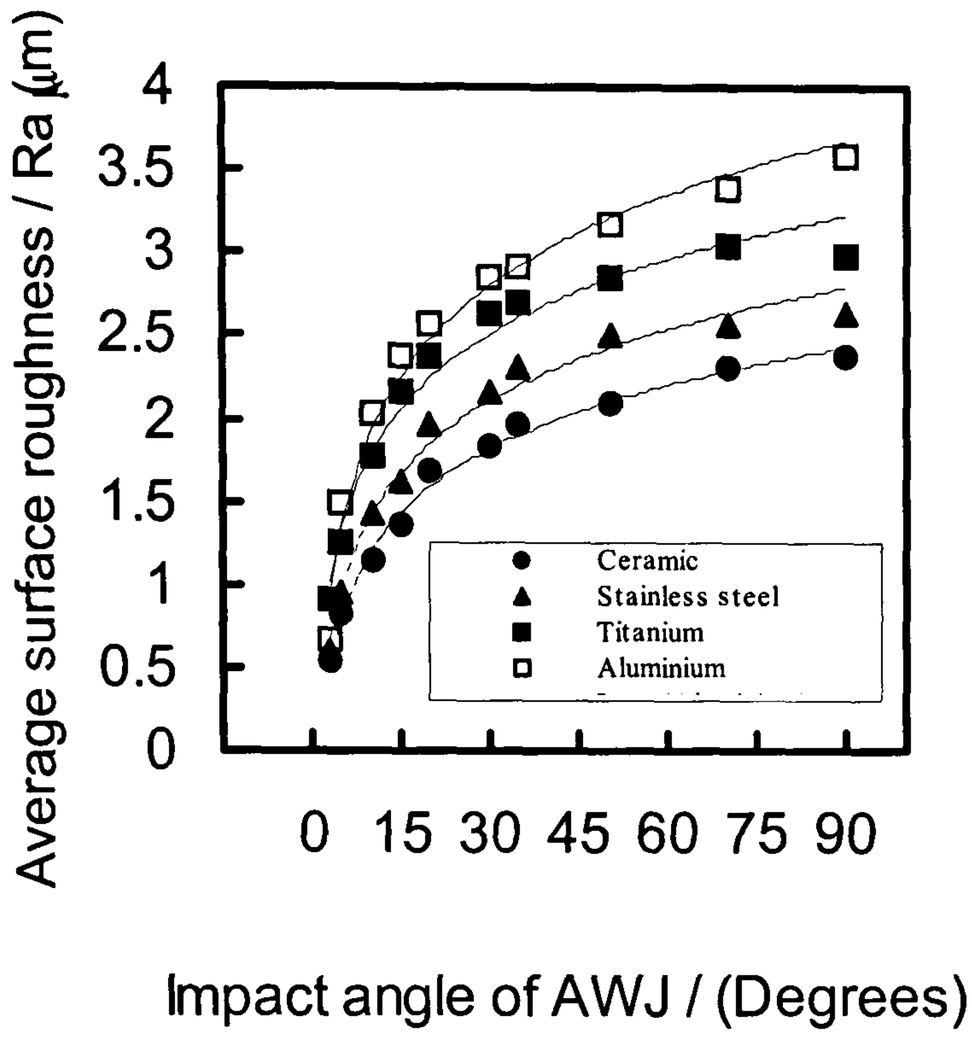

Figure 2.24 Surface Roughness Ra vs Impingement angle indicating improvement in surface finish as the impingement angle decreases [from Li et al. 1996a].

Although erosion conditions provided by stationary low pressure particle laden fluids are different from those seen in moving high pressure particle laden fluids, the surface morphology is similar and is affected by grit size, grit shape, grit hardness and, perhaps the most important factor, impingement angle. Low impingement angles result in 'scratch like' surfaces whilst high impingement angles result in a deformed, indented, cratered surface.

2.7.3 Grit embedment.

Grit embedment is the entrapment of impacted particles in the surface of a material. In the area of wear of materials, there are a number of research studies which document the nature of grit embedment caused by erosion of surfaces with relatively low particle velocities [Ives and Ruff, 1977, Neilson and Gilchrist, 1968, Stachowiak and Stachowiak, 2000, Armada et al.1991, Zu et al. 1991]; however, there is relatively little published research on the effect of processing parameters on the embedment of grit into component surfaces during milling with AWJ. In work concerning abrasion of materials,

it has been suggested [Stachowiak and Stachowiak, 2000] that particle shape, rather than particle hardness, is the key factor in determining the level of grit embedment in a surface

Ramulu and Raju [1993] conducted research on abrasive water jet cutting of aluminium and a Metal Matrix Composite (MMC) at impingement angles of 5° to 25°. No embedded grit was seen in the MMC, but embedded grit was seen in the aluminium specimens. Ramulu concluded that this was due the fact that MMC, being harder than the aluminium was more resistant to penetration by the grit.

2.7.3.1 Particle shape.

A more rounded particle is less likely to be embedded than a angular shaped grit whose pointed shape acts as a sharp indentor and therefore is more likely to penetrate into the surface of a material. The point on an angular particle has less surface area than a rounded particle to distribute the impact force, and thus will penetrate deeper and is more likely to become embedded. Stachowiak and Stachowiak [2000] who fed a slurry onto rotating brass discs, found that glass beads produced the least grit embedment, whilst sand and garnet produced four times more grit embedment. Silicon carbide produced six times and quartz eight times more grit embedment than glass beads. The surface morphology produced by the glass beads was smooth round dents due to plastic deformation and very little material was removed. Silica sand and garnet produced a mixture of indents and scratches and this was due to ploughing and cutting. The highest roughness was produced by quartz and silicon carbide particles. The shape of the scratches correlated well to the particle shapes. They suggested that the morphology of the worn surface is strongly dependent on the shape of the abrasive particles.

2.7.3.2 Impingement angle.

Armada et al. [1999] attempted to quantify levels of grit embedment, and indicated that, when grit blasting steel with alumina, a reduction in blasting angle from 90° to 75° resulted in a 13% reduction in grit embedment. Arola et al. [2002b] quantified the residual grit embedment following abrasive water jet peening of Ti6Al4V using image software analysis. They observed coverage of 17.5% in selected areas and 7% total area coverage. Chen et al. [2002] quantified levels of grit embedment by comparing the number of particles embedded in selected areas on AWJ through-cut surfaces, while

comparing the effectiveness of grit embedment reduction by oscillating jet as opposed to using straight AWJ cutting techniques.

Ives and Ruff [1977] conducted research on the erosion of copper utilising an air blast laden with aluminium oxide grit and concluded that embedded grit occurs at angles as low as 20°. At an impingement angle of 90°, the grit embedment is more severe. Neilson and Gilchrist [1968] also observed a similar effect when eroding aluminium with aluminium oxide. Arola et al [2002b] also concluded that impingement angles of 90° produced the most grit embedment whilst at lower impingement angles the grit embedment was reduced. Griffiths et al. [1999] in grit blasting research, similarly found that grit blasting at 45° reduced grit embedment compared to grit blasting at 90°.

A number of workers [Hashish, 1991, Li et al. 1996b, Ramulu and Raju, 1993, Ives and Ruff, 1977, Zu et al. 1991] have reported that grit embedment consisted of particles which are fragments of the original grit; some of these papers discuss the fracture mechanism of the grit and its embedment. Hashish [1991] states that particle fracture plays a significant role in the embedding process. Moreover, Ives and Ruff [1977] proposed that particles already embedded in a surface will be impacted by later incoming particles, causing fracture and deeper embedment (Fig. 2.25). They also observed that at low impingement angles of 20° the parent metal flattens and folds around the particle in a classic ploughing removal of material. This scenario could result in the embedded grit becoming completely embedded by the parent material, below the surface of the parent material and remain undetected. The visual inspection of such a component would pass the component as being acceptable, when such a discontinuity may result in component failure.

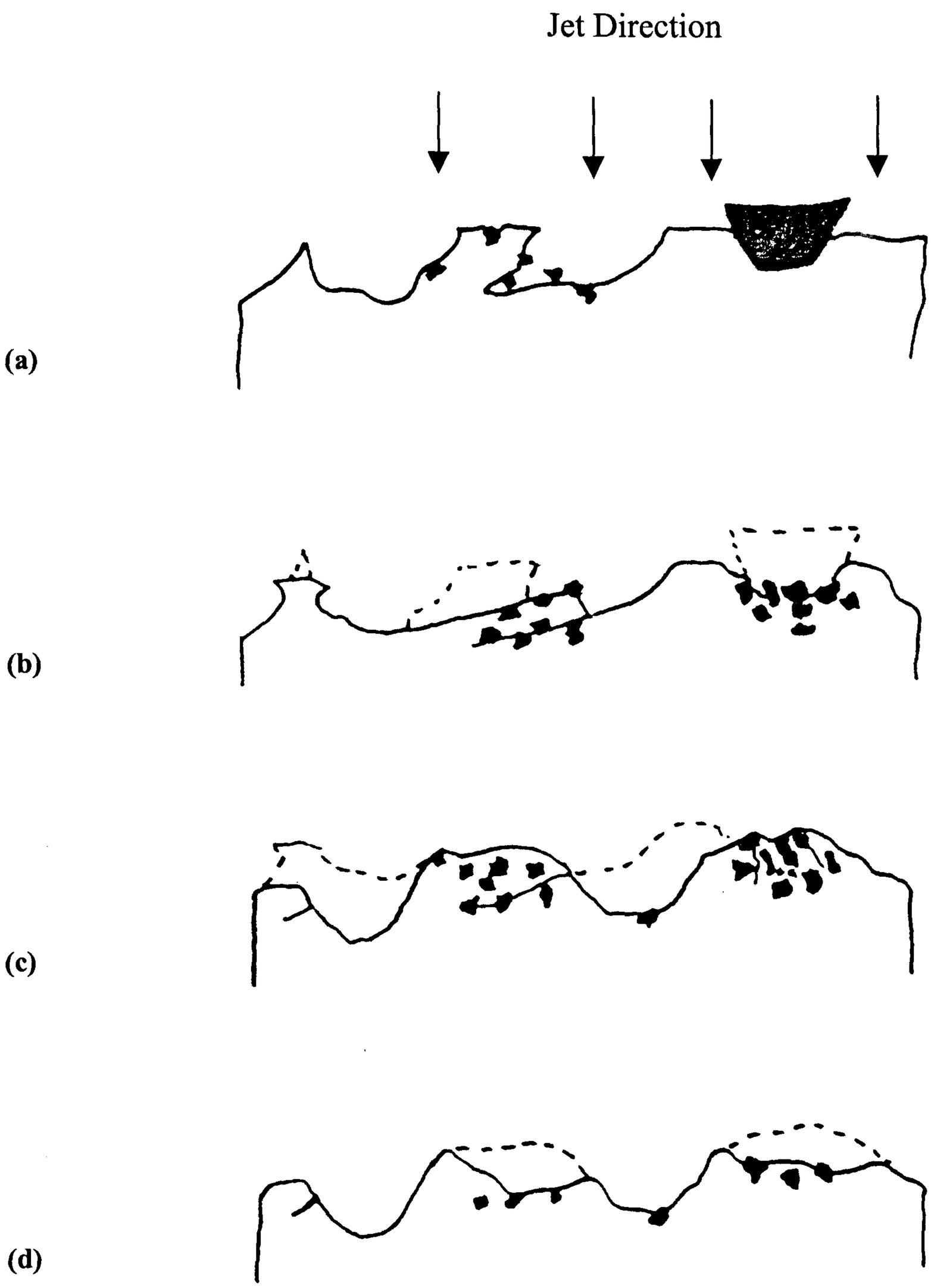

Figure 2.25 Model depicting mechanism for grit embedment. (a) Particle impacting material. (b) Impacting particle fractures. Second impacting particle folds previously fractured particle further in to the material burying grit particles beneath the surface. (c) Impacting particles of grit erode and deform surface (d) Impacting particles erode embedded particles exposing previously covered grit [Ives and Ruff, 1977].

Singh and Jain [1995] made similar observations in their research. They detected embedded grit below the material surface of the parent metal. They cut a surface with AWJ and then 'tumbled' components in a ball mill with large abrading objects, to remove surface defects such as burrs. They suggested that the post treatment method of tumbling pushed the grit further into the material and covered the embedded grit with parent metal. In studies of erosion of copper, Ives and Ruff [1977] indicated that at high impact angles (90°), extensive grit embedment occurred whilst at low impact angles the grit embedment was much less severe. Hashish [1989c] observed a similar tendency in AJW machining, although no methodology was provided to quantify the level of grit embedment.

2.7.3.3 Reduction of embedded grit.

If embedded grit has a detrimental effect on the fatigue life of abrasive water jet machined components, then depending upon the application its removal may be important.

Research conducted by Griffiths et al. [1999] suggests that using a low vibratory brushing technique does not remove any embedded grit, whilst casting replica material (a two part plastic resin) removed some grit. Such a process is not an economically viable solution for industry. However they suggest that in industry, ultrasonic techniques have successfully removed embedded grit.

Another method of removing grit is suggested by Hashish [1996c] who investigated the methodologies of abrasive water jet milling. He recommended that after milling a surface by AWJ, switching off the abrasive grit supply and traversing over the workpiece with a pure high pressure water jet can be employed to flush out and clear unwanted debris and embedded grit. However, he does not mention any settings for this process or whether the 'water peening process' that may take place induces any residual stress in the component surface. However, this technique will not remove particles of grit deeply covered with base/parent metal. However, Singh and Jain [1995] stated that once the particles were covered with base/ parent metal they were difficult to remove even after chemical milling.

The best solution would be to produce no embedded grit at all during the abrasive water jet milling process. The use of low impingement angle will reduce the risk of grit embedment but the literature suggests that the use of low impingement angle will not entirely guarantee its complete removal. Only cryogenic and ice jet machining processes

offer a possible solution of avoiding the problem of embedded grit since no grit is used [Li et al. 1996a], [Hashish, 1998b],[Chen 2002].

However, the removal of the embedded grit itself may leave voids as possible stress raisers from which fatigue cracks may initiate.

2.7.4 The effects of grit embedment and surface morphology.

Surface morphology and grit embedment affect two key areas in the aerospace industry, namely the fatigue life of a component and surface adhesion capability for the application of coatings.

2.7.4.1 Surface adhesion.

Embedded grit, if not removed from the surface of the AWJ machined material, may affect the post operational requirement of the component. For example, Leidheiser et al. [1984] conducted research into the effect of embedded grit on the delamination of epoxy paint from steel panels pre - treated with air blasted grit. Steel panels were air blasted with various grits and coated with epoxy paint and subjected to an electrolyte bath. They found that the type of grit used affected the delamination rate; alumina blasted panels yielded the lowest delamination rate whilst, those blasted with silicon carbide had a substantial rates of corrosion.

Grit embedment also affects the adhesion of alumina coatings employed as thermal barriers in the aerospace industry. Griffiths et al. [1999] investigated the adherence of plasma sprayed alumina coating on to carbon steel sheets prepared by air blasted grit at 90° and 45° followed by spray coating. They found that blasting at 45° and spraying at 90° yielded the best adhesion for the sprayed coating. They concluded that the increased adhesion was due to the improved saw tooth profile morphology and the reduction in embedded grit, arising from the employment of the low angled blasting process.

Therefore grit embedment can cause premature failure of paints and thermal barrier coatings by causing delamination through poor adhesion. It should be noted that there is a lack of published research on the delamination of coatings resulting from embedded grit induced by AJW-CDM.

2.7.4.2 Fatigue.

Abrasive water jet machining can be used for through-cutting of materials or for milling pockets in components. The effect of embedded grit is an unknown factor on the fatigue life of such items and so is a major concern for the aerospace industry where the control of fatigue is important. Fatigue failure occurs where a component is subjected to cyclic loading which results in fatigue cracks developing from an initiation point, (often called stress raisers or notches) in the form of dents, sharp scratches, grooves, sharp corners, sudden changes in section, inclusions, porosity etc that are produced on the component by manufacturing processes. The concern is that embedded grit, or the morphology and associated roughness of the water jet machining process may provide the initiation source for fatigue to occur.

Singh and Jain [1995] compared the fatigue behaviour of materials when through-cut by laser and abrasive water jet cutting. Their research indicated that whilst there was no heat affected zone, the abrasive water machined component failed before the laser machined component. Fordham et al. [1997] showed that AWJ cut components had embedded grit in the through-cut surface and the surface finish was considered to be rough. It was concluded that these two factors had shortened the fatigue life of the component.

A methodology to improve fatigue life of AJW machined components would be to induce a residual stress, from the manufacturing process itself or by shot peening or to eliminate grit embedment.

2.7.4.3 Residual stress.

A review of the literature suggests that one benefit of grit blasting, AWJ machining and pure water jet cutting is that a residual stress can be induced into the component being machined. Compressive residual stress is beneficial in improving fatigue life [Leverant et al. 1979]. However, there are two distinct methodologies aimed at replacing grit/bead or shot peening techniques for inducing compressive residual stresses. One is AWJ peening, where the abrasive water jet is applied to the surface of a component with abrasive grit entrained into the jet stream under a set of conditions with minimal erosion taking place. The other methodology is water jet peening, where a pure water jet is applied to the surface of a component under a set of conditions with minimal erosion taking place. No abrasive grit is used in water jet peening.

2.7.4.3.1 Water jet peening.

Water jet peening has been extensively researched as a possible replacement for shot peening to induce a beneficial residual stress. Tonshoff et al. [1995] has induced a residual compressive stress of 500 MPa in turned and ground surfaces of rotating bending non/notched specimens made from SAE G5115 (German specification: 16MnCr5) steel. A 31% increase in fatigue life was detected. Tonshoff observed that there was an increase in the surface roughness values. Arola et al. [2002b] also observed an increase in surface roughness particularly if the water pressure was too high. Tonshoff's research indicates that water jet peening generates a residual stress approximately 50% lower than that of steel shot peening. They utilised a constant water jet pressure and observed that the residual stress was a maximum value when the peening time duration is fifteen seconds. They also suggest that high impingement angles yield higher residual stresses. Tonshoff et al. state that a flat nozzle, described as an asymmetrical nozzle, elliptical in shape whose bore dimensions are determined by appropriate x and y dimensions yield a residual stress values approximately twice that when peening with a axisymmetrical round nozzle with a constant diameter.

Ramulu et al. [2000] also employed two different types of nozzles, but did not describe the physical characteristics of nozzles. Clearly nozzle design has an influence on generation of residual stress by water jet peening, but the reasons for this were not made clear. They suggest that an increase in water jet pressure and a decrease in stand off distance increase the magnitude of the residual stress. However, a decrease in stand off distance results in an increase in surface roughness.

Arola et al. [2002b] agree that an increase in water pressure results in an increase in residual stress (Fig. 2.26). They also noted that materials respond differently to the peening process employed; Commercially Pure Titanium responds better to water jet peening whilst Ti6Al4V alloy responds better to abrasive water jet peening.

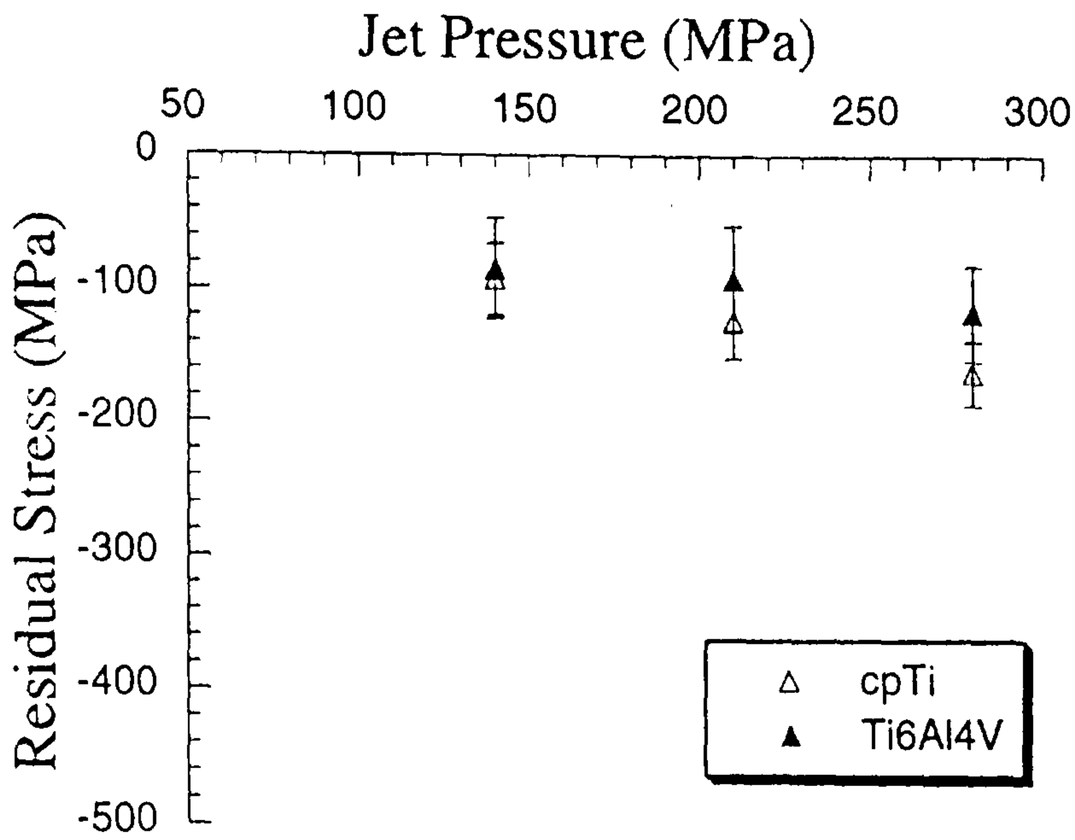

Figure 2.26 Water jet peening of commercially pure titanium and titanium alloy Ti6Al4V showing the increase in residual stress as the water pressure is increased [Arola et al. 2002b].

Conditions for inducing maximum residual stress for water peening are high water pressure, high jet impingement angle, short stand off distance, short duration time and optimised nozzle design. The material properties of the target material also affect residual stress inducement.

Tonshoff [1993] suggests that the mechanism for residual stress inducement by water peening is based on water drop impingement. High pressures are developed as a drop impinges on the material sufficient to deform the material and induce a residual stress at the point impact. Tonshoff demonstrated that machine ground specimens had higher residual stress induced by water jet peening than polished specimens that were water jet peened under the same conditions. He suggested that impact pressures are higher for ground surfaces than polished surfaces because the rough ground surface delays the radial flow of the droplet allowing more impact pressure to be transferred. A polished smoother surface finish allows the water droplet to flow away more easily, and so less of the impact pressure is transferred.

However, research conducted by Hirano et al. [1997] suggests that cavitation is responsible for the inducement of residual stress by water jet peening. Cavitation is where air bubbles implode near the surface of the material being impinged by the water jet. The implosion of the air bubble creates a pressure wave, which plastically deforms the surface of the material and induces a residual stress.

Only a few models have been derived to predict the residual stress induced by water jet peening. A model devised by Colosimo et al. [2000] uses an energy based method to predict surface roughness, erosion and residual stress. Another model for predicting residual stress for water jet peening by Daniewicz and Cummings [1999] employs a commercial Finite Element Analysis (FEA) modelling package ('ANSYS 5.2'). They suggest that residual stress is due to sub - surface deformation and that the residual stress is reduced as the erosion and surface roughness increase.

2.7.4.3.2 Abrasive water jet peening.

Arola and Ramulu [1997a, 1997b] investigated the magnitude of stress fields generated by the abrasive water jets for through-cutting and found that magnitude of the stress fields increased as the abrasive grit size increased. However, further research by Arola et al. [2002b] on abrasive water jet peening found that for the abrasive water jet peening of Ti6Al4V, a decrease in grit size resulted in an increase in the magnitude of stress fields. Therefore, conditions for inducing stress for through-cutting may be different from those required for peening where no through-cutting takes place. In contrast to pure water jet peening, they noted that increasing the water pressure reduced the magnitude of the residual stress by about 50%. This trend was also observed for commercially pure titanium (Fig. 2.27). This observation is in contrast to that for grit blasting, where Guilemany et al. [1996] suggest that an increase in blasting pressure results in an increase in the residual stress.

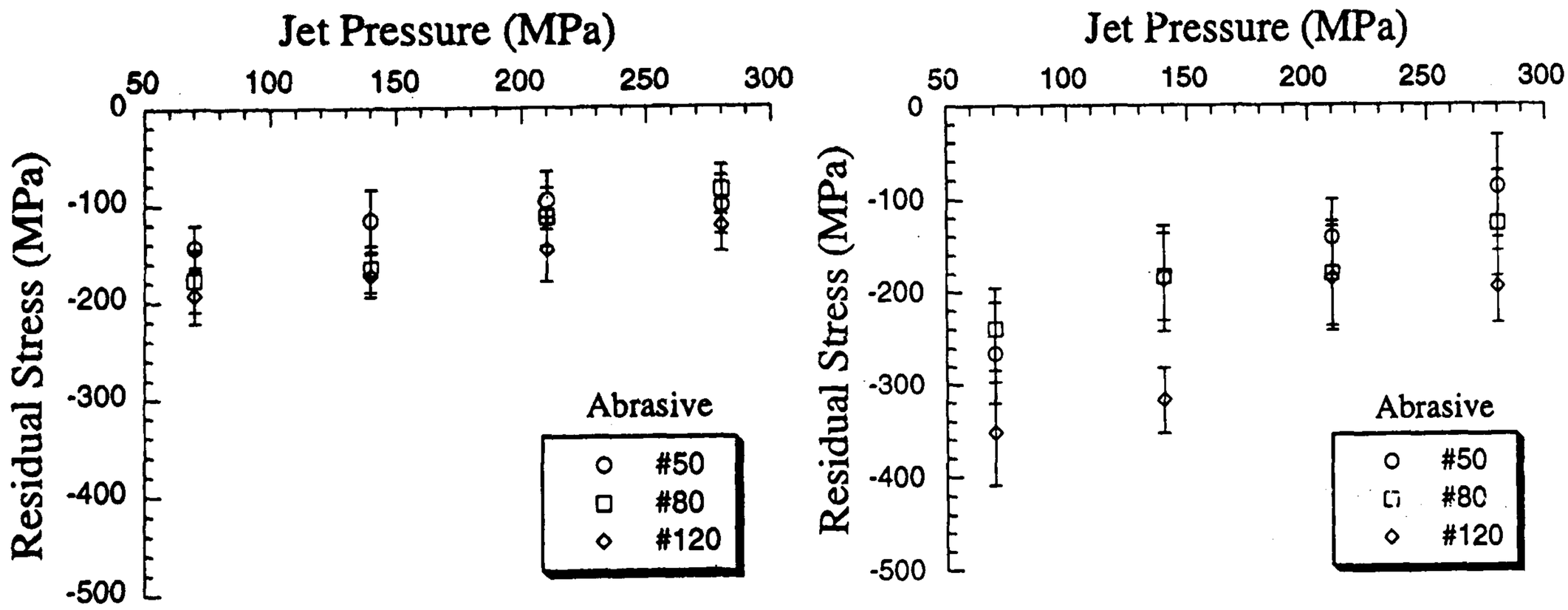

Figure 2.27 Abrasive water jet peening of (a) commercially pure titanium and (b) titanium alloy Ti6Al4V showing that residual stress increased as the water pressure and grit size decreased [Arola et al. 2002b].

Research conducted by Badwi et al. [1986] on grit blasting suggests that a decrease in grit size results in an increase in residual stress. Badwi et al. [1996] and Guilemany et al. [1996] noticed a decrease in residual stress as the impingement angle is decreased from a normal angle impingement.

For abrasive water jet peening the conditions required for inducing maximum residual stress are water pressures lower than those for pure water jet peening, a short stand off distance, a short duration time and small sized grit. The material properties of the target material also affects residual stress inducement. The mechanism for the inducement of residual stresses by abrasive water jet machining for through-cutting is due to subsurface deformation and strain hardening according to research conducted by Arola et al. [2002b]. The magnitude of residual stress occurring in AWJ machining of metals depends on the extent of metal strain hardening behaviour and abrasive attack angles at impingement [Arola and Ramulu, 1997a, 1997b]. No published research was available for models predicting the residual stress induced during abrasive water jet peening.

2.8 Chemical milling - the process to be replaced.

The chemical milling process has been used in manufacturing for many years, being employed for the manufacture of decorative patterns on 16th century suits of armour, while the application of chemical milling to general engineering began in 1927 with the chemical etching of filters and printing equipment. [Harris, 1976 pp 15]. Therefore, chemical milling can be considered a mature process, but there is little published research on the application of chemical milling of titanium alloys. However, chemical milling is a process that can be employed to machine materials that are difficult to machine conventionally. Further, the chemical reaction employed to remove material by etching is a zero or very low stress (force) process [Koster and Field, 1973] and so can be used to remove unwanted material from thin walled components without distortion or inducing unwanted stresses. However, research by Koster and Field, suggests that the chemical milling of Ti6Al4V induced a residual stress of 275 MPa at a depth of 0.01 mm, a magnitude similar to that observed in abrasive and water jet peening [Arola et al. 2002b]. Moreover, the chemical milling process has been reported by Koster and Field [1973] to have little or no effect on the fatigue life of components manufactured from titanium. Harris [1976 pp 117 - 130] also argues that chemical machining has no or little effect on the fatigue life of components manufactured from titanium while aluminium, high tensile steel and stainless steel exhibited a 15% reduction in fatigue life.

2.8.1 Basic principles.

There are normally five main steps in chemical milling: cleaning, masking, scribing, etching, demasking. The material substrate is initially cleaned to ensure mask adhesion, and reduce etch inhibition resulting from contamination by foreign matter that may act as a barrier to the etch. Masking is the application of a barrier of chemically-resistant material (neoprene rubber or resin/wax coatings) to define the areas which are to be left unetched. Masking operations are followed by a scribing operation to define accurately the etch area and to allow the removal of unwanted mask material. Etching may be in the form of an acid bath or an acid spray operation. Once the depth of material removal is achieved the etched component is removed and cleaned to prevent continued etching by the etchant, and the masking material removed.

2.8.2 *Limitations of the chemical milling process.*

2.8.2.1 Geometry.

The corner geometry of the bottom of chemically milled pockets is generally that of a radius form (Fig. 2.28b). Chamfers are possible (Fig. 2.28c) with the control of etchant formulation but sharp faced edge geometry is not possible (Fig. 2.28a). The geometric form of the corner of the chemical milled pocket is described by eq. 2.5.

Where:-

$$Etch\ factor = \frac{A}{R}$$

$$A = mask\ overlap$$

$$R = Depth\ of\ etch$$

Eq. 2.5

Fig. 2.29 shows the etching of the pocket edge geometry; this type of etching is termed 'eat back'. The eat back is also controlled by the formulation of the etchant. Etch factors of 1:1 result in a radius equal to the etch depth [Souffrant, 1972]. However, pocket edge geometry is also affected by other factors. Poor scribing to define the area to be etched can result in poor geometry. Fig. 2.30 shows how poor scribing technique results in channels and ridges where the etchant has exaggerated surface defects [Harris, 1976]. Incorrect scribing posture can result in irregular pocket sizes and radii (Fig. 2.31). Therefore, scribing requires skill and time to ensure errors so described are reduced or eliminated. Further, gas trapped in the edge geometries will prevent the presentation of etchant to the material to be etched and therefore reduce etch rate, resulting in poorly defined edge geometries (Fig.2.32). Poor control of etchant formulation and concentration also affect etch rate, which results in dishing and channelling (Fig.2.33).

Chemical milling of titanium can result in depth control of ± 0.05 mm and surface roughness values of 0.08 to 1.5 μm [Harris, 1976]. However, material removal by etchant follows the contour of the existing surface affecting the surface waviness of a component that is chemical milled.

A major limitation of chemical machining is the long manufacturing time arising from the process of cleaning, scribing and masking/demasking operations but also the etching time to mill to the required depth. The type of etchant required is dependent on the material to be etched. The time of etch is dependent on the etch formulation and the

corrosion resistance of the material. Time of etch is also depth dependent and not area dependent, therefore, both small and large areas to be milled to the same depth take the same time to etch.

The rate of etching affects the control of depth, surface roughness and time to etch. Shuford [1970] suggests that etchants for titanium with an etch rate of 18 - 38 μm min^{-1} result in poor depth control but in short etch times (etch to depth of 1mm takes 26 - 55 minutes). A decrease in etch rate to 5 - 13 μm min^{-1} (etch to depth of 1mm takes 76 - 200 minutes) enables depth control to ± 0.025 mm to be achieved. The control of depth and surface waviness is affected by the grain structure which alters the etch rate resulting in an irregular depth (Fig. 2.34). A non-uniform surface also affects etch rate and depth in a similar way.

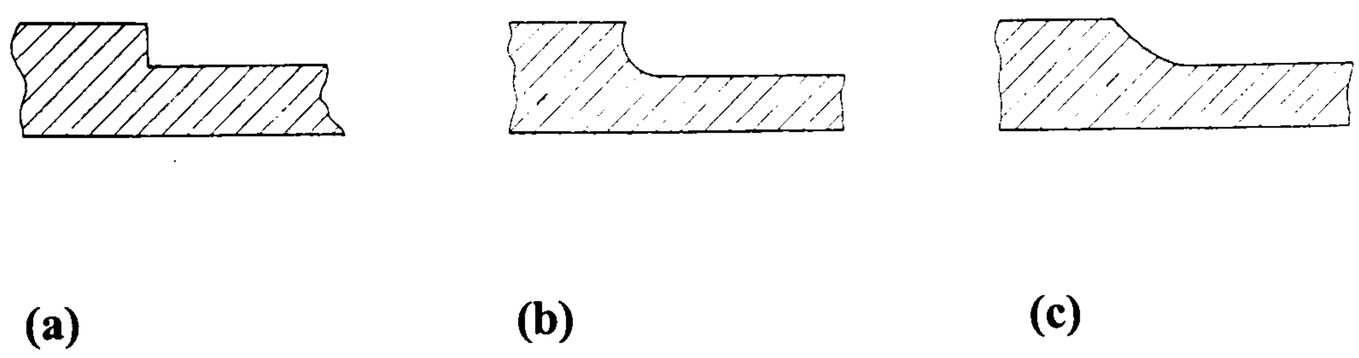

Figure 2.28 Pocket edge geometry limitations: (a) Not possible with chemical milling; (b) typical geometry; (c) possible with etchant control [Harris, 1976.]

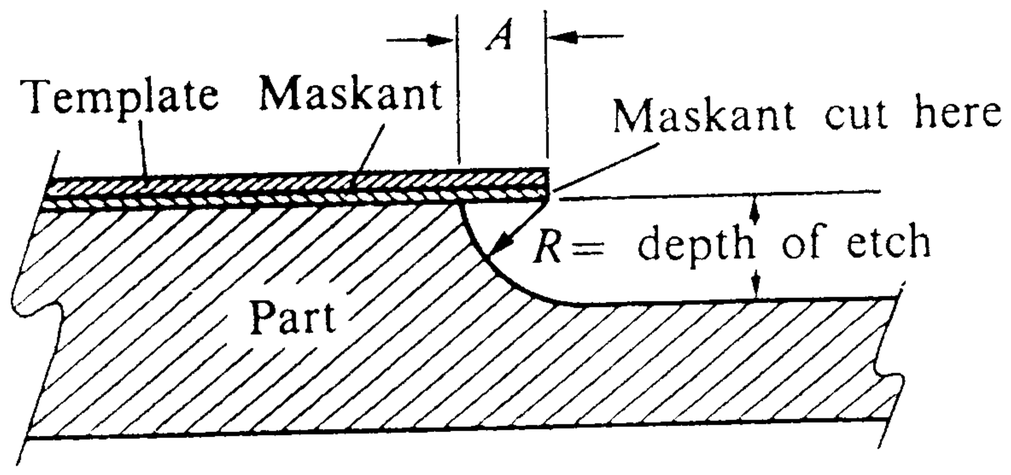

Figure 2.29 Relationship of mask geometry and etch depth [Harris, 1976, Souffrant, 1972]

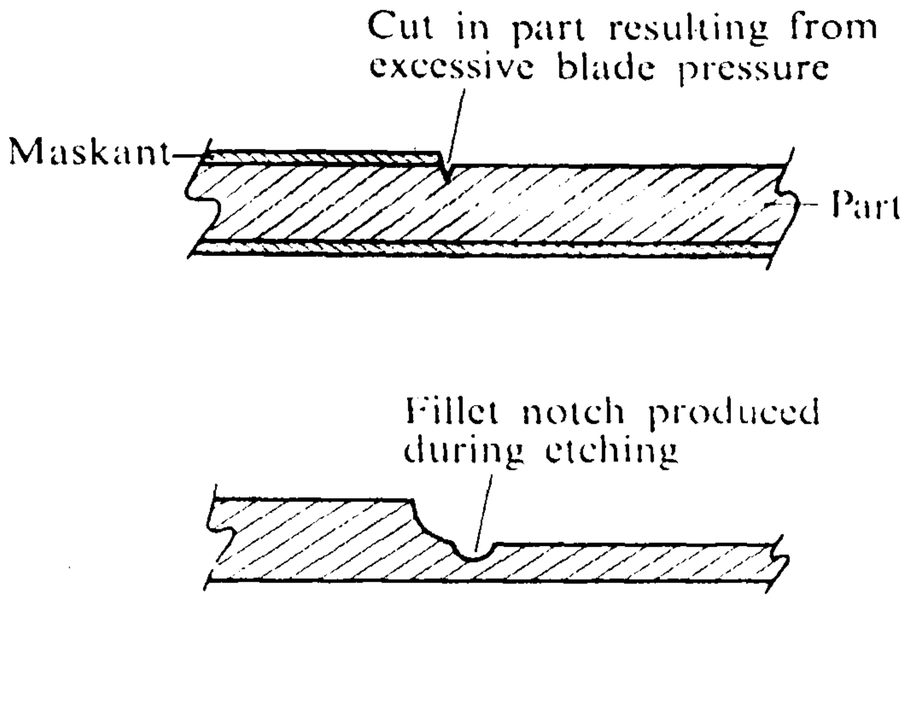

Figure 2.30 (a) Before etching; excessive scribing pressure results in surface defect. (b) After etching; defect is exaggerated [Harris, 1976].

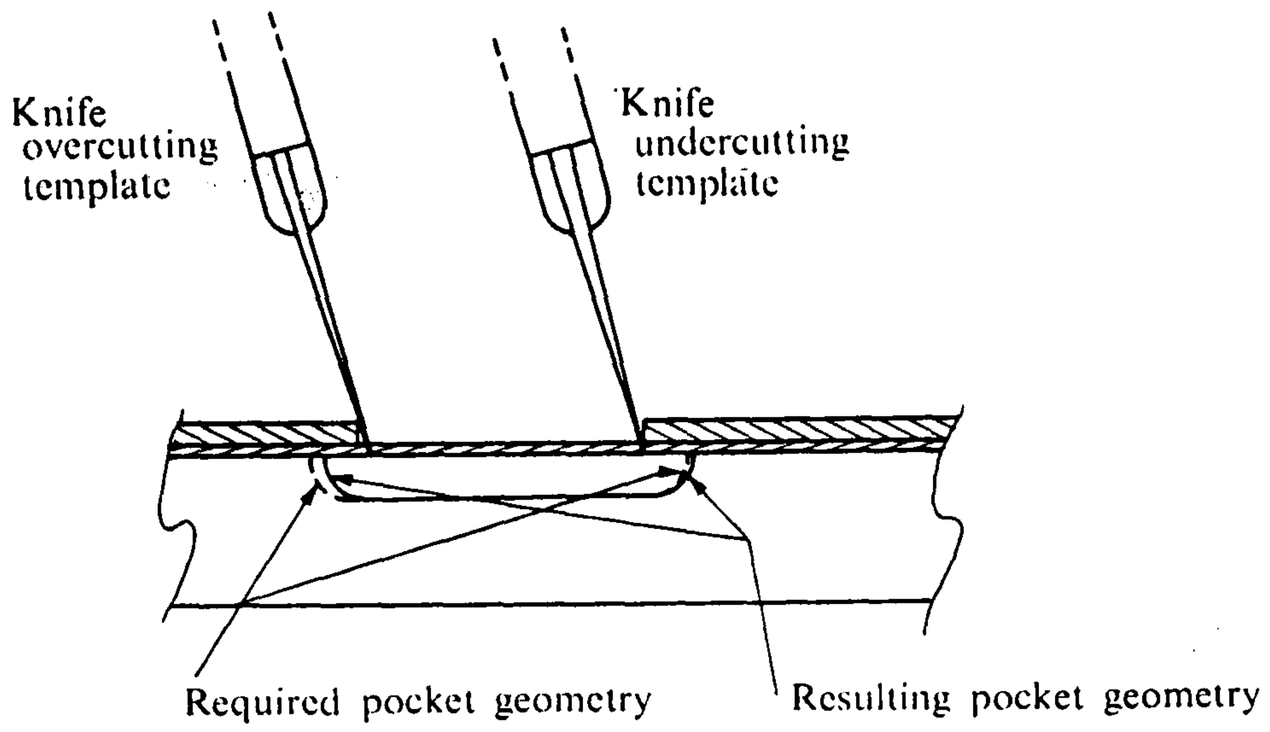

Figure 2.31 Scribing the maskant from the template. Scribing at an angle results in pocket geometry inaccuracies [Harris, 1976].

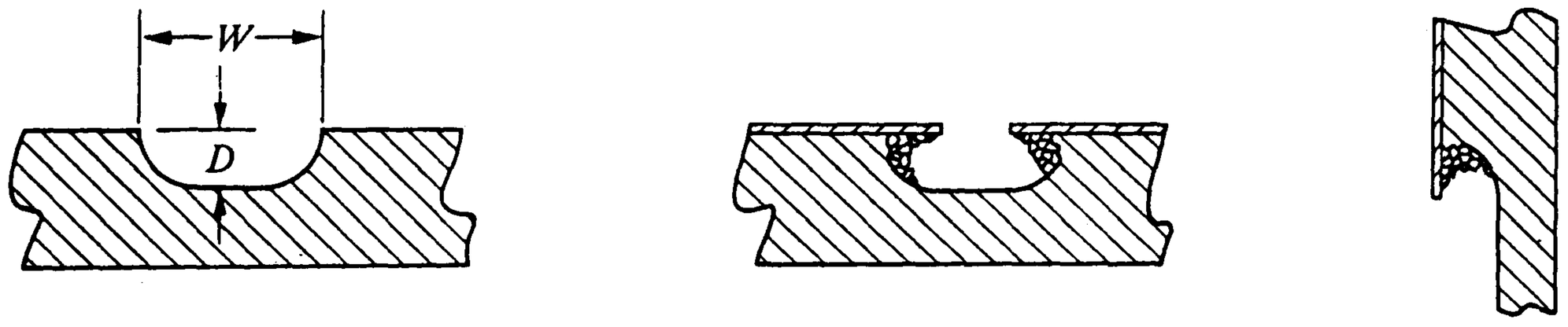

(a) **(b)** **(c)**

Figure 2.32 Examples of gas bubble entrapment. (a) Desired pocket geometry; (b) Horizontal gas entrapment; (c) Vertical gas entrapment [Harris, 1976].

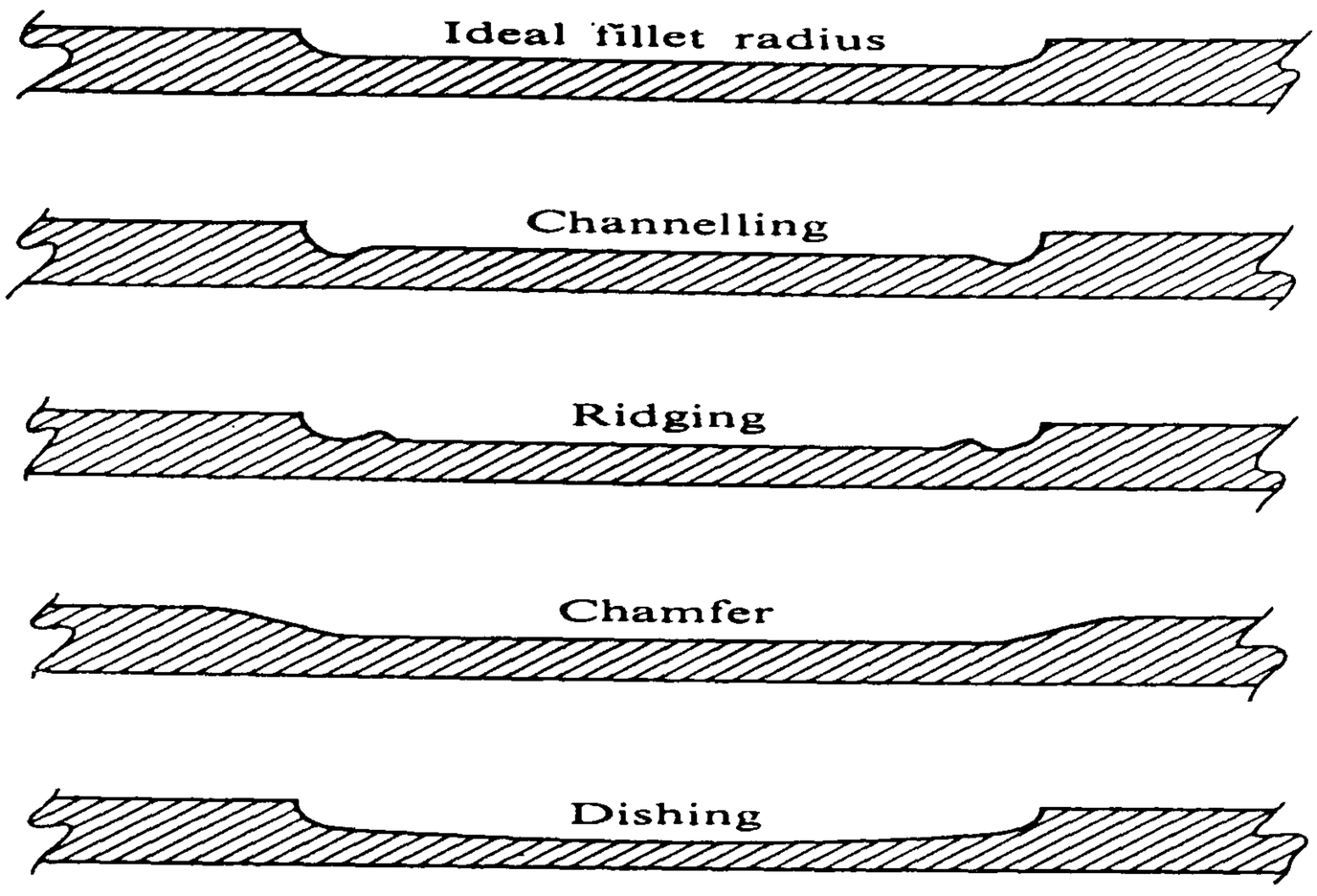

Figure 2.33 Further examples of geometry anomalies resulting from poor etching, scribing and masking techniques [Harris, 1976].

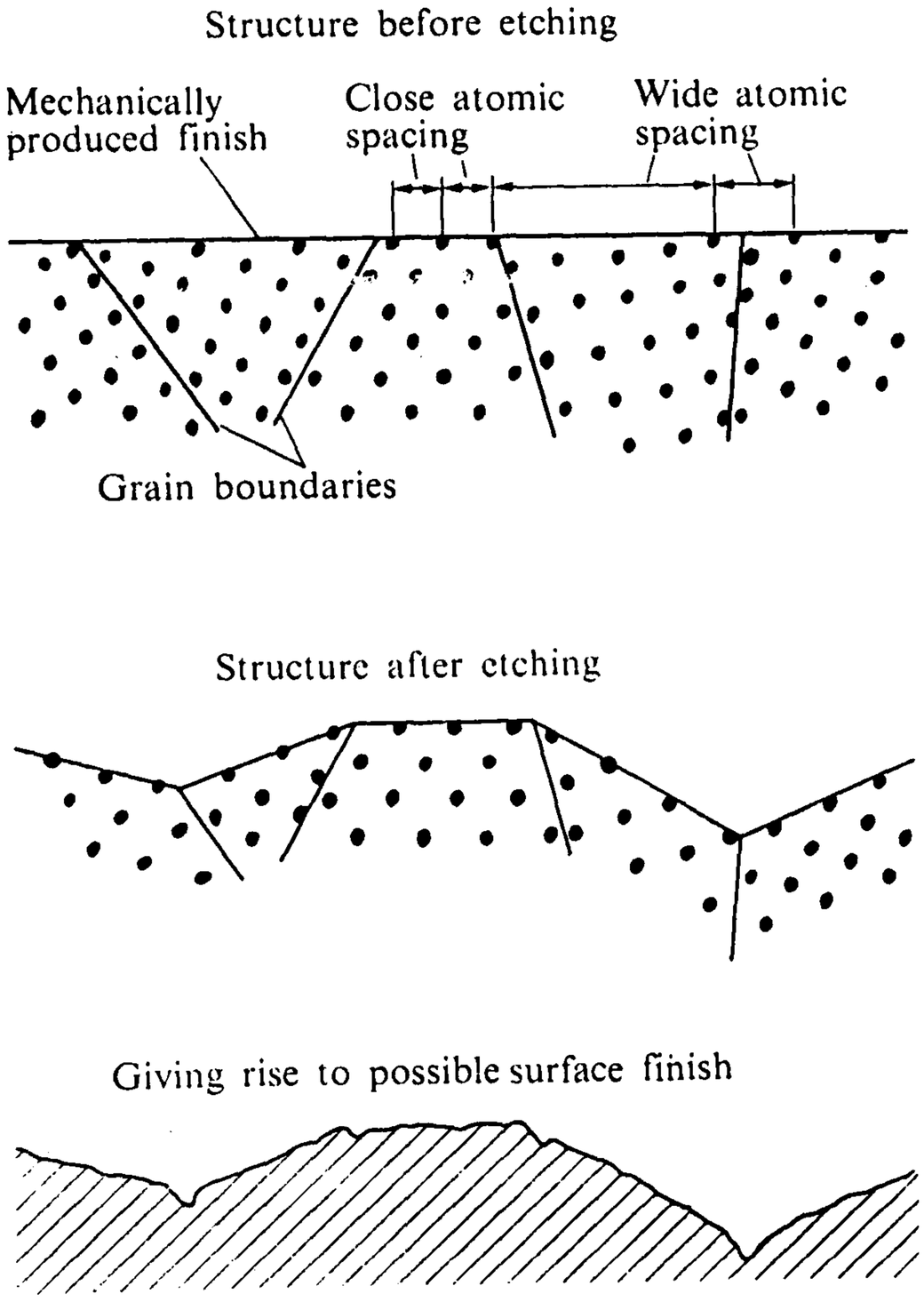

Figure 2.34 The micro effect of etching action at the surface of a material [Harris, 1976].

Another mechanical limitation of chemical machining is one of hydrogen embrittlement of materials resulting from the absorption by the material of hydrogen gas liberated from the chemical reaction between the etchant and the material to by etched. Hydrogen embrittlement results in micro-cracking and consequently mechanical failure of the component. This phenomenon can occur when processing steel and titanium and its alloys and can be reduced by heat treatment to diffuse the hydrogen to atmosphere, or by formulating the etchant to prevent the formation of hydrogen gas.

2.8.2.2 Economics.

The chemical milling of titanium is problematic since titanium has an inherent resistance to corrosion. The etchants employed to remove material chemically from the surface of titanium and its alloys are generally formulations of hydrofluoric acid with nitric or chromic acid. These etchants are corrosive, toxic and carcinogenic chemicals requiring high value capital plant, manufactured from chemically resistant high cost materials with fume and effluent disposal systems to protect operatives and the environment from the discharge of contaminants. Thus, meeting the environmental, health and safety legislation to reduce exposure to legal infringement defence costs and fines results in high overhead recovery costs and manufacturing costs when compared to conventional machining techniques [Harris, 1976]. Changing Government legislation since the 1970's, long manufacturing times and increased environmental disposal costs are becoming an increasing cost burden to the chemical milling process [Harris, 1976]. The economic and legislative pressure is obvious and more so now with the introduction of the 1990 Environmental Protection act and its following provisions on integrated pollution prevention and control (SI 1991/472; SI 2000/1973) requiring companies to expend more money on capital equipment to reduce emissions. Authorisation notice numbers: AL7316 BB8575, AP2472, AL8576, AL9050 AP6451, issued under the 1990 Environmental Protection Act for four companies employing chemical milling, show that over a period of six years from 1994 to 2000 there have been two distinct changes in the environmental disposal of effluents arising from chemical milling process. These are the introduction of changes to capital equipment (effluent) to meet reduced emissions and additional administration for monitoring and recording of discharges, both resulting in the need for companies to establish environmental management systems. Accordingly the British Standards Institute (BSI) introduced the BS EN ISO 14001 'Environmental management systems' in 1996. Such changes increase the environmental disposal costs associated with chemically milled components.

2.9 Summary of literature.

The literature review indicates that the abrasive water jet machining process is complex. There are a number of parameters which play a significant role in the production of kerf characteristics, such as w*ater jet pressure, abrasive flow rate, traverse speed, grit size*, whilst other parameters such as stand off distance, manufacturing strategy, and number of passes are less significant. The importance and optimisation of significant parameters for through-cutting is well documented. However, for pocket and linear milling the significant parameters for producing good kerf geometry are not well documented. The literature suggests that for pocket and linear milling, the traverse speed plays a significant role in the control of the flatness and depth. Also, whilst some research has examined the surface roughness and surface waviness of through-cut surfaces [Chao et al. 1992, Hashish, 1992a], there is little published research on the effect of grit size and traverse speed on the surface roughness and surface waviness of AWJ-CDM kerfs or milled pockets.

Other areas of importance which must be understood in the employment of AWJ-CDM are those of *milling strategy, jet impingement angle, lateral (jet) increment step size, number of passes*. The utilisation of cut masks must also be explored and their role in the control of the primary and secondary milled profile geometry (secondary milling caused by water jet deflection) understood.

The effect of jet impingement angle on the tendency for grit embedment, for low pressure particle laden fluid streams is well documented. However, this is not well documented for the erosion process by high pressure particle laden fluid streams as seen in abrasive water jet cutting.

Thus, this research seeks to investigate the role of a number of parameters on the material and AJW-CDM process characteristics of material removal, roughness, waviness, morphology and grit embedment.

Chapter 3

3 Experimental methodology.

3.1 Brief Description of AWJ machine.

Fig. 3.1 shows the main components of the AJW apparatus, consisting a water tank, pump and filter, hydraulic intensifier, and cutting head assembly which houses the orifice mixing chamber and nozzle. Water is pumped from a tank to a hydraulic intensifier, where low pressure water is raised to a high pressure. The water jet pressure is measured before the water is passed through an orifice to form a jet of fast moving water. The jet of water passes into a mixing chamber where abrasive grit, initially at rest, is entrained into the water by the Bernouli effect. The abrasive feed rate so formed is controlled by a mechanical device; however, due to changes in operating parameters a variation of 5% in feed rate was observed. The water and abrasive enter a nozzle to focus the jet and control the size of the water jet acting on the target material. An abrasive water jet exits the nozzle at high speed (a velocity of 525 m s^{-1} under the influence of a water pressure of 137.9 MPa [Momber and Kovacevic, 1998]). The water jet is turbulent in nature, and the velocity and distribution of the entrained grit particles will resemble the velocity profile of the water jet [Momber and Kovacevic, 1998]. The abrasive water jet erodes the target material, after which the energy of the abrasive water jet is reduced by the water mass located in the catcher tank.

3.2 Design of experiments.

The aims of the research are to investigate the areas identified in the literature review where there is little published research on abrasive water jet controlled depth milling. These areas concern the role of the process variables of nozzle traverse speed, grit size, jet impingement angle, jet increment and number of passes of the jet, on the process characteristics of material removal rate, depth of cut, surface roughness and waviness, surface morphology and the presence of embedded grit. Such work will allow the selection of the process variables to enable the manufacture of components such as the engine rib seen in Fig. 3.2 by AJW-CDM to set requirements. Also using this information as a base, the dependence of fatigue life, residual stress, and coating adhesion on the processing parameters can be established in future work.

The complexity of the process and the need to understand the interdependency of process variables on the material characteristics requires the utilisation of a parametric study, where the process variables remain set at constant values with the variable under investigation being altered accordingly.

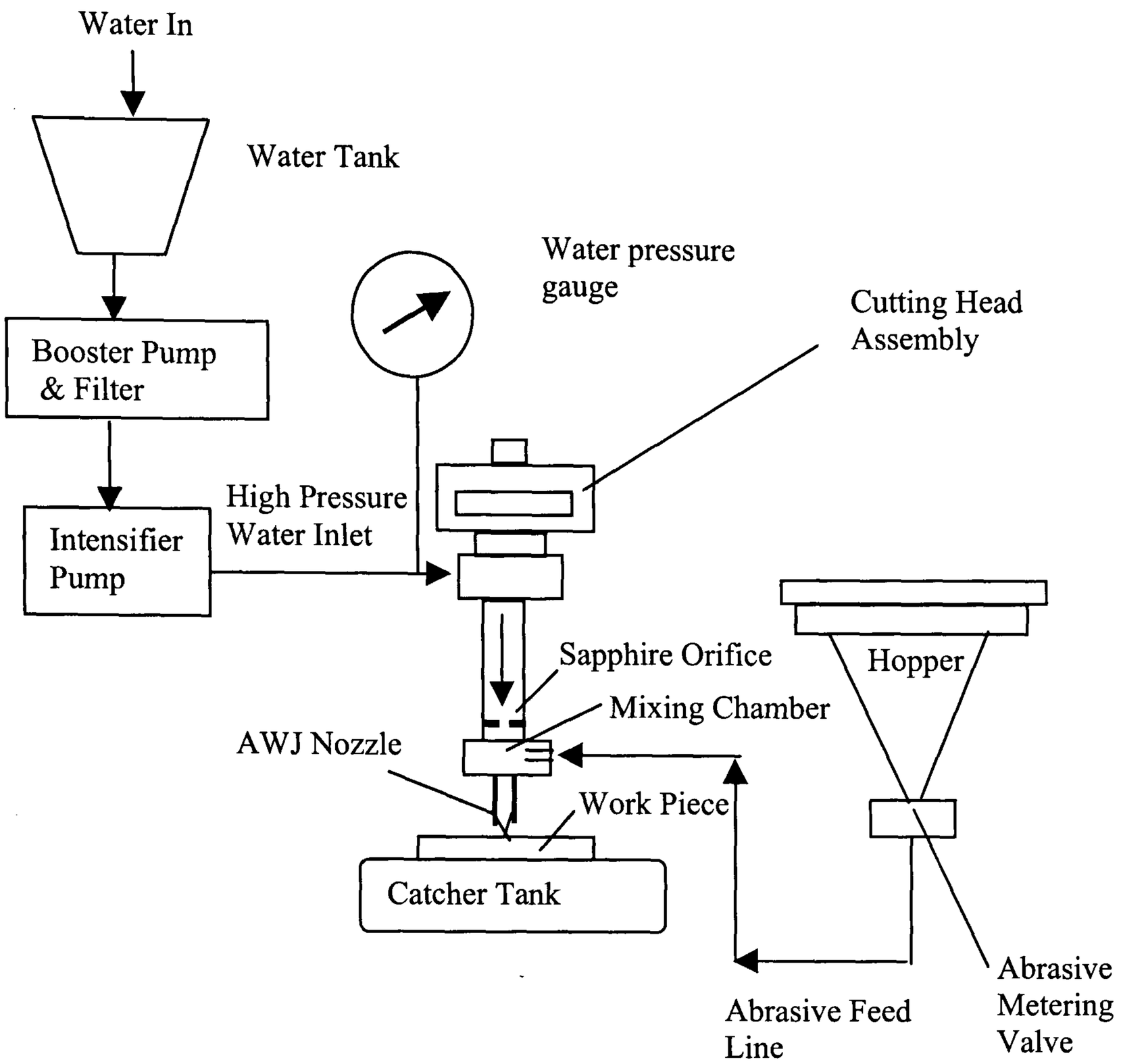

Figure 3.1 Schematic diagram of the abrasive water jet apparatus for AJW-CDM [adapted from Kovacevic et al. 1995b].

Machine:	Hydro Technologies Serial No 1000-1.
Control:	Siemens 810D.
Table Size:	2 000 mm x 1 500 mm. Y axis moves the X axis beam
Intensifier:	1000-01-AA
Intensifier power:	22 kW
Traverse speed:	0.003 m s^{-1} (200 mm min^{-1}) to 5 m s^{-1} (300 000 mm min^{-1})
Orifice Diameter:	0.25 mm.
Nozzle Diameter:	1 mm.
Nozzle Length	75 mm
Working Pressures:	34.4 MPa (5 000 psi) to 258.6 MPa (37 500 psi).
Stand off Distance:	3mm to 150 mm
Abrasive Flow Rate (AFR):	0.005 kg s^{-1}

Table 3.1 Description of the AWJ process settings.

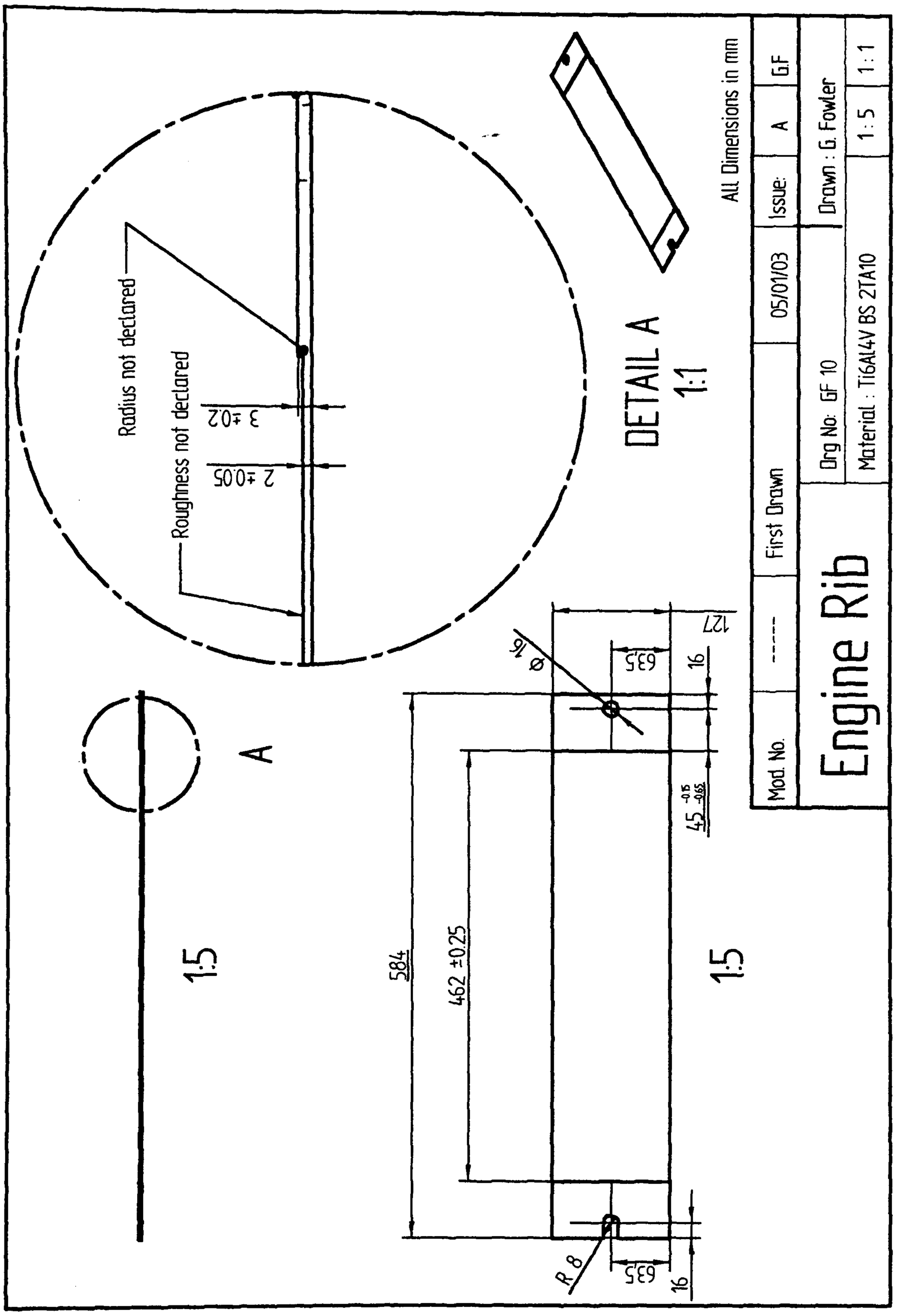

Figure 3.2 Engine rib drawing showing the currently chemical - milled feature in the Plan and Detail view A: a slot 462 mm x 127 mm wide x 1 mm deep which is to be machined by AJW-CDM.

3.3 Description of the apparatus.

The milling trials were conducted with a commercial AWJ apparatus (Hydro Technologies, North Shields, Tyne & Wear, UK). Details of the machine and process settings are given in Table 3.1 In normal working, the AWJ nozzle assembly traversed above stationary testpieces on a gantry (termed *linear milling*) (Fig. 3.3a). This was limited to traverse speeds of 0.166 m s^{-1} (10 000 mm min^{-1}). To extend the range of velocities available, a rotary table onto which the testpieces were attached was employed, above which the AWJ nozzle assembly was kept stationary (termed *rotary milling*). This allowed traverse speeds up to 5 m s^{-1} (300 000 mm min^{-1}) to be achieved. Single passes of the jet were used at low traverse speeds whereas at higher traverse speeds (where the amount of material removed per pass was low), multiple passes were employed.

Further, the AWJ machine on which the milling trials were conducted is a two axis (X and Y axis) machine and was not equipped to allow jet impingement at angles other than 90°. Therefore, apparatus was designed and manufactured to allow the water jet to be angled from 90° to 15° (Fig. 3.3b). The modified machine was used to investigate the role of impingement angle on the material removal characteristics.

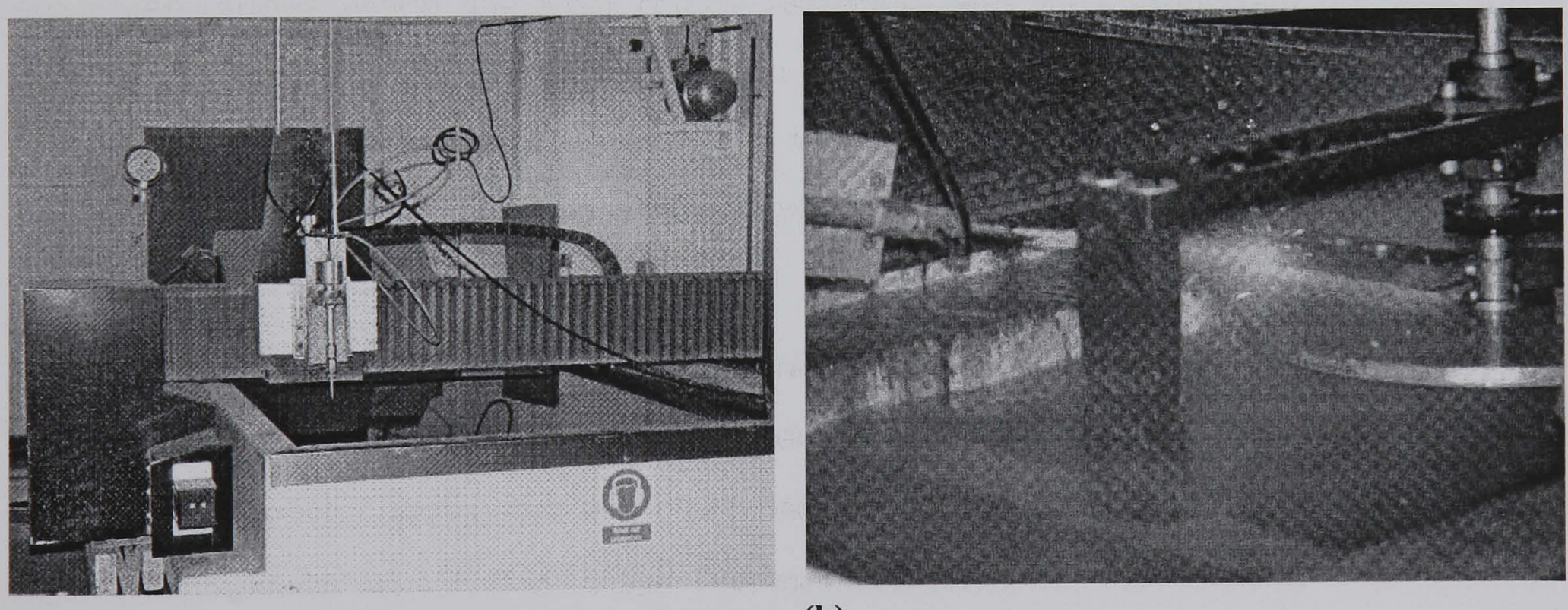

(a) (b)

Figure 3.3 Experimental water jet milling equipment for linear and rotary milling. (a) Linear milling. (b) High traverse speed water jet angled milling employing rotary table.

3.4 Materials.

The abrasive employed was Garnet of three size ranges, namely 180 μm (80#), 125 μm (120#) and 75 μm (200#). The 180 μm (80#) and 125 μm (120#) grit was supplied by GMA Garnet (Middlewich, Cheshire) and the 75 μm (200#) grit was supplied by Kuhmichel (Friarmill, Stafford).

The abrasive particle morphologies can be observed in Fig. 3.4. All the grit fractions fall into the size regime declared by the suppliers. It can be seen that the 180 μm (80#) and 100 μm (120#) grit are sub-angular in shape, (Fig. 3.4a and Fig. 3.4b) while, the smaller 75 μm (200#) grit is more angular.

The material which was the subject of the milling trials was a titanium alloy, Ti6Al4V supplied by Rolls-Royce plc. Specimens were in the form of cuboids 50 mm wide, 230 mm long and 17 mm thick. However, for the cut mask investigation, the cuboid size was reduced to 50 mm wide, 30 mm long and 17 mm thick, to allow for clamping into a fixture. The average as - received surface waviness of each sample was 5 μm and the average surface roughness was Ra 0.3 μm.

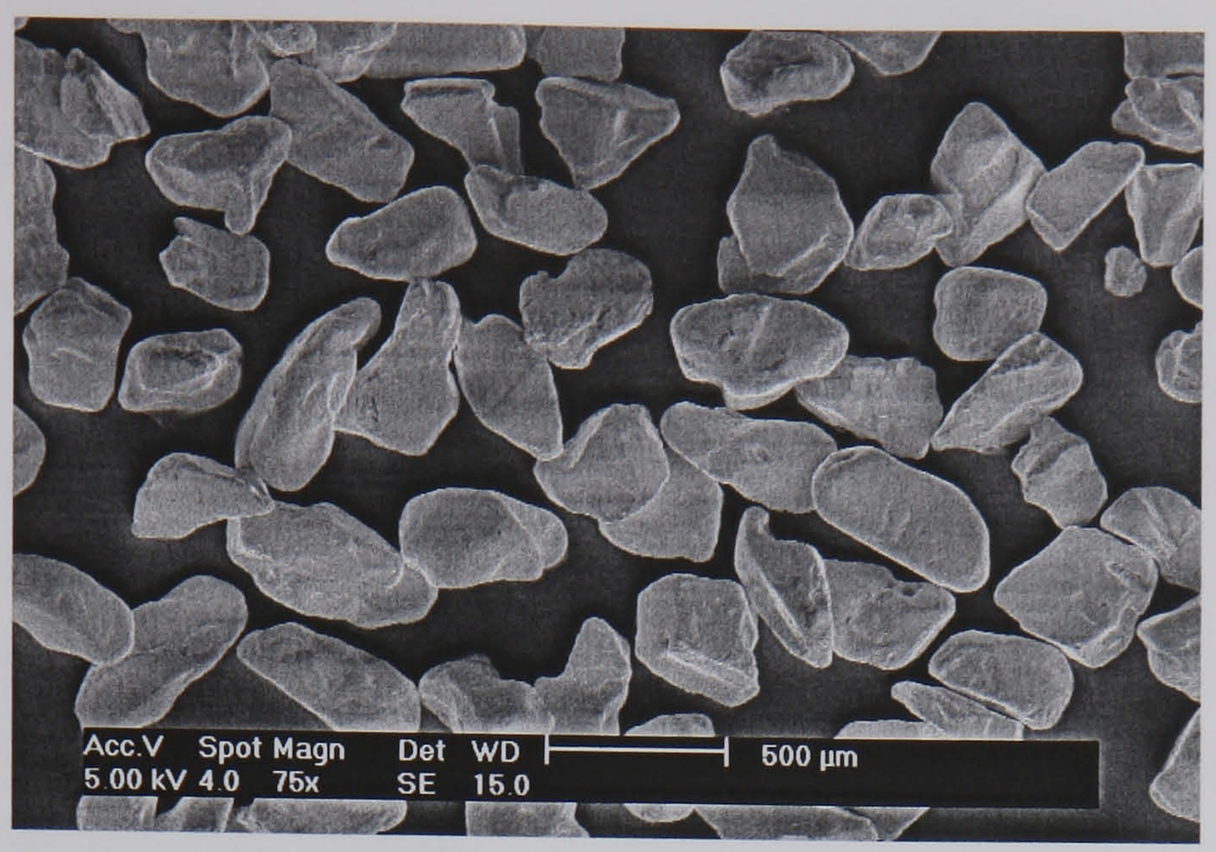

(a)

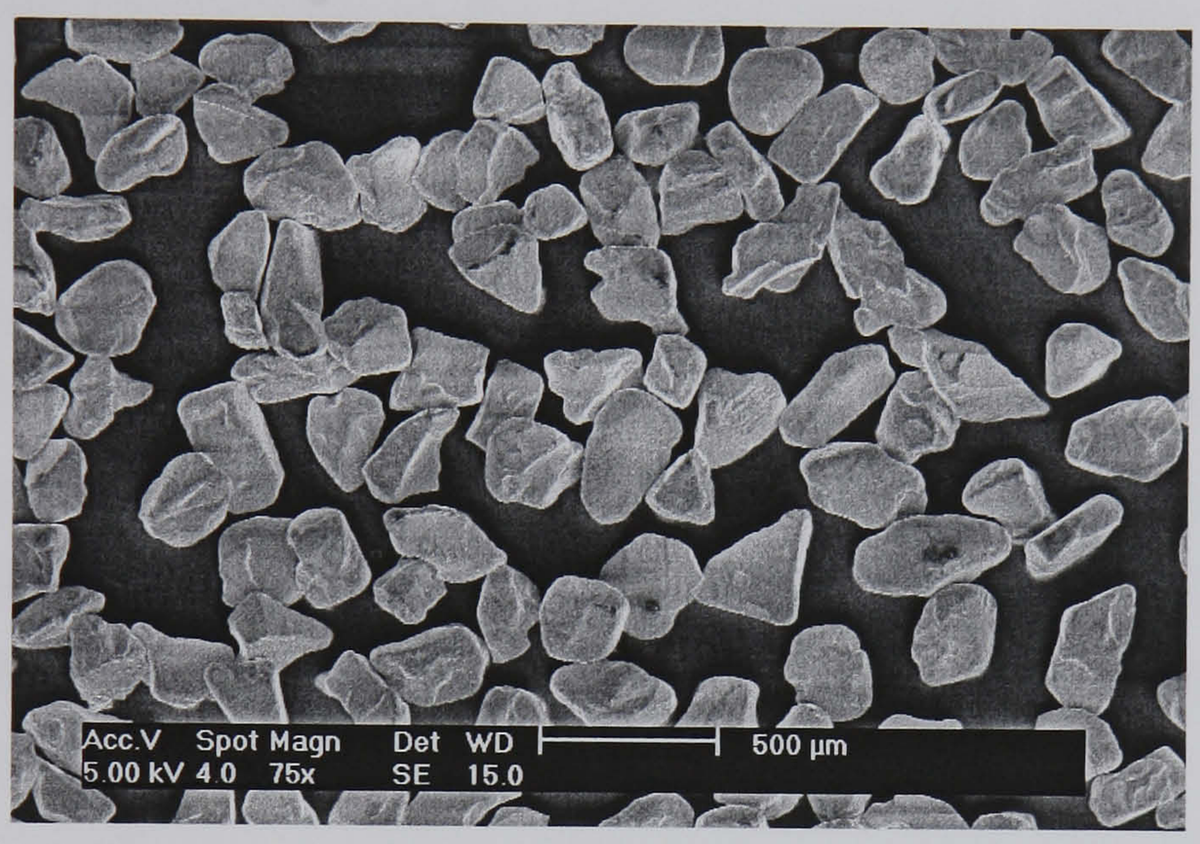

(b)

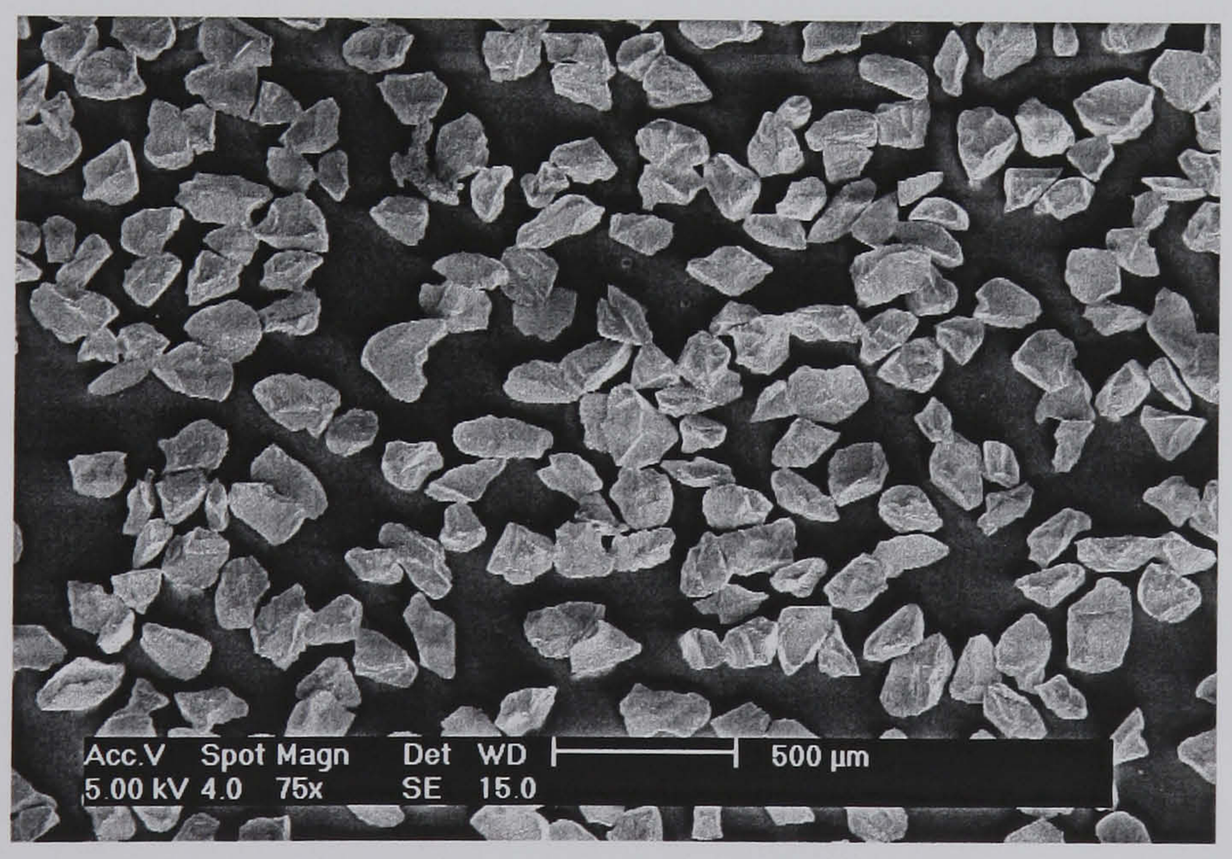

(c)

Figure 3.4 SEM micrograph illustrating the characteristic size and shape of the garnet grit; (a) 180 µm (80#) GMA garnet grit; (b) 100 µm (120#) GMA garnet grit; (c) 75 µm (200#) Kuhmichel garnet grit.

3.5 Fixed Process settings.

The abrasive flow rate, orifice (diameter 0.25 mm) and nozzle (diameter 0.25 mm, length 75 mm) were maintained at nominally constant values. The stand off distance was generally set at 3 mm, although a few trials were also conducted at 10 mm. Literature indicates that the material removal rate is relatively insensitive to stand-off distance between 2 mm and 5 mm and is maximised in this region, while stand-off distances above 5 mm result in a small decrease in the material removal rates [Hashish, 1987, Laurinat et al. 1993, Ojmertz, 1997a].

In order to ensure consistency in the collected data the cutting head was always traversed in the X - direction on the machine gantry.

The specimens were placed on the machine bed gratings and held in place using temporary fixturing. The jet was traversed across the largest face, parallel to its shortest edge in linear milling and with the radius of the table parallel to the longest face in rotary milling. Each experiment was repeated three times and the data presented are an average of the individual measurements. The actual average abrasive flow rate during each test was also measured by measurements of mass of abrasive consumed during the time of operation.

The path of the head across the specimen was as follows:

Linear Milling:

Dwell 40 mm from the edge of the specimen for 3 s; start traverse in X direction; travel in X direction for 130 mm; dwell for 3 s.

Rotary Milling:-

Dwell for 3 s, start rotary traverse and run for time t seconds to achieve required number of passes of the jet; stop the machine with no end dwell.

All water jet cutting was conducted in air, with the water bed level set level with the machine grating (i.e. below the specimen surface).

3.6 Process Variable settings.

The process variables were altered using suitable incremental changes in accordance with the area under investigation.

3.6.1 Role of milling parameters.

3.6.1.1 Jet traverse speed.

In order to investigate the role of jet traverse speed, the specimens were linear and rotary milled with single and multiple passes of the jet under fixed process conditions. The maximum and minimum traverse speeds were 5 m s^{-1} (300 000 mm min^{-1}) and 0.003 m s^{-1} (200 mm min^{-1}) respectively. The influence of the jet traverse speed was investigated as a function of the abrasive grit size and jet impingement angle.

3.6.1.2 Water jet pressure.

The effect of water jet pressure as a function of traverse speed was investigated by linear milling specimens with single passes of the jet under fixed process conditions. The maximum and minimum pressures were 258.6 MPa (37 500 psi) and 68.9 MPa (10 000 psi) and maximum and minimum traverse speeds were 0.166 m s^{-1} (10 000 mm min^{-1}) and 0.003 m s^{-1} (200 mm min^{-1}) respectively.

3.6.1.3 Stand off distance.

In order to investigate the role of stand off distance as a function of traverse speed, specimens were linear milled with single passes of the jet under fixed process conditions. Stand off distances of 3 mm and 10 mm were employed. The maximum and minimum traverse speeds were 0.166 m s^{-1} (10 000 mm min^{-1}) and 0.003 m s^{-1} (200 mm min^{-1}) respectively.

3.6.1.4 Jet step increment.

To examine the role of jet step increment to mill large areas the water jet was moved across the workpiece in a prescribed path. Jet increment is defined as the movement of the jet in the Y axis, between successive passes of the jet as a fraction of the jet width (Fig. 3.5). For instance, a ¾ jet increment involves 0.75 mm of movement of the head in

the y axis since the jet width is 1 mm. Lateral passing is defined as the traversing of the jet across the workpiece with a given jet increment. In Fig. 3.5, a milling pattern with ten lateral passes is shown. A depth pass is defined as the number of times a particular milling pattern is repeated. For a single line cut, the number of passes is simply equal to the number of passes of the jet over the workpiece. However, for a milling pattern as defined in Fig. 3.5, two depth passes (for example) would consist of two repeats of the pattern (20 passes of the jet over the workpiece in total).

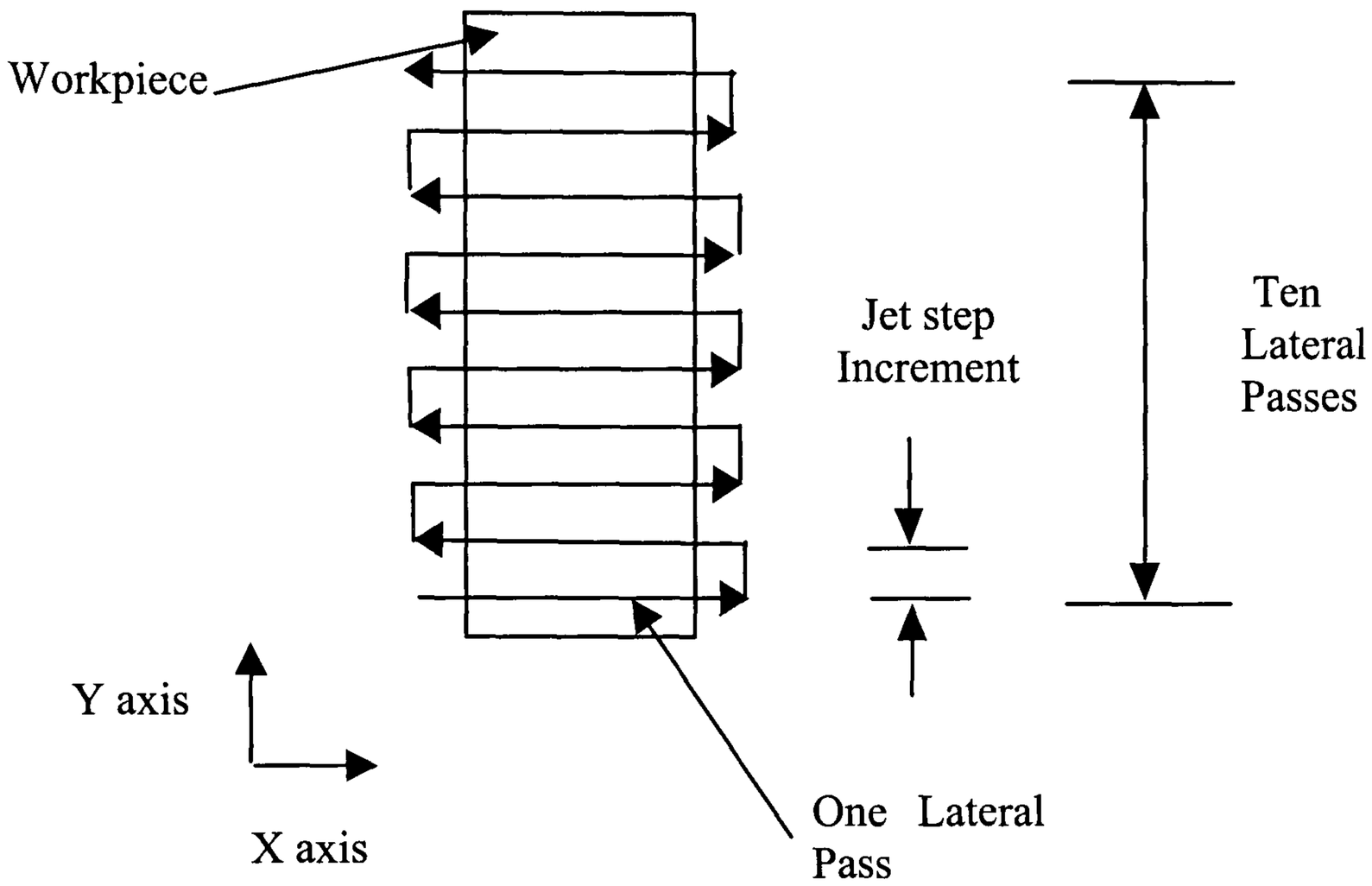

Figure 3.5 Schematic diagram showing a lateral pass pattern consisting of 10 lateral passes.

3.6.1.5 Jet impingement angle (including forward and backward milling).

The literature indicates that the jet impingement angle has an influence in AJW-CDM on surface roughness and morphology. To examine the effect of the jet impingement angle, specimens were linear and rotary milled. Four traverse speeds were investigated, namely 0.003 m s^{-1}, 0.016 m s^{-1}, 0.166 m s^{-1} and 5 m s^{-1}. The jet impingement angle (defined as the minimum angle between the jet axis and the plane of the specimen surface (Fig. 3.6)) was incremented in 15° intervals from 15° to 90°. The water jet was traversed in two directions, both parallel to the direction of the jet axis projected onto the plane of the specimen. In forward milling, the direction of the jet axis projected onto the plane of the specimen was in the same direction as the direction of movement of the jet across the specimen whereas in backward milling, the direction of the jet axis projected onto the plane of the specimen was opposite to that of the direction of movement of the

jet across the specimen. Such definitions are illustrated in Fig. 3.6. In order, to investigate the effect of multiple passes of the jet under the given milling mode (e.g. forward), the water jet was switched off, returned to its original start position before being restarted and passed over the sample again. A key interest in milling as a function of jet impingement angle is the effect of not only multiple passes of the jet over a single line but also of milling larger areas. Therefore, experiments were also conducted where the water jet was incremented by ¼ jet width to generate 10mm wide slots.

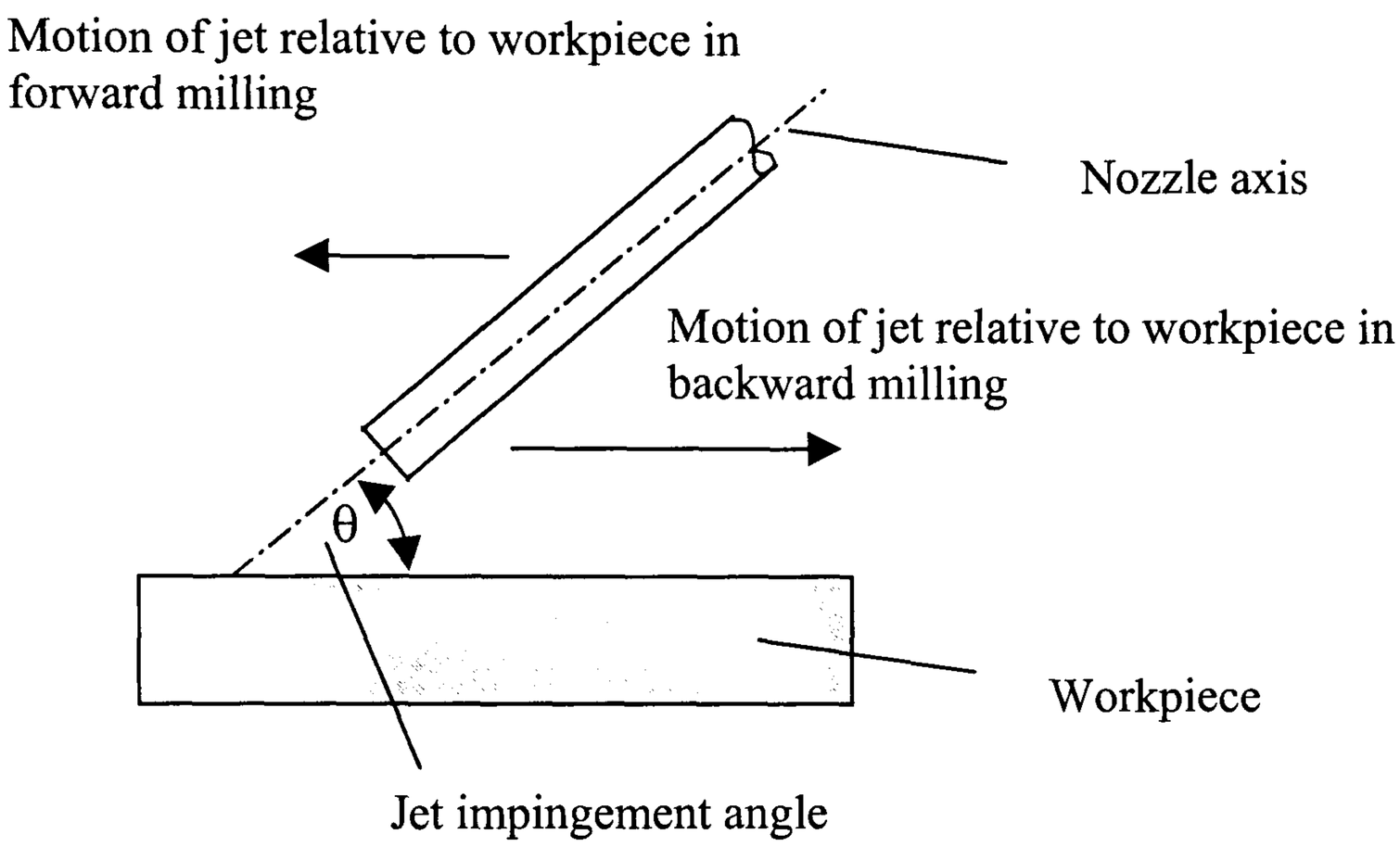

Figure 3.6 Schematic diagram illustrating relative motions in forward and backward milling operations.

3.6.1.6 Cut mask investigation.

The investigation into the employment of cut masks is of particular importance to the industrial application of AWJ milling. Fig. 3.2 shows a component of interest, currently manufactured by chemical milling where manufacture by AWJ-CDM is being investigated. Cut masks may provide a manufacturing solution for AWJ-CDM of this component. Test specimens were mounted in a fixture, with the mask clamped over the specimen with the cut hole in the mask centred over the specimen.

Parameters for milling were selected on the basis of previous findings from this work. The jet impingement angle was 90° in all experiments and the nozzle pressure was set at 137.9 MPa (20 000 psi). The traverse speed was set at 0.166 m s^{-1} (10 000 mm min^{-1}). The abrasive size employed was 180 μm (80#). The jet increment was set at ¼ of the

jet and the number of depth passes conducted was 20. The stand off distance was set at 3 mm from the top of the mask.

Metallic masks were manufactured from 2 mm rolled plate so that the mask height could be built up in increments from 2 mm to 6 mm. The masks were produced with 4 location holes to allow the mask to be clamped on to a fixture. The holes through which milling was conducted were as follows:-

- straight sided 25 mm square hole with no corner radii;
- straight sided 25 mm square hole with 6 mm corner radii;
- straight sided 25 mm round hole.

Mask material selection was based on cost, availability, machinability by conventional methods and resistance to erosion. The ductile materials of low carbon steel, stainless steel and Nimonic alloy were selected by Rolls - Royce plc. It was assumed that Ti6Al4V mask would erode in the same manner as the target material. Alumina and boron carbide are brittle materials chosen to compare with the ductile materials; although they are relatively expensive and difficult to machine, they possess hardness values much higher than garnet (the erodent) and are thus erosion resistant. Masks were manufactured from the following materials (table 3.2).

Material	**Supplier**	**Waviness (Wt) Avg.**	**Roughness (Ra) Avg.**	**Hardness (H_v)**
Low Carbon Steel BS 1409 HR2	Smiths Metal Centres Ltd, Attenborough, Nottingham	4.17 μm	0.708 μm	111 kgf mm^{-2}
Stainless Steel 304	Smiths Metal Centres Ltd, Attenborough, Nottingham	15 μm	0.345 μm.	189 kgf mm^{-2}.
Nimonic alloy PK33	Rolls-Royce, Derby	4 μm	0.32 μm	249 kgf mm^{-2}.
Ti6Al4V	Rolls-Royce, Derby	5 μm	0.3 μm.	330 kgf mm^{-2}
Alumina 4 mm thick	B P, Sunbury on Thames	15 μm	0.4 μm	1 800 kgf mm^{-2}
Boron Carbide 5mm thick	B P, Sunbury on Thames	10 μm	0.5 μm.	3 200 kgf mm^{-2}

Table 3.2 Description of the mask materials.

3.6.1.7 Water jet cutting front investigation.

In order to examine the cutting action at the water jet front a fixed set of process parameters were employed. The jet impingement angle was set at 90° in all experiments and the nozzle pressure was set at 137.9 MPa (20 000 psi). Three traverse speeds were employed namely 0.003 m s^{-1} (200 mm min^{-1}), 0.016 m s^{-1} (1 000 mm min^{-1}), and 0.166 m s^{-1} (10 000 mm min^{-1}). The abrasive sizes employed were 180 μm (80#) and 75 μm (200#). The water jet was traversed in the x direction; the water jet was traversed 30 mm along the specimen to a selected point where upon the water pressure was switched off. The water pressure and the abrasive grit flow reduce to zero very rapidly. The cutting front is thus captured in an instant of time and its morphology was preserved. The samples were sectioned appropriately (See Fig. 5.1) so that the cutting front itself could be examined to identify the material removal mechanism (See chapter 5).

3.7 Measurement and examination of process and workpiece characteristics.

3.7.1 Mass loss and cutting efficiency.

Initially, the mass of the specimens before and after each cut was established using a Sartorius Electronic balance with a resolution of 0.01g. The specimens were weighed three times in a dry state at the start of each experimental cut. After each experimental cut, the specimens were washed to remove loose abrasive, dried and re weighed again three times. However, the mass loss of samples was very small in some cases and in these cases, direct measurement of mass loss was of limited accuracy since the mass of the specimen is large compared to the small mass loss. To determine the mass loss and ascertain the material removal rate (the parameter of interest) a methodology was developed to measure the material removal rate using the alternative measurement of depth of material removed.

It was shown (see section 3.7.2) that the cross sectional area of a kerf was proportional to its depth. Using this, the volume of material removed can be estimated from the measurements of kerf depth provided that the profile is constant. Knowing the density of the material, the material removal rate (mass removed per second) can be calculated.

3.7.2 Depth of cut.

The depth of cut was measured using the following techniques. Cuts up to 0.21 mm deep were measured by traversing the probe of a Talysurf surftronic 3P across the cut, normal to the direction of the cut. The resolution of the Talysurf surftronic 3P is 0.1 μm and the probe stylus has a radius of 5 μm. Cuts deeper than 0.21 mm were measured using a Mitotoyo Dial Test Indicator with a resolution of ± 0.01 mm modified by the addition of a fine needle probe to gain access to the bottom of narrow cuts. Measurements were taken at 5 mm spacings along the track.

3.7.3 Determination of material removal rate.

The efficiency of the process is defined by the material removal rate. We may define the normalised material removal rate, E_n, as the mass of sample removed per unit mass of abrasive impinging on the sample. Thus we may write that:-

$$E_n = \frac{M\,V}{m_a\,l_{real}} \qquad \text{Eq. [3.1]}$$

where M is the sample mass loss (kg), l_{real} is the length of the cut (m), m_a is the mass flow rate of the abrasive (kg s^{-1}) and V is the relative speed of the machine head with respect to the specimen (m s^{-1}).), l_{real} is defined as follows:-

$$l_{real} = l_s \times n \qquad \text{Eq.[3.2]}$$

l_s being the length of the specimen along which the cut is made and n the number of passes of the jet over the specimen.

If m_a is the abrasive flow rate is considered to be constant, then removing m_a from equation [3.1] yields the material removal rate E_m (kg s^{-1}) which can be defined as

$$E_m = \frac{M\,V}{l_{real}}$$

Eq.[3.3]

The material removal rate E_d (kg s^{-1}) can also be defined in terms of the geometry of the material removed, which eliminates the need to know directly the mass loss (the mass loss is derived from the volume loss).

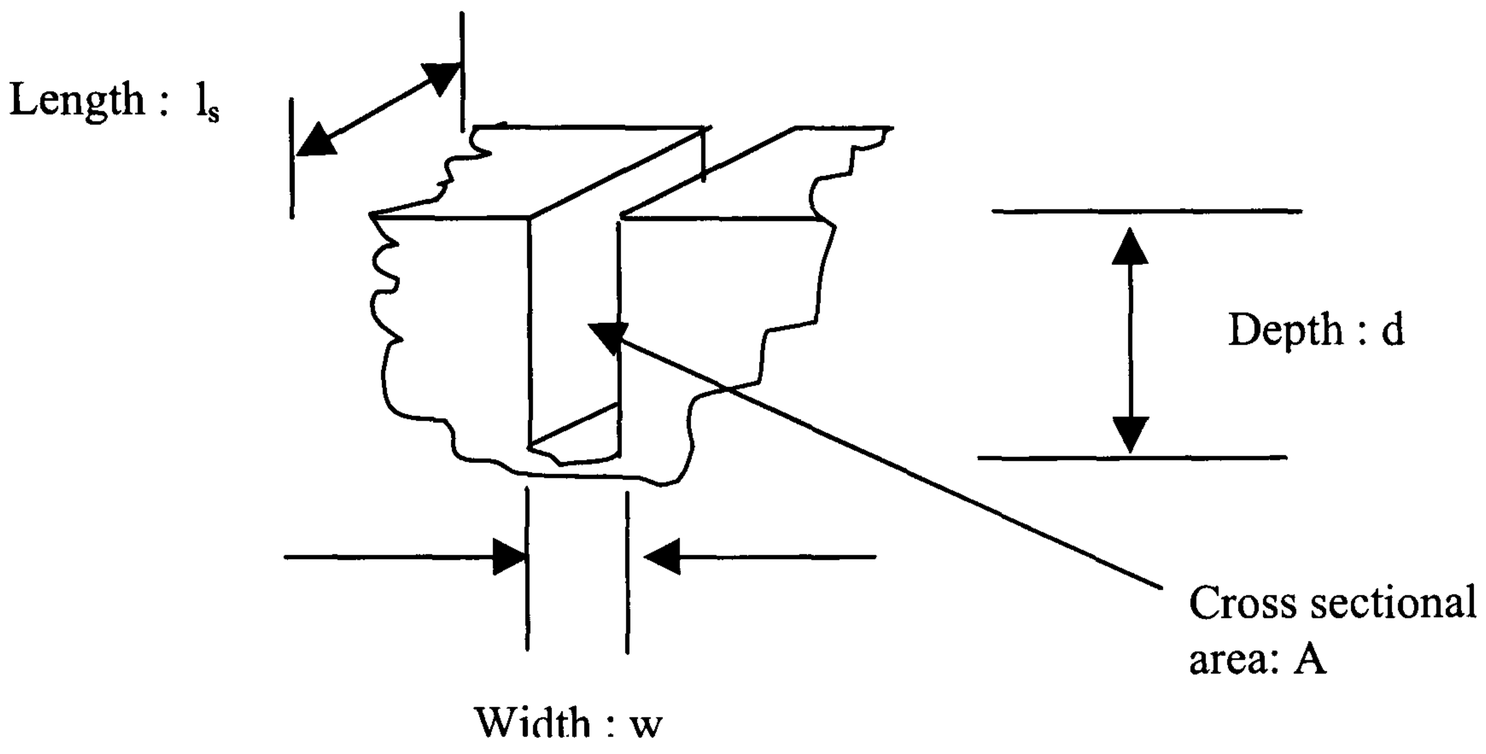

Figure 3.7 Diagram of abrasive water jet slot cut one jet width wide, across the width of a specimen using multiple passes of the jet.

The volume of material removed, *v*, is given by:

$$v = A\,l_s$$

Eq.[3.4]

And thus the mass loss, *M*, is given by:

$$M = A\,l_s\,\rho$$

Eq.[3.5]

Where ρ is the density of the material being cut.

Substituting equation [3.5] in to equation [3.3] yields E_d which is the material removal rate per pass of the water jet, defined as a function of area as follows:-

$$E_d = \frac{\rho A V}{n}$$

Eq.[3.6]

To examine the relationship between the cross-section area *A*, and the depth of cut *d*, the depth and area of a number of single line cuts, linear and rotary milled with single and multiple passes of the jet using large and small grit were examined. The depth and profile of cuts with shallow depths of 0.21 mm were captured accurately with a profilometer; the profile data can be manipulated using appropriate software such as 'Origin' to accurately derive the cross sectional area. However, where the depth was deeper than 0.21 mm, it could only be measured using a Dial test indicator with an extension probe. However, these deeper cuts allow the mass loss to be measured more accurately and in such cases the average cross sectional area can be derived from the mass loss measurements.

The cross sectional area (measured directly by profilometer or derived from measurement of the mass loss) was plotted against the depth of the single line cuts to ascertain whether area is a simple function of depth. The data shown in Fig. 3.8 indicate that the area is proportional to the depth over a wide range of depths, and thus the simple measurement of depth can be used to determine the cross sectional area indirectly and therefore the material removal rate.

Thus from Fig. 3.8 **if the depth, *d*, is measured in mm** then:

$$A = 0.8d$$

Eq.[3.7]

The material removal rate E_d can be given by Eq 3.8:

$$E_d = \frac{0.8\rho\, dV}{n} \quad \{\text{kg s}^{-1}\}$$

Eq.[3.8]

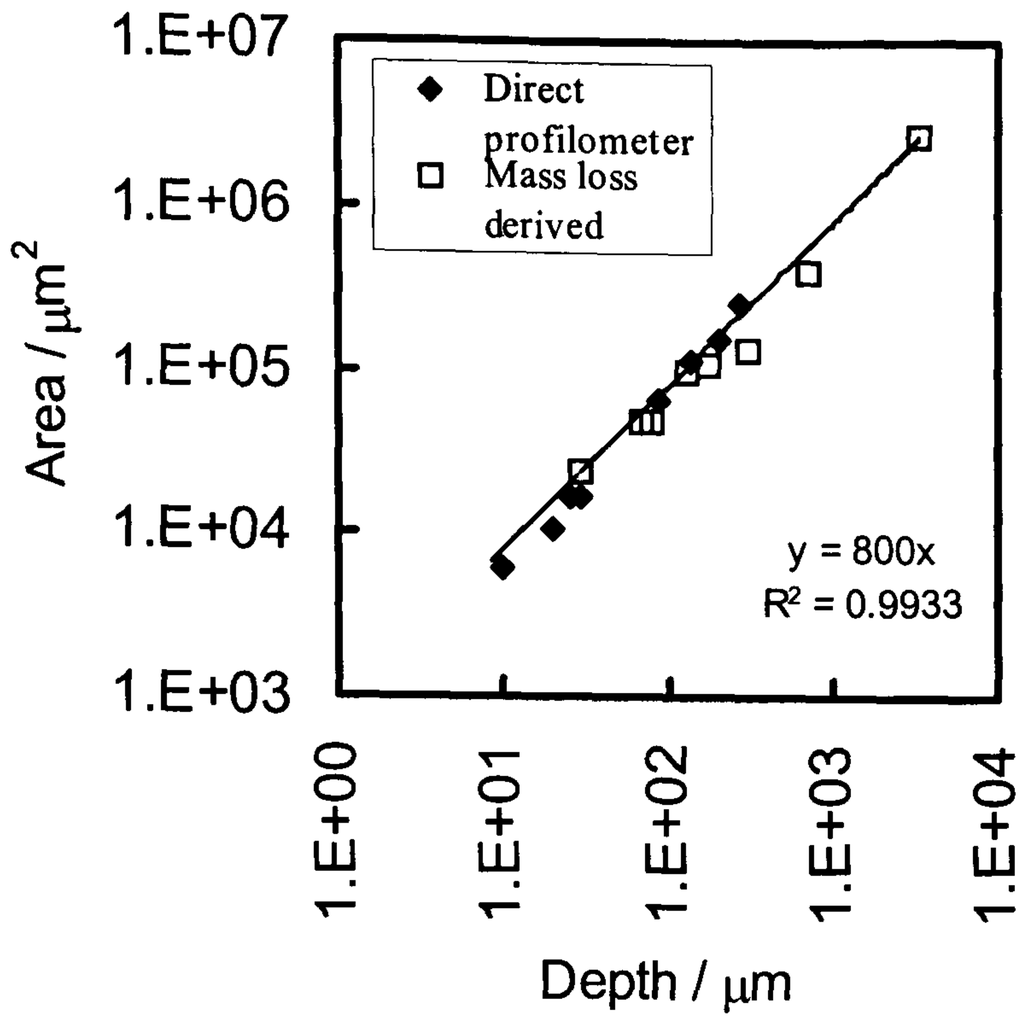

Figure 3.8 Area of single cut tracks vs depth for a wide range of milling conditions. Areas measured both directly with the profilometer and indirectly from mass loss measurements. Note: log scale. Regression line refers to both data sets.

In cases where a slot had been milled by lateral passing, the cross-sectional area *A* was defined as:

$$A = wd \qquad \text{Eq.[3.9]}$$

In this case the slot width, *w*, was given by:

$$w = w_j + [w_j j_i \times (n_{lat} - 1)] \qquad \text{Eq.[3.10]}$$

where w_j is the jet width and j_i is the jet increment and n_{lat} is the number of lateral passes in the milling pattern.

3.7.4 Surface roughness and waviness.

There are a number of techniques employed to measure surface roughness. The method employed to measure the surface roughness during this investigation was Ra (the Arithmetric Mean of the departures of the profile from the mean line, throughout a prescribed sampling length). It is the most widely employed international parameter for a measure of roughness. [Rank Taylor Hobson, 1985a, 1985b, 1994]. Further, a survey of the literature indicates that the majority of the published research has employed Ra as the measure of roughness.

The surface roughness was measured using a Talysurf Surftronic 3P profilometer. Measurements were made over a distance of 8 mm with a cut-off length of 0.8 mm and processed with a Gaussian filter. During measurements, the stylus was centred in the AWJ machined track and traversed along the centreline of the track. A standard Taylor and Hobson 02 stylus with a tip radius of 5 μm was employed.

The profile of the bottom of the kerf, as discussed earlier, is undulating following milling at low jet traverse speeds but the undulation is reduced as the traverse speed increases. This undulation is called surface waviness. It can be measured using a Talysurf surftronic 3P (Fig. 3.9).

The surface waviness *Wt* (i.e. total height of the undulation over the sampling length) is the sum of the height of the highest peak height (top of undulation) and the deepest valley depth (bottom of undulation) within the sampling length (Fig. 3.9) [Rank Taylor Hobson, 1985a, 1985b, 1994]. The measure of surface waviness, *Wt*, was selected so that results obtained via the profilometer could be compared to results measured with a Dial Test Indicator. Measurements over the same sampling distance provide a suitable methodology for comparing waviness results.

Fig. 3.9 illustrates a typical output from the surface measuring equipment. The surface roughness and waviness values have not been normalised.

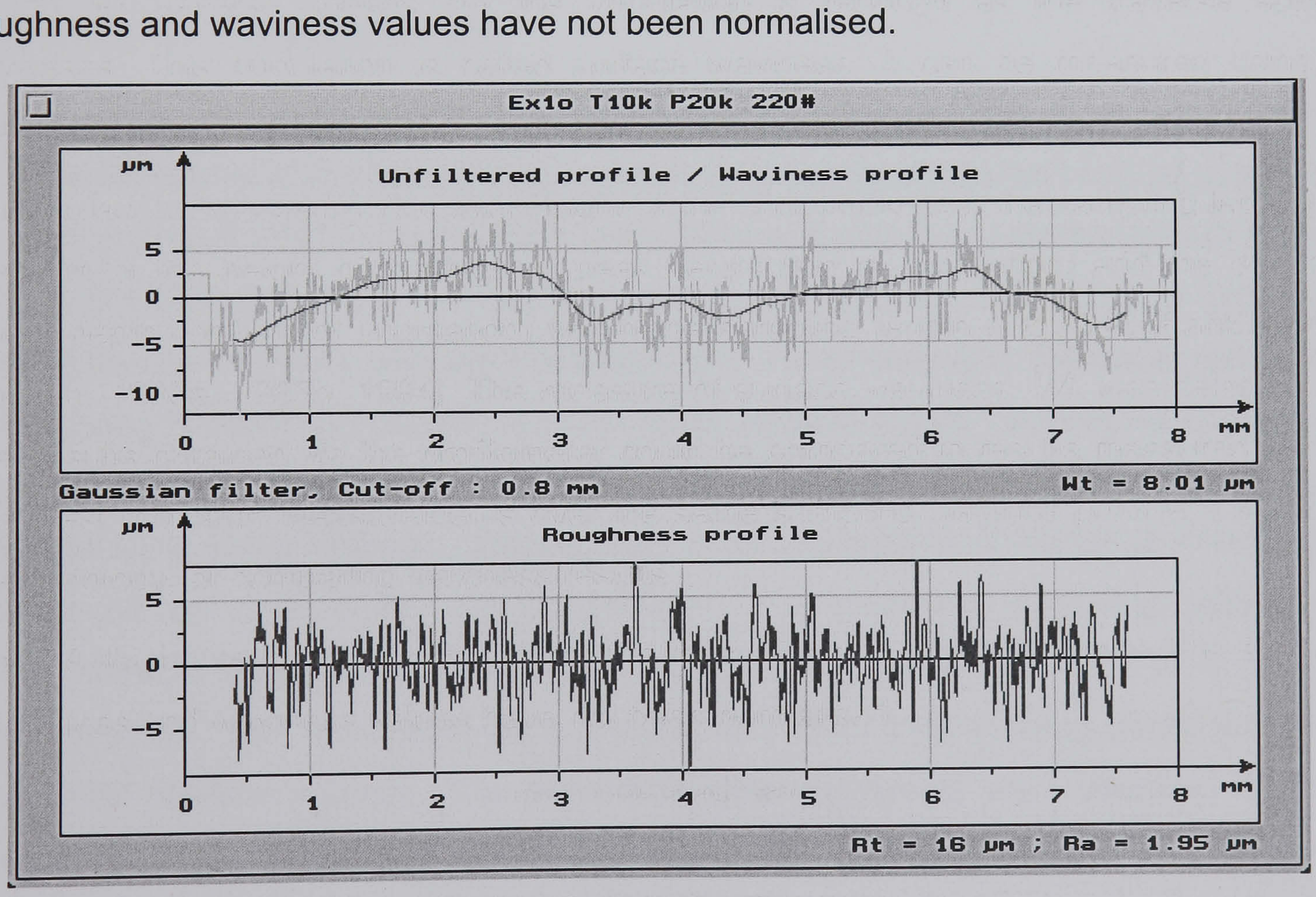

Figure 3.9 Typical output from surftronic 3P measuring equipment showing surface roughness and surface waviness values.

3.7.5 Grit embedment and surface morphology.

The morphology of the surface of the testpiece material following AWJ milling was examined by scanning electron microscopy (SEM) at 15 kV in secondary electron mode using a Philips XL30 with a LaB_6 filament, while grit embedment was examined in back scatter electron mode (BSE).

Assessment of the level of embedded grit has been conducted by a few researchers. Chen et al. [2002] counted the number of particles of grit embedded per unit area, while Griffiths et al. [1999] and Arola et al. [2001] assessed the percentage area of embedded grit as a proportion of the total area under consideration.

The level of grit embedment in this research was assessed using SCION image analysis software (SCION IMAGE BETA 4.02 for windows, free shareware software available from scioncorp.com) on SEM BSE images to detect the ratio of the number of dark pixels, representing the grit and light pixels representing the Ti6Al4V. However, since no established methodology for assessing grit embedment was available the accuracy of the methodology also needed to be established. Iron location mapping by SEM EDX analysis of the same area was performed to assess the accuracy of grit levels being analysed by the SCION technique on BSE images. Iron mapping was employed since it was an element unique to the grit.

A major concern following AJW-CDM is the presence of sub-surface grit where grit has been buried beneath the parent metal surface by a variety of mechanisms as suggested by Ives and Ruff [1977]. Therefore in order to investigate the presence of sub-surface grit, AJW-CDM tracks were sectioned using a process that induces no further garnet grit embedment or removes existing embedded grit. To achieve this, the track was plated with a layer of cobalt to prevent the subsequent removal of grit. To plate the specimens, they were first degreased for 30 minutes in an alkaline (pH13) Alcan deruster solution, followed by a basic cathodic cleaning etch in an electrolyte of NaOH at 4 volts and current density of 20 A dm^{-2} for 120 seconds. The specimens were then plated in a cobalt chloride electrolyte at a potential of 4 volts and current density of 50 A dm^{-2} for 3600 seconds. The specimens were washed and dried before being sectioned using wire EDM erosion process. The specimens after sectioning were mounted in SEM compound and polished with decreasing sized silicon carbide papers finishing with a diamond lap.

3.8 Experimental errors.

3.8.1 Abrasive feed pipe wear.

Increasing wear of the abrasive feed pipe internal diameter and pinholes in the abrasive feed pipe, has the potential to reduce the vacuum generated by the Bernoulli effect; a reduced vacuum reduces the abrasive flow rate resulting in a reduced depth of cut. In order to minimise these effects, the vacuum was measured using a vacuum gauge and maintained by pipe replacement at a constant value of 27± 1 mm of mercury, at a machine operating pressure of 258.6 MPa (37 500 psi).

3.8.2 Abrasive feed rate.

The abrasive feed rate is controlled by a mechanical device and so for deliberate bulk changes (e.g. increase in water jet pressure) to the Bernouli effect that result in an increased abrasive flow rate can be accommodated can be easily controlled to 5 g s^{-1}. However, due to small changes in operating parameters a variation of 5% in the abrasive feed rate was observed.

3.8.3 Orifice and nozzle wear.

Orifice and nozzle wear due to machine operation result in changes in the characteristics of the abrasive waterjet. Therefore, to minimise these effects, both the orifice and nozzle were changed following 50 hours of running, in accordance with the manufacturer's guidelines [Hydro Technologies, 1998]. Inspection of the orifice and nozzle following removal indicated that wear was negligible in this period.

3.8.4 Water pressure.

Water pressure affects the particle velocity, and thus the material removal. The water pressure gauge is calibrated and the variation in water pressure is ± 3.4 MPa, (500 Psi). The affect of water pressure was minimised by conducting maintenance checks and replacing the intensifier, water pump seals following 500 hours of running in accordance with the manufacturer's guidelines [Hydro Technologies, 1998]. Inspection of the intensifier, water pump seals following removal indicated that wear was negligible in this period

3.8.5 Repeatability.

The repeatability of the process is the ability of the process to maintain the outputs of material removal rate, roughness and waviness at consistent values for the same set of cutting conditions. It is of concern since the experimental results will be employed to establish the process characteristics. To assess the repeatability of the process, ten experiments were conducted with the same parameter conditions and the process characteristics of material removal rate, waviness and roughness values were measured. It was found that the process characteristics of material removal rate, waviness and roughness experienced a variation of ± 5% about an average value.

It should be noted that the abrasive grit is supplied as a mesh size, e.g. 80#. The particles of grit fall into a range of sizes that follow a Gaussian distribution with an average particle size. Therefore, variations in the repeatability of the process characteristics may also be due to the effect of small changes in particle size and distribution, particularly where particle size has a functional effect on a process characteristic [Momber and Kovacevic, 1998].

Chapter 4

4 Process Characterisation in AWJ milling.

The AJW-CDM process is less mature than that of through-cutting with little published research on the process characteristics of, material removal rate, surface roughness and waviness, grit embedment and surface morphology. Before the chemical milling process can be successfully replaced by an AJW-CDM process, the effect of the process variables of water jet pressure, jet traverse speed, grit size, jet step increment, jet impingement angle and number of the passes of the jet that determine the characteristics of material removal rate, surface roughness and waviness, grit embedment and surface morphology need to be established. This chapter seeks to identify the effect of the process variables on the process and work piece characteristics.

4.1 Role of jet traverse speed and grit size on process characteristics.

4.1.1 Results.

Fig. 4.1 shows the effect of traverse speed on material removal rate for the two grit sizes examined. It can be seen that material removal rate (E_d) for both grit sizes is high at the lowest traverse speed examined and decreases rapidly with increasing traverse speed. The material removal rate at the higher traverse speeds is lower for the smaller grit, being approximately 18×10^{-6} kg s^{-1} with the larger 180 μm (80#) grit, and approximately 10×10^{-6} kg s^{-1} with the smaller 75 μm (200#) grit.

Fig. 4.2 shows SEM micrographs of the surface morphology of the bottom of two tracks milled with 180 μm (80#) abrasive grit, one with a traverse speed of 0.0166 m s^{-1} (1 000 mm min^{-1}) (Fig. 4.2a) and the other with a traverse speed of 0.166 m s^{-1} (10 000 mm min^{-1}). The former track exhibits clear directionality indicative of abrasive impinging at a low angle whilst the latter has a cratered appearance with little evidence of directionality, indicative of predominantly normal impact of the particles.

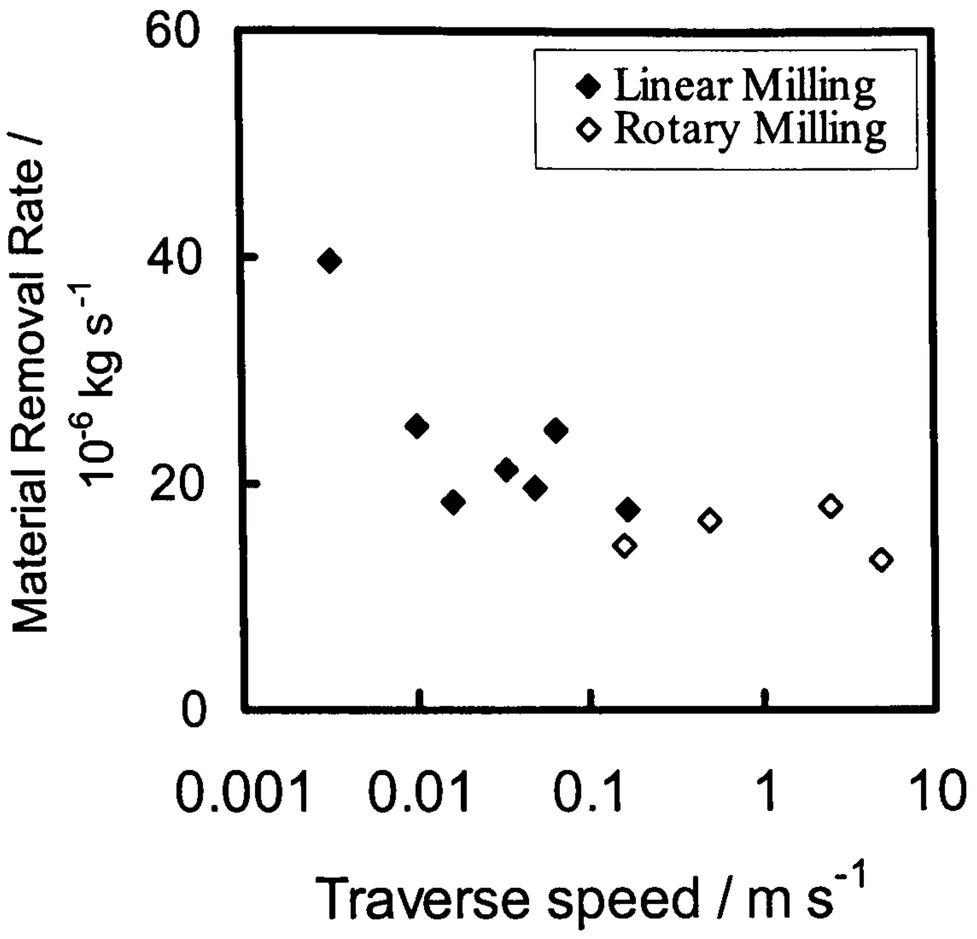

(a)

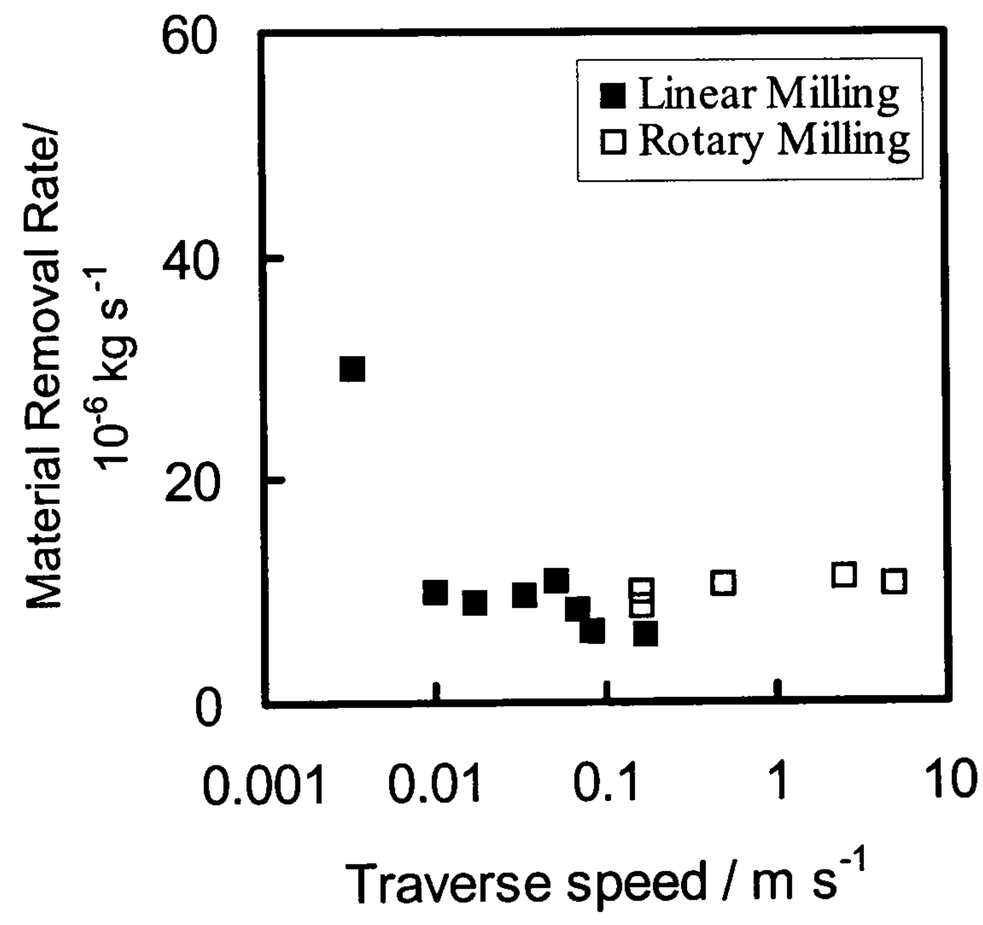

(b)

Figure 4.1 Material removal rate during AWJ-CDM of Ti6Al4V as a function of jet traverse speed: Water jet pressure 137.9 MPa (20 000 psi), Stand off distance 3mm, jet impingement angle 90° (a) with 180 μm (80#) garnet grit; (b) with 75 μm (200#) garnet grit.

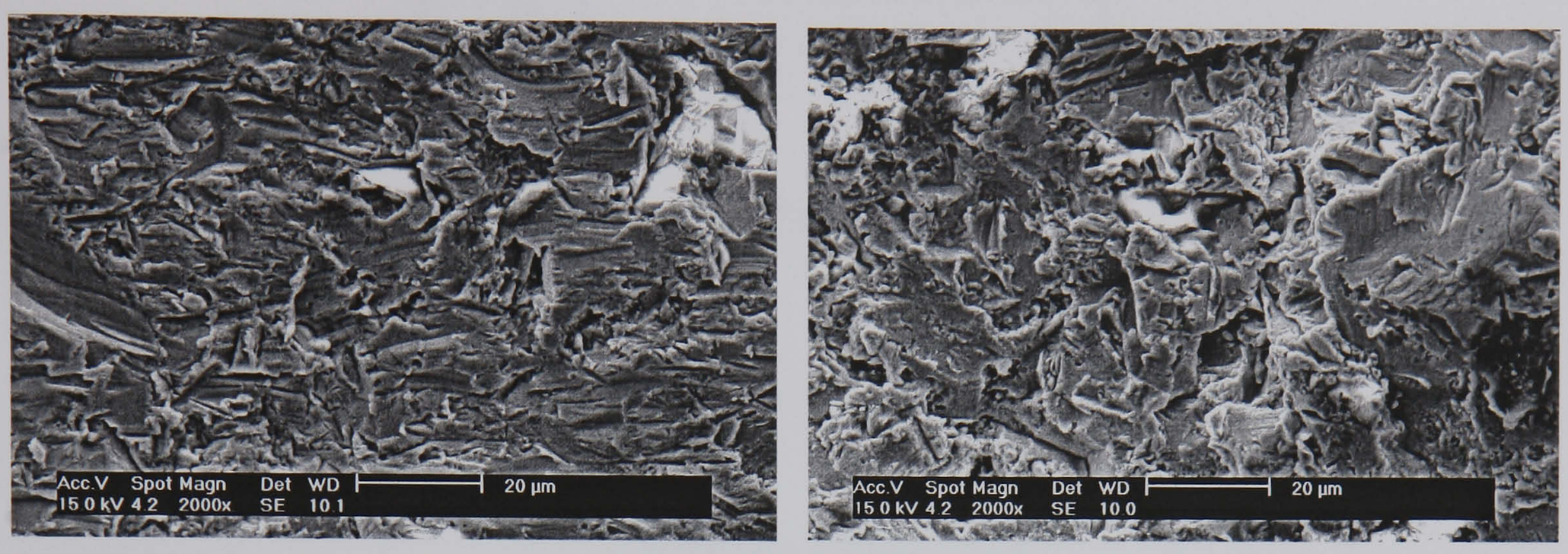

(a) (b)

Figure 4.2 SEM micrographs of the bottom of AWJ-CDM tracks in Ti6Al4V using 180 µm (80#) garnet grit following a single pass of the jet: Water jet pressure 137.9 MPa (20 000 psi), Stand off distance 3mm, jet impingement angle 90° (a) with a jet traverse speed of 0.0166 m s^{-1} (1 000 mm min^{-1}); (b) with a jet traverse speed of 0.166 m s^{-1} (10 000 mm min^{-1}).

Fig. 4.3 shows the effect of jet-workpiece traverse speed on the surface waviness of the kerf for the two grit sizes examined. Higher waviness values were observed for lower traverse speeds but these have not been included on the graph for clarity. It can be seen that an increase in traverse speed results in a reduction in surface waviness for both grit sizes, with the reduction being most significant for the larger grit (Fig. 4.3a). It can also be seen that at all traverse speeds, the surface waviness is greater with the larger grit than with the smaller grit.

Although the effect of traverse speed on surface waviness has been examined in Fig. 4.3, one must also note that the depths of the kerfs have also changed accordingly, and as such it is unclear whether the surface waviness is dependent on the traverse speed or the depth of the kerf. In light of this, a small number of kerfs were cut to approximately the same depth at a range of traverse speeds (using an appropriate number of passes of the jet to achieve the desired depth). Fig. 4.4 shows the surface waviness as a function of traverse speed for the two grit sizes; for the 180 µm (80#) grit, the depth of cut was 3.47 ± 0.1 mm and for the 75 µm (200#) grit, the depth of cut was 2.5 ± 0.1 mm. Fig. 4.5 shows four slots from Fig. 4.4, two milled with the 180 µm (80#) grit and two milled with the 75 µm (200#) grit. The dependence of surface waviness on traverse speed can clearly be seen, with a significant reduction in waviness at the higher traverse speed.

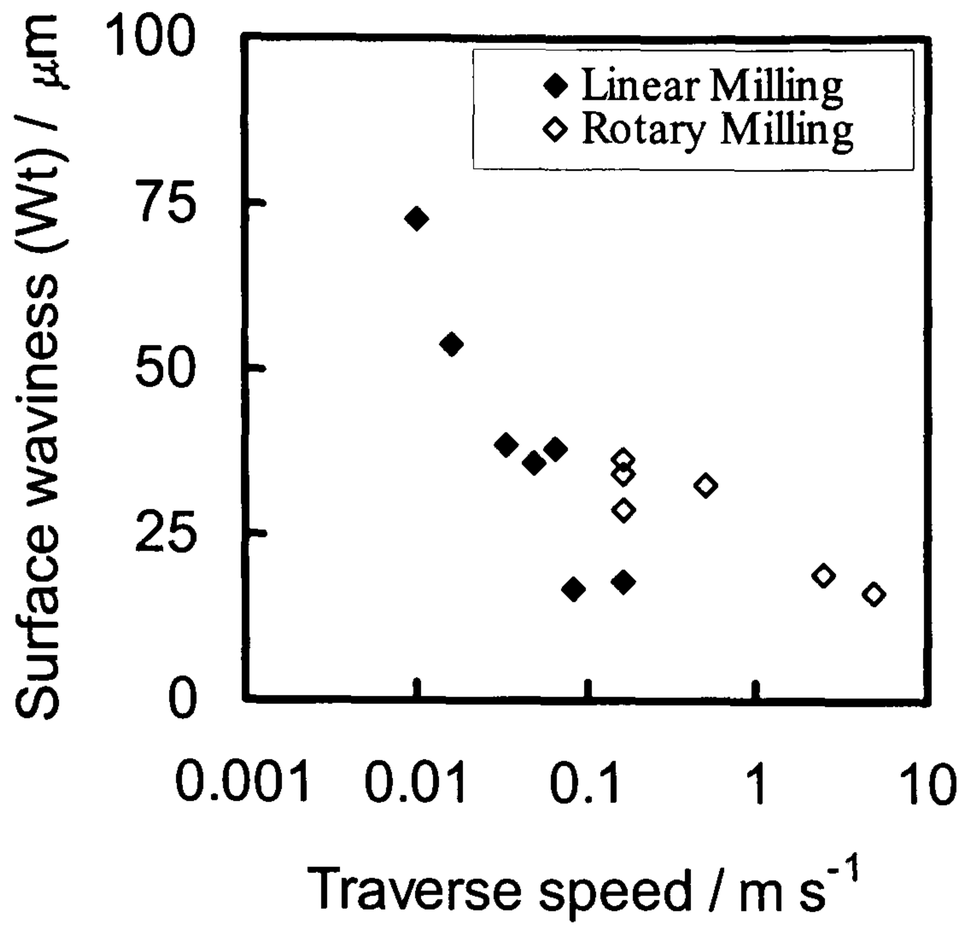

(a)

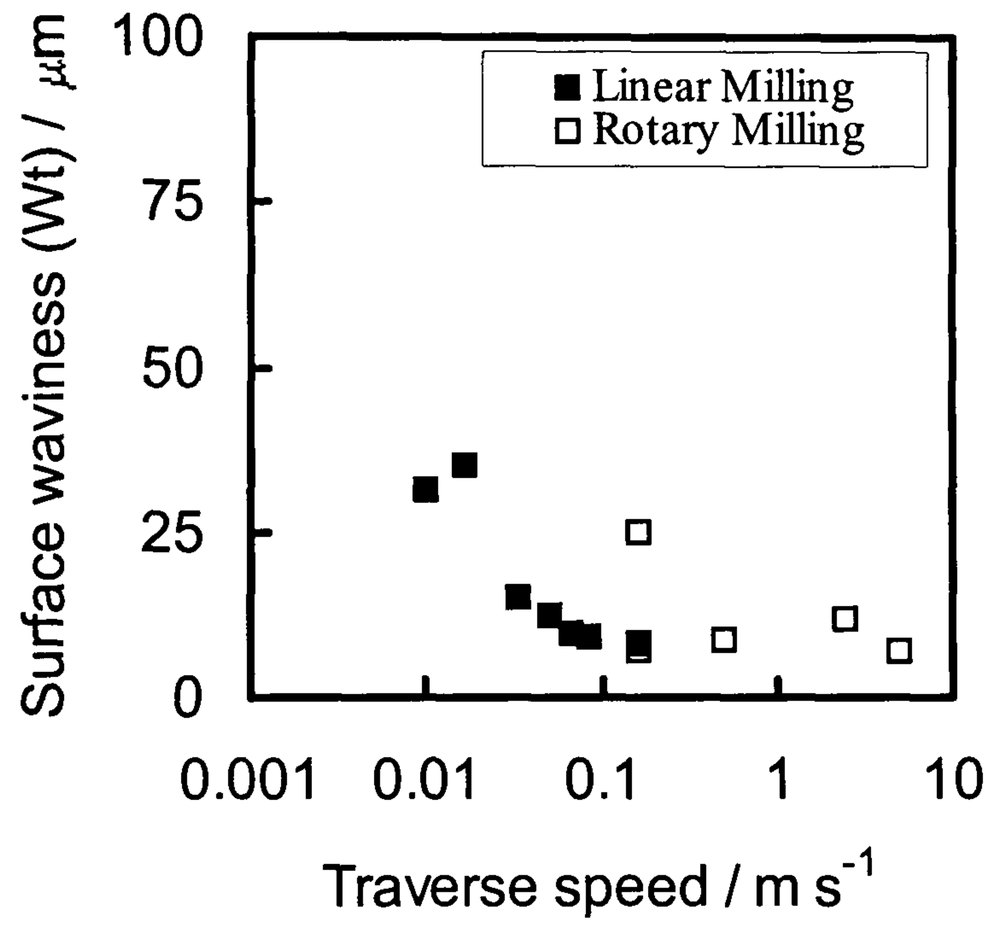

(b)

Figure 4.3 Surface waviness developed during AWJ-CDM of Ti6Al4V as a function of jet traverse speed: Water jet pressure 137.9 MPa (20 000 psi), Stand off distance 3mm, jet impingement angle 90° (a) with 180 μm (80#) garnet grit; (b) with 75 μm (200#) garnet grit. Measurements taken after one pass of the jet in linear milling and twenty passes of the jet in rotary milling.

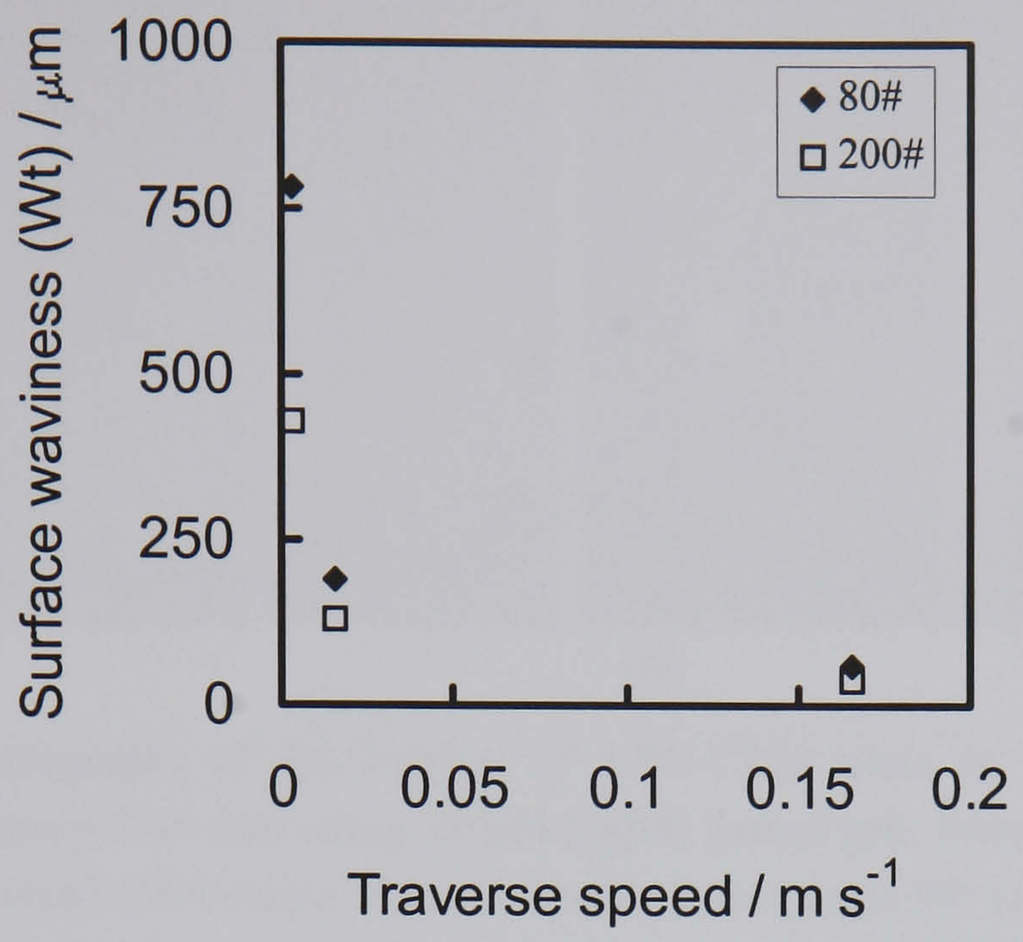

Figure 4.4 Surface waviness developed during AWJ-CDM of Ti6Al4V to an approximately constant depth as a function of jet traverse speed; Water jet pressure 137.9 MPa (20 000 psi), Stand off distance 3mm, jet impingement angle 90°. Milled depth of 3.47 ± 0.1 mm and 2.5 ± 0 .1 mm with 180 μm (80#) garnet grit and 75 μm (200#) garnet grit respectively.

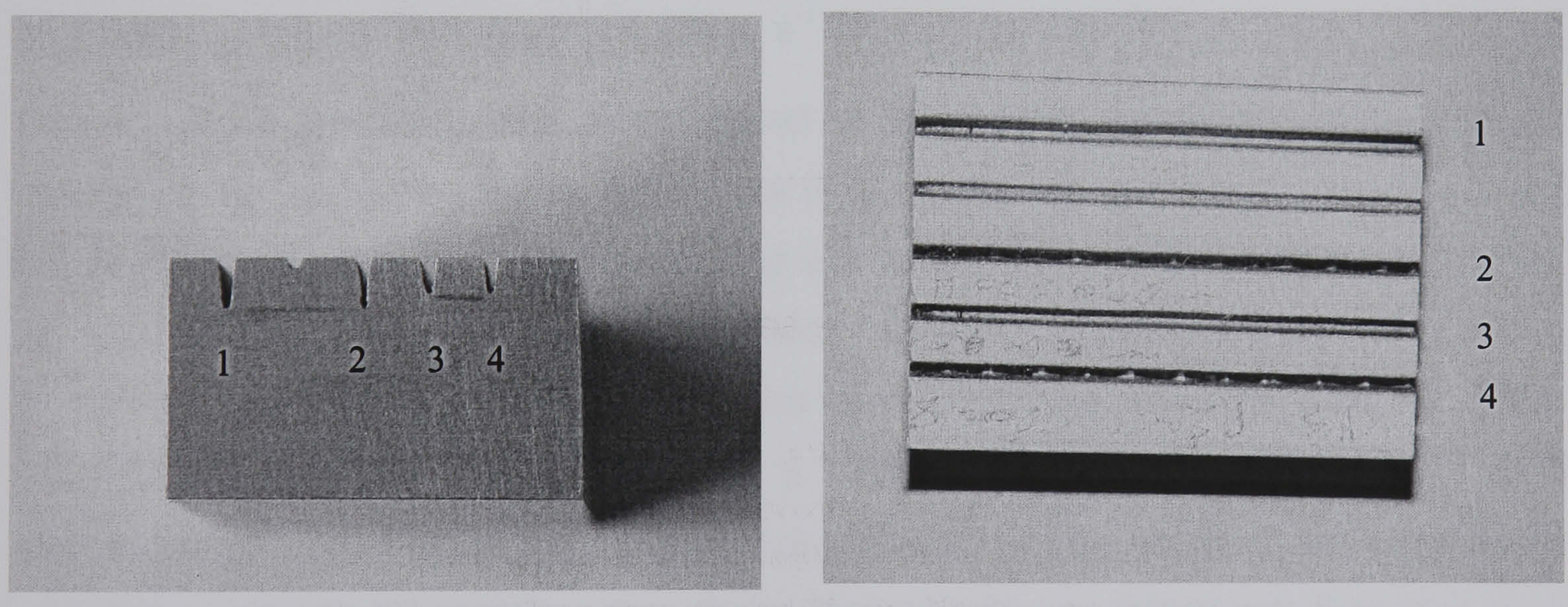

(a) **(b)**

Figure 4.5 (a) End view and (b) plan view of slots AWJ milled in Ti6Al4V. With each grit size, slots were milled with different jet traverse speeds to give slots of approximately the same depth; Water jet pressure 137.9 MPa (20 000 psi), Stand off distance 3mm, jet impingement angle 90°. Slot 1: depth = 3.37 mm, traverse speed = 0.166 m s^{-1} (10 000 mm/min^{-1}), 173 jet passes, 180 μm (80#) grit; Slot 2: depth = 3.41 mm, traverse speed 0.003 m s^{-1} (200 mm min^{-1}), 1 jet pass, 180 μm (80#) grit; Slot 3: depth = 2.49 mm, traverse speed 0.166 m s^{-1} (10 000 mm min^{-1}), 110 jet passes 75 μm (200#) grit; Slot 4: depth = 2.41 mm, traverse speed 0.003 m s^{-1} (200 mm min^{-1}), 1 jet pass, 75 μm (200#) grit.

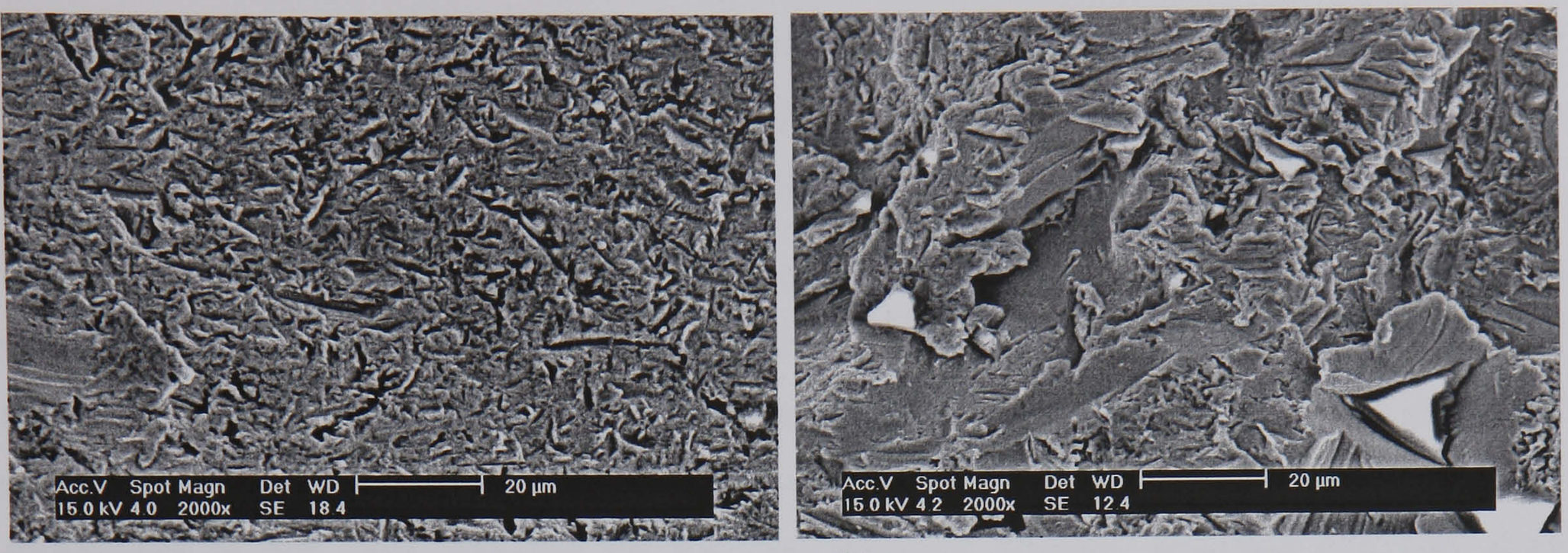

(a) (b)

Figure: 4.6 SEM micrographs of the bottom of AWJ-CDM slots in Ti6Al4V cut to a depth of approximately 2.49 mm using 75 µm (200#) garnet grit. Water jet pressure 137.9 MPa (20 000 psi), stand off distance 3mm, jet impingement angle 90° (a) jet traverse speed = 0.003 m s^{-1} (200 mm min^{-1}), 1 jet passes; (b) jet traverse speed = 0.166 m s^{-1} (10 000 mm min^{-1}), 110 jet passes.

Fig. 4.6 shows the surface morphology of the bottom of two slots milled with 75 µm (200#) grit to the same depth as a function of traverse speed. A striated, directional morphology was observed following milling at a traverse speed of 0.003 m s^{-1} (200 mm min^{-1}) whilst a cratered surface morphology was generated by traversing the jet over the workpiece at the higher speed of 0.166 m s^{-1} (10 000 mm min^{-1}).

Fig. 4.7 shows the effect of traverse speed on the surface roughness of the bottom of the kerf, with single jet passes in the case of linear milling and twenty passes of the jet for the rotary milling. It can be seen that increasing the traverse speed results in an increase in kerf roughness. For both grit sizes, there is a substantial increase of 100% in roughness on increasing the traverse speed from 0.003 m s^{-1} (200 mm min^{-1}) to 0.166 m s^{-1} (10 000 mm min^{-1}) with then only a slight increase in roughness with further increases in traverse speeds. At all traverse speeds, the roughness of test pieces milled with 180 µm (80#) grit is higher than that milled with 75 µm (200#) grit. It is later shown (see Fig. 4.10) that the number of passes of the jet across the workpiece has only a small effect on the surface roughness.

Fig. 4.8 shows the development of depth of cut with multiple passes of the nozzle across the workpiece with both large and small grit sizes at two traverse speeds. It can be seen that in all cases, the cumulative depth of cut increased linearly with number of passes. In a similar manner to Fig. 4.1, it can be seen that the material removal rate is always higher with the larger grit size and is significantly higher at the lower traverse speed.

Fig. 4.9 shows the development of surface waviness with multiple passes of the nozzle across the workpiece at two traverse speeds with both large (Fig. 4.9a) and small (Fig. 4.9b) grit sizes. It can be seen that there is a general increase in waviness with number of passes and thus with depth of cut. For both grit sizes, the waviness is significantly higher at the lower traverse speeds. Also, the waviness is higher for the larger grit size.

Fig. 4.10 shows the development of surface roughness with multiple passes of the nozzle across the workpiece at two traverse speeds with both large (Fig. 4.10a) and small (Fig. 4.10b) grit sizes. For both sizes of grit, the surface roughness does not change significantly with number of passes and thus with depth of cut. The surface roughness is not very different for the two traverse speeds selected (c.f. Fig. 4.7); however, the roughness developed with the 180 μm (80#) grit is around 5.5 μm whereas that developed with the 75 μm (200#) grit is round 3.0 μm.

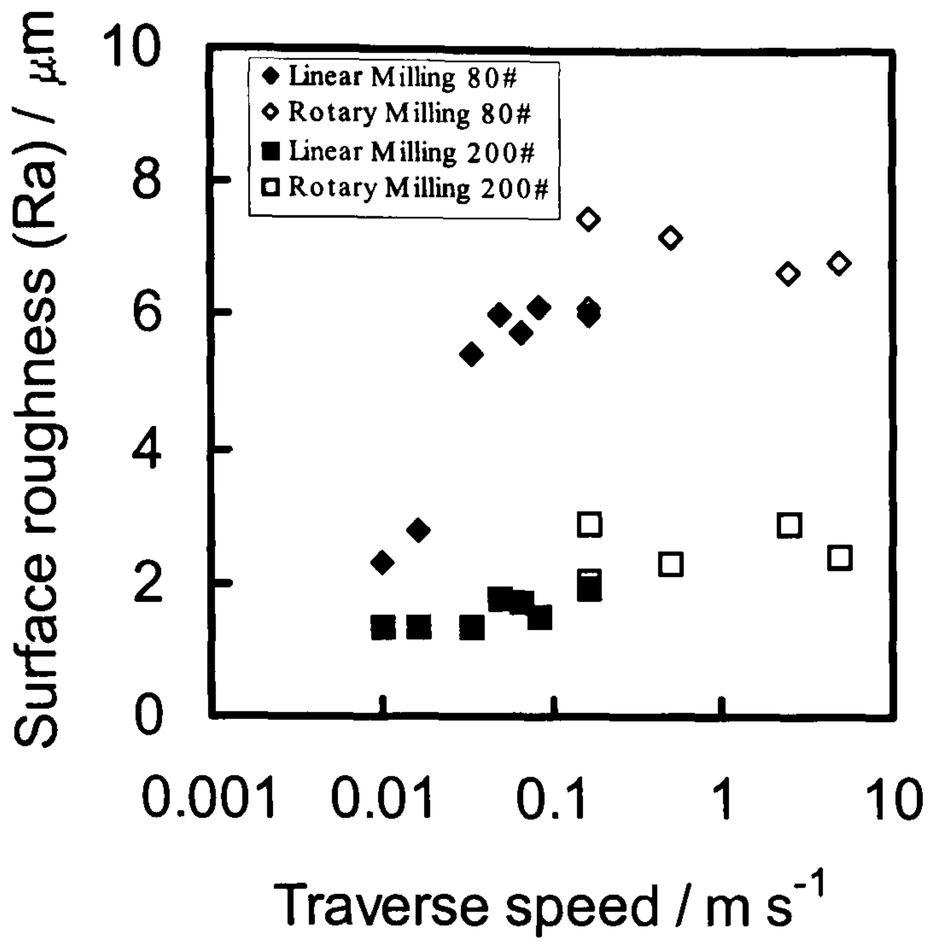

Figure 4.7 Surface roughness developed during AWJ-CDM of Ti6Al4V as a function of jet traverse speed with both 180 μm (80#) garnet grit and 75 μm (200#) garnet grit. Water jet pressure 137.9 MPa (20 000 psi), Stand off distance 3mm, jet impingement angle 90°. Measurements taken after one pass of the jet in linear milling and twenty passes of the jet in rotary milling. (Note: Traverse speed on log scale)

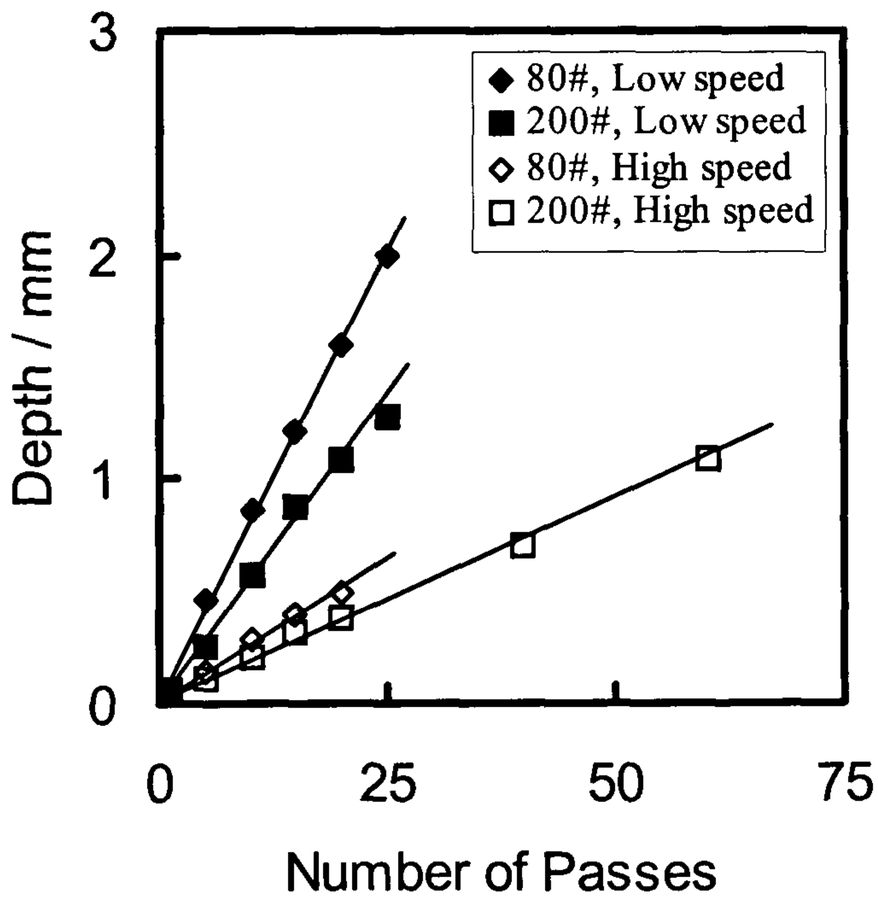

Figure 4.8 Depth of cut as a function of number of jet passes during linear AWJ-CDM of Ti6Al4V for two grit sizes (80# and 200# garnet) and two jet traverse speeds. Low traverse speed = 0.05 m s^{-1} (3 000 mm min^{-1}); high traverse speed = 0.166 m s^{-1} (10 000 mm min^{-1}); Water jet pressure 137.9 MPa (20 000 psi), Stand off distance 3mm, jet impingement angle 90°.

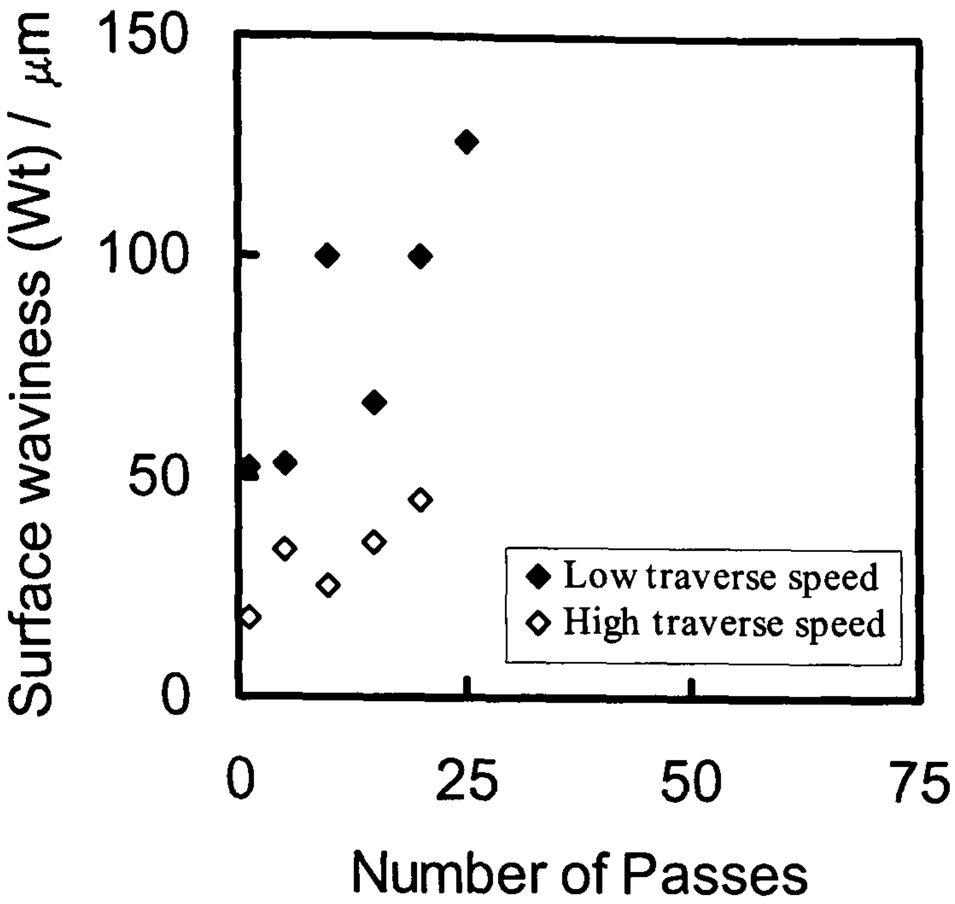

(a)

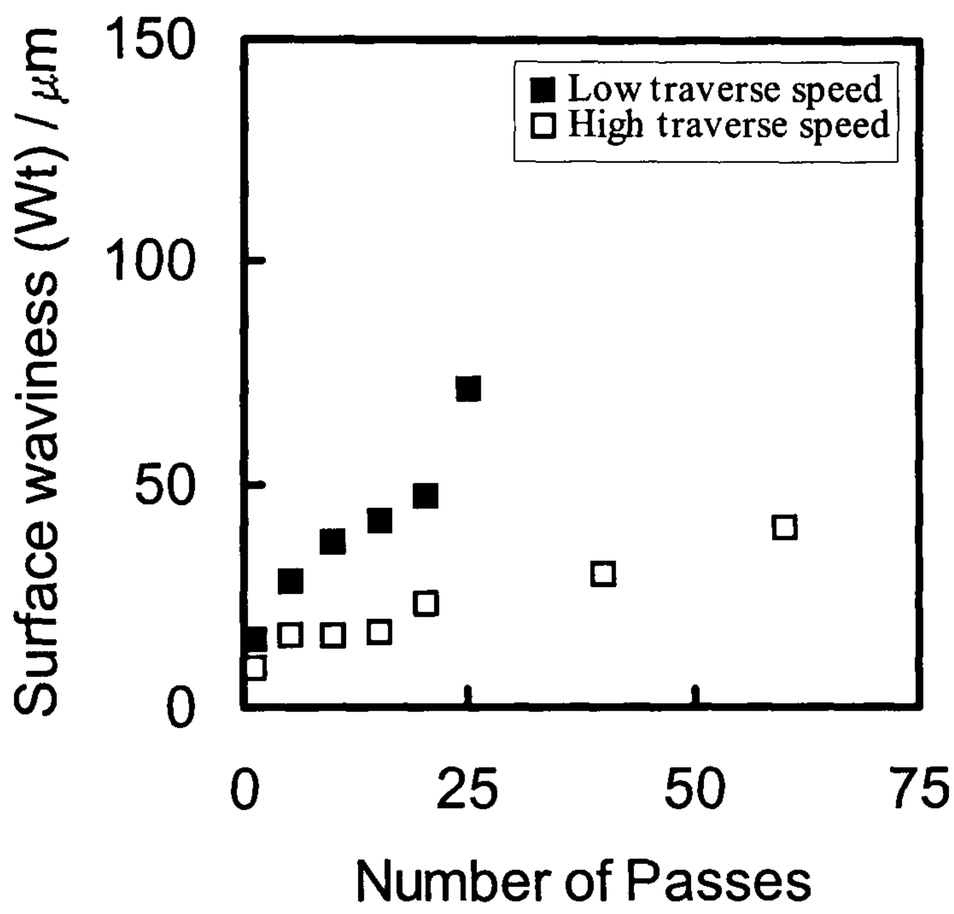

(b)

Figure 4.9 Surface waviness developed during linear AWJ-CDM of Ti6Al4V as a function of number of jet passes at high (0.166 m s^{-1}) and low (0.05 m s^{-1}) jet traverse speeds: Water jet pressure 137.9 MPa (20 000 psi), Stand off distance 3mm, jet impingement angle 90° (a) with 180 μm (80#) garnet grit; (b) with 75 μm (200#) garnet grit.

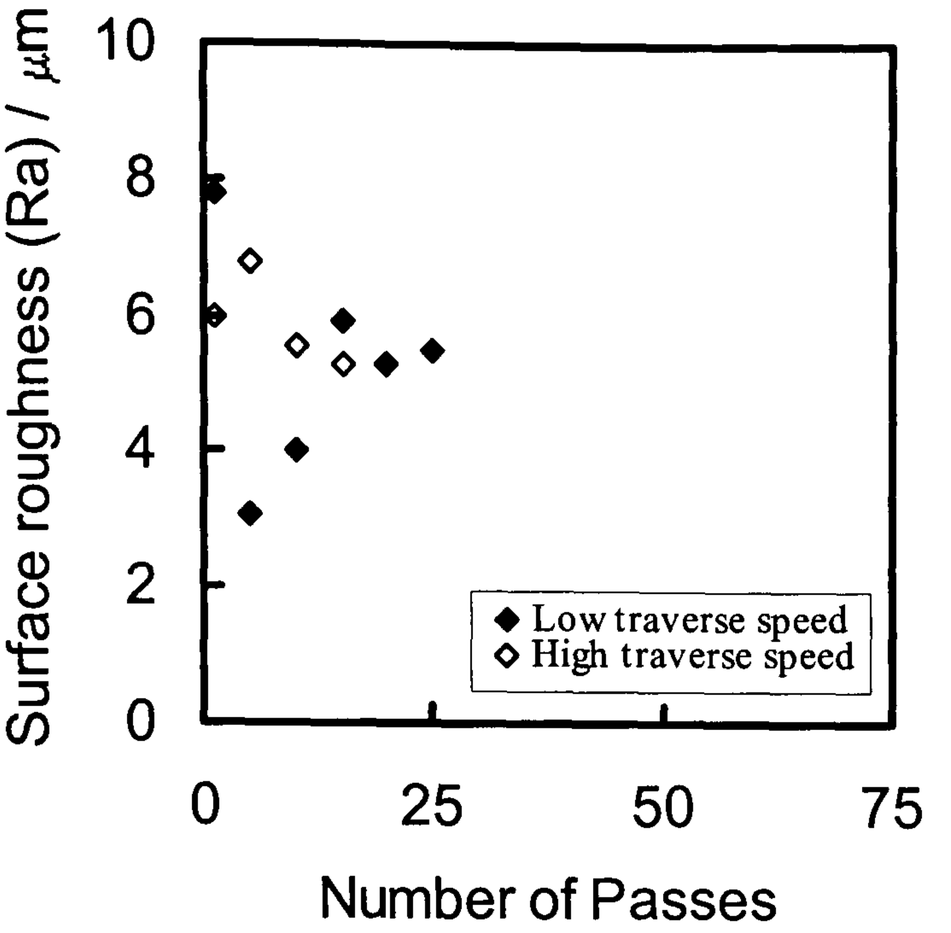

(a)

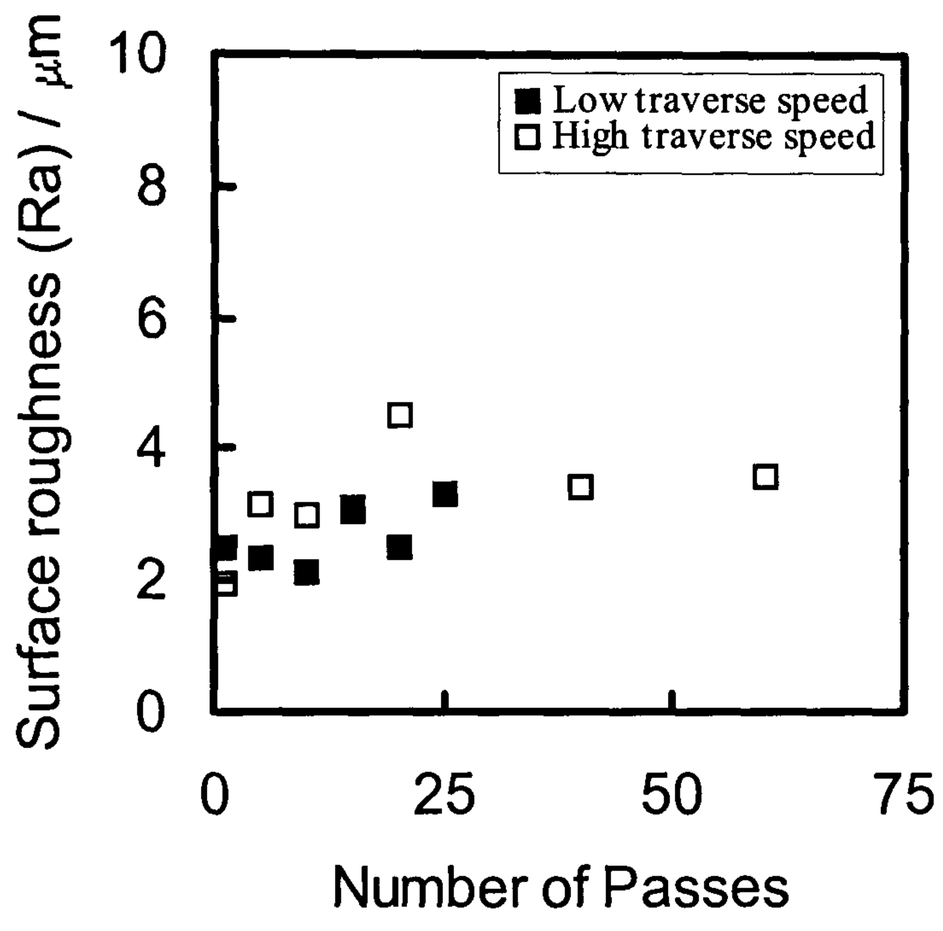

(b)

Figure 4.10 Surface roughness developed during linear AWJ-CDM of Ti6Al4V as a function of number of jet passes at high (0.166 m s^{-1}) and low (0.05 m s^{-1}) jet traverse speeds: Water jet pressure 137.9 MPa (20 000 psi), Stand off distance 3mm, jet impingement angle 90° (a) with 180 μm (80#) garnet grit; (b) with 75 μm (200#) garnet grit.

4.1.2 Discussion.

4.1.2.1 The influence of jet traverse speed on material removal rate.

Fig. 4.1 shows that the material removal rate decreased significantly from its value at the lowest traverse speed (for normal jet angles) to an approximately constant value at the higher speeds. The transition to the lower constant value was more abrupt with the smaller grit size. Such a significant change in material removal rate suggests a change in mechanism of material removal. At low traverse speeds, a deep cut is formed. Much of the cutting is performed at very low angles of attack on the leading edge of the kerf face. A schematic diagram illustrating this is shown in Fig. 4.11c and 4.11d. Since the erosion takes place at low impact angles by a microcutting mechanism, it has an enhanced erosion rate [Hashish, 1998a, Bitter 1963a, 1963b]. At high jet traverse speeds, the depth of cut is small and the leading edge of the kerf face makes up a very small proportion of the total cutting area (Fig 4.12b). The micrographs in Fig. 4.2 support the mechanisms proposed in Fig. 4.11 and Fig. 4.12. Fig. 4.2a shows the bottom of the kerf following milling at low traverse speeds. Here, there has been some channelling of the jet to run along the bottom of the kerf. There is evidence of directionality associated with particles striking the surface at low impacts as the jet has flowed along the kerf [Bitter, 1963a, 1963b, Li et al. 1996b, Summers, 1995]. Fig. 4.2b (where no channelling of the jet has occurred shows no evidence for directionality and only evidence for normal impact of the abrasive particles onto the workpiece surface. It can also be seen by comparing Fig. 4.1(a) and Fig. 4.1(b) that as the grit size is decreased, the material removal rate also decreased. Such behaviour may be expected since in erosion research, the material removal rate is often seen to decrease as the particle size drops below about 100 μm (whilst the material removal rate is independent of the particle size for larger particles sizes) [Hashish, 1998a], [Hashish, 1987], [Ruff and Wiederhorn, 1979], [Sheldon and Finnie, 1968].

4.1.2.2 The influence of jet traverse speed on roughness and waviness.

Surface waviness appears to develop due to irregularities formed during the milling process itself. Once formed, irregularities are propagated since they form disturbances to the pattern of flow of the water jet; such turbulence then further promotes local material removal. A number of publications [Hashish, 1991, Hashish, 1998a, Ojmertz, 1993, Liu, 1998] have indicated that if a non-uniformity in depth exists or is created, it will not be removed, but instead is exaggerated by subsequent passes of the jet. To

reduce surface waviness requires the traverse speed of the abrasive water jet to be increased (Fig. 4.3). As such, the tendency to form any irregularities at all is reduced (since the depth of cut per pass is reduced as the traverse speed is increased) and thus waviness is reduced. Hashish [1987] suggested that a traverse speed of 0.016 m s^{-1} (1 000 mm min^{-1}) should be exceeded to achieve surface uniformity; the data reported in this thesis supports his recommendation. It is also notable that the waviness is significantly lower for the smaller particle size (Fig. 4.3). This may be due to the smaller particles generating smaller irregularities during the milling process, since smaller size grit generates smaller impact craters than the larger grit particularly during milling at higher traverse speeds. The ease of the smaller grit to follow the streamlines of the water jet and thus not result in impact with the workpiece as the jet flowed around irregularities may also help to reduce surface waviness.

Fig. 4.3 shows data which were derived from either single passes or twenty passes of the jet over the workpiece. However, in each case, the depth to which the cut was made is not the same (since it too is dependent on the traverse speed). Thus it was not clear whether Fig. 4.3 showed an intrinsic link between traverse speed and surface waviness, or whether the link was between the depth of cut and the surface waviness. Fig. 4.4 presents further data concerning the surface waviness developed at different traverse speeds where the number of passes was altered to make the overall depth of the kerf the same in all cases. Here, it is proved unambiguously that the surface waviness is indeed dependent upon the jet traverse speed. Fig. 4.5 shows a macrograph of a sample with cuts generated at two different traverse speeds. It is clear that the waviness is significantly reduced by the use of higher traverse speeds for both grit sizes. Fig. 4.6 shows micrographs of the bottom of two kerfs (both ~ 2.49 mm deep), one milled at a traverse speed of 0.003 m s^{-1} (200 mm min^{-1}) (Fig 4.6a) and the other at 0.166 m s^{-1} (10 000 mm min^{-1}) (Fig 4.6b). Again, it is clear that at low traverse speeds (Fig. 4.6a) there is directionality in the bottom of the kerf indicating cutting at low attack angles from the channelled jet. However, despite the fact that the kerf is the same depth (but also approximately the same depth in front of the jet as well as behind it), no evidence of directionality is observed on the bottom of the kerf following milling at the higher traverse speed (Fig. 6b). This indicates that the walls of the kerf are not in themselves sufficient to cause the jet to channel along the bottom of the kerf.

Fig. 4.7 shows that the surface roughness of the bottom of the kerf is also dependent on the jet traverse speed. For the larger abrasive particles, the surface roughness is low at the lowest traverse speeds (where the waviness is high). This phenomena was also seen by Ojmertz [1997a]. However, there is a rapid increase in roughness to a value in

excess of 5 μm for the larger 180 μm (80#) grit as the traverse speed is first increased from 0.003 m s $^{-1}$ (200 mm min^{-1}) to 0.166 m s^{-1} (10 000 mm min^{-1}). Only a small increase in roughness occurs as the traverse speed is increased above 0.166 m s^{-1} (10 000 mm min^{-1}). A similar trend is exhibited with the smaller grit but it is less pronounced. As indicated by Fig. 4.2 and Fig. 4.6, there is a shift in dominant mechanism as the jet traverse speed is increased from low angle, directional cutting at low traverse speeds to high angle deformation at high traverse speeds. This shift in mechanism is responsible for the increase in roughness with increasing traverse speed.

Since both traverse speed and number of passes affect the way that material is removed in AWJ milling, a series of trials were performed using just two traverse speeds and varying instead the number of passes of the jet. Fig. 4.8 shows that the depth to which material is removed increases linearly with number of passes. This linear dependence has also been seen by Hashish [1998a]. Due to changes in dominant mechanism as discussed earlier, the depth of cut is always larger with the lower traverse speeds. Also, the depth to which material is removed is again shown to be much higher for larger grit sizes.

Fig. 4.9 shows the development of surface waviness at two traverse speeds for both sizes of grit. Whilst in all cases the initial waviness was not too large, the experiments at the lower traverse speeds showed a significant increase in waviness as the number of passes increased. However, it is notable that at the higher traverse speeds the increase in waviness is much more gradual, particularly in the case of the 75 μm (200#) grit at 0.166 m s^{-1} (10 000 mm min^{-1}). The investigation has shown that as the number of jet passes increased then the surface waviness also increased, whereas the investigations by Ojmertz [1996] did not see any trend. However, whilst the graphs of material removal rate (Fig. 4.1) indicated that there was little difference between 0.05 m s^{-1} (3 000 mm min^{-1}) and 0.166 m s^{-1} (10 000 mm min^{-1}), there clearly is a significant difference in the development of the kerf. Any small aberrations in the surface become more exaggerated as the number of passes increases leading to very high waviness. It is clear that to stop significant increases in surface waviness with the two grit sizes employed here requires a traverse speed greater than 0.05 m s^{-1} (3 000 mm min^{-1}).

Fig. 4.10 shows that for both sizes of grit employed and at both traverse speeds examined, there is little dependence of kerf surface roughness with increasing number of passes of the jet. As such, the roughness is developed at the micro-scale and is independent of the total number of particles striking the surface, material characteristics [Hashish, 1991] and particle size and thus is independent on the depth of cut. In contrast, surface waviness is a more macro-scale measurement; waviness develops

because of perturbations caused in the AWJ milling process but once formed, it is exaggerated by subsequent jet passes. This latter explanation explains the research findings of Hashish, Ojmertz and Liu [Hashish, 1987, Ojmertz, 1993, Ojmertz, 1997a, Liu, 1998]. High traverse speeds reduce the formation of significant irregularities in the surface and thus waviness can be improved i.e. reduced in value.

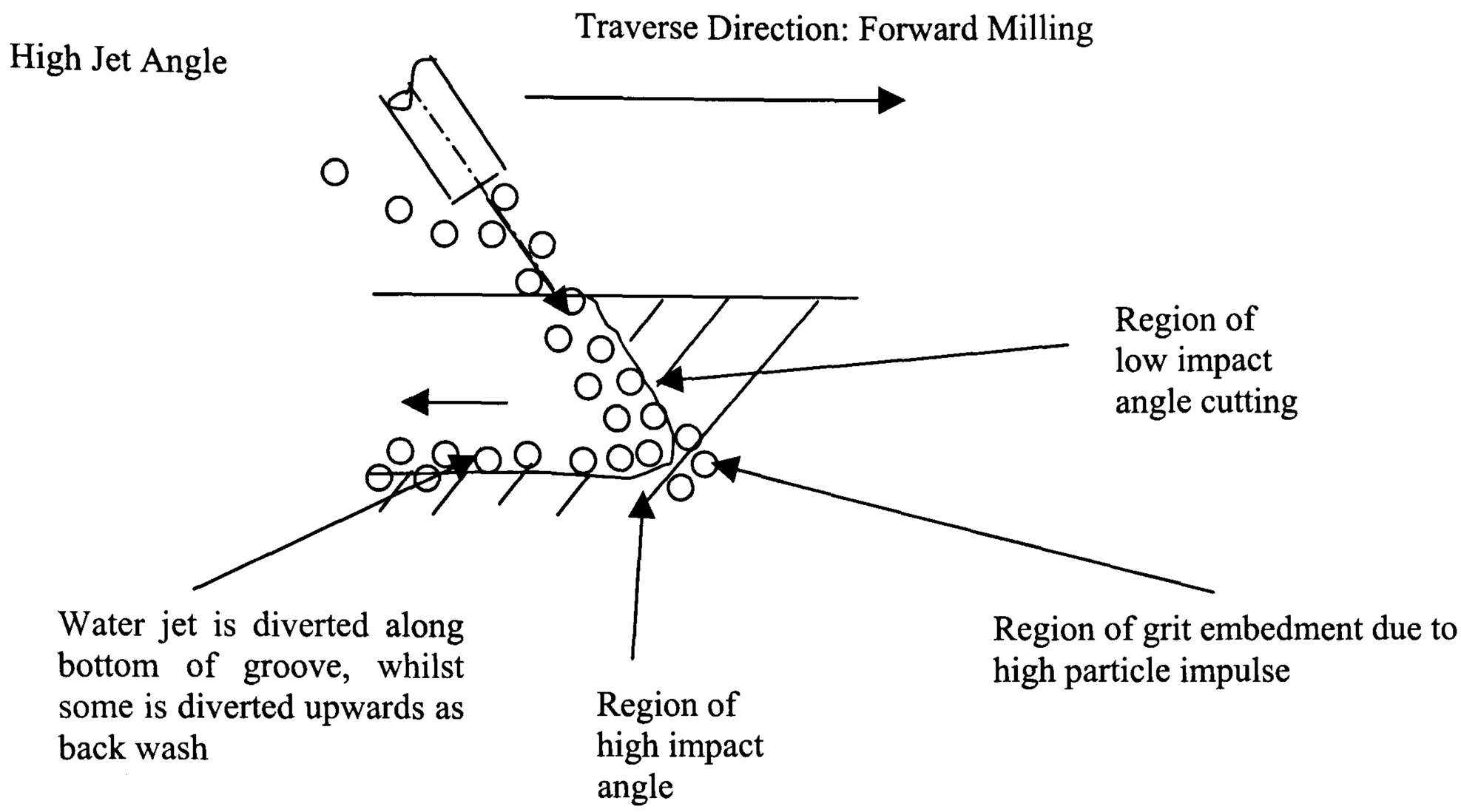
High Jet Angle
Traverse Direction: Forward Milling
Region of low impact angle cutting
Water jet is diverted along bottom of groove, whilst some is diverted upwards as back wash
Region of high impact angle
Region of grit embedment due to high particle impulse

(a)

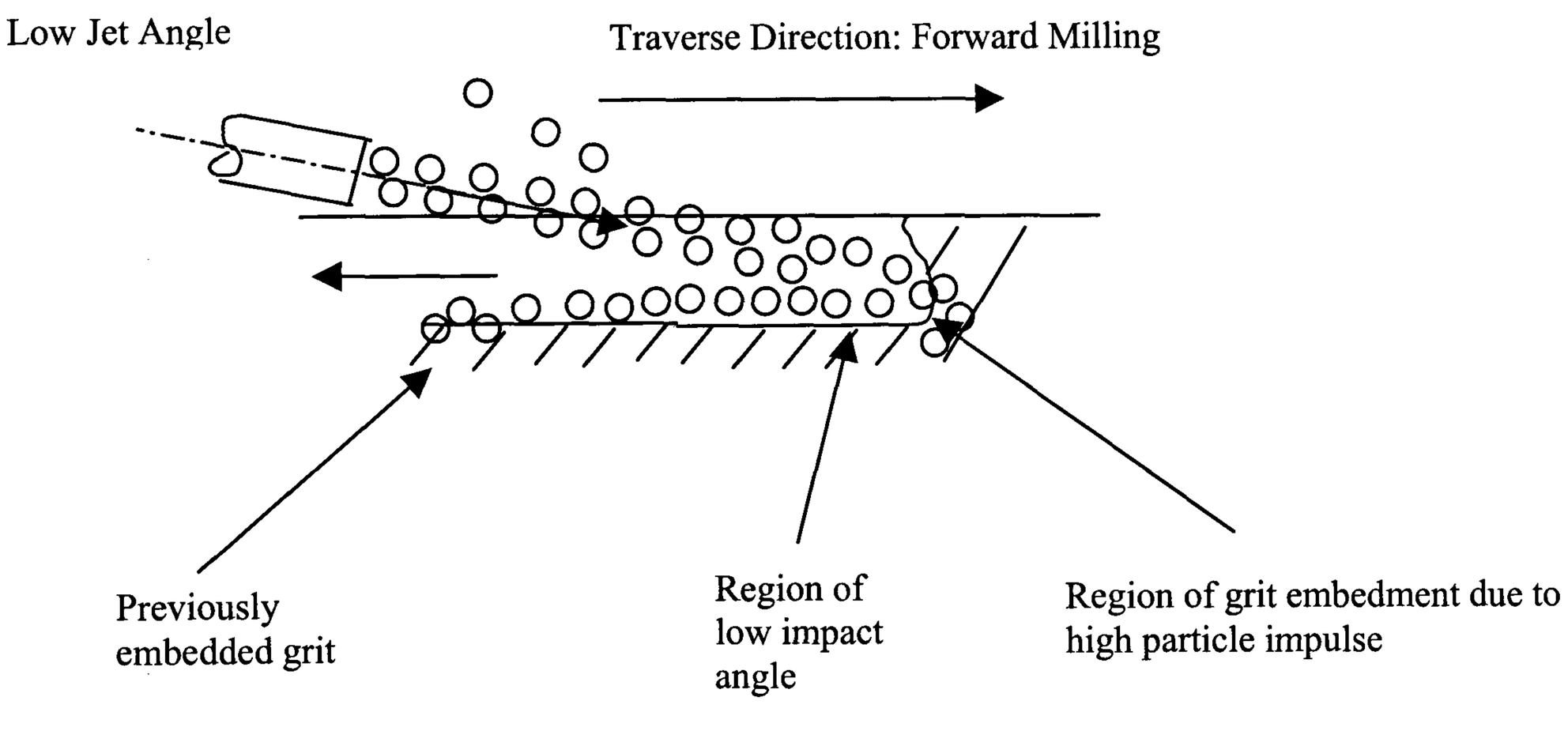
Low Jet Angle
Traverse Direction: Forward Milling
Previously embedded grit
Region of low impact angle
Region of grit embedment due to high particle impulse

(b)

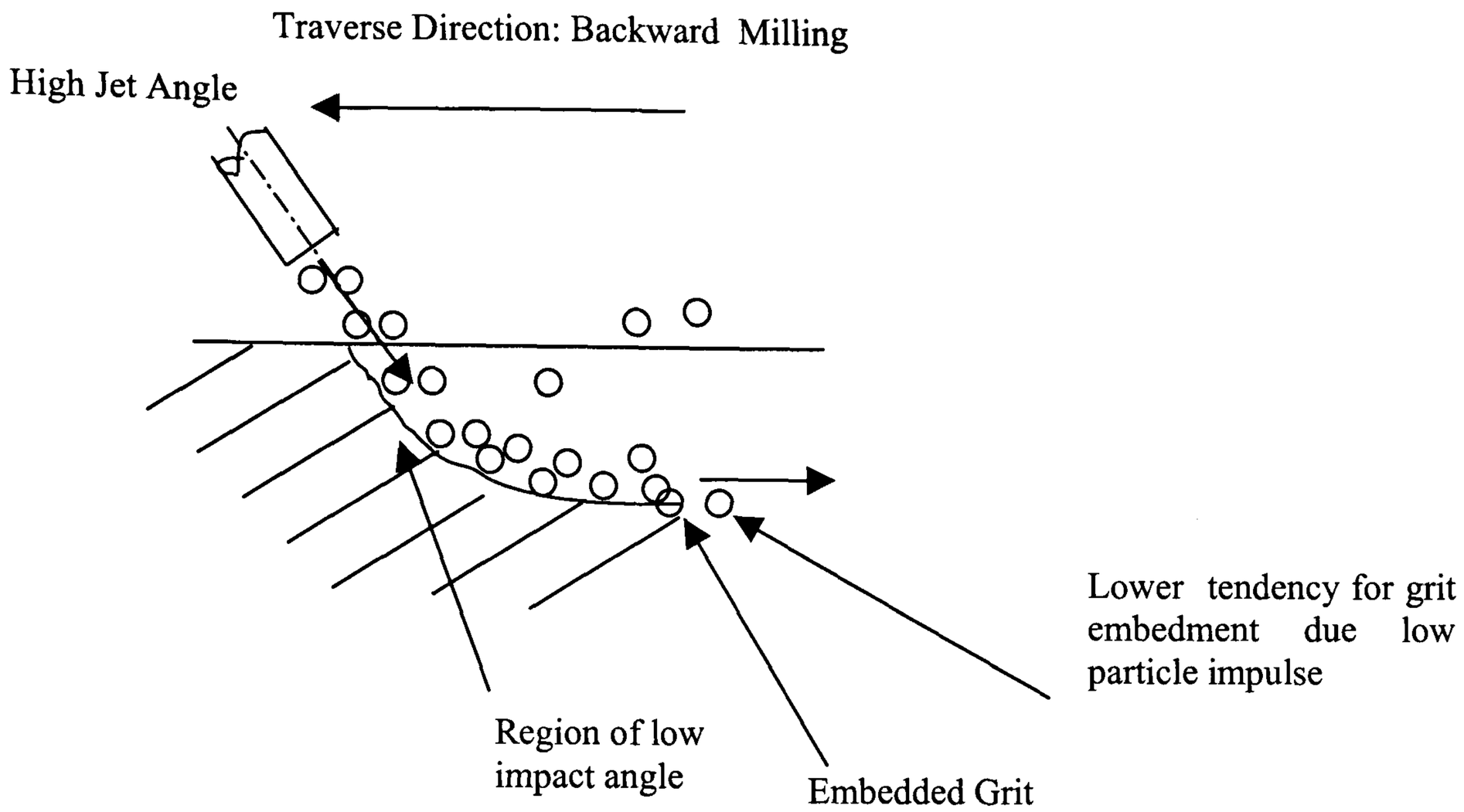

(c)

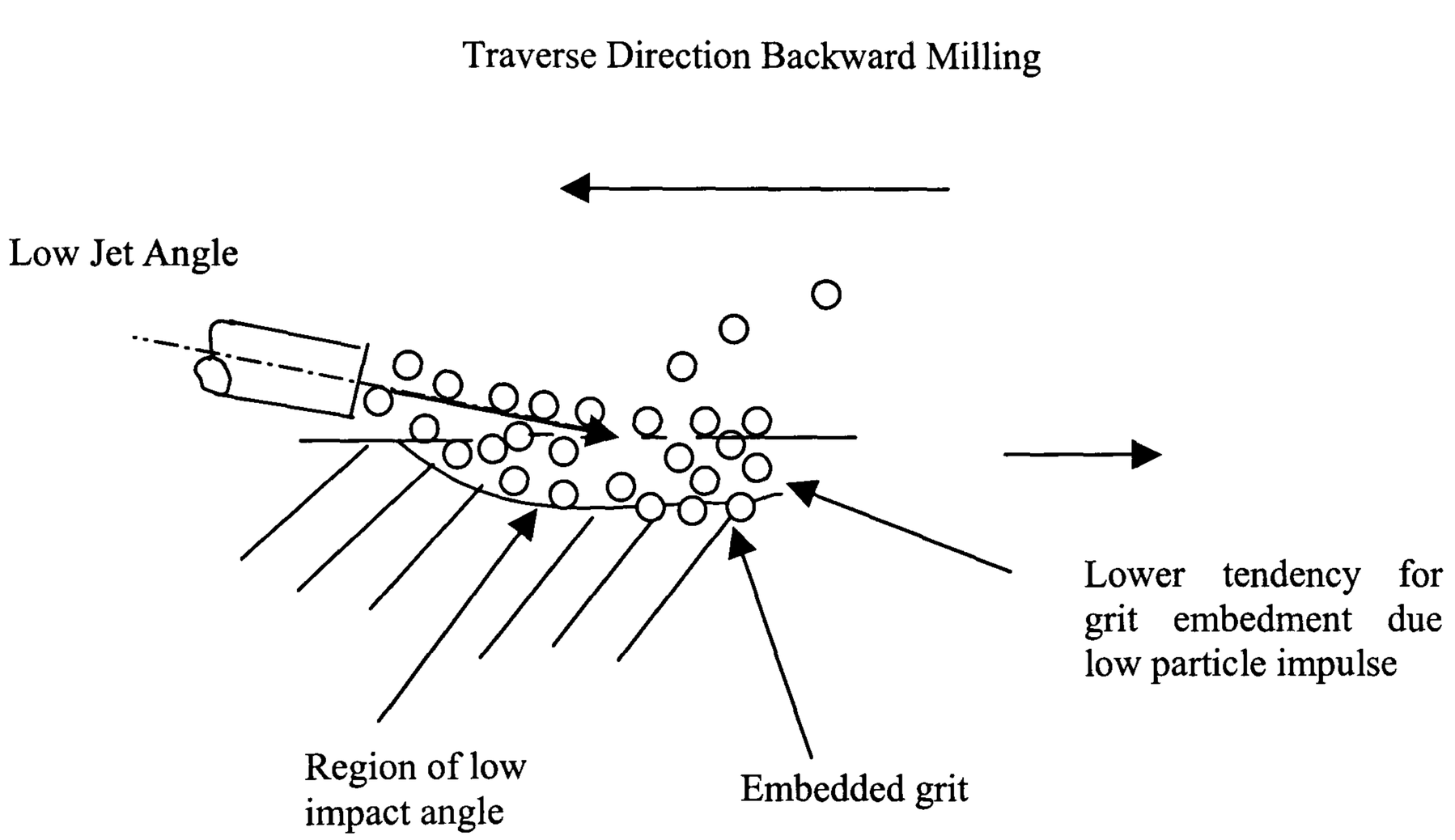

(d)

Figure 4.11 Schematic diagram of flow patterns in AWJ milling with a low jet traverse speed: (a) high jet impingement angle, forward milling; (b) Low jet impingement angle, forward milling; (c) High jet impingement angle, backward milling; (d) Low jet impingement angle, backward milling.

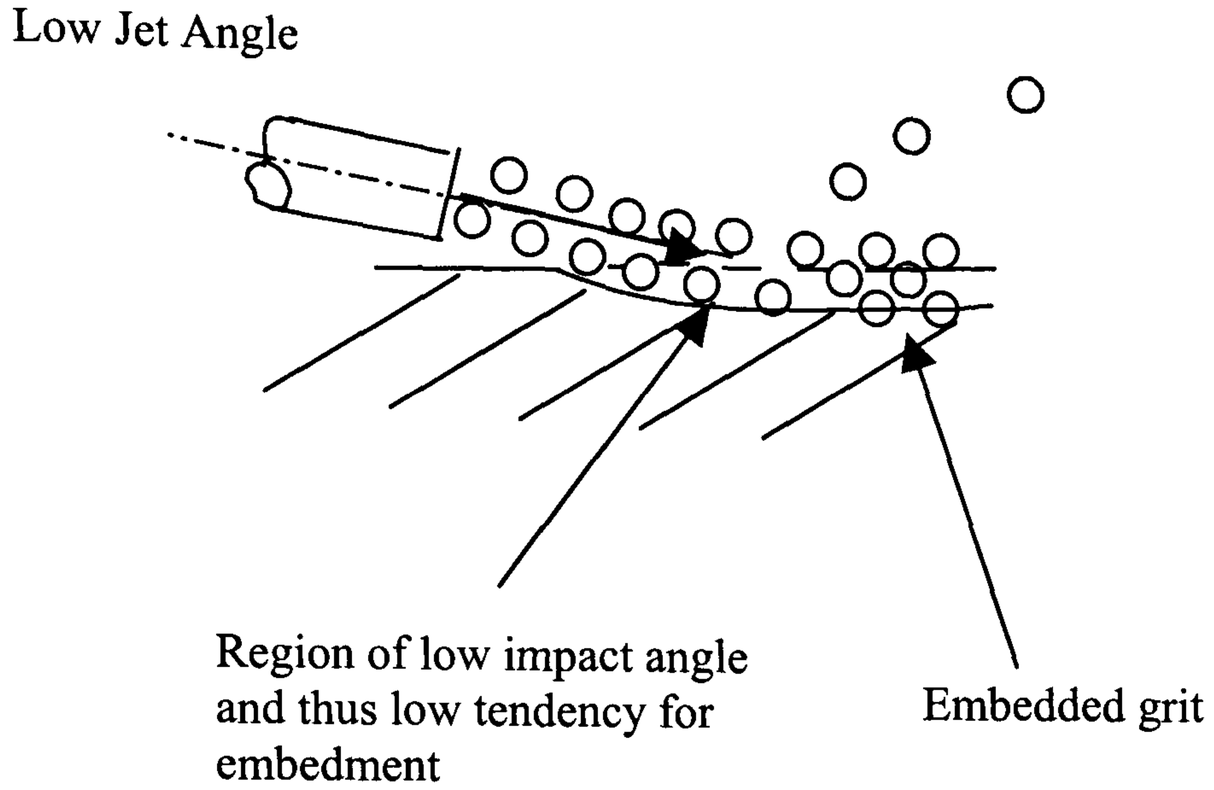

(a)

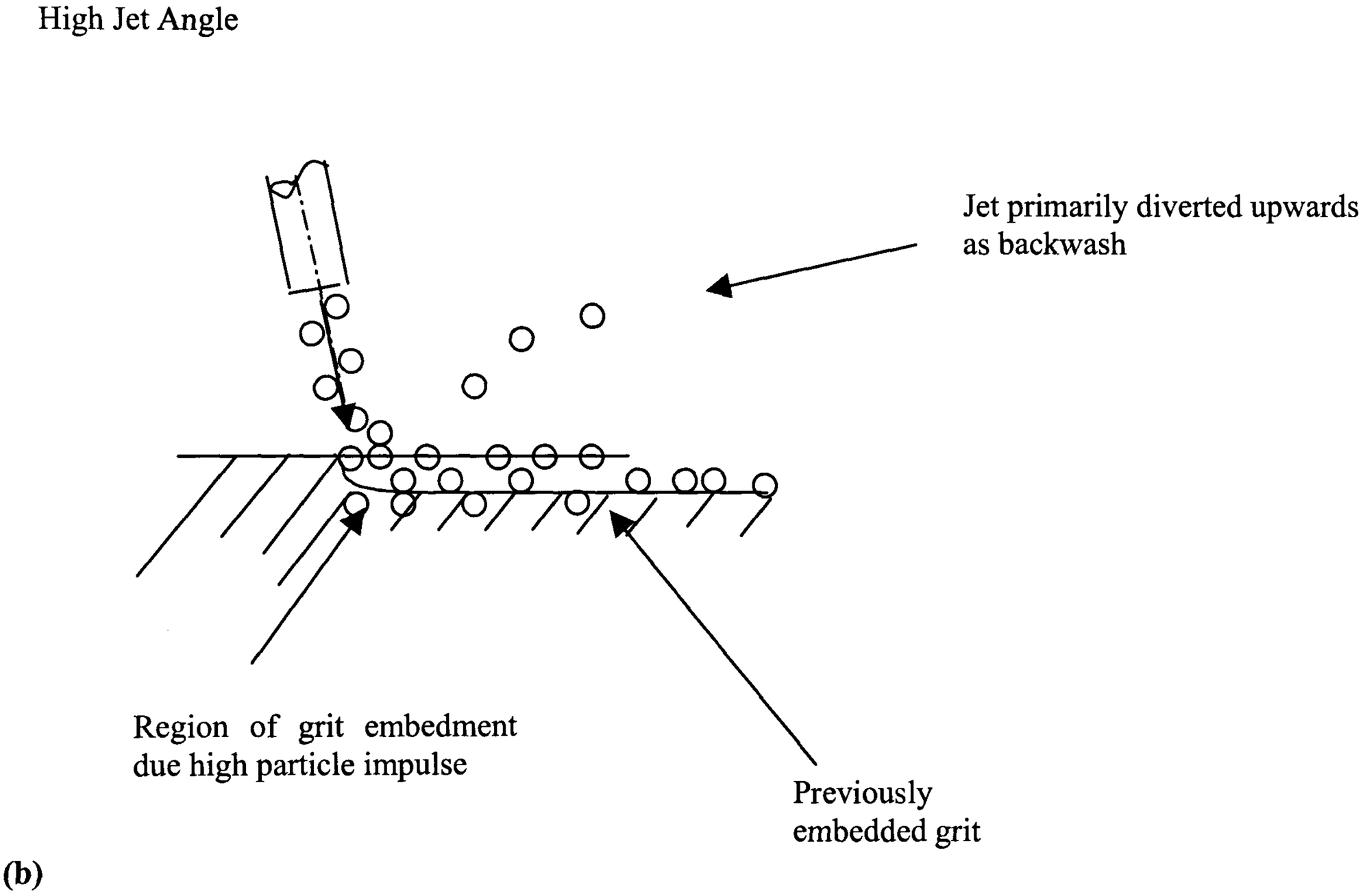

(b)

Figure 4.12 Schematic diagram of flow patterns in AWJ milling with a high jet traverse speed: (a) low impingement angle, backward or forward milling; (b) high impingement angle, backward or forward milling.

4.2 Role of water jet pressure, stand off distance and jet increment on process characteristics.

4.2.1 Results.

Fig. 4.13 shows the effect of traverse speed and water jet pressure on material removal rate for two grit sizes when milling with single passes of the water jet. At all jet traverse speeds, the material removal rate increased with increasing pressure. It can also be seen that material removal rate (E_d) for both grit sizes is high at the lowest traverse speed examined and decreases rapidly with increasing traverse speed as seen previously (Fig. 4.1). This trend is observed over the range of water jet pressures examined. The material removal rate at the higher traverse speeds and water jet pressure is approximately 60×10^{-6} kg s^{-1} with the larger 180 μm (80#) grit (Fig. 4.13a), and approximately 20×10^{-6} kg s^{-1} with the smaller 75 μm (200#) grit (Fig. 4.13b).

Fig. 4.14 shows the development of roughness and waviness as a function of traverse speed and water jet pressure. For all traverse speeds investigated it can be seen that an increase in water jet pressure results in an increase in surface waviness. Moreover, water pressure has a much stronger influence on surface waviness at the lower traverse speed, than at higher traverse speeds (Fig. 4.14a and Fig. 4.14b). For high traverse speeds the employment of high water jet pressure results in an approximate 50% increase in surface waviness whilst at lower speeds a six fold increase in waviness is observed for both grits. However, an increase in water jet pressure has a no strong influence on roughness across the range of jet traverse speeds examined. For both grit sizes examined, the roughness values increase by approximately 16% as the speed increases from 0.0166 ms^{-1} to 0.166 ms^{-1} (Fig. 4.14c). It should also be noted that milling with the smaller abrasive grit can result in a 50% reduction in roughness and waviness compared with the larger grit.

In Fig. 4.15a it can be seen that a three fold increase in stand off distance reduces the material removal rate by approximately one third for the large grit size; for the smaller grit the reduction was much larger depending on traverse speed. Whilst the influence of the jet traverse speed and particle size are evident in Fig. 4.15b and 4.15c, no strong influence of the jet stand off distance is observed on the development of either roughness or waviness.

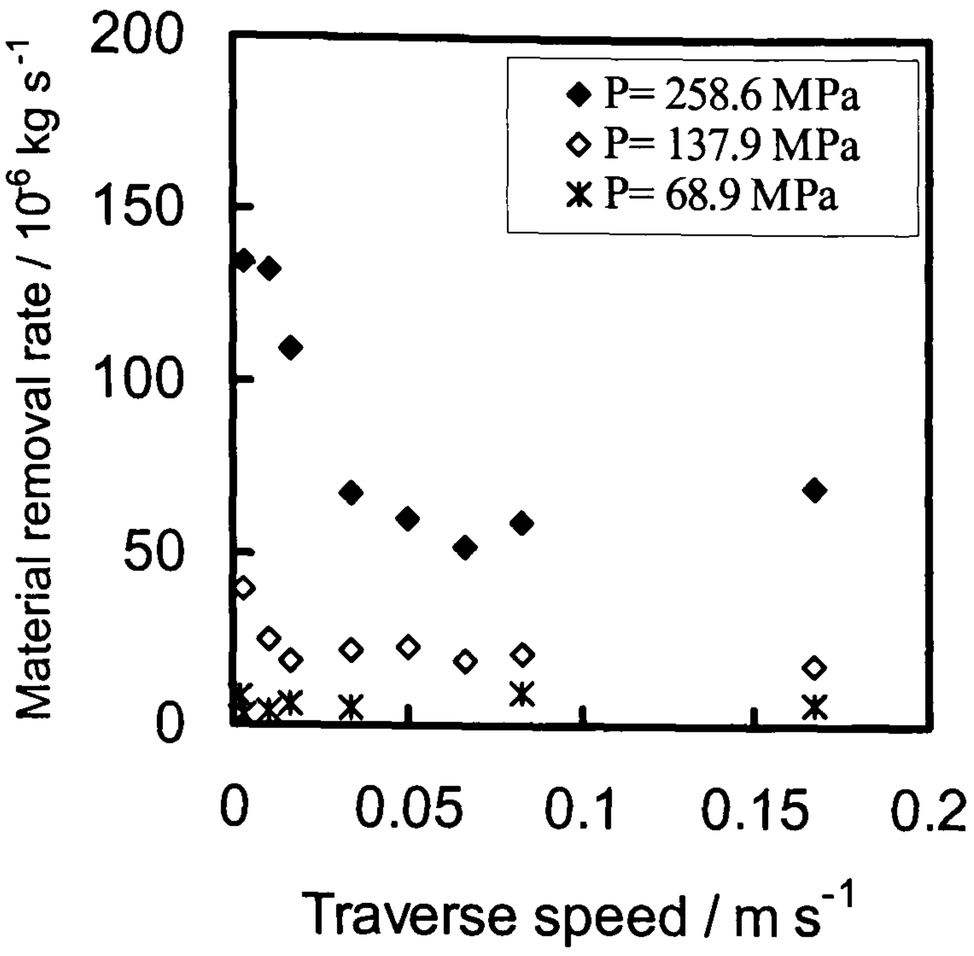

(a)

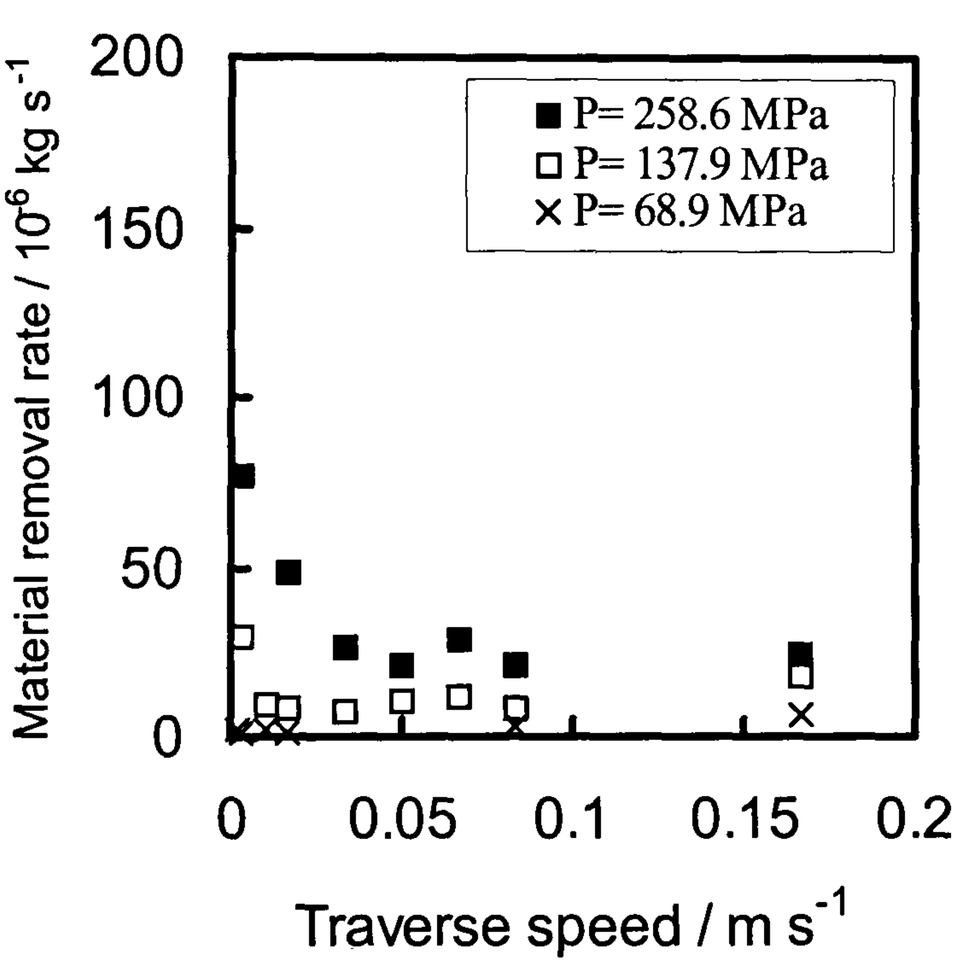

(b)

Figure 4.13 Material removal rate during AWJ-CDM of Ti6Al4V as a function of jet traverse speed: with water jet pressures (as indicated in the legend) of 258.6 MPa (37 500 psi), 137.9 MPa (20 000 psi), and 68.9 MPa (10 000 psi); stand off distance 3mm, jet impingement angle 90°; (a) with 180 μm (80#) garnet grit; (b) with 75 μm (200#) garnet grit.

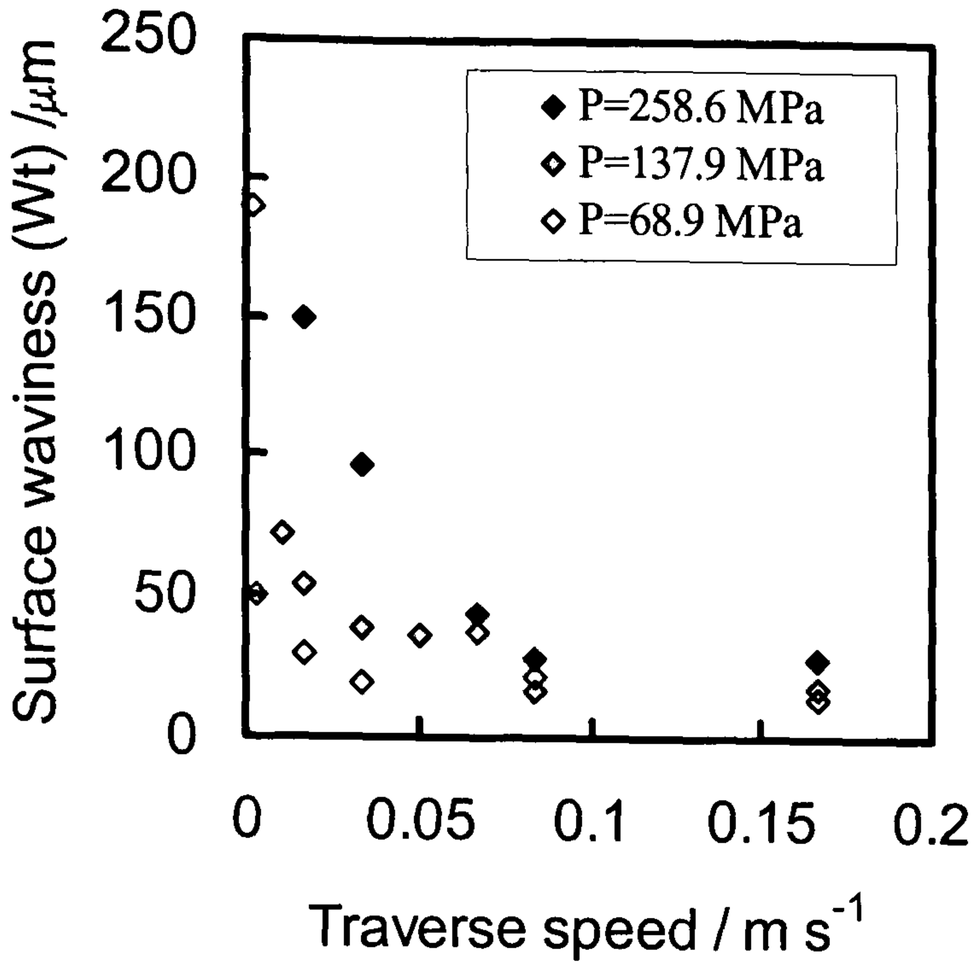

(a)

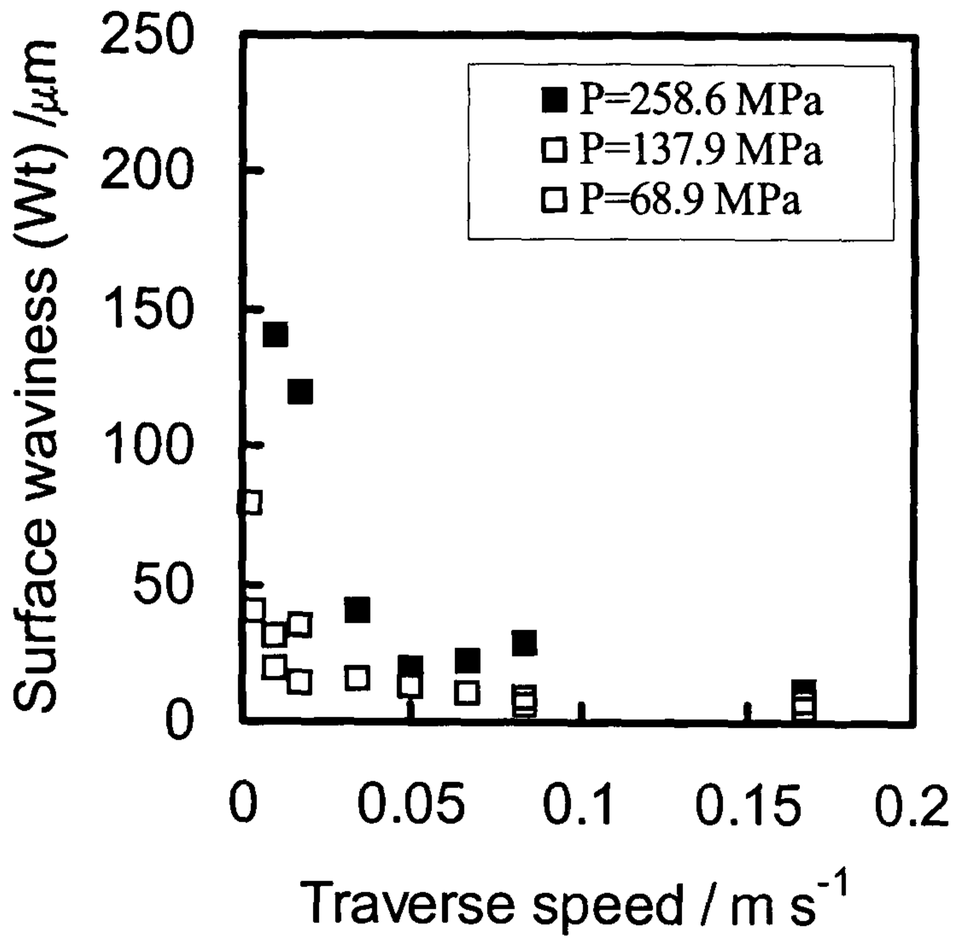

(b)

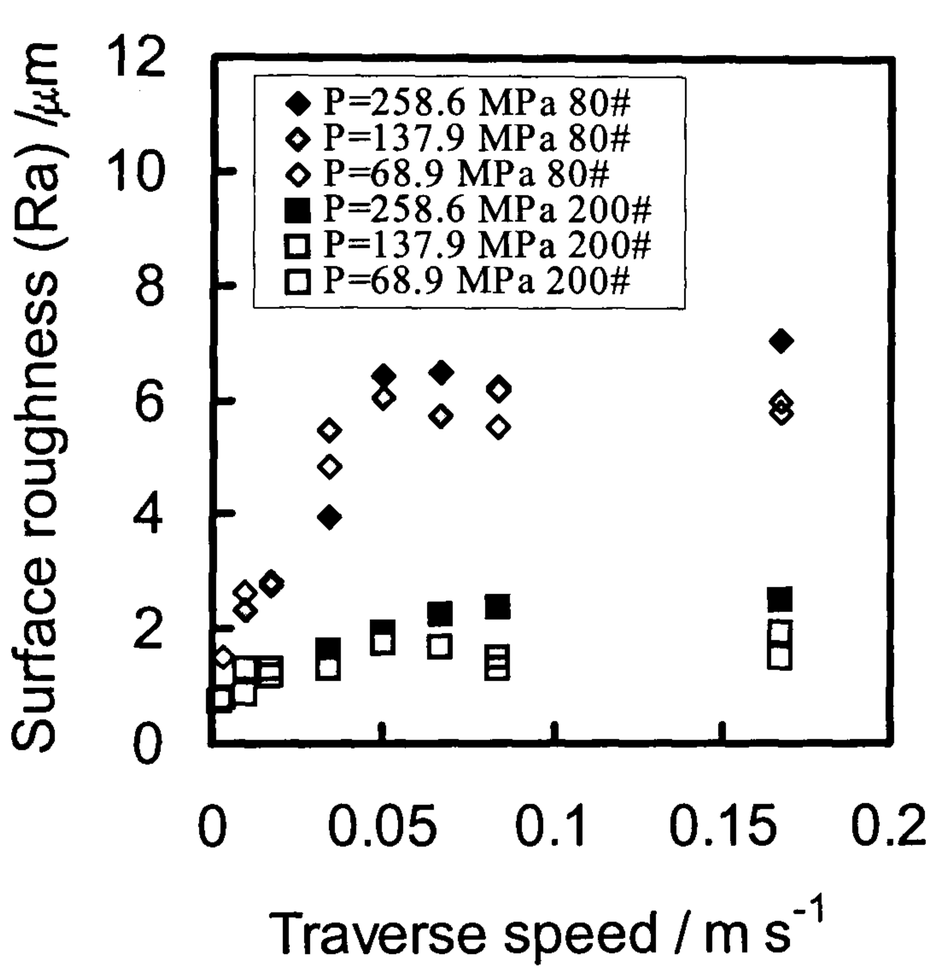

(c)

Figure 4.14 Surface waviness and roughness developed during AWJ-CDM of Ti6Al4V as a function of jet traverse speed: Milling with a range of water jet pressures (as indicated in the legend) of 258.6 MPa (37 500 psi), 137.9 MPa (20 000 psi), and 68.9 MPa (10 000 psi), stand off distance 3mm, jet impingement 90° (a) Surface waviness developed when milling with 180 μm (80#) garnet grit; (b) Surface waviness developed when milling with 75 μm (200#) garnet grit. (c) Surface roughness developed when milling with 180 μm (80#) and 75 μm (200#) garnet grit.

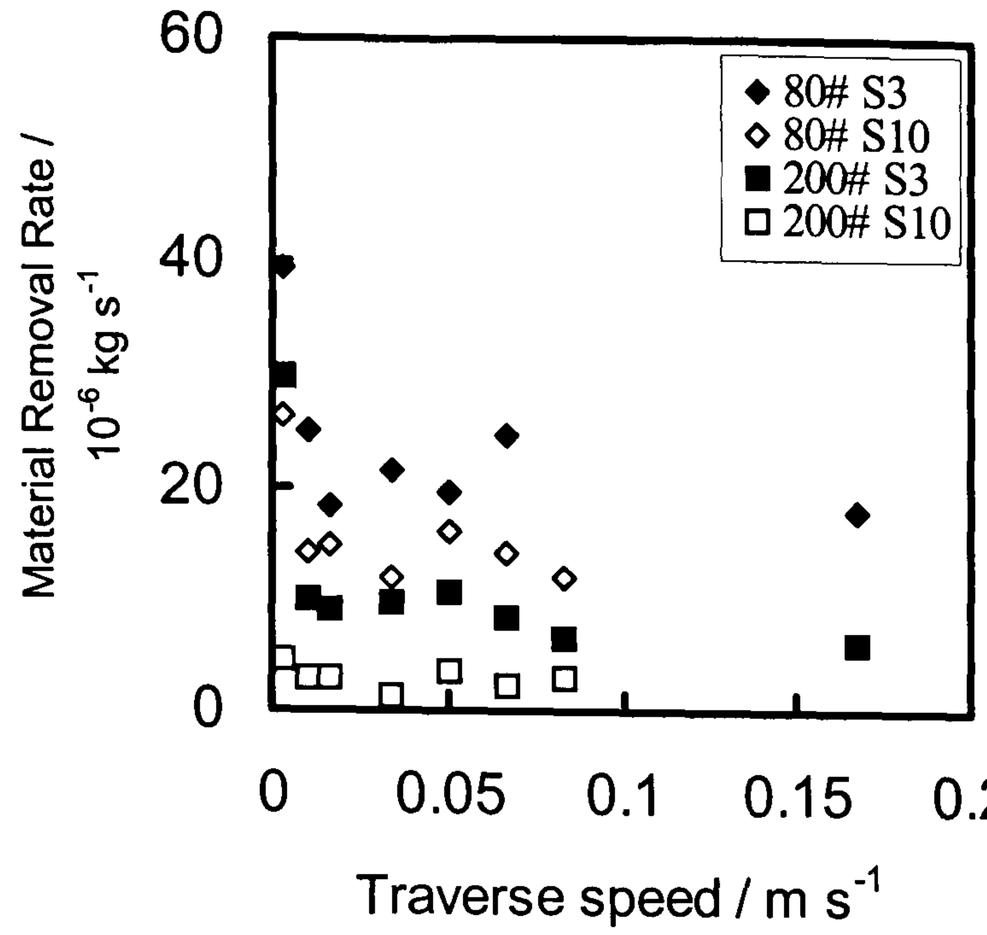

(a)

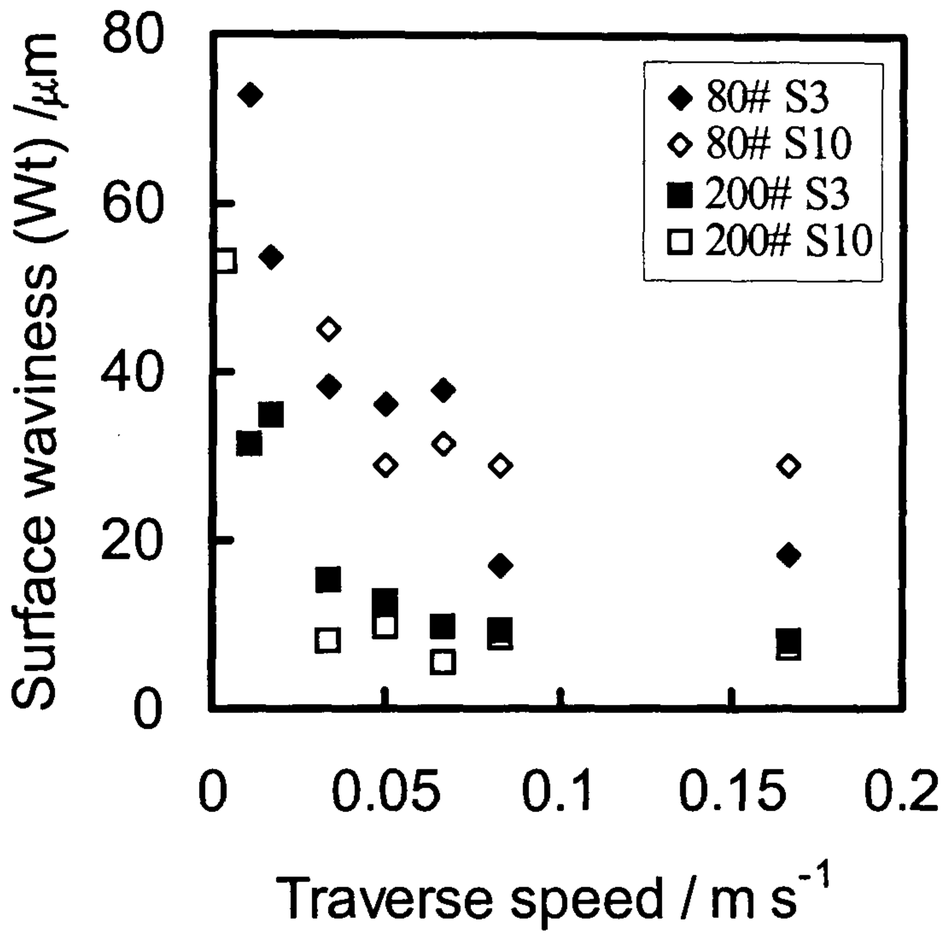

(b)

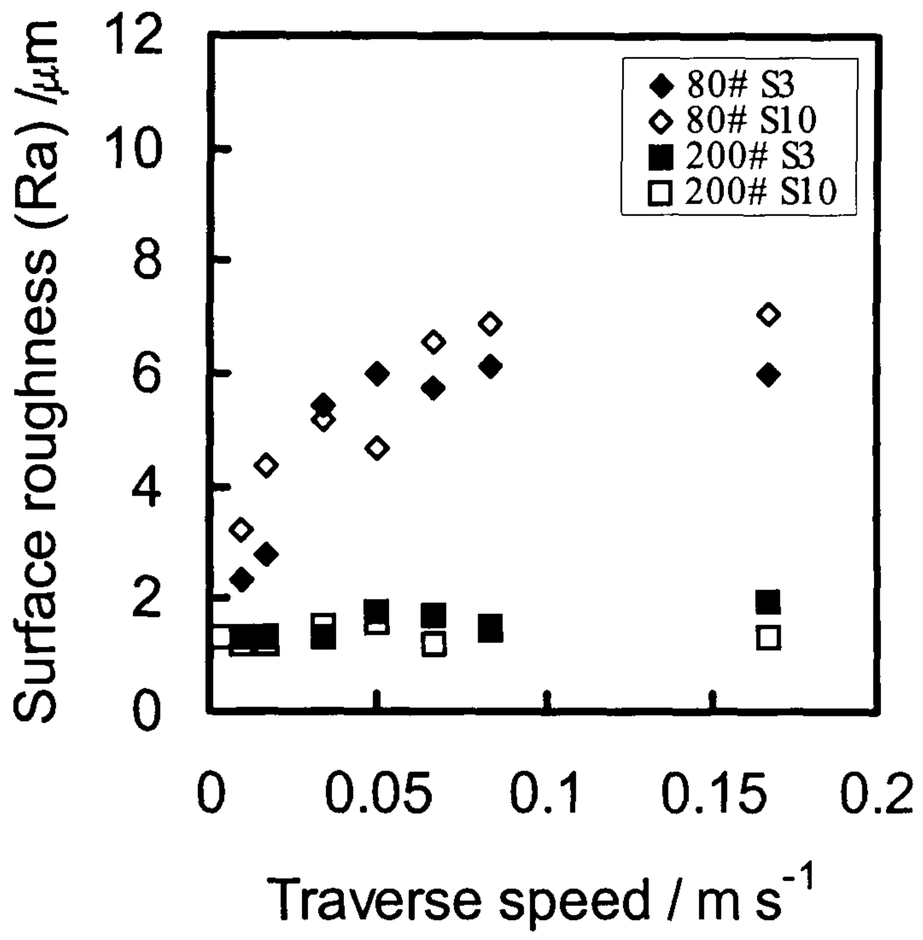

(c)

Figure 4.15 Material removal rate, surface waviness and roughness developed during AWJ-CDM of Ti6Al4V as a function of jet traverse speed, with stand off distances (as indicated in the legend) of 3 and 10 mm; Water pressure 137.9 MPa (20 000 psi), jet impingement angle 90°. (a) Material removal rate developed when milling with 180 μm (80#) and 75 μm (200#) garnet grit. (b) Surface waviness developed when milling with 180 μm (80#) and 75 μm (200#) garnet grit. (c) Surface roughness when milling with 180 μm (80#) and 75 μm (200#) garnet grit.

To examine industrially relevant milling of large areas, the influence of jet overlap or increment and lateral passing was investigated. Fig. 4.16a shows material removal rate as a function of number of lateral passes of the nozzle for two different jet increments across the work piece to mill a wide slot. Milling was conducted once across the workpiece with a prescribed milling pattern (Fig. 3.5) using two grit sizes, at high jet traverse speed. It can be seen that the material removal rate for both grit sizes was approximately constant with number of passes, and that the employment of small jet increments resulted in a modest increase in material removal rate. Milling with small sized grit size as expected results in a significant reduction in material removal rate. For the case of milling once with the described milling pattern (Fig. 3.5), grit size is the controlling factor on waviness (Fig. 4.16b) and roughness (Fig. 4.16c) which are independent of jet increment and number of lateral passes. However, this is not the case for multiple passes of the jet over the same milling pattern. Fig. 4.17 shows development of roughness and waviness when milling a wide slot with a large 180 μm (80#) and a small 75 μm (200#) garnet grit. Multiple passes of the jet over the same area result in a larger increase in waviness (Fig. 4.17a) than that seen earlier with multiple jet passes over the same single line (Fig. 4.9). This is as a result of jet increment exaggerating the waviness. Multiple passes of the jet (Fig. 4.17b) have no significant influence on roughness (as seen earlier in Fig. 4.10 for milling of a single line), for milling large areas. Moreover, water jet pressure also has no significant influence on roughness, (Fig. 4.18b) but does have a strong influence on waviness. Fig. 4.18a shows that an increase in water jet pressure results in an increase in waviness.

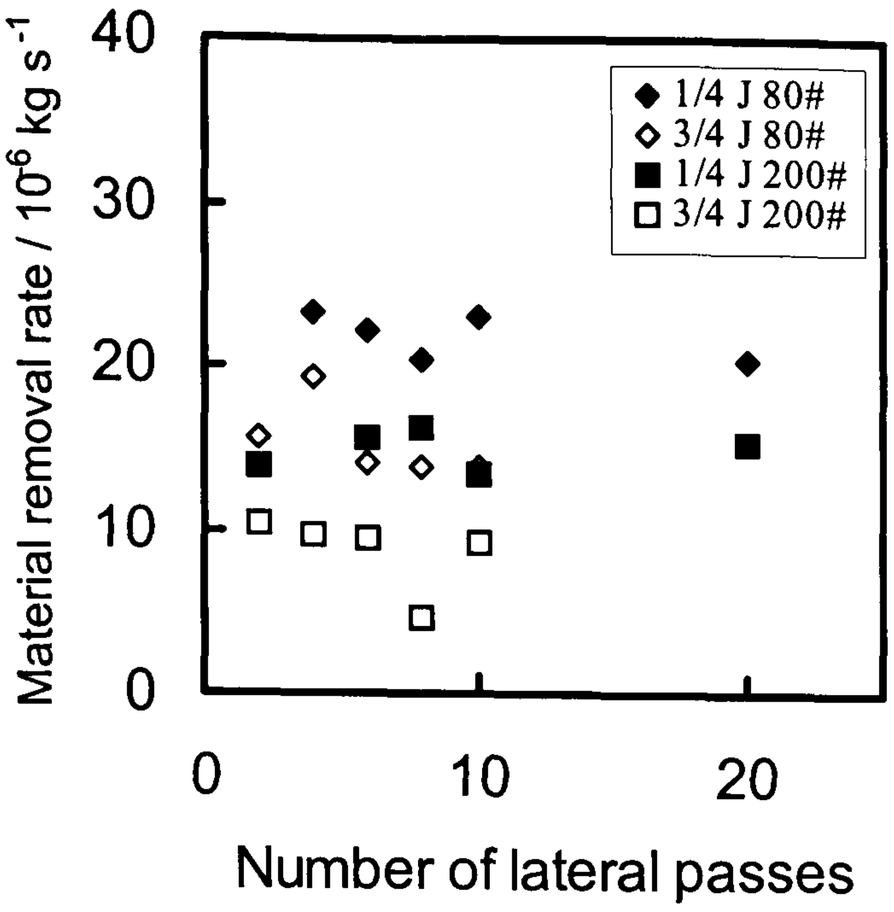

(a)

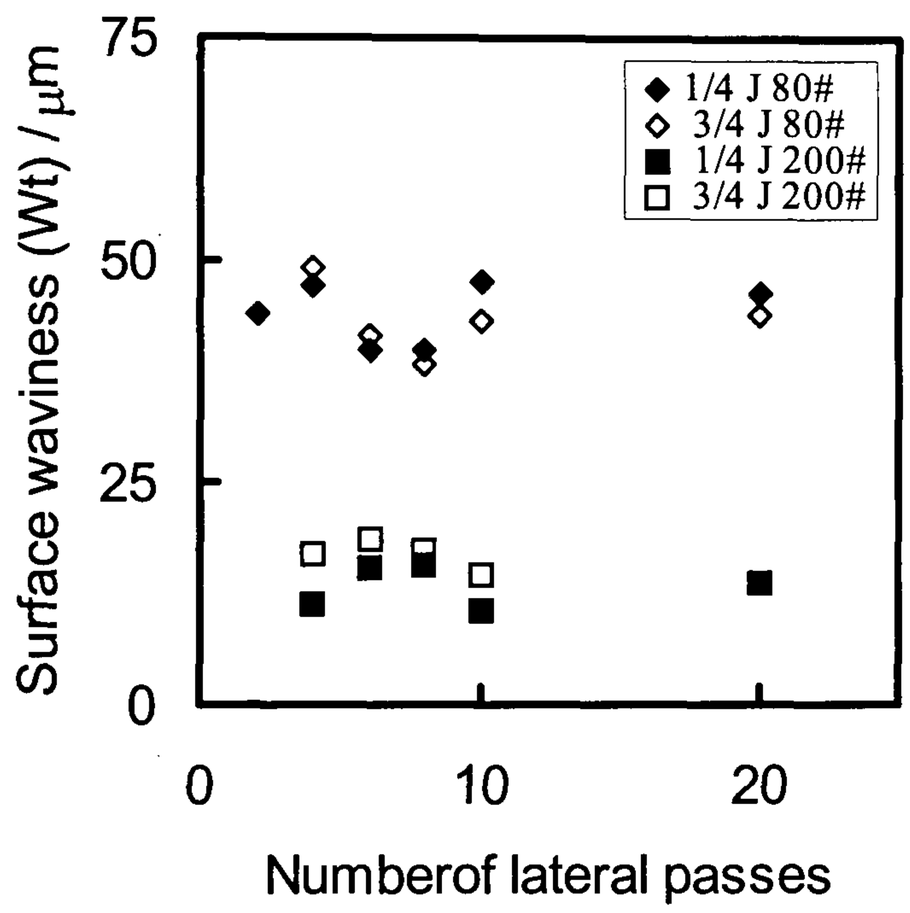

(b)

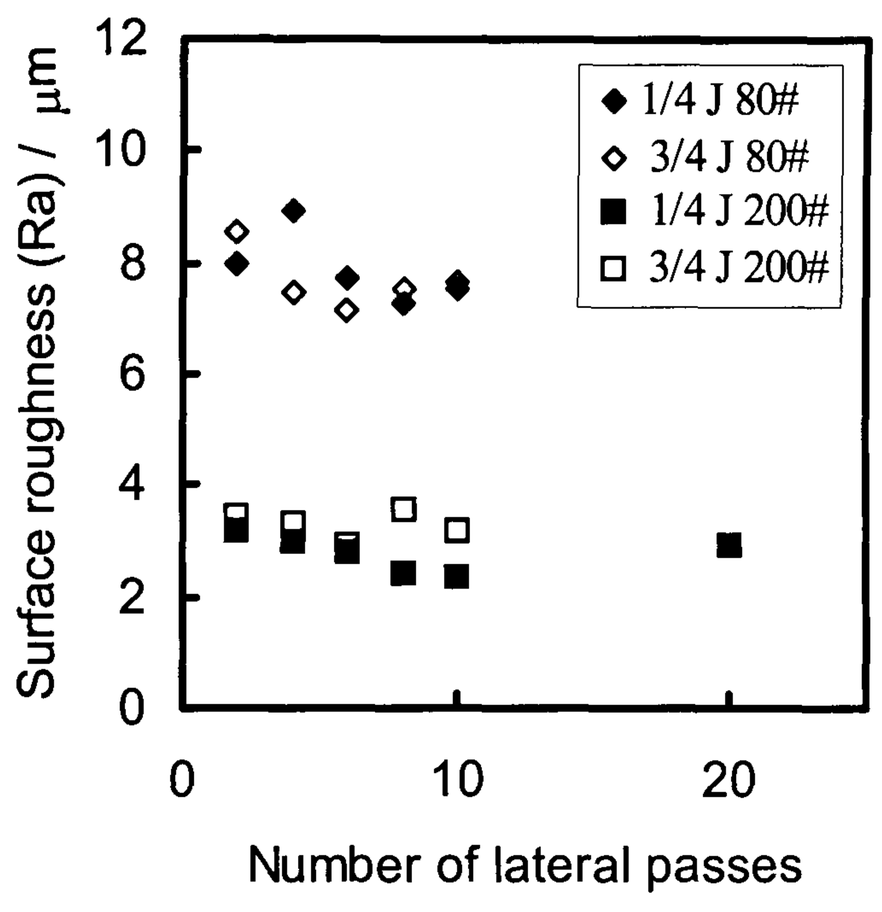

(c)

Figure 4.16 Material removal rate, surface waviness and roughness developed during AWJ-CDM of Ti6Al4V as a function of lateral jet passes, with high traverse speed (0.166 m s^{-1}) and 180 µm (80#) and 75 µm (200#) garnet grit; water pressure 137.9 MPa (20 000 psi), stand off distance 3 mm, jet impingement angle 90°. (a) Material removal rate developed when milling with jet increments of ¼ and ¾. (b) Surface waviness developed when milling with jet increments of ¼ and ¾. (c) Surface roughness developed when milling with Jet increments of ¼ and ¾.

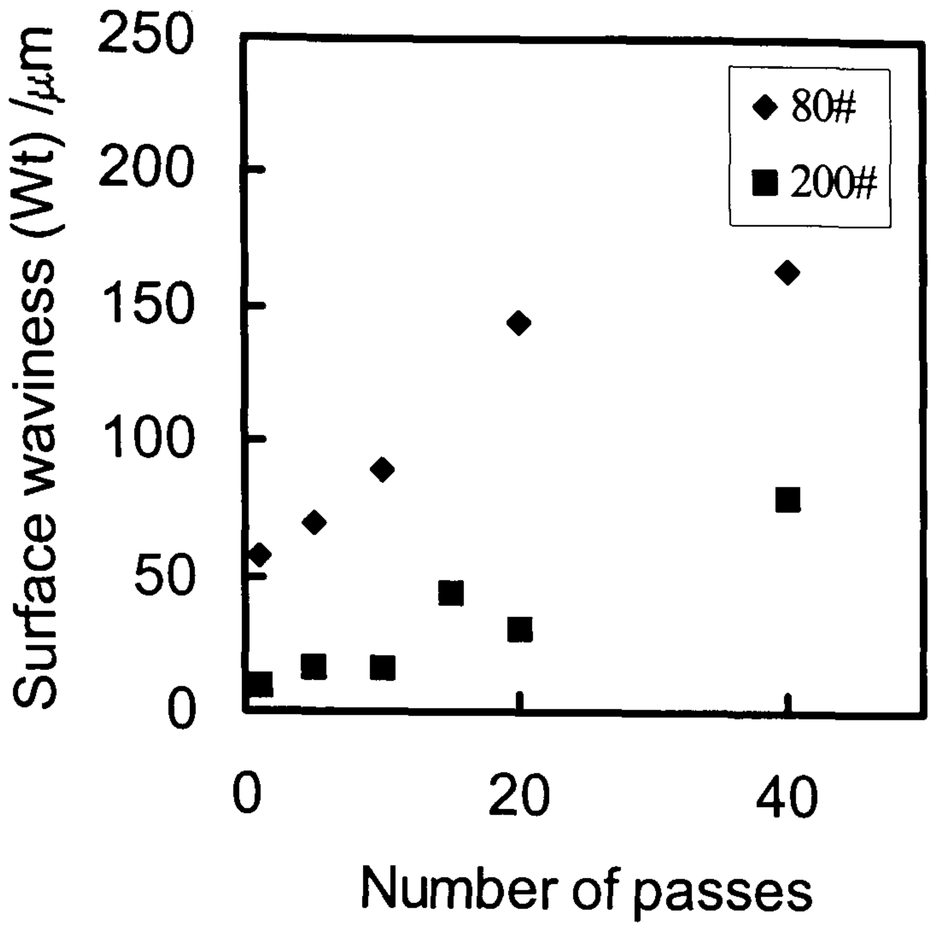

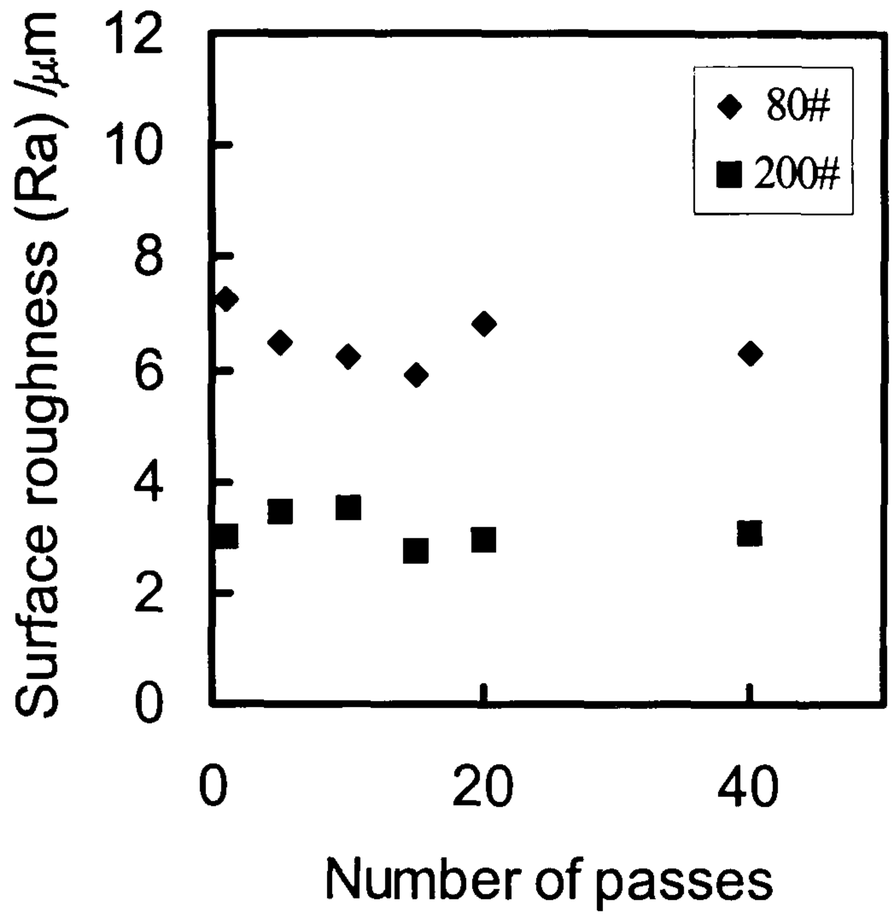

(a) **(b)**

Figure 4.17 Surface waviness and roughness developed during AWJ-CDM of Ti6Al4V as a function of number of depth passes of the jet, milling at high traverse speed (0.166 m s^{-1}): Water jet pressure 137.9 MPa (20 000 psi); stand off distance 3 mm, jet impingement angle 90°; with 180 μm (80#) and 75 μm (200#) garnet grit; (a) Surface waviness developed when milling with ¼ jet increment. (b) Surface roughness developed when milling with ¼ jet increment.

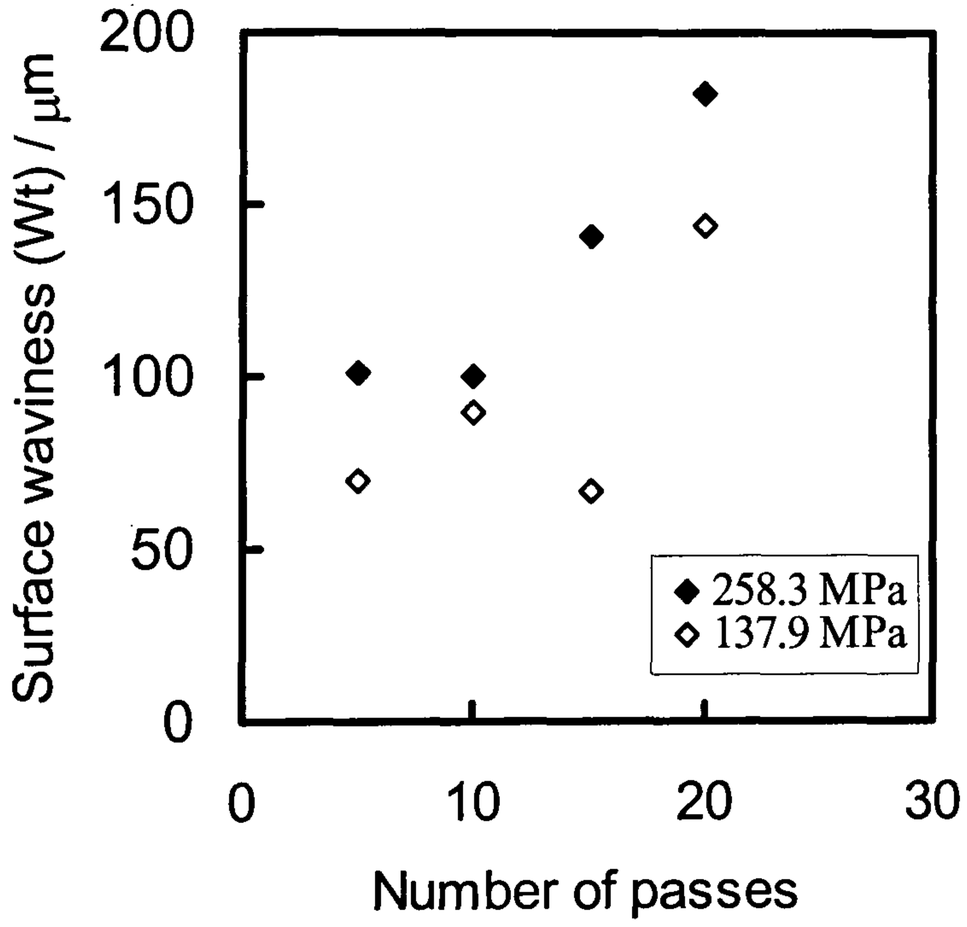

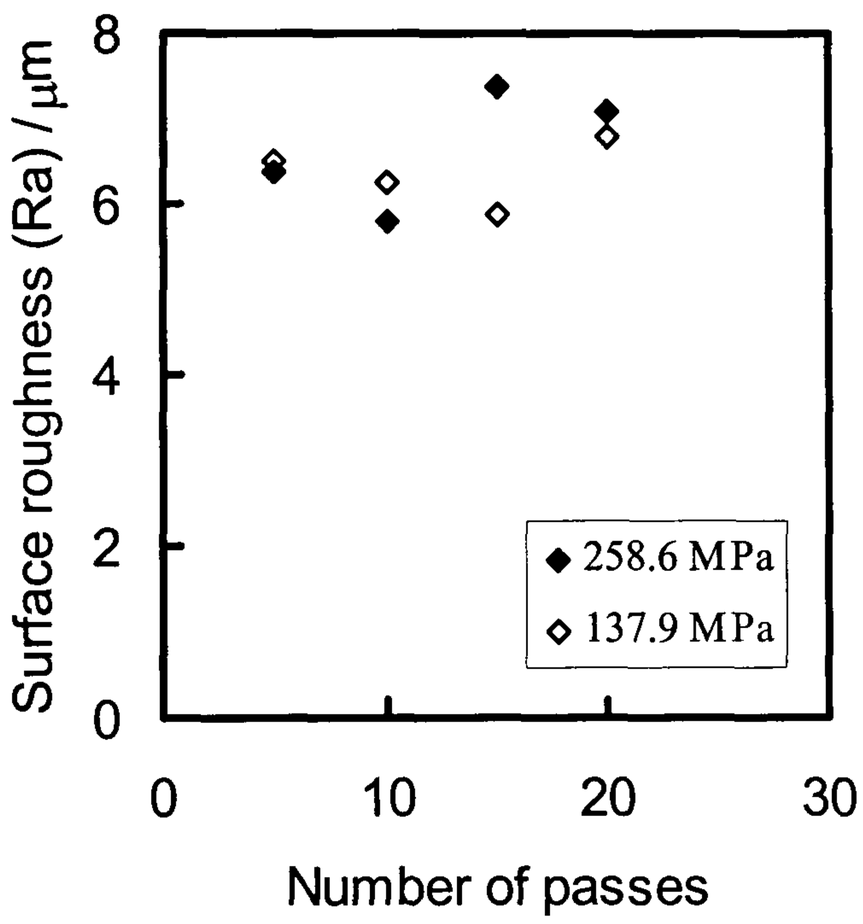

(a) **(b)**

Figure 4.18 Surface waviness and roughness developed during AWJ-CDM of Ti6Al4V as a function of number of depth passes of the jet, milling at high traverse speed (0.166 m s^{-1}): Water jet pressures 258.6 and 137.9 MPa (37 500 & 20 000 psi), stand off distance 3 mm, jet impingement angle 90°, jet increment ¼ J. (a) Surface waviness developed when milling with 180 μm (80#) garnet grit; (b) Surface roughness developed when milling with 180 μm (80#) garnet grit.

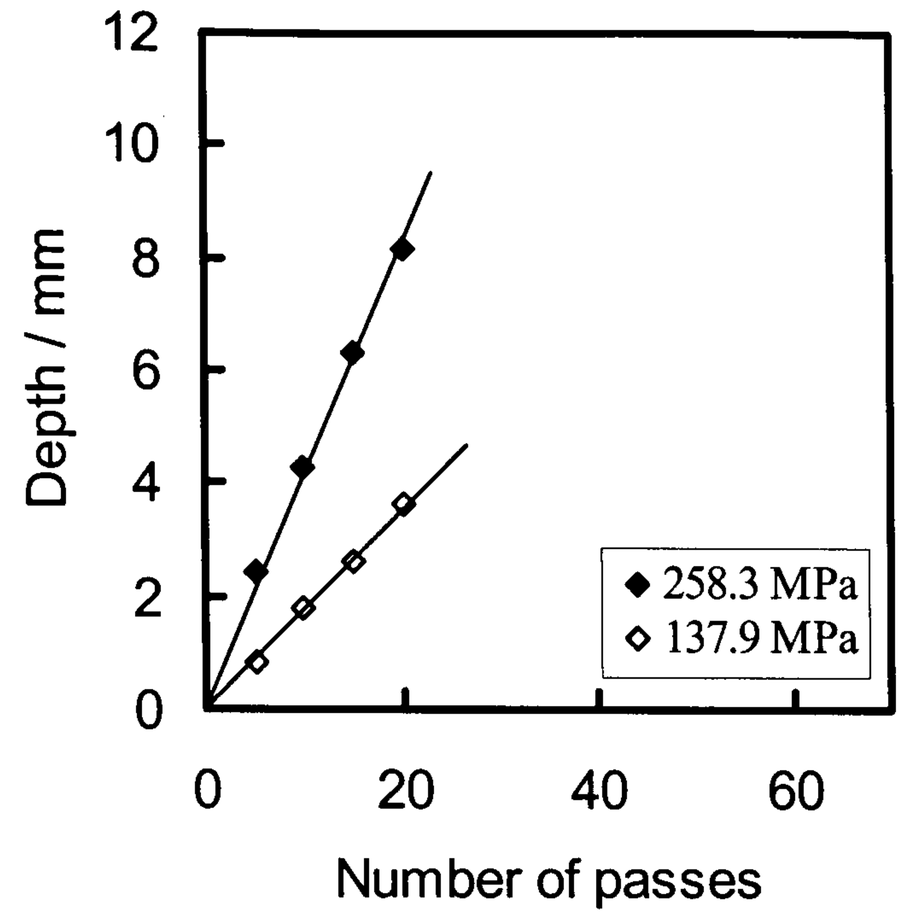

(a)

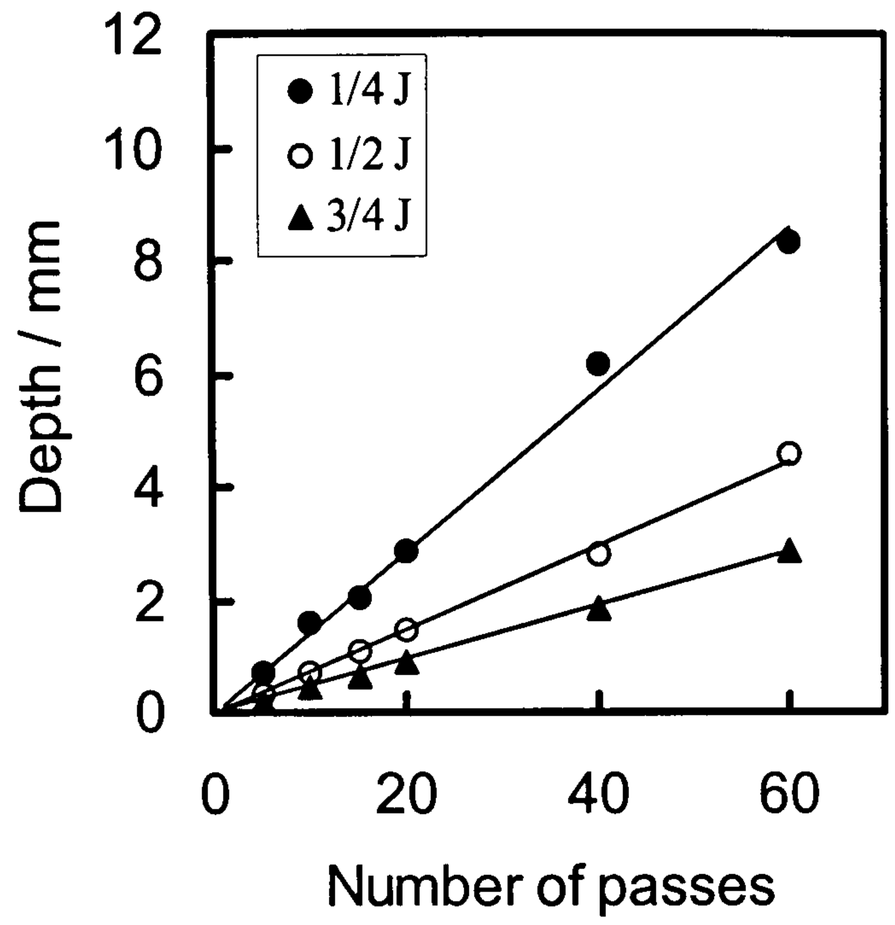

(b)

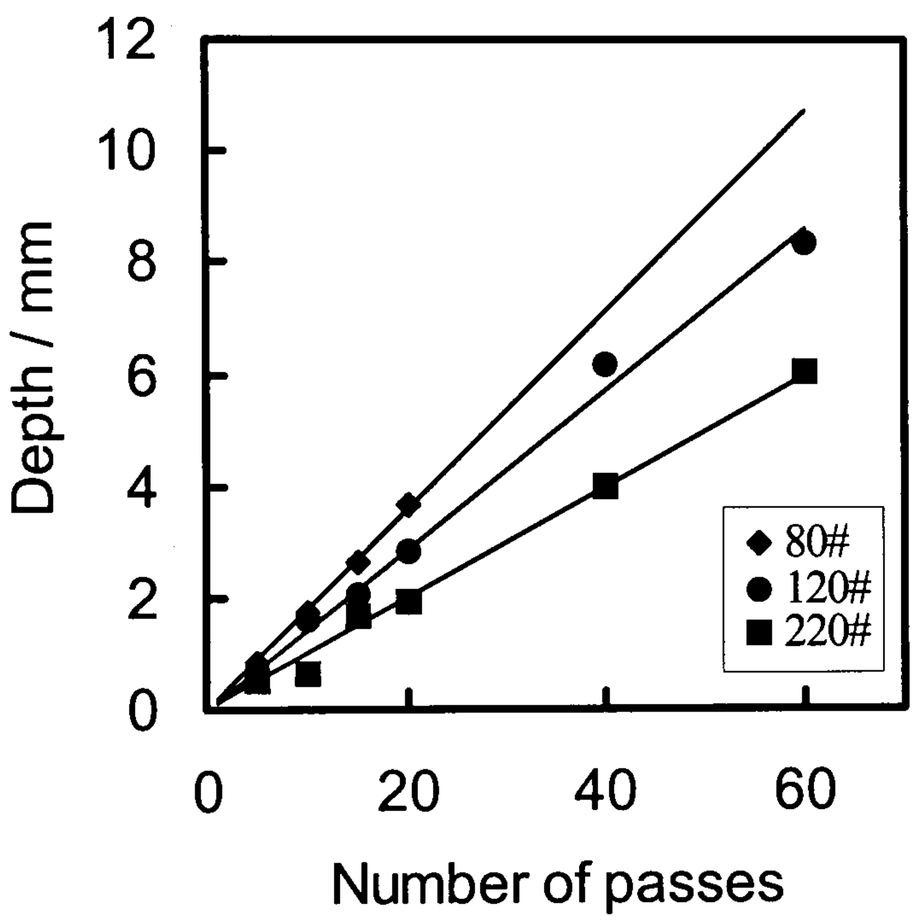

(c)

Figure 4.19 Depth as a function of jet passes during linear AWJ-CDM of Ti6Al4V high traverse speed 0.166 m s^{-1} (10 000 mm min^{-1}). (a) Depth developed when milling at set water jet pressures 258.6 MPa and 137.9 MPa (37 500 & 20 000 psi); stand off distance 3 mm, jet impingement angle 90°, Jet increment set at ¼ J with 180 μm (80#), garnet grit. (b) Depth developed with 100 μm (120#) garnet grit when milling under increasing jet increment ¼ - ¾ J. (c) Depth developed at a set jet increment of ¼ J when milling with 180 μm (80#), 100 μm (120#) and 75 μm (200#) garnet grit

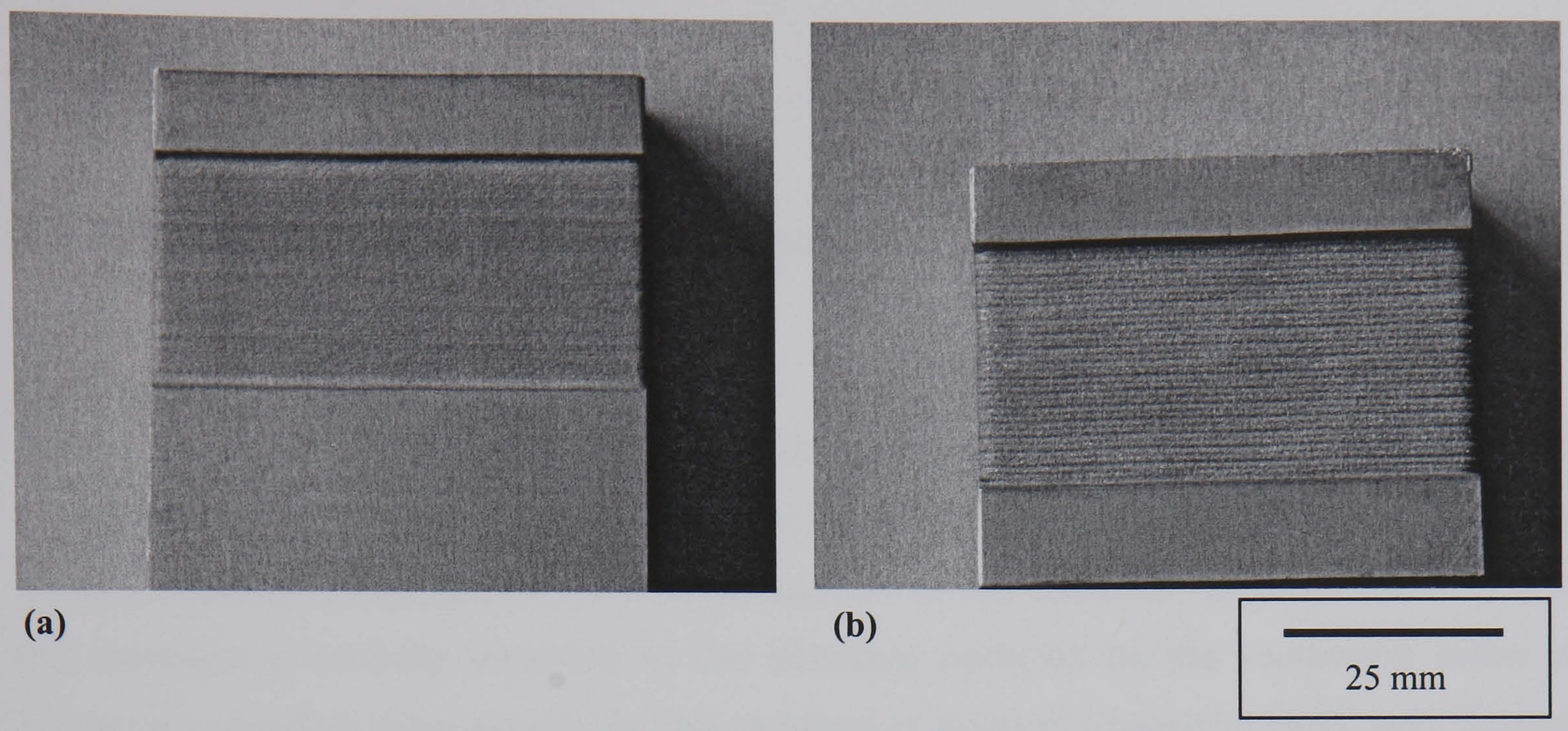

Figure 4.20 Macrographs showing the development of lay marks when AJW-CDM Ti6Al4V alloy: High traverse speed (0.166 m s^{-1}): with 180 μm (80#) garnet grit; and increasing jet increment: Water jet pressure 137.9 MPa (20 000 psi), stand off distance 3 mm, jet impingement angle 90°. (a) Jet increment ¼ Jet diameter; (b) Jet increment ¾ Jet diameter.

A linear relationship was observed between the depth of cut and number of passes of the jet when milling large areas with high and low water jet pressures (Fig. 4.19a), small and large jet increments (Fig. 4.19a), large and small grit sizes (Fig. 4.19a). One dominant feature arising from the investigation of jet increments (irrespective of multiple passes of the jet, water jet pressure and grit size employed to achieve the required depth) has been the presence of laymarks. Laymarks are surface features or marks left behind by the manufacturing process. Fig. 4.20 shows the development of laymarks when high speed milling with the described milling pattern (Fig. 3.5) with multiple passes of the jet. It can be seen that a larger jet increment resulted in more pronounced lay marks (Fig. 4.20b). Lay marks were observed with both grit sizes.

4.2.2 Discussion.

4.2.2.1 The influence of water pressure and stand off distance on material removal rate.

An increase water pressure results in an increase in material removal rate; the increase in material removal rate is observed for both grit sizes examined (Fig 4.13) and all traverse speeds investigated. This enhancement of the material removal rate is due to the increase in velocity imparted to the abrasive particles by the increased water jet pressures allowing more energy for the purpose of erosion (Hashish [1999] and Ojmertz [1997a]). Fig. 4.15 shows that the material removal rate decreased by a third as the stand off distance was increased. Laurinat et al. [1993] suggest that the material removal rate is relatively insensitive to stand off distance between 2 mm and 5 mm and is at a maximum in this region; with stand-off distances above 5 mm, the material removal rates decrease [Hashish, 1987, Ojmertz, 1997a], as also demonstrated in this research. The reduction in material removal rate is a result of the drop jet particle velocity as the stand off distances increases [Hori 1990].

4.2.2.2 The influence of water pressure and stand off distance on roughness and waviness.

When low speed milling, water pressure has a strong influence (a six fold increase) on waviness and a lesser influence (a 50% increase) when high speed milling where waviness is generally lower as a consequence of the higher traverse speed (Fig. 4.14b).

Since an increase in water pressure promotes an increase in material removal rate it will also promote deeper aberrations as the grit penetrates deeper into the material. This can be seen in Fig. 4.14a and Fig. 4.14b, where the surface waviness increased as water jet pressure increased for all jet traverse speeds and grit sizes investigated.

Fig. 4.14c shows that water jet pressure has no influence on the surface roughness at low jet traverse speeds, (below 0.016 m s^{-1} (1 000 mm min^{-1})) but does have a slightly stronger influence at high traverse speed (0.166 m s^{-1} (10 000 mm min^{-1})). During low speed milling, the water jet is diverted along the bottom of the kerf, where microcutting is prevalent. Therefore, little increase in roughness is observed. At high traverse speed where particle - substrate impact occurs at normal angles, the particle performs as an

indenter (Fig. 2.1 chapter 2) with the depth and area of indentation dependent on the shape of the particle and its velocity. Particle impacts at low velocity (low water jet pressures) result in small indentations in the target material. With small shallow indentations, the surface roughness is reduced. At higher particle velocities (high water jet pressures), where the indentations areas are correspondingly deeper, the surface roughness increases as observed in Fig. 4.14c.

Fig. 4.15b and 4.15c show that the stand off distance has little influence on the waviness and roughness. Hashish [1987] suggests that an increase in stand off distance results in a wider, shallower kerf as the water jet impingement area increases (Fig. 2.15). This, according to Horri [1990] is due to a reduction in the water jet velocity and the change in the jet velocity profile as the stand off distance increases. Stand off distance controls particle impact velocity, and reduces the aberrations and therefore the waviness is reduced. At high traverse speeds where the particle performs as an indentor at normal jet angles, waviness and roughness may be reduced by increasing stand off distance due to the formation of shallower craters as a result of lower impact velocities [Li et al. 1996b]. However, the experimental data suggest that while this may be the case for waviness (Fig. 4.15b) where a slight decrease occurs in high speed milling, for roughness, (Fig. 4.15c) this is not the case since the roughness increased slightly when high speed milling.

4.2.2.3 The influence of lateral passing and jet increment on material removal rate.

Although the traverse speed and jet impingement angle are contributors to material removal by their influence on the material removal mechanism, the material removal rate can be increased as a result of mechanical movement of the water jet position. Fig 4.16a shows that small jet increments of 0.25 mm (¼ of the jet diameter) result in an approximate 30% increase in material removal rate when compared to milling with a 0.75 mm (¾ of the jet diameter) increment. Ojmertz [1997a] [Hashish, 1998a], also observed an increase in material removal rate when the jet increment was reduced when milling aluminium as did Paul et al. [1998] when milling a square pocket in steel. The increase in material removal rate arises from the fact that the water jet cuts deeper on ¼ jet increment. Fig. 4.21 shows that 25% of the jet diameter of the water jet is cutting on the edge of new material, while 75% of the jet diameter is cutting the bottom of previously machined material for three jet increments. Material removal is time dependent and for small jet increments the water jet spends more time over previously

machined areas removing more material at the bottom of the previously cut kerf than the edge of new material. With the ¾ jet increment, the water jet spends less time cutting the previously machined surface with less of the water jet (25% area) and so removes less material, even though 75% of the water jet diameter is cutting on the edge of unmachined material. Fig. 4.16a suggests that edge cutting with small increments is more efficient than material removal than larger jet increments. Ojmertz [1997a] suggests an alternative solution that the part of the water jet that is exposed to the previously cut surface material causes more pronounced water jet interaction with the surface resulting in an accelerated rate of penetration.

An increase in number of *lateral passes* (cf. Fig. 3.5) to increase slot width results in a constant material removal rate for both jet increments and grit sizes (Fig. 4.16). The increasing lateral passes manufacture a flat geometric feature known as a slot. The constant material removal rate suggests a consistent material removal process thus allowing depth control.

4.2.2.4 The influence of lateral passing and jet increment on waviness and roughness.

In the case of milling once with the prescribed milling pattern (Fig. 3.5), jet increment and lateral passes have no strong influence on surface waviness or roughness (Fig 4.16b and Fig. 4.16c). Ojmertz [1996, 1997a] also observed no significant increase in waviness between jet increments of 0.25 mm and 0.75 mm (¼ - ¾ jet increment). However, Fig. 4.17 shows that an increasing jet increment does have a strong influence when milling with multiple passes of the jet over the same milling pattern (to increase depth of the milled area). In Fig. 4.17a it can be seen that as the depth increases by the employment of multiple passes of the jet, waviness increased rapidly for small jet increments. Moreover, in Fig. 4.17b it can be seen that multiple passes of the jet have no strong influence on roughness which remains constant and this was seen previously with multiple passes of the jet over a single line. Initially the specimen surface is smooth and flat; milling once with the prescribed milling pattern to mill a large area results in the development of laymarks (Fig. 4.20) which are recorded in Fig. 4.16. The multiple passes of the jet to increase depth exaggerate the laymarks leading the rapid rise in waviness (Fig. 4.17a). Large jet increments as in Fig. 4.20b result in more pronounced lay marks than those produced by small jet increments (Fig. 4.20a); these lay marks are a result of the AJW-CDM process and are the aberrations responsible for the significant increase in waviness.

Figs. 4.16 and 4.17 demonstrate that to minimise laymarks (Fig. 4.20a) and to be able to mill large areas with low waviness and roughness requires high speed milling with low water jet pressure using small sized grit and small jet increments.

Laymarks were also observed by Hashish [1998a]. Questions have been raised concerning their role as stress raisers in the initiation of fatigue particularly if the laymarks are normal to the direction of cyclic loading [Leverant et al.1979].

Although surface waviness increased rapidly as the depth increased, the linearity in depth observed earlier when employing multiple passes of the jet over a single line is still observed when milling large areas with small and large jet increments (Fig. 4.19b). This linearity in depth is also observed when milling with any grit size (Fig. 4.19c) and also under increased water jet pressures (Fig. 4.19a). This linear dependence has also been seen by Hashish [1998a]. Due to changes in dominant mechanism as discussed earlier, the depth of cut is always larger with the smaller jet increment and high water jet pressures. More significantly, the depth to which material is removed is again shown to be much higher for larger grit sizes.

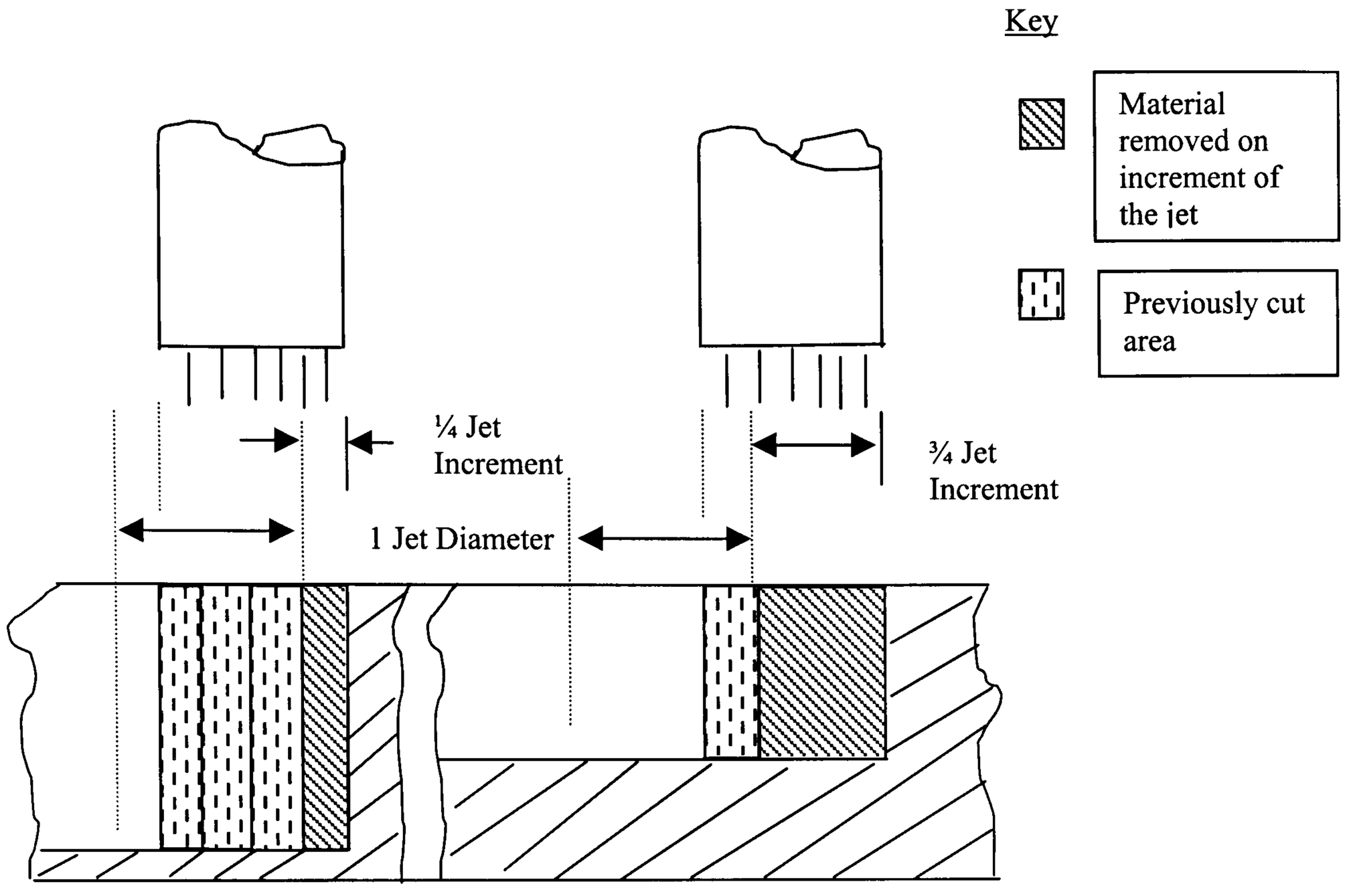

(a)

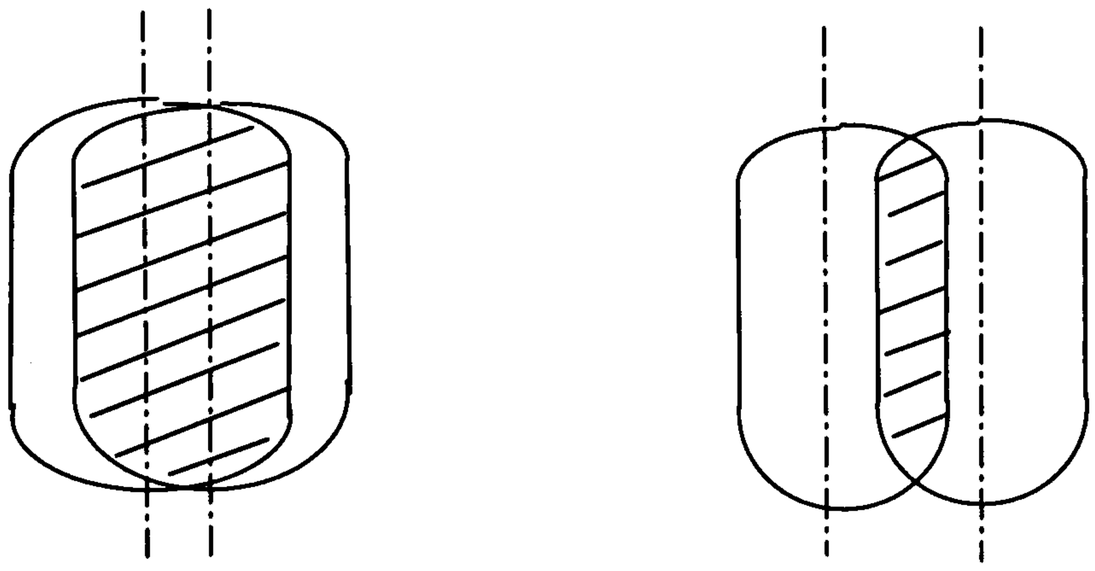

¼ Jet increment.
Area overlapped:
75%.

¾ Jet increment.
Area overlapped:
25 %.

(b)

Figure 4.21 Jet increments of ¼ and ¾ Jet diameter indicating areas of overlap when AJW-CDM: (a) Sectional view. (b) Plan view.

4.3 Role of jet impingement angle on process characteristics.

4.3.1 Results.

Fig. 4.22 shows the effect of jet impingement angle on material removal rate and surface profiles for milling at a low traverse speed of 0.003 m s^{-1}. It can be seen that material removal rate (E_d) for both grit sizes is high at high jet impingement angles, irrespective of milling direction (Fig. 4.22a and 4.22b). The material removal rate is very low at the low impingement angles and peaks at around 60° for both grit sizes. Interestingly, in contrast to the work of Hashish [1998a], it is observed that the material removal rates are very similar for the two grit sizes. Fig. 4.22c shows that the surface waviness is relatively low at low jet impingement angles, but then increases rapidly at jet impingement angles above 45°. In light of these very high recorded waviness values (which make these conditions totally unsuitable for controlled-depth milling), the surface roughness was not recorded at angles greater than 45° at this traverse speed. However, at the low jet impingement angles, it was observed that the surface roughness increased with increasing impingement angle. At the low traverse speed represented in this figure, the milling direction appears to have no strong influence on material removal rate, roughness or waviness.

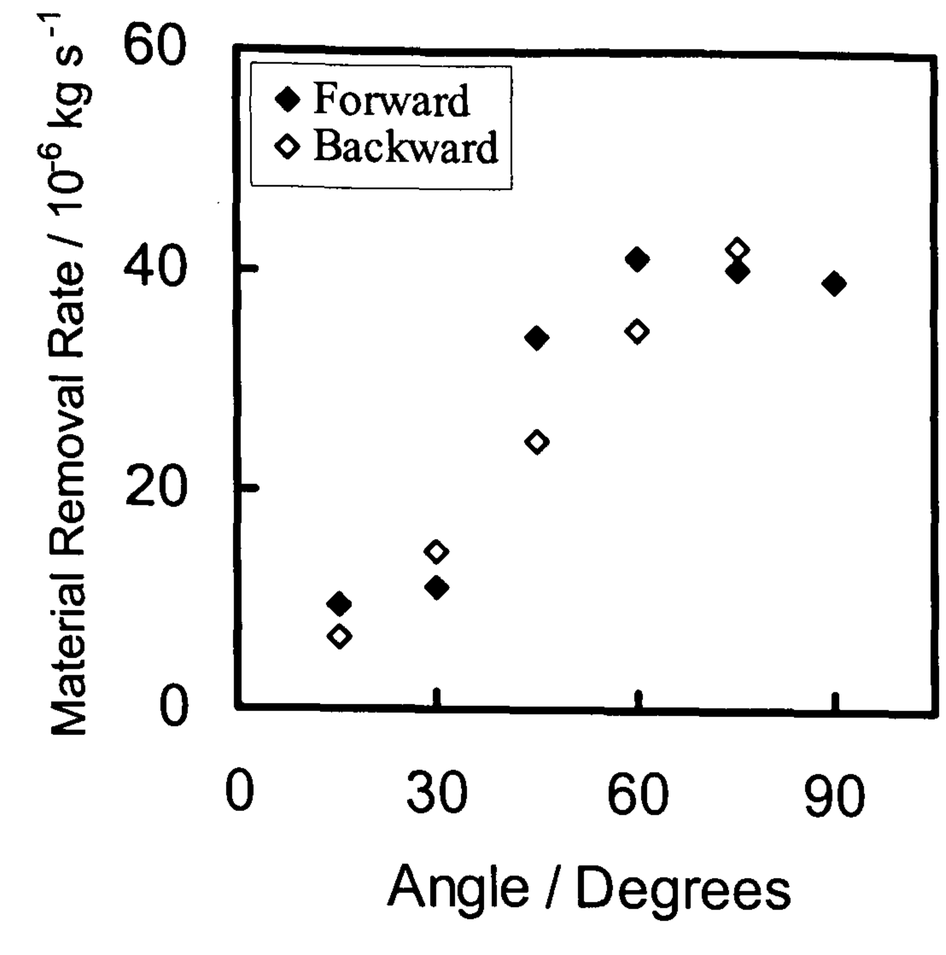

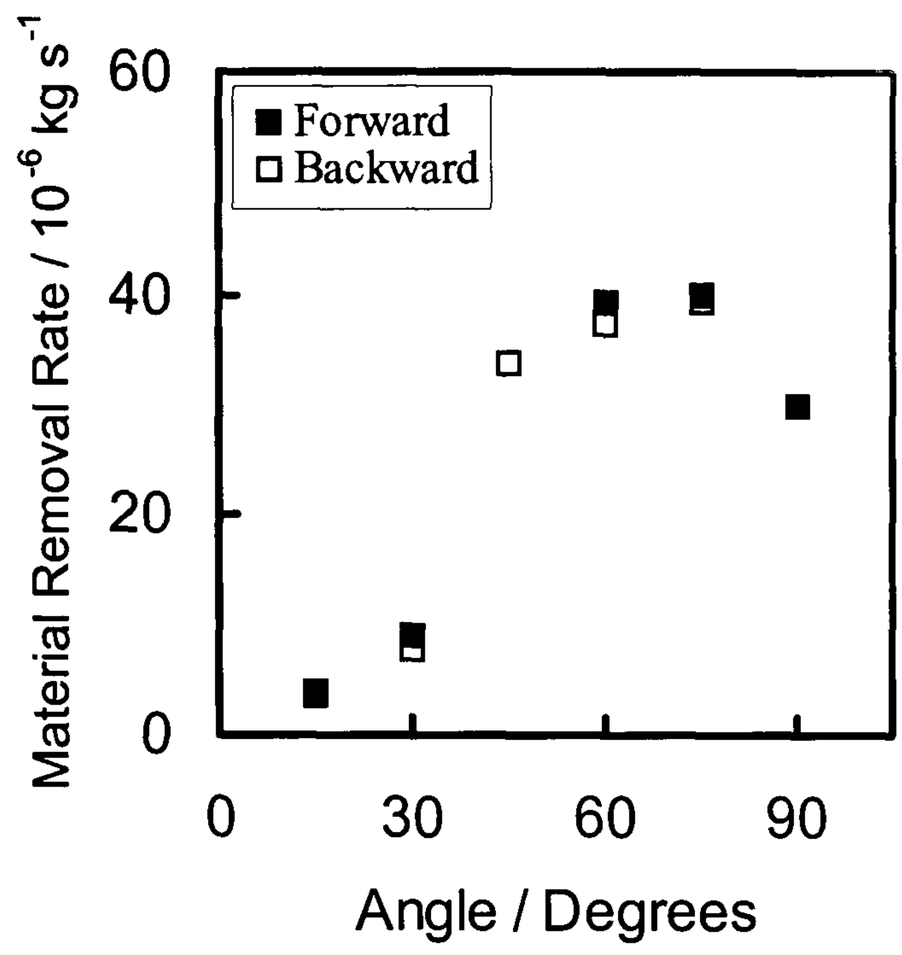

(a)

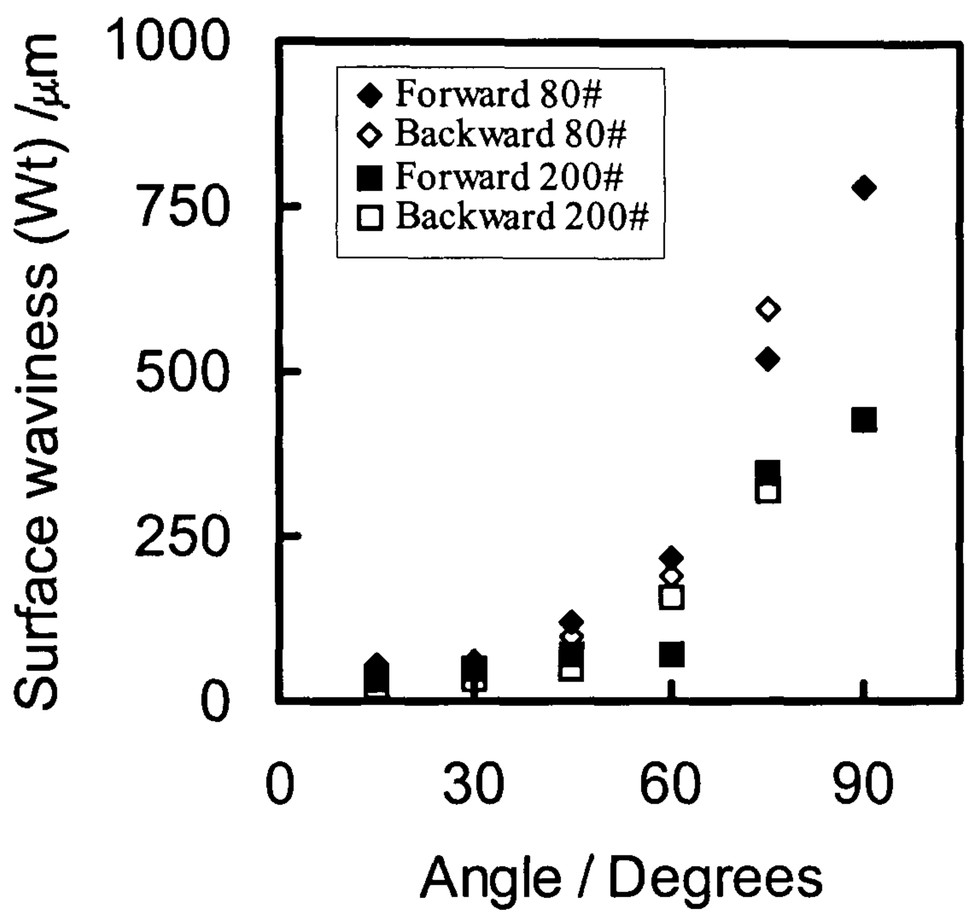

(b)

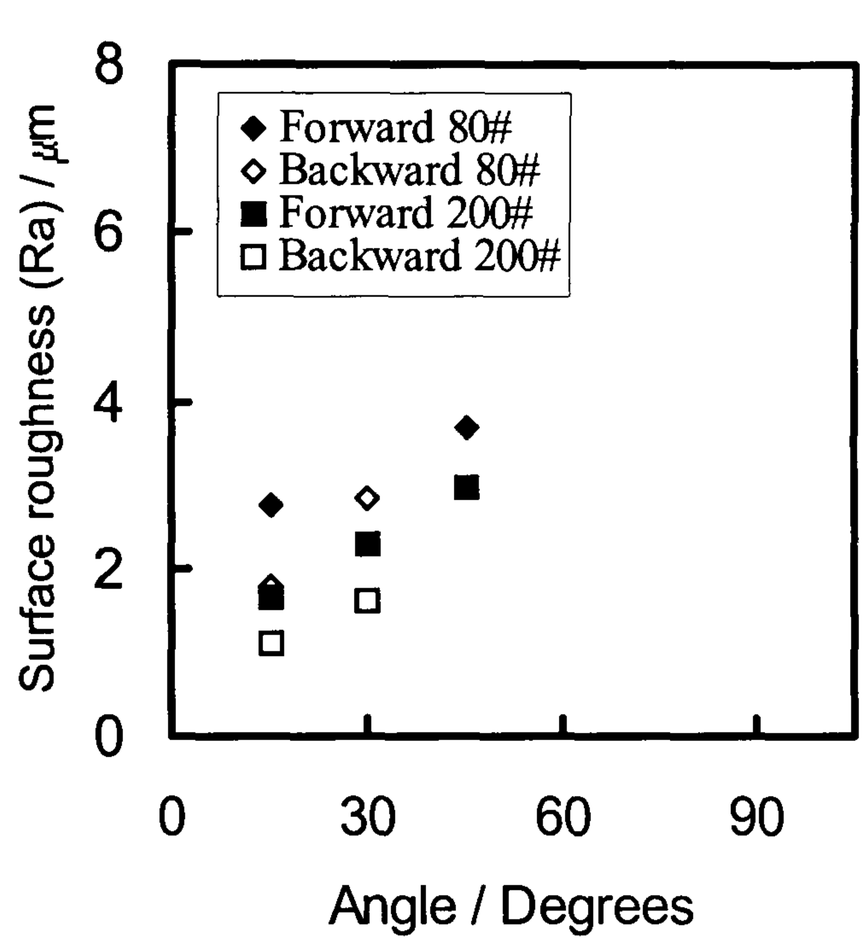

(c)

(d)

Figure 4.22 Material removal rate, surface waviness and roughness developed during AWJ-CDM of Ti6Al4V as a function of jet angle at low traverse speed (0.003 m s^{-1}); water jet pressure 137.9 MPa (20 000 psi), stand off distance 3mm. Material removal rate developed when milling (a) with 180 μm (80#) garnet grit (b) with 75 μm (200#) garnet grit (c) Surface waviness developed when milling with 180 μm (80#) and 75 μm (200#) garnet grit (d) Surface roughness developed when milling with 180 μm (80#) and 75 μm (200#) garnet grit.

Fig. 4.23 shows the effect of jet impingement angle on material removal rate and surface profiles for milling at an intermediate traverse speed of 0.0167 m s^{-1}. It can be seen that material removal rate (E_d) for both grit sizes is again low at low impingement angles and then peaks at some intermediate angle before generally falling away as the impingement angle is increased towards the normal (Fig 4.23a and 4.23b). Unlike at the lower traverse speed, there appears to be some difference in the variation of material removal rate with impingement angle with milling direction; for both grit sizes, backward milling results in a definite peak in material removal rate whereas in forward milling, the change in material removal rate over the impingement angles 30° to 90° is not as large. The surface waviness is low at the low jet impingement angles (Fig. 4.23c) and rises rapidly as the impingement angle increases. For the large grit size, the waviness continues to increase with impingement angle, but for the smaller grit size, the waviness is approximately constant over the impingement angle range 45° to 90°. There is no strong effect of milling direction on the variation of waviness with jet impingement angle. Unlike the waviness, the surface roughness (Fig. 4.23d) does not show very low values at the low impingement angles. In all cases, it rises slowly as the impingement angle increases and then decreases at normal jet impingement. Forward milling at this traverse speed results in significantly higher values of surface roughness than that developed during backward milling, the differences being greater for the larger grit size. It is clear that for this traverse speed, the milling direction does have an effect on the variation of material removal rate and surface roughness with jet impingement angle.

Fig. 4.24 shows the effect of jet impingement angle on material removal rate and surface profiles for milling at a high traverse speed of 5 m s^{-1}. In this case, milling has been conducted for 92 passes of the jet over the workpiece. In light of other research (presented in section 4.4) which demonstrated that forward and backward milling became indistinguishable processes at high jet traverse speeds, only forward milling has been considered. It can be seen that for both grit sizes (Fig. 4.24a), the material removal rate (E_d) is lowest at the lowest impingement angles and increases with increasing impingement angle to around 60°, where upon it decreases as the impingement angle moves towards the normal. Fig. 4.24b shows that low jet impingement angles result in a low surface waviness for both grit sizes; the waviness increases significantly as the impingement angle increases for the larger grit size, with the increase being much more modest for the smaller grit size. There is a distinct peak in waviness at a jet impingement angle of 60° for the larger grit size. The low jet impingement angle also results in low values of surface roughness for both grit sizes (Fig. 4.24c). For the smaller grit size, the surface roughness maintains a relatively low value for jet impingement

angles between 30° and 90° whilst for the larger grit there is an increase in roughness with jet impingement angle, with a plateau being attained at around 60°.

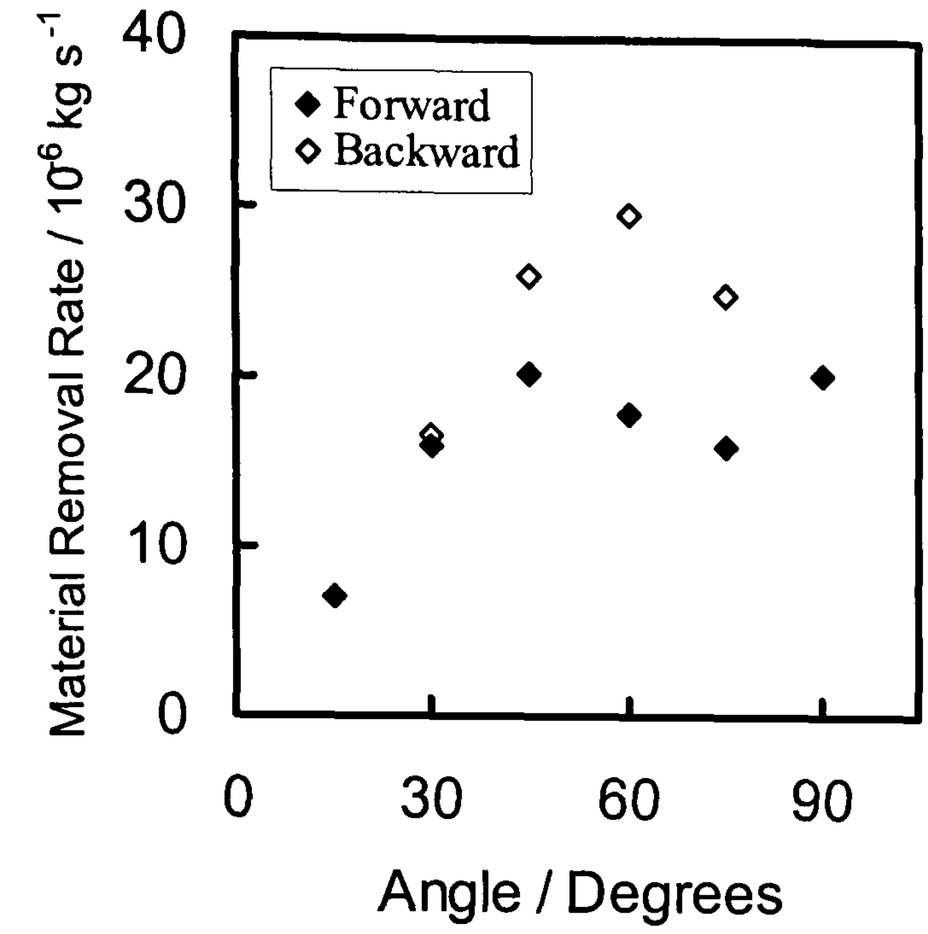

(a)

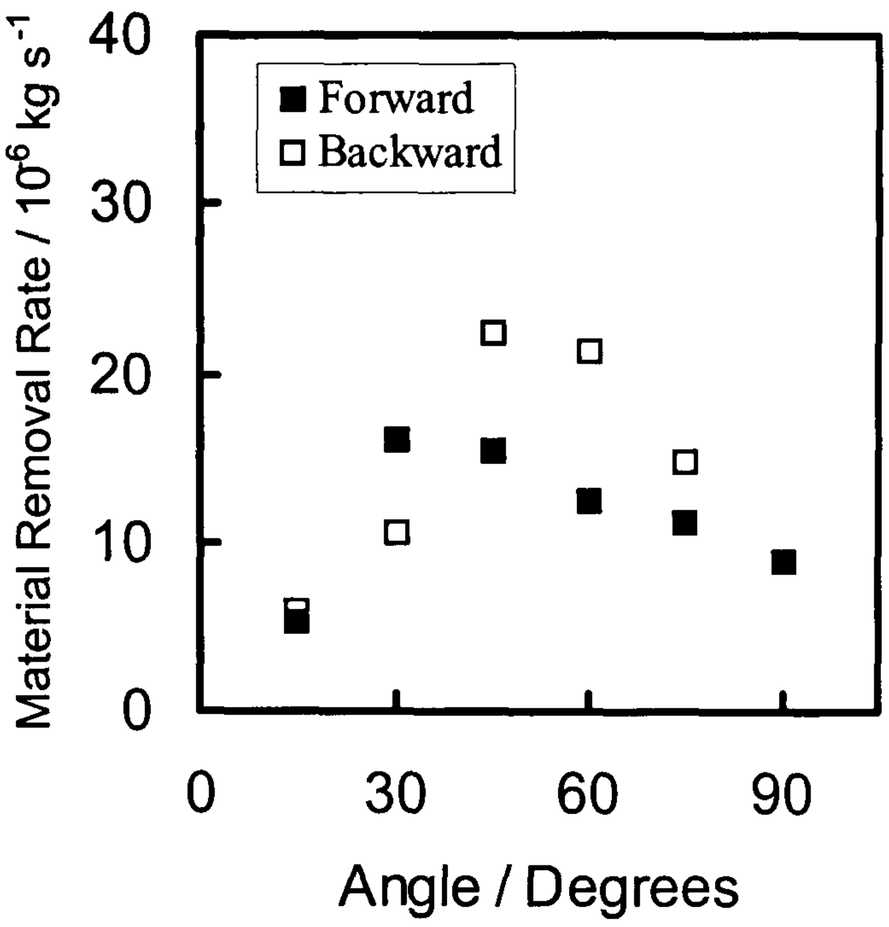

(b)

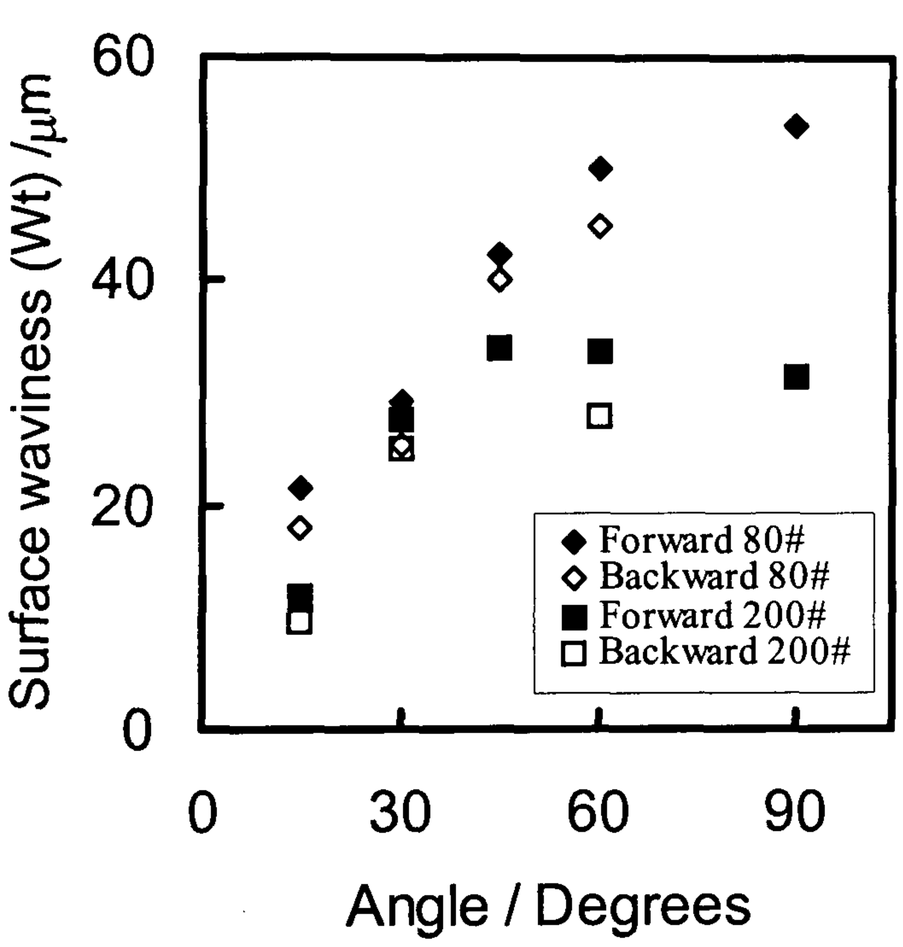

(c)

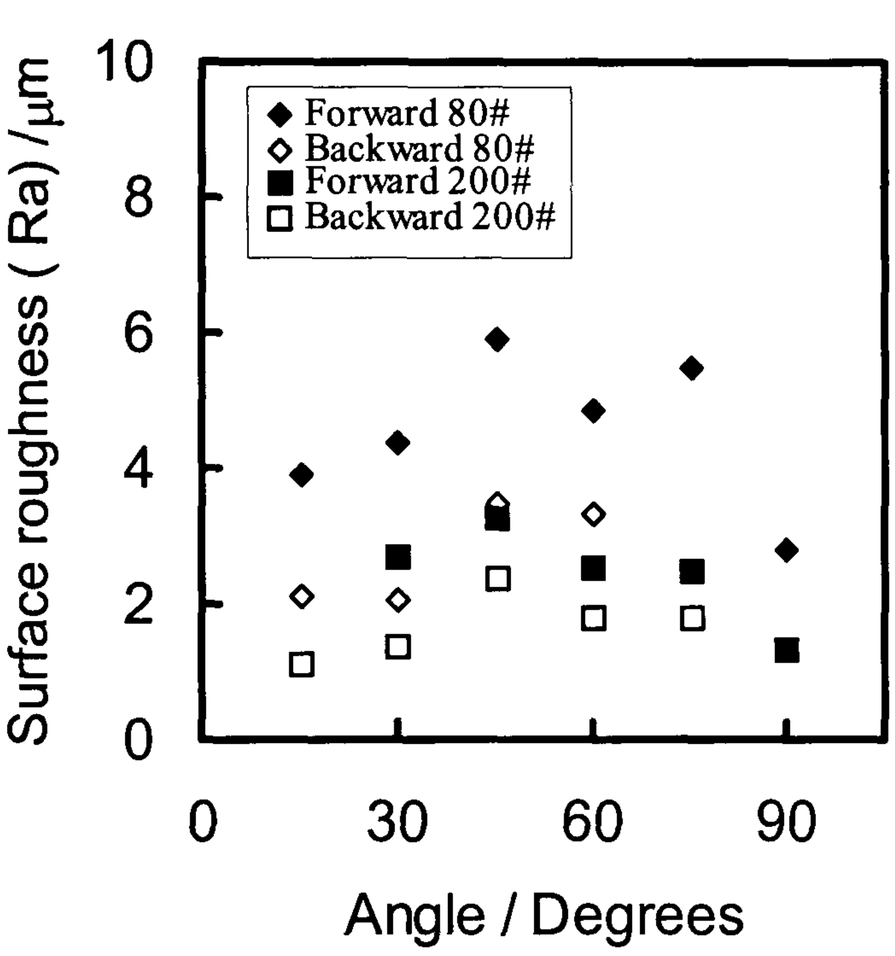

(d)

Figure 4.23 Material removal rate, surface waviness and roughness developed during AWJ-CDM of Ti6Al4V as a function of jet angle at medium traverse speed (0.0166 m s^{-1}); water jet pressure 137.9 MPa (20 000 psi), stand off distance 3mm: Material removal rate developed when milling (a) with 180 μm (80#) garnet grit (b) with 75 μm (200#) garnet grit (c) Surface waviness developed when milling with 180 μm (80#) and 75 μm (200#) garnet grit (d) Surface roughness developed when milling with 180 μm (80#) and 75 μm (200#) garnet grit.

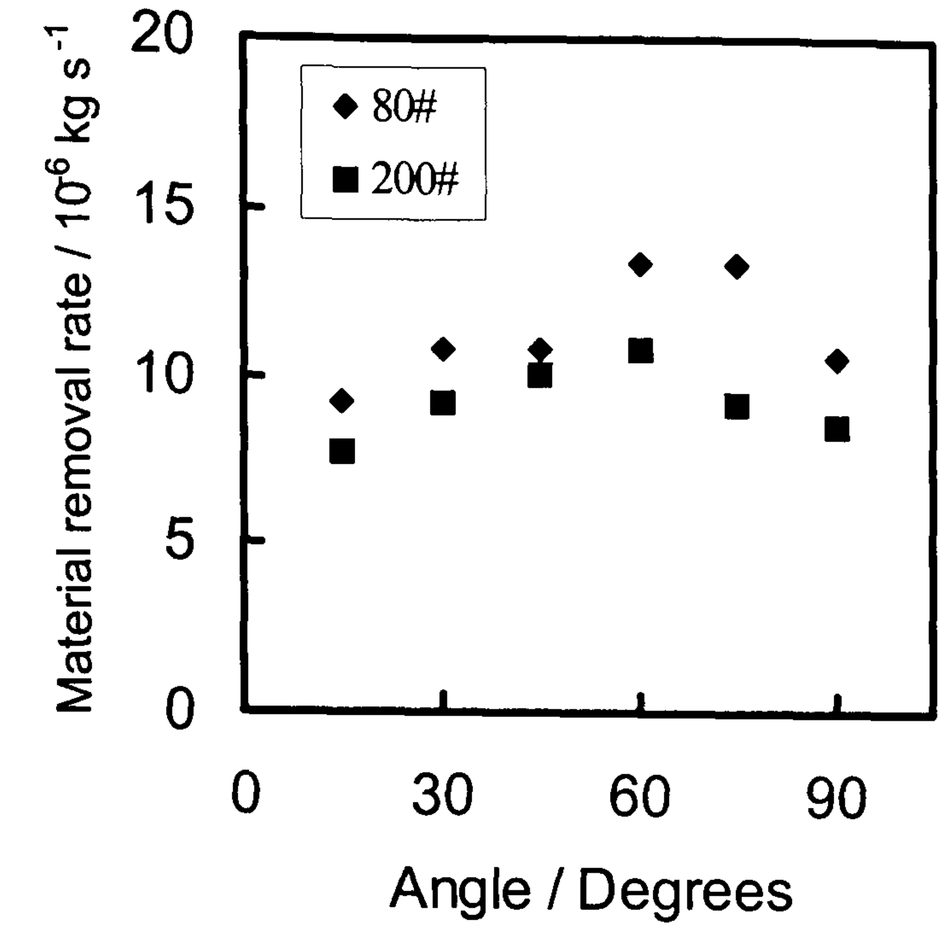

(a)

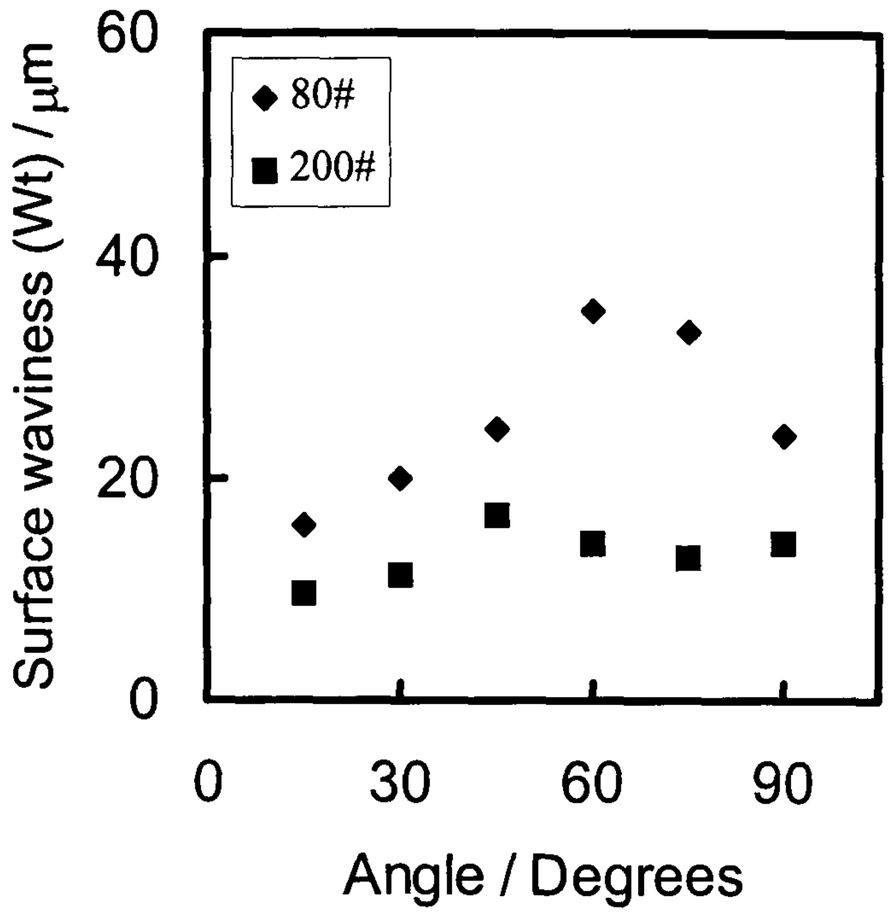

(b)

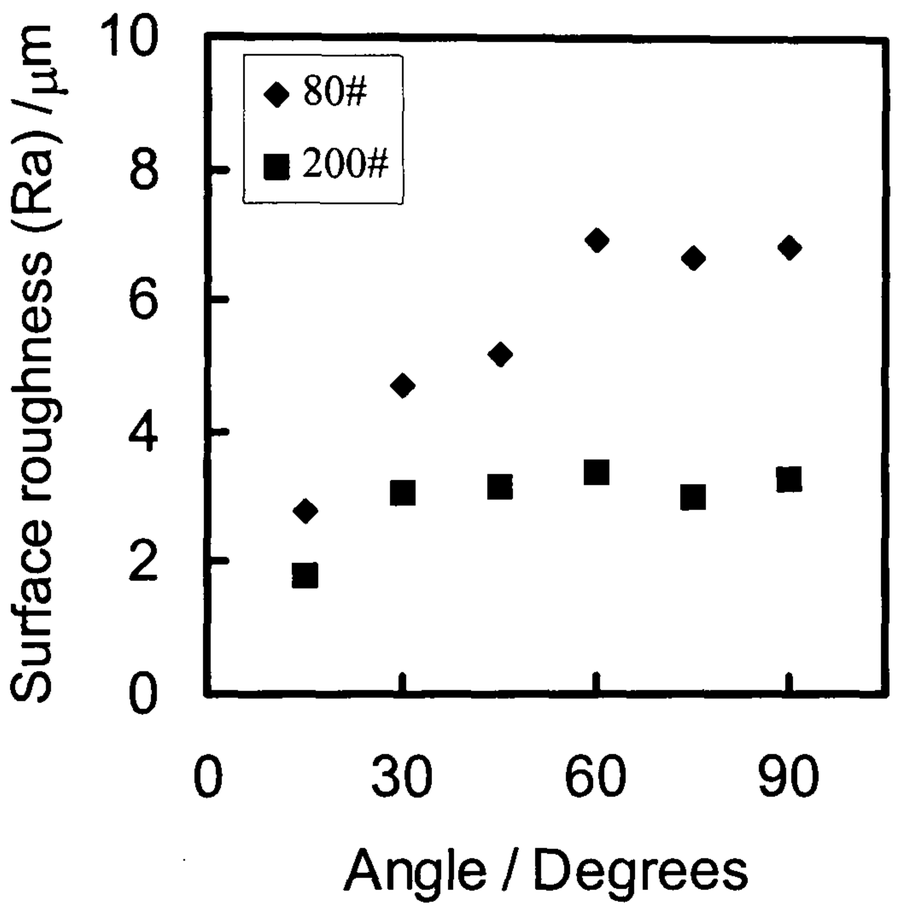

(c)

Figure 4.24 (a) Material removal rate, (b) surface waviness and (c) roughness development during AWJ-CDM of Ti6Al4V as a function of jet angle at high traverse speed (5 m s^{-1}); water jet pressure 137.9 MPa (20 000 psi), stand off distance 3mm: with 180 µm (80#) garnet grit and 75 µm (200#) garnet grit and 92 jet passes.

To examine the variations of material removal rate, surface waviness and roughness with number of passes of the jet (and thus amount of material removed), experiments were conducted at the high jet traverse speeds at two jet impingement angles. The high traverse speed was chosen as the most promising for development of low values of surface roughness and waviness required from a milling process. Instead of the milled area being a single track over which the jet is passed a number of times, a more industrially relevant case of a slot 10 mm wide was milled. Multiple passing of the jet was employed to achieve this, with a 0.25 mm overlap (¼ jet diameter increment) between adjacent passes [Ojmertz, 1997a]. Fig. 4.25 shows the development of depth of cut, roughness and waviness with multiple passes of the nozzle across the workpiece. It can be seen that in both cases, the depth of cut increased linearly with number of passes (Fig. 4.25a) and that the material removal rate was higher at the higher impingement angle (as expected from the data presented in Fig. 4.24a). It can also be seen that there is a general increase in waviness with number of passes of the jet for both impingement angles high and also thus with depth of cut (Fig. 4.25b). However, Fig. 4.25c shows that the surface roughness exhibits almost no variation with number of passes of the jet.

Fig. 4.26 shows SEM micrographs of the surface morphology of the bottom of four tracks forward milled with 180 μm (80#) abrasive grit, at both high and low jet impingement angles and high and low jet traverse speeds. At low jet impingement angles, a grooved directional morphology was observed (Fig. 4.26a and 4.26b), irrespective of traverse speed, indicative of abrasive impinging at a low angle. The morphology developed at high impingement angles is dependent on jet traverse speed; following milling at low traverse speeds, clear directionality, with some cratering is observed (Fig. 4.26c), indicative of abrasive impinging at a low angle. However, following milling at high traverse speeds (Fig. 4.26d), the track has a cratered appearance, indicative of predominantly normal impact of the particles.

The mechanism of material removal from the workpiece was examined over a wide range of conditions. Fig. 4.27 shows the regimes of development of various surface morphologies as a function of processing conditions. Figs. 4.27a, 4.27b and 4.27c show representative SEM images of the various types of morphology observed. Figs. 4.27d and 4.27e illustrate regimes where the different morphologies are developed as a function of jet impingement angle and traverse speed, for both forward passing (Fig 4.27d) and backward passing (Fig. 4.27e). Experiments were carried out with both the large and small garnet grit sizes and it was found that the maps developed for Fig. 4.27 were representative of the development of morphology for both of the grit sizes. It can

be seen that at the lower traverse speeds, there were differences between the morphologies developed in forward and backward passing of the jet. Both modes generally resulted in a grooved surface morphology, but in forward passing, some mixed cratered and grooved morphology was observed at intermediate jet impingement angles. At the higher traverse speed, development of surface morphology was independent of whether forward or backward milling was employed. Low impingement angles resulted in the development of a grooved morphology whereas impingement angles of above about 45° resulted in a cratered morphology.

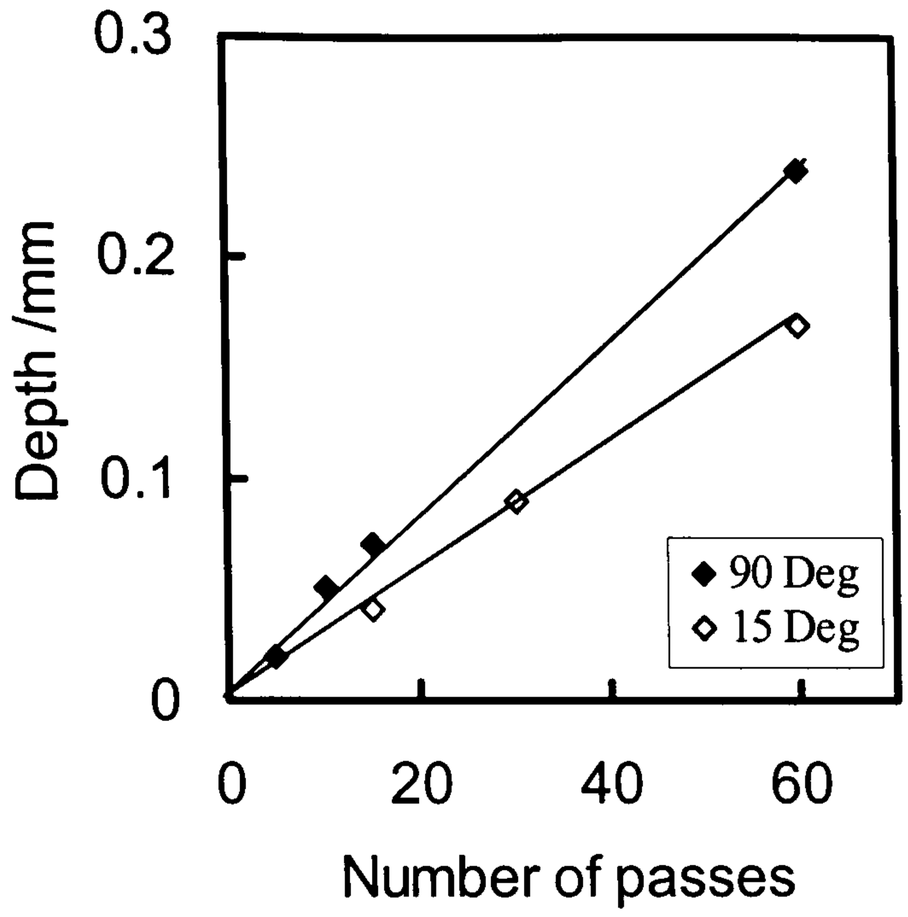

(a)

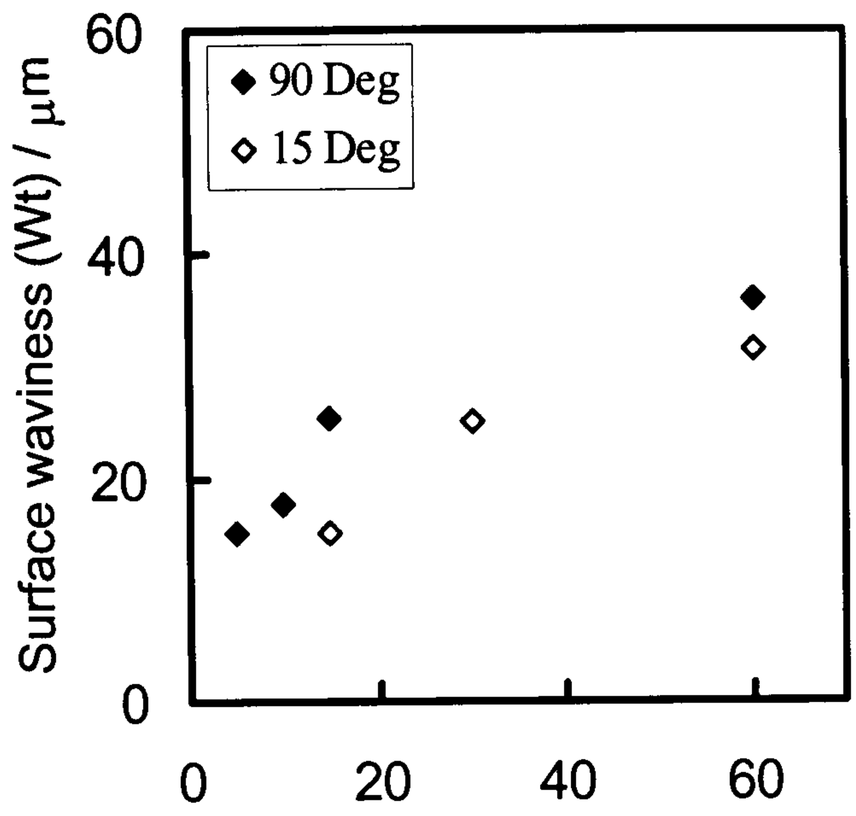

(b)

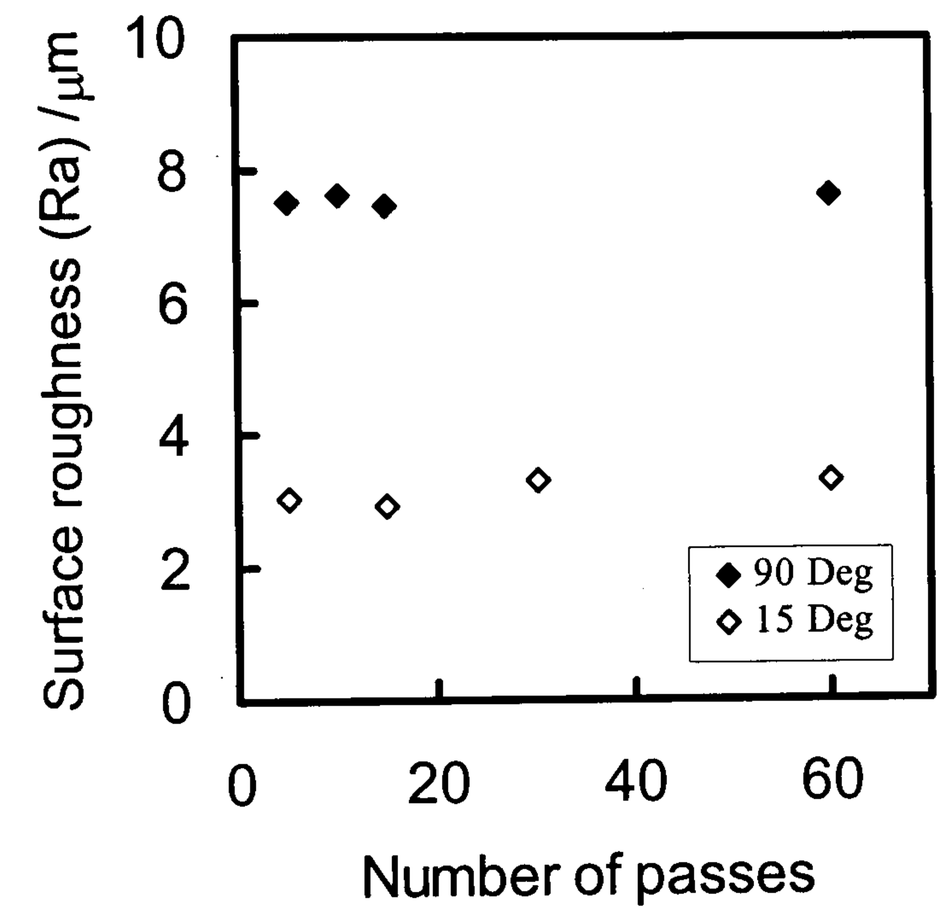

(c)

Figure 4.25 (a) Depth of cut, (b) surface waviness and (c) roughness developed during AWJ-CDM of Ti6Al4V as a function of number of jet passes: high traverse speed (5 m s^{-1}); water jet pressure 137.9 MPa (20 000 psi), stand off distance 3mm: with 0.25mm (¼) jet overlap and 180 µm (80#) garnet grit. Milling at jet angles of 90° and 15°.

Direction of Jet Travel

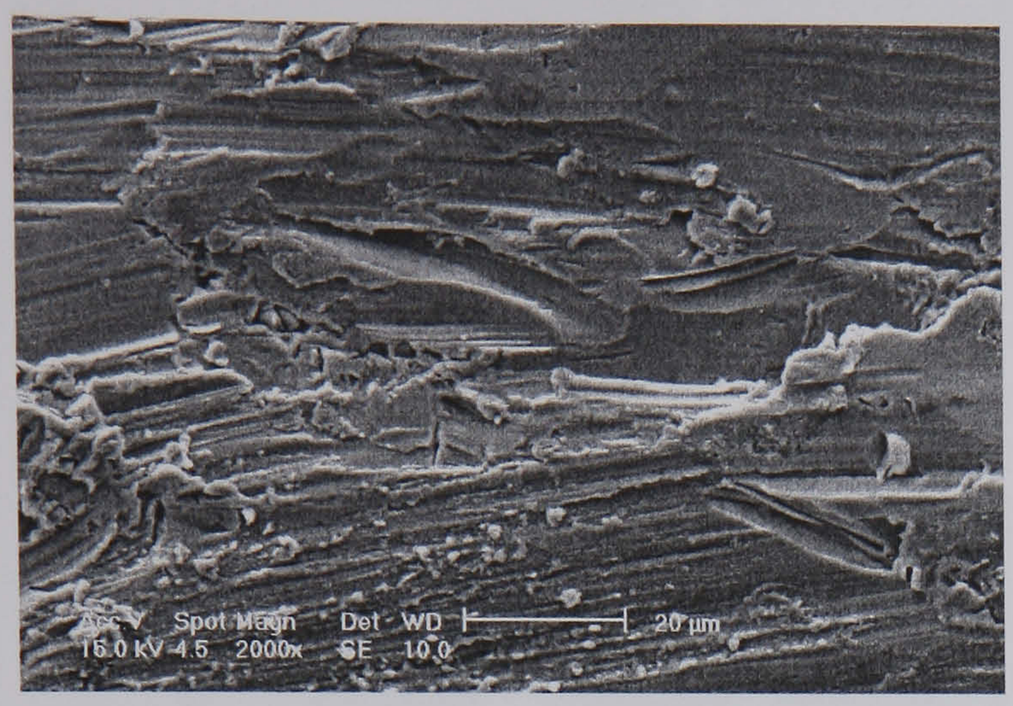

(a)

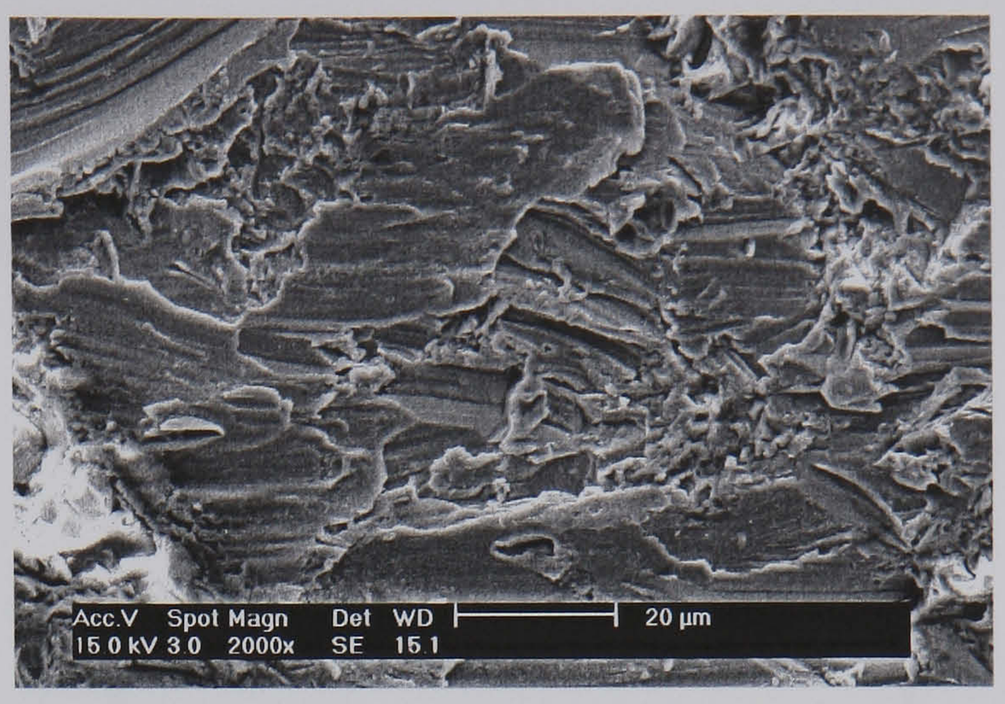

(b)

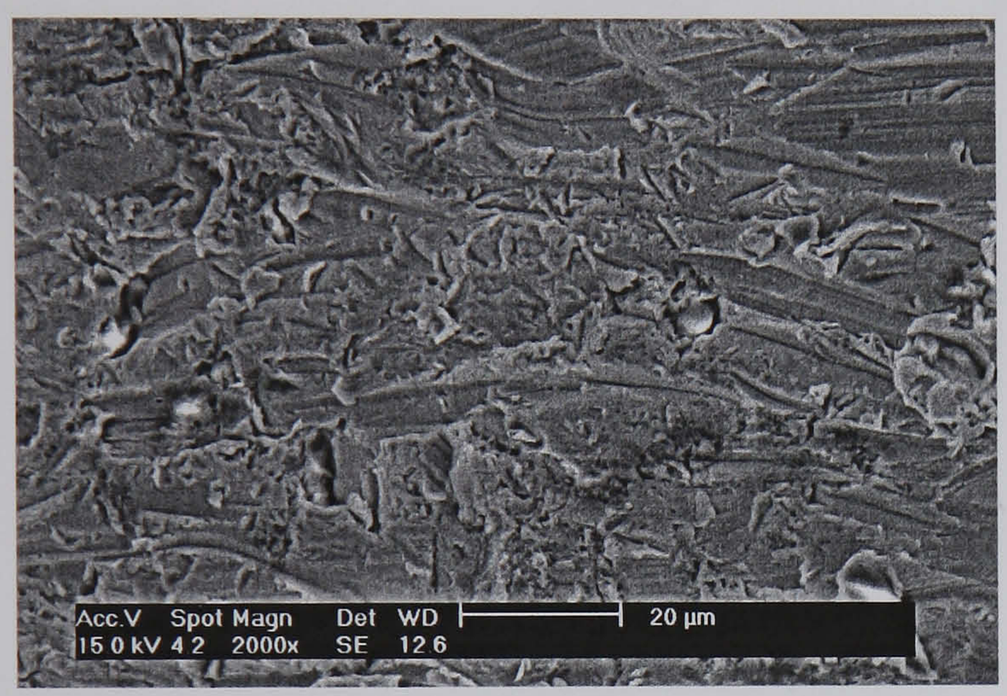

(c)

(d)

Figure 4.26 SEM micrographs of the bottom of AWJ-CDM tracks in Ti6Al4V using 180 µm (80#) garnet grit forward milling with a 92 passes of the jet; water jet pressure 137.9 MPa (20 000 psi), stand off distance 3mm: (a) Low traverse speed = 0.003 m s^{-1}, jet angle = 15°; (b) High traverse speed = 5 m s^{-1}, jet angle = 15°; (c) Low traverse speed = 0.003 m s^{-1}, jet angle = 90°; (d) High traverse speed = 5 m s^{-1}, jet angle = 90°.

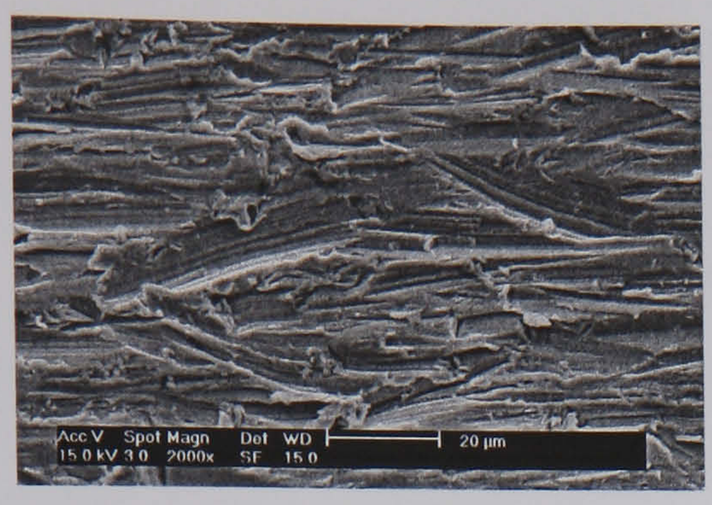

(a)

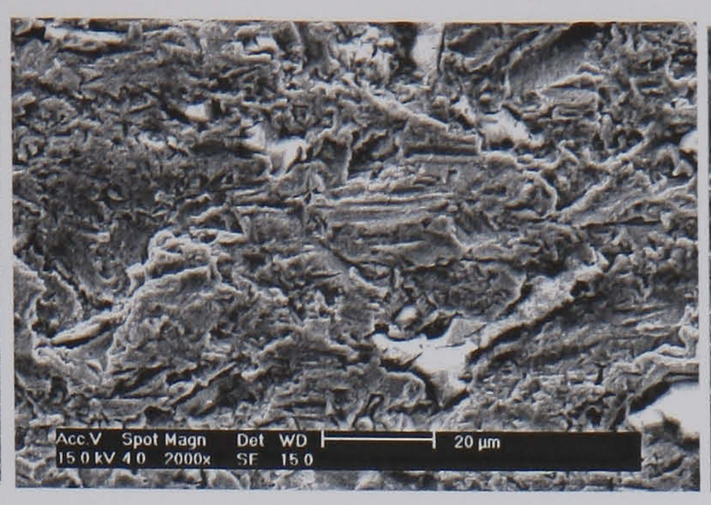

(b)

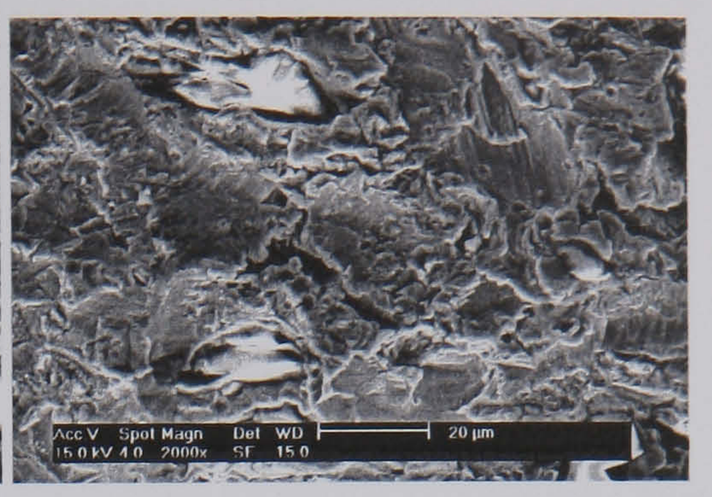

(c)

20 µm

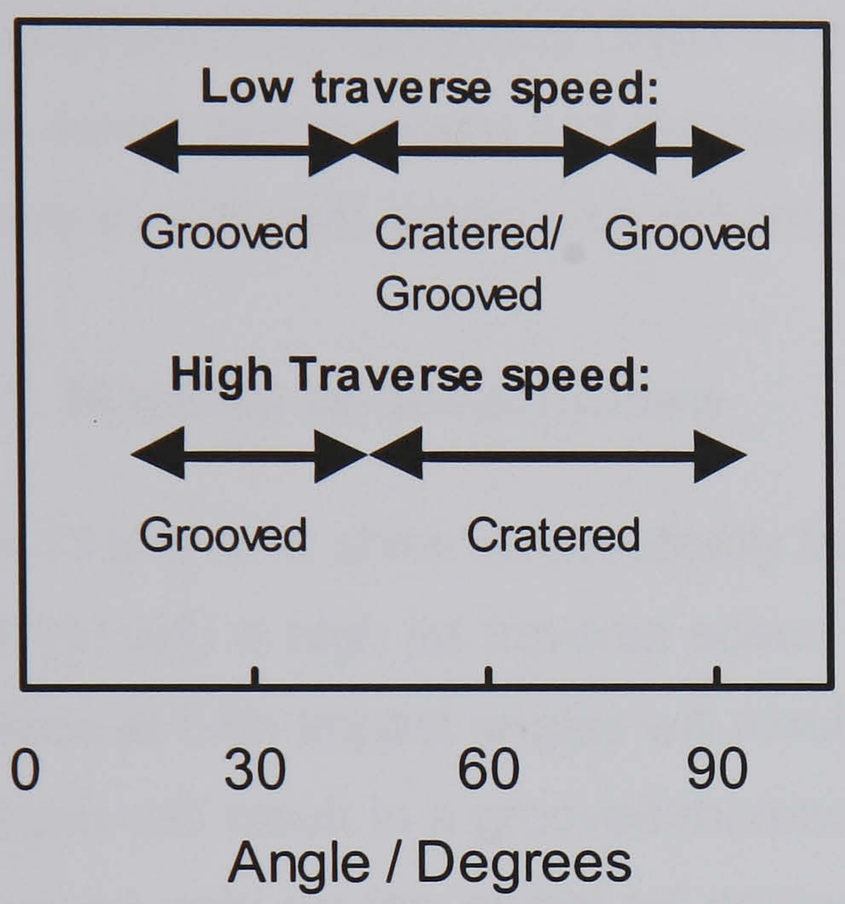

(d)

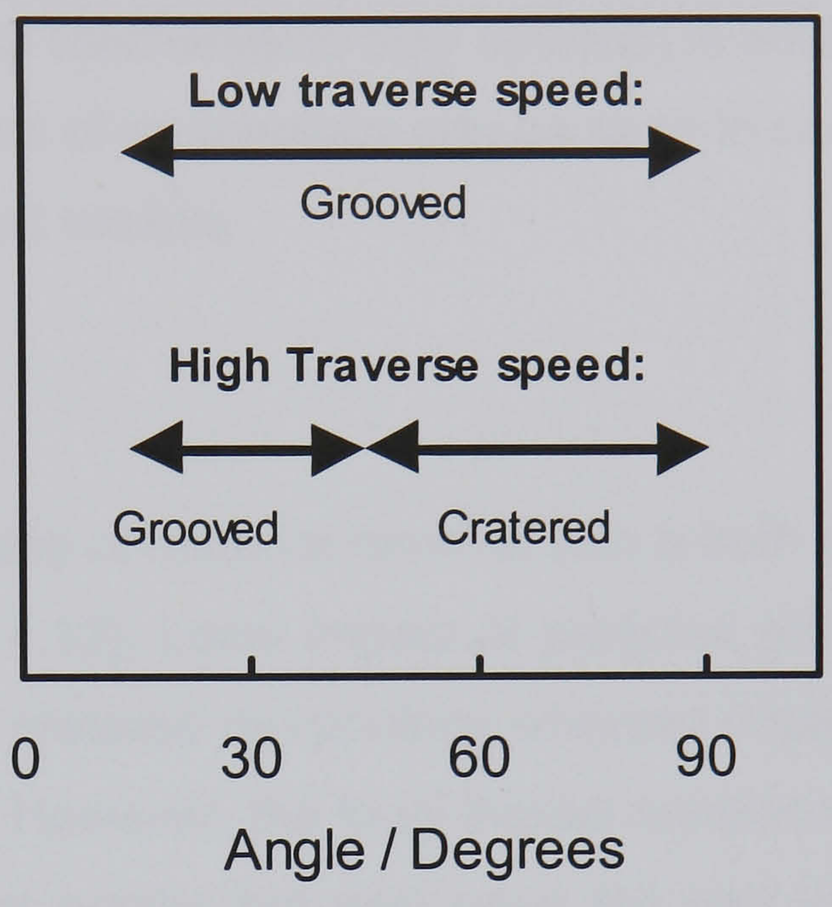

(e)

Figure 4.27 Generalised morphology developed during AWJ-CDM of Ti6Al4V as a function of jet impingement angle following a single pass of the jet with two grit sizes: 180 µm (80#) and 75 µm (200#) garnet grit and with high (5 m s^{-1}) and low (0.003 m s^{-1}) jet traverse speeds; water jet pressure 137.9 MPa (20 000 psi), stand off distance 3mm. SEM micrographs of representative morphologies: (a) grooved morphology; (b) mixed grooved and cratered morphology; (c) cratered morphology. Map of morphologies as a function of processing conditions. (d) Morphologies developed in forward milling; (e) Morphologies developed in backward milling.

4.3.2 Discussion.

The results presented indicate that not only is the material removal rate dependent on jet impingement angle, but also the surface characteristics, such as roughness, waviness and morphology. Moreover, the dependence on impingement angle varies with grit size, milling direction and jet traverse speed. To allow a rationalisation of the observations made, a model indicating the mechanisms by which material is removed (and the processing conditions under which such mechanisms may operate) is outlined. Further details of this model and the development of morphology can be seen in section 4.4 which investigates work piece grit embedment models.

4.3.2.1 Material removal modes

Figs. 4.11 and 4.12 show schematically the modes of material removal with a both a low (Fig. 4.11) and a high jet traverse speed (Fig. 4.12). Local impact of particles with the workpiece at high impact angles will result in a cratered morphology whereas impact at low angles will result in a grooved morphology. However, the local impact conditions do not depend only on the global jet impingement angles but also upon the kerf shape developed in the material by previous material removal. In low speed milling, the depth of material removed per pass can be large (section 4.4). Fig. 4.11a illustrates the situation for milling at a high jet impingement angle in forward mode. A deep groove is formed and much of the cutting is performed at very low angles of attack on the leading edge of the kerf face. As the particles reach the area where the kerf front face and the bottom of the groove intersect, impact at high angles will result. Some particles will leave the impact zone by flowing along the already milled groove and thus develop directional grooving, such as seen in Fig. 4.26c. Similar evidence of grooving associated with particles striking the surface at low impact angles as the jet has flowed along the groove has been reported by other workers [Li et al. 1996b, Summers, 1995]. Fig. 4.11b illustrates the change in the situation as the jet impingement angle is reduced in low traverse speed forward milling. Here again, much of the material removal is performed by the jet on the kerf front wall. However, at these low impact angles, the back edge of the jet will actually strike the groove bottom at a low impact angle, producing a grooved morphology, such as seen in Fig. 4.26a.

Fig. 4.11c illustrates the situation for a high jet impingement angle in backward milling mode. Here the kerf front wall exhibits a smooth transition into the groove bottom. The natural tendency of the fluid stream will be to be diverted and flow along the groove

bottom so that a grooved morphology is produced. Fig. 4.11d again shows that there will be a greater tendency for the particles to strike the surface at an angle close to the global jet impingement angle.

It has been shown that the morphology of the groove is influenced by local impact conditions, which depend upon traverse speed as well as the jet impingement angle. Flow of particle-laden fluid along a groove can result in significant material removal and a change in morphology from that expected. In backward milling, all impacts and flow of the particle-laden fluid tend to lead to a grooved morphology. In forward milling, high impact angles result in some cratering along with grooving by fluid flow along the groove whereas low impact angles result in grooving, primarily from the back edge of the jet.

At high jet traverse speeds, the situation is much less complex than for low jet traverse speeds, since in this case the effect of milling mode (forward or backward) becomes insignificant. The jet impingement angle also has a much stronger influence on the surface morphology of surface milled with a high jet traverse speed. A cratered morphology is observed at high jet impingement angles (such as seen in Fig. 4.26d) and a directional grooved morphology is observed at low jet impingement angles (such as seen in Fig 4.26b). In the current investigation, a cratered morphology was observed when high speed milling at jet impingement angles above 45° and a directional grooved morphology at jet impingement angles below 45°. Fig. 4.12 illustrates the modes of material removal with high jet traverse speeds. In all cases, the depth of cut is small and the leading edge of the kerf face makes up a very small proportion of the total cutting area. The small depth of cut per pass is the primary reason why forward and backward milling result in very similar behaviour. As a result, the local particle impact angles are generally the same as that of the jet impingement angle. Also, since the local height of the material being milled in the current pass is very similar to that of the surrounding material (not the case for low jet traverse velocities), then the tendency of the particle laden fluid to run along the groove is also reduced. Thus, due to the lack of fluid channelling, the surface morphology is as expected, with directional grooving at low jet impingement angles and cratering at high impact angles.

4.3.2.2 Angular dependence of material removal rate.

For a ductile material such as Ti6Al4V, the classic angular dependence of erosion rate would exhibit a maximum at an angle somewhere between 30° and 45° [Yerramareddy and Bahadur, 1993], with very low erosion rate at low impingement angle. It is proposed that cutting is the most efficient mode of material removal, but that for cutting to operate

efficiently there must be a normal force (provided by the component of velocity normal to the surface) and motion parallel to the surface. If the impact angle is too small, then the depth of cut is small and little material is removed; however, if the impact angle is large, then there is little lateral motion over which a chip can be generated. However, it is clear that in AWJ-CDM, not only the impact angle, but also the jet traverse velocity and milling mode affect the angular dependence of material removal rate.

The model proposed in Fig. 4.11 and 4.12 shows that the local impact angle of a particle is controlled by the jet impingement angle, jet traverse speed and milling mode, and it is these three parameters in combination which thus govern the material removal rate. At low traverse speeds (Fig. 4.22), material is removed primarily by impacts on the kerf front face, where low angle cutting operates irrespective of the global jet impingement angle. However, at low jet impingement angles, the momentum of the jet is altered less by impact with the workpiece than it is at higher impact angles. This higher momentum change at the higher impact angles results in greater forces being applied to the workpiece; however, unlike in the case of conventional erosion, the fluid stream carries the particles laterally along the workpiece (see for example Fig. 4.26c) and thus is able to remove the material by cutting. Thus, the material removal rate increases as the jet impingement angle increases at these low jet traverse speeds.

As the traverse speed is increased, the kerf front face height is reduced until at very high traverse speeds it is negligible and, as outlined in Fig. 4.12, the local particle impact angle is the same as the overall jet impingement angle. At the intermediate traverse speed of 0.0166 m s^{-1}, the angular dependence of material removal rate is complex. In backward milling (where the fluid and grit motion is less complex - see Figs. 4.11c and 4.11d), a maximum in material removal rate appears. This is now the appearance of classic erosion behaviour. However, the peak is at around 60°; this is a somewhat higher angle than that observed by Hashish [1989c] where the maximum material removal rate for the AWJ milling of Ti6Al4V with 150 μm (100#) garnet grit at a somewhat higher jet traverse speed of 0.068 m s^{-1} was 30°. Maxima at between 30°and 60° were observed for stainless steel depending on AWJ process conditions. Differences between the angle for maximum material removal rate observed in this work and that observed in the erosion literature [Hashish, 1989c, Yerramareddy and Bahadur, 1993] may result again from the difference between the jet impingement angle and the local particle impact angles which will be much more strongly affected by the high density fluid carrier in the abrasive water-jet process. Conversely, Zu et al. [1991] found that in their research on slurry and free fall erosion of aluminium that the maximum erosion occurred at impingement angles of 40 - 50°. Angles much higher than the 20°

observed by Finnie [1960]. They also observed grit embedment and this may change the erosion conditions since the surface is a mix of embedded grit and parent material thus changing the material properties [Ives and Ruff, [1977]. Ives and Ruff [1977] suggested that material with high concentrations of embedded particles will exhibit different properties to that of the surrounding parent. Thus, the resulting composite structure may be more resistant to erosion and impingement angles for maximum erosion may be susceptible to change. This investigation has shown grit embedment to exist for the traverse speeds and jet impingement angles examined (Fig. 4.30). Moreover, secondary machining is also observed (Fig. 5.5) and so embedded grit coupled with the mechanics of secondary machining may be a contributing to the erosion conditions that may affect the impingement angle at which maximum erosion is said to occur.

At this traverse velocity, it is noticeable that the material removal rate is different for forward and backward milling. Fig. 4.11 shows how the local impact conditions will be very different for the two modes of milling. In the case of backward milling (see Figs 4.11c and 4.11d), there will be very few particles striking the workpiece at a high local impact angle and thus all the impacts will be relatively efficient in terms of material removed. However, in the case of forward milling, there will be more particles impacting at high impact angles which reduces the material removal rate in this case.

As the jet traverse speed is increased even further, then the local particle impact angle tends towards that of the jet impingement angle. Fig. 4.22a shows the angular dependence of material removal rate in this case, with a peak in removal rate at an angle around 60°. Again, this is higher than that observed in the erosion literature [Hashish, 1989c, Yerramareddy and Bahadur, 1993].

When the material removal rates at the three traverse speeds are compared, it is noticeable that at the high jet impingement angles, there is a general decrease in removal rate as the traverse speed increases. This is due to the move from low local particle impact angles at low traverse speeds (which more efficiently remove material) to high local particle impact angles at high traverse speeds. The same is true at intermediate jet impingement angles. However, at low jet impingement angles, the differences in material removal rate for the different jet traverse speeds are small, since in all cases now the local impact angles are low (and similar to the jet impingement angle).

It can also be seen that at each traverse speed, the material removal rate is slightly lower for the smaller grit size. However, this is not a strong effect, and the true effect of

the particle size itself as expected from the erosion literature [Hashish, 1998a, Hashish, 1987, Ruff and Wiederhorn, 1979, Sheldon and Finnie, 1968] is masked by the fact that the different particle sizes will follow the fluid flow streamlines in the jet differently, and thus for any given jet impingement angle, the local particle impact angles will vary with particle size.

4.3.2.3 Angular dependence of surface waviness and surface roughness.

Surface waviness appears to develop due to irregularities formed during the milling process itself. Once formed, irregularities are propagated since they form disturbances to the pattern of flow of the water jet which then further promotes local material removal. A number of workers [Hashish, 1998a, Liu, 1998, Ojmertz, 1993] have suggested that if a non-uniformity in depth exists or is created, it will not be removed, but instead is exaggerated by subsequent passes of the jet. To reduce surface waviness requires the traverse speed of the abrasive water jet to be increased or the jet angle to be decreased as seen in Fig. 4.22c, Fig. 4.23c and Fig. 4.24b. As the traverse speed is increased, the tendency to form any irregularities at all are reduced (since the depth of cut per pass is reduced) and thus the waviness is reduced. A low jet impingement angle results in lower waviness at all traverse speeds since again the depth removal per pass is lowest at low impingement angle. Carter et al. [1980] also report that ripples were not observed in erosion studies for impact angles below 25°. Also, as the traverse speed increases, high impact angles result in cratering which may then develop into waviness, whereas at lower jet impingement angles, the surface height variations are less as the particles cut along the surface. The surface waviness and roughness are both reduced by the adoption of low jet angle for both high and low traverse speeds but the reduction in waviness is more dramatic at low traverse speeds.

Whilst the surface waviness formed during AWJ-CDM is on a large scale, the development of waviness has been previously reported in studies on material erosion in both dry and slurry environments [Carter, 1980], [Finnie and Kabil, 1965], [Zu et al. 1991], [Sheldon and Finnie, 1968] and attributed to the fundamental mechanisms of material removal. In AWJ-CDM no evidence for this ripple formation was seen although it may be the precursor for the development of waviness.

It is also notable that the waviness is significantly lower for the smaller particle size at all traverse speeds (Fig. 4.22c, Fig. 4.23c and Fig. 4.24b). This may be due to the smaller particles generating smaller irregularities during the milling process, since smaller size

grit generate smaller impact craters than the larger grit, particularly during milling at higher angles at higher traverse speeds. The ease of the smaller grit to follow the streamlines of the water jet and thus not result in impact with the workpiece as the jet flowed around irregularities may also help to reduce surface waviness.

Changes in local surface morphology affect the roughness of the surface produced. The surface morphology at low jet angles is striated with directional grooving at both high and low traverse speeds. The morphology above impingement angles of approximately 45° is still striated at low traverse speed (Fig. 4.26c) due to particle laden fluid running along the groove following the initial impact and removing *local* irregularities (this flow does not remove gross irregularities, but enhances them due to turbulence and thus enhances surface waviness). However, at these impingement angles, the morphology changes to a cratered appearance at high traverse speed (Fig. 4.26d). This change in morphology appears to be responsible for the reduction is roughness as the jet angle decreases. The striated surface is smooth, while the cratered surface appearance is rough.

At all traverse speeds, an increase in surface roughness is observed at the jet impingement angle is increased from 15° to 45°. At the intermediate jet traverse speed (Fig. 4.23d), the behaviour is complex with a peak in roughness at 45° and the lowest roughnesses being observed for normal jet impingement. This is in contrast to the work of Li et al. [1996b] where a significant reduction in roughness at a jet impingement angle of 20° was observed for a number of materials (including titanium alloy) when backward milling at low traverse speeds of 0.021 m s^{-1}. Ojmertz [1993] also saw a dramatic reduction in roughness and waviness on reduction of the jet impingement angle from 90° to 30° when backward milling steel and aluminium at a traverse speed of 0.026 m s^{-1}. At the highest traverse speed (Fig. 4.24c), there is an increase in roughness with increasing jet impingement angle up to a point where no further increases are observed. At this traverse speed, local particle impact angle is similar to the jet impingement angle and thus the stability in roughness at the higher impact angles must associated with the nature of the impact process itself. At the high traverse speed there is a shift in dominant mechanism from impact deformation at high jet impingement angle (Fig. 4.26d) to one of directional cutting (Fig. 4.26b) at low jet impingement angle. This shift in mechanism is responsible for the decrease in roughness with decreasing jet angle since the grooved morphology is smooth compared to that of the rougher deformation morphology.

At all traverse speeds, a reduction in particle size results in a decrease in roughness across the range of jet impingement angles. The smaller particles produce impact damage at smaller scales due to their lower momentum and this is observed in the

roughness measurement. Also, the smaller particles are better able to follow the fluid streamlines and thus there will be a greater tendency for the particles to strike the surface at lower impact angles, thus resulting in low angle cutting with the associated reduction in roughness.

It is clear from Figs. 4.22 and Fig. 4.23 that the milling mode (forward or backward) influences the development of roughness, whereas its effect on the development of waviness is small. The difference in roughness with milling mode is most clearly seen in Fig. 4.23d. Forward milling results in higher roughness than backward milling for both particle sizes; moreover, the difference is greatest for the larger particle size. It has already been argued that the low roughness is associated with local particle impact at lower angles (not necessarily a low jet impingement angle) whilst high local impact angles result in higher roughness. Fig. 4.27b and 4.27d exhibit a mixed morphology of craters and directional grooving indicating a change to higher local impacts, and Fig. 4.27a and Fig. 4.27e exhibit a directional grooved morphology indicating a change to low local impacts at intermediate jet impingement angles. The implication from Fig. 4.23d is that changing the milling mode from forward to backward results in a higher proportion of particle impact at lower local angles, thus reducing roughness; this is proposed in the model illustrations in Fig. 4.11.

To investigate the effect of number of passes of the jet on the process efficiency and development of surface morphology at low impact angles, a series of trials were performed using just two jet angles (15° and 90°) at high traverse speed as a function of number of passes of the jet. Rather than multiples passes over a single line, a slot 10 mm wide was milled with jet increments of 0.25 mm over the width of the slot. Fig. 4.25a shows that the depth to which material is removed increases linearly with number of passes for both high and low jet angles. This linear dependence at high jet impingement angles has also been seen by Hashish [1998a]. This indicates that the process is controllable and there are no changes in behaviour with milling depth in the range examined. Fig. 4.25b shows the development of surface waviness with number of passes of the jet. Waviness is seen to increase with number of passes of the jet as any perturbations produced early in the process are exaggerated with further milling [Ojmertz, 1993, Ojmertz, 1997a, Hashish, 1987, Liu, 1998]. The waviness developed is greater than 30 μm at high numbers of passes. However, the rate of increase of waviness with number of passes appears to be decreasing, indicating that a plateau may be reached at high numbers of passes. As also seen in Fig. 4.24b, the waviness is slightly higher at the high impact angle. However, the use of low impact angles does not

limit the development of waviness in the process, which may be a limitation to the industrial applicability of this process.

In these experiments, it is noticeable that the material removal rate and surface waviness are not very different for the two jet impingement angles employed. However, the surface roughness can be significantly reduced by the use of a lower impingement angle. Fig. 4.24c shows that this effect may less significant when smaller grit is employed, whereupon the roughness is smaller across the range of impingement angles.

4.4 Workpiece grit embedment following AJW milling of titanium alloy.

4.4.1 Results.

There is little in the way of published research on the fatigue characteristic of AJW-CDM components. A few researchers have identified in some instances in AJW cut components where embedded grit [Fordham et al. 1997, Singh and Jain, 1995] has resulted in fatigue life reduction or where embedded grit from cleaning operations has caused coating delamination [Grififths et al. 1999]. The roughness [Struck, 1990], [Wagner et al. 1984], [Arola and Williams 2002a] and morphology [Fordham et al. 1997, Leverant et al. 1979] characteristics of AJW cut components have also influenced fatigue failure. The role of the AJW-CDM generated surface morphology and grit embedment on determination of component service life is not known, and this requires further work.

However, as a precursor to this, investigations were conducted to establish the effect of the process variables of traverse speed, grit size and jet impingement angle on the process characteristic of grit embedment. The characterisation of grit embedment is required as an input to the assessment of fatigue life debits, when manufacturing components using the AJW-CDM process.

Fig. 4.28 shows back scattered electron images (BSE) and Fe k line X-ray localisation (dot) map images of the water jet backward milled surfaces, milled under a variety of conditions. It can be seen that the back scattered images consist of a white background indicating the presence of metal atoms from Ti6Al4V with small darker patches dispersed over the area of analysis, indicating the presence of grit.

Figure 4.28 Grit embedment developed during AWJ-CDM of Ti6Al4V as a function of jet angle; water jet pressure 137.9 MPa (20 000 psi), stand off distance 3mm (a) high traverse speed of 0.166 m s^{-1} (10 000 mm min^{-1}) high jet angle: 90°; (b) High traverse speed of 0.166 m s^{-1} (10 000 mm min^{-1}) Low angle 15°; (c) Low traverse speed of 0.003 m s^{-1} (200 mm min^{-1}) Low angle 15°; backward milling with a single pass of the jet: with 180 μm (80#) garnet grit.

Table 4.1 compares the EDX spot analysis of the grit particle identified bottom left in Fig. 4.29a (chosen so that the sampling volume would be encompassed entirely within the particle) against the chemical analysis of the grit supplied by the Manufacturer, GMA Garnet. It can be seen that the EDX analysis compares favourably with the chemical analysis as supplied by the manufacture. Therefore, the particle of grit can be established as being garnet from the AJW-CDM process.

Table 4.2 compares the BSE pixel image analysis against the EDX Fe pixel image analysis of four backward AJW-CDM single pass tracks. The area percentage of the embedded grit was measured. It can be seen that the two methods of measurement compare favourably. As such, the BSE image analysis method was used in further analysis due to its simplicity.

Material	GMA Analysis (wt. %)	SEM EDX Analysis (wt %)
SiO_2 (as silicate)	36%	37.1%
Al_2O_3	20%	21.0%
FeO & Fe_2O_3	32%	30.4%
TiO_2	2%	2.7%
MnO	1%	0.8%
CaO	2%	1.2%
MgO	6%	6.6%

Table 4.1 Comparison of manufacturer's average chemical composition (wt. %) to the SEM EDX (energy dispersive X ray) analysis (wt. %) (oxides) of the grit particle identified in Fig. 4.29 left bottom. [GMA Garnet, 2001].

Jet Traverse Speed	Jet Impingement Angle	Grit Size	SCION BSE	SCION Fe k
High	Low	Large	6.5%	9.8%
High	High	Large	36.2%	40.7%
High	High	Small	10.9%	7.1%
Low	Low	Large	6.6%	4.2%
Low	Low	Small	5.9%	6.4%

Table 4.2 Comparison of Scion software analysis of SEM BSE micrographs to Scion software analysis of SEM Fe k line (Dot map) micrographs. Speed: Low = 0.003 ms^{-1} (200 mm min^{-1}); High = 0.166ms^{-1} (10 000 mm min^{-1}); Jet angle: High = 90°; Low = 15°; Grit size: Large = 180 μm (80#) Small = 75 μm (200#). Water jet pressure 137.9 MPa (20 000 psi), stand off distance 3 mm.

Fig. 4.29 shows SEM micrographs of the surface morphology of the bottom of a single track following AWJ milling. Embedded grit fragments are clearly seen (the darker contrast features in BSE image due to their lower average atomic number), and have been identified as garnet using EDX spot analysis techniques. The largest particles of grit observed are less than 50 μm in size (Fig. 4.29) with many particles of a much smaller dimension, some only 20 μm in size. Much of the embedded grit is severely fragmented. Fig. 4.29b shows sub surface grit some 20 - 30 μm below the surface of the material. The encapsulated grit fragments are about 20 μm in size. The white surface layer is a cobalt plating used in the verification process. The examination of the garnet grit before and after milling helps to identify the severity of fragmentation. Grit in the 'as received' condition (Fig 4.29c) has many sub rounded regularly sized particles (180 μm

avg.); after milling (Fig. 4.29d), the size of the particles of grit are reduced to a few large particles (100 μm avg.) with numerous small particles (fragments less than 50 μm). All the particles possess irregular sharp edged faces indicative of fracture.

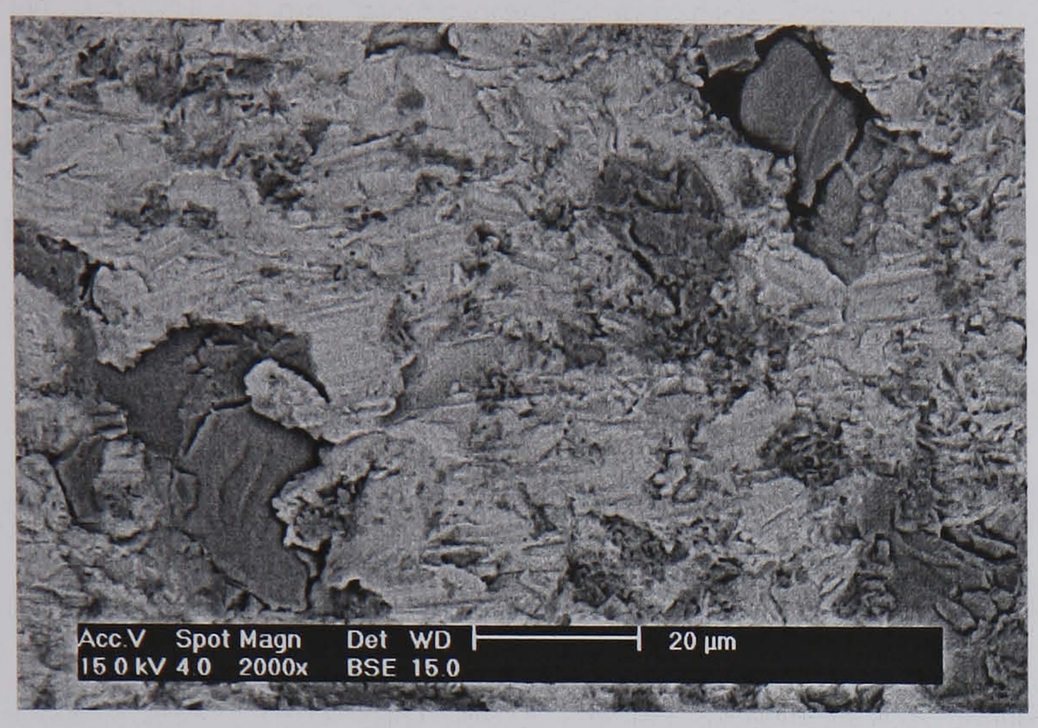

(a)

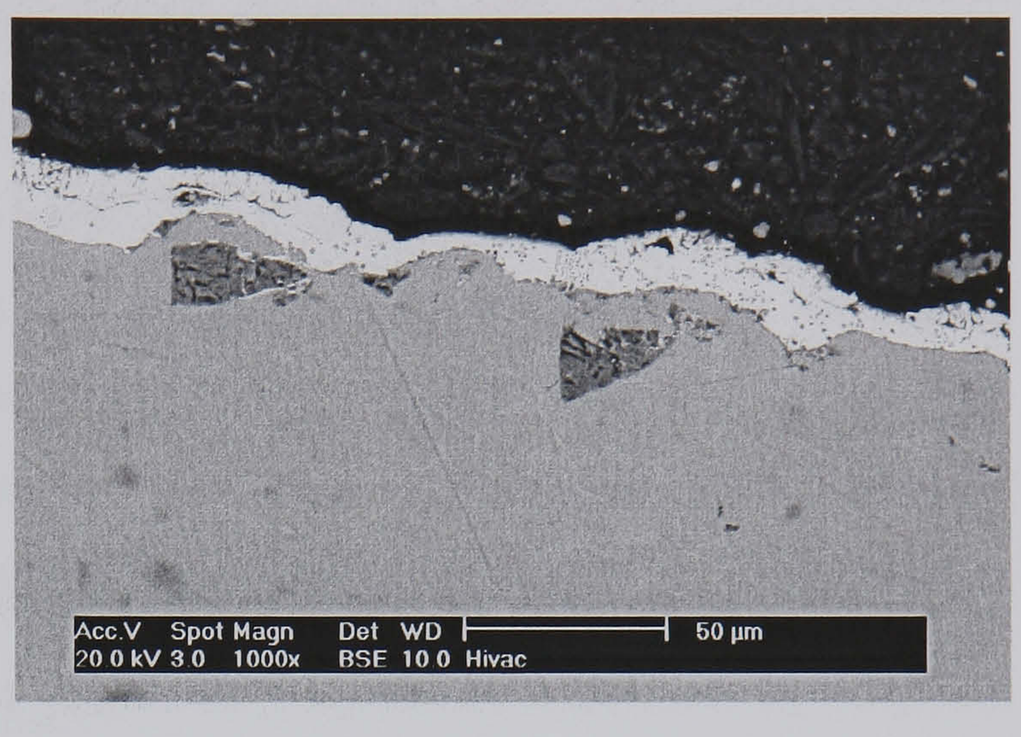

(b)

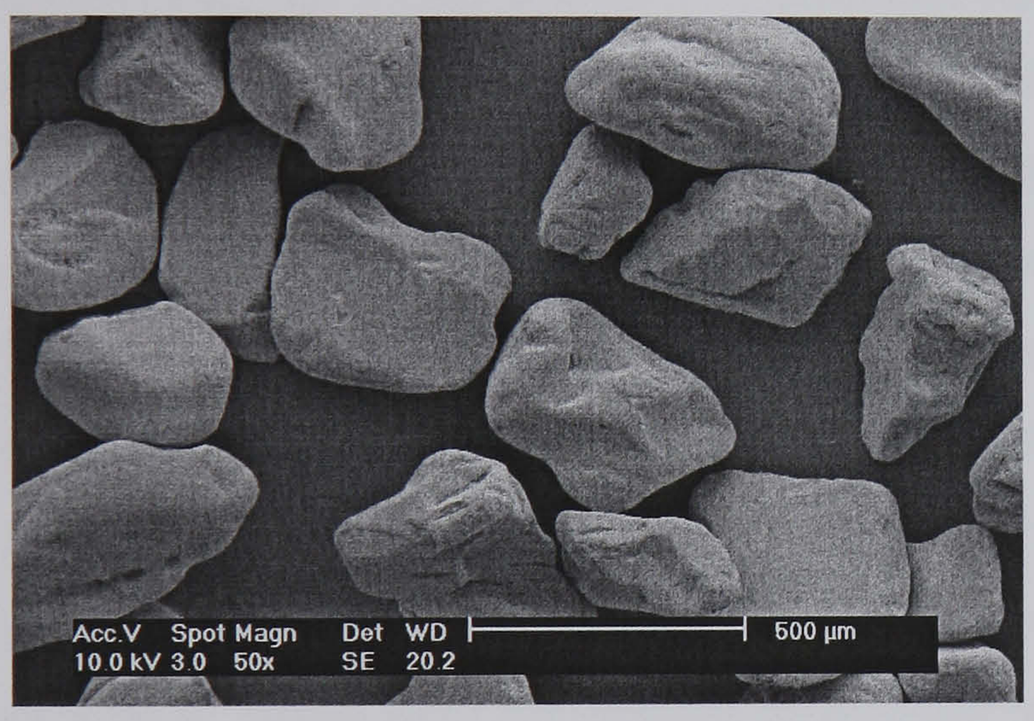

(c)

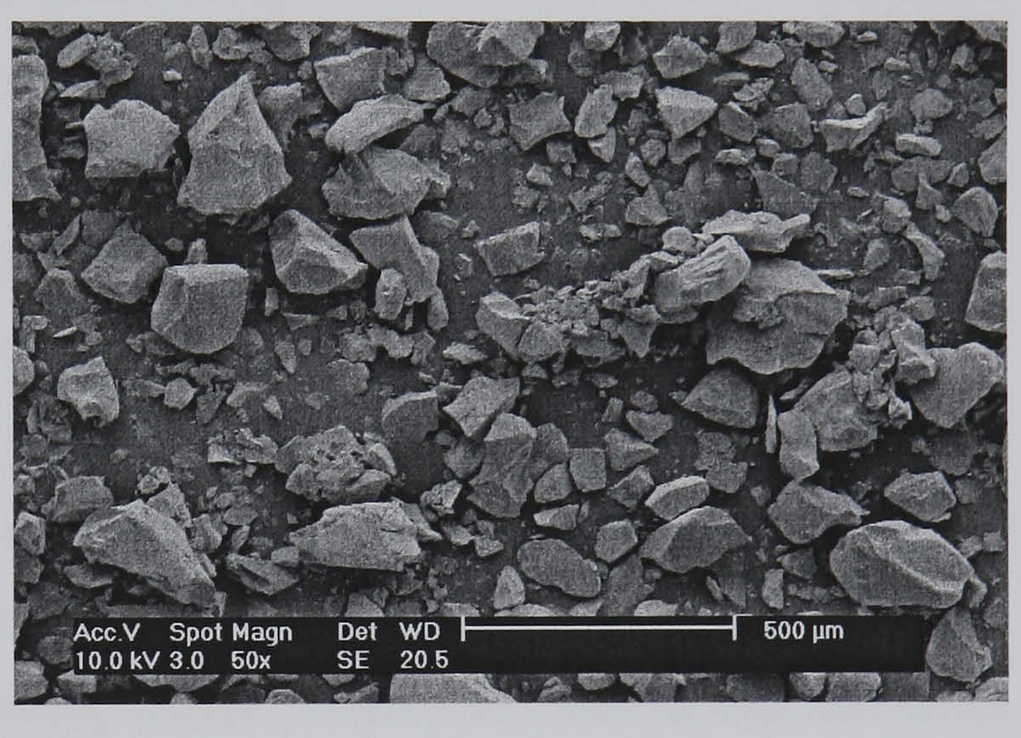

(d)

Figure 4.29 SEM micrographs of the bottom of AWJ-CDM tracks in Ti6Al4V indicating grit embedment: water jet pressure 137.9 MPa (20 000 psi), stand off distance 3 mm. (a) SEM showing embedded grit trapped by ears of metal following a multi jet pass operation. (Bottom left, top right). (b) SEM showing sub surface embedded grit of the AJW-CDM surface. (c) SEM micrograph of 80# garnet grit in 'as received'condition. (d) SEM micrograph of 80# garnet grit after a single milling operation.

Fig. 4.30 shows the development of grit embedment as a function of jet impingement angle when forward and backward milling with large and small grit sizes over a range of jet traverse speeds. At low traverse speeds of 0.003 m s^{-1} (Fig. 4.30a), both grit sizes exhibit similar levels of grit embedment for each set of milling conditions investigated. However, two different types of behaviour with impact angle can be seen depending upon whether milling is being conducted in the forward or backward directions. In forward milling, there is a peak in the area fraction of embedded grit at around a 60° jet impingement angle. However, in backward milling, the degree of grit embedment is lower than for forward milling at all angles up to 90° (where forward and backward milling are the same process). At an impingement angle of 30°, there is a five-fold difference in level of embedment between forward and backward milling. The degree of grit embedment in backward milling increased with impingement angle up to 75° with a slight reduction for milling at 90°.

At higher jet traverse speeds of 0.166 m s^{-1}, a significantly different behaviour was observed. Fig. 4.30b shows that both grit size and milling direction (forward or backward milling) have little effect on grit embedment behaviour at these higher speeds. There is a general trend of a monotonic increase in level of grit embedment with jet impingement angle. At the lowest impingement angle investigated (15°), the area fraction of grit was between 10 and 15% whereas at the highest impingement angle (90°), area fractions of up to 40% were recorded. Since the effect of milling direction on grit embedment is small at the high traverse speed of 0.166 m s^{-1}, it was concluded that this trend would prevail at jet traverse speeds of 5 m s^{-1}. Therefore, experiments at this higher jet traverse speed of 5 m s^{-1} were only conducted in forward milling mode. Moreover, due to the low dose of particles per pass and low material removal rates, samples milled with this jet traverse speed were examined after ninety two passes of the jet. Fig. 4.30c shows the data for level of grit embedment under these conditions. Comparison with the data in Fig. 4.30b, shows that there is little difference in grit embedment behaviour between the two traverse speeds of 0.166 m s^{-1} and 5 m s^{-1}.

To examine the development of grit embedment with multiple doses of particles onto a milled surface, as seen with multiple passes of the jet in Fig. 4.30c, a sample was milled with both the large and small grit and a jet traverse speed of 0.166 m s^{-1}; the level of grit embedment was measured as a function of the number of passes of the jet over the workpiece. Fig. 4.31 shows the development of grit embedment under these conditions. It can be seen that there was no discernable change in level of grit embedment with the number of passes of the jet indicating that steady state is reached early in the milling

process. It can also be seen that the grit size has no strong influence on grit embedment.

In an attempt to understand the mechanisms controlling grit embedment, the mechanism of material removal from the workpiece was examined over a wide range of conditions. Fig. 4.27 shows the regimes of development of various surface morphologies as a function of processing conditions.

It is clear from Fig. 4.30a and Figs. 4.27d and 4.27e that at low jet traverse speeds, the angle of jet impingement and the milling mode (forward or backward milling) have a significant influence on the level of grit embedment and the morphology of the milled surface. In an attempt to better understand the changes in milling behaviour, SEM was employed to examine surface characteristics; Figs. 4.32 - 4.35 show SEM micrographs of the milled surfaces (showing grit embedment with BSE and surface morphology with SE) for both forward and backward milling with a low jet traverse speed of 0.003 m s^{-1}, with the jet impingement angle increasing from Fig. 4.32 to Fig. 4.35.

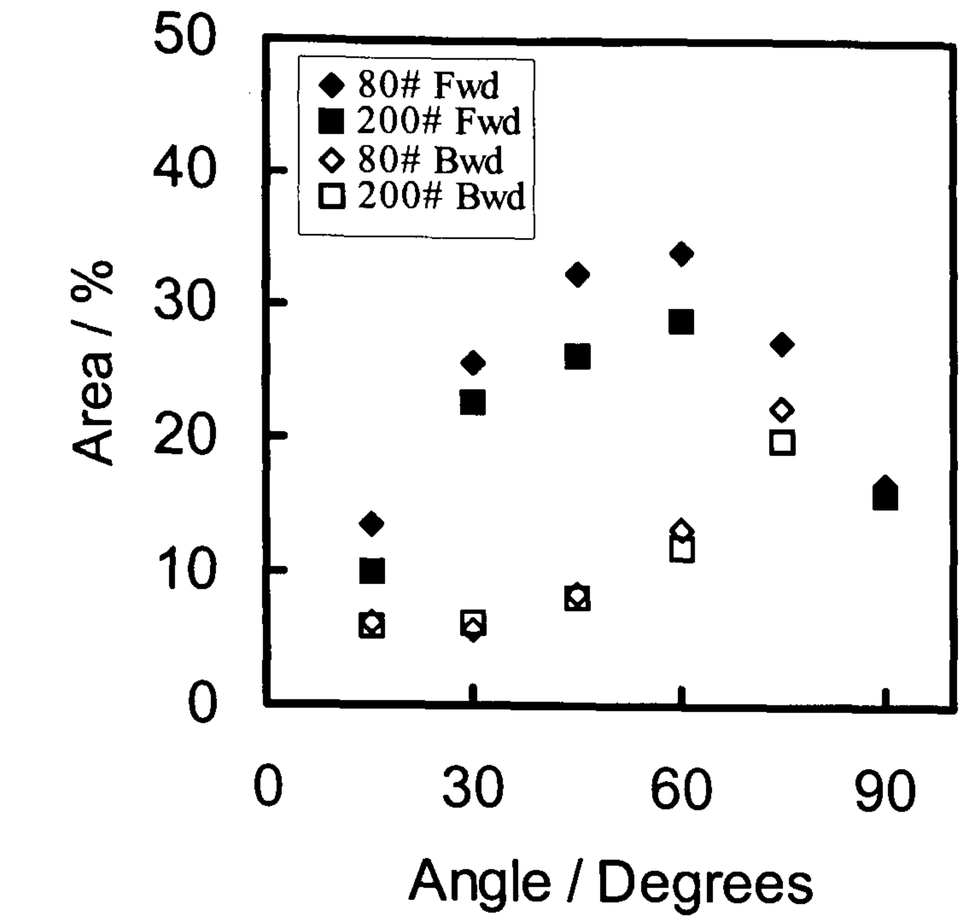

(a)

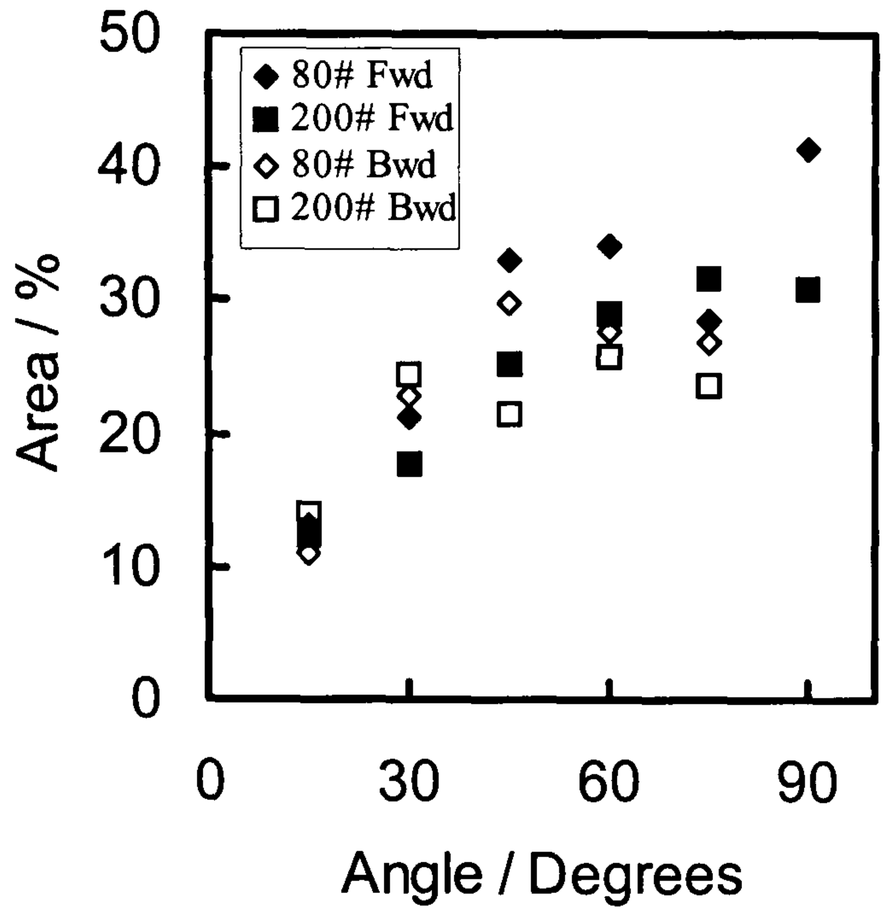

(b)

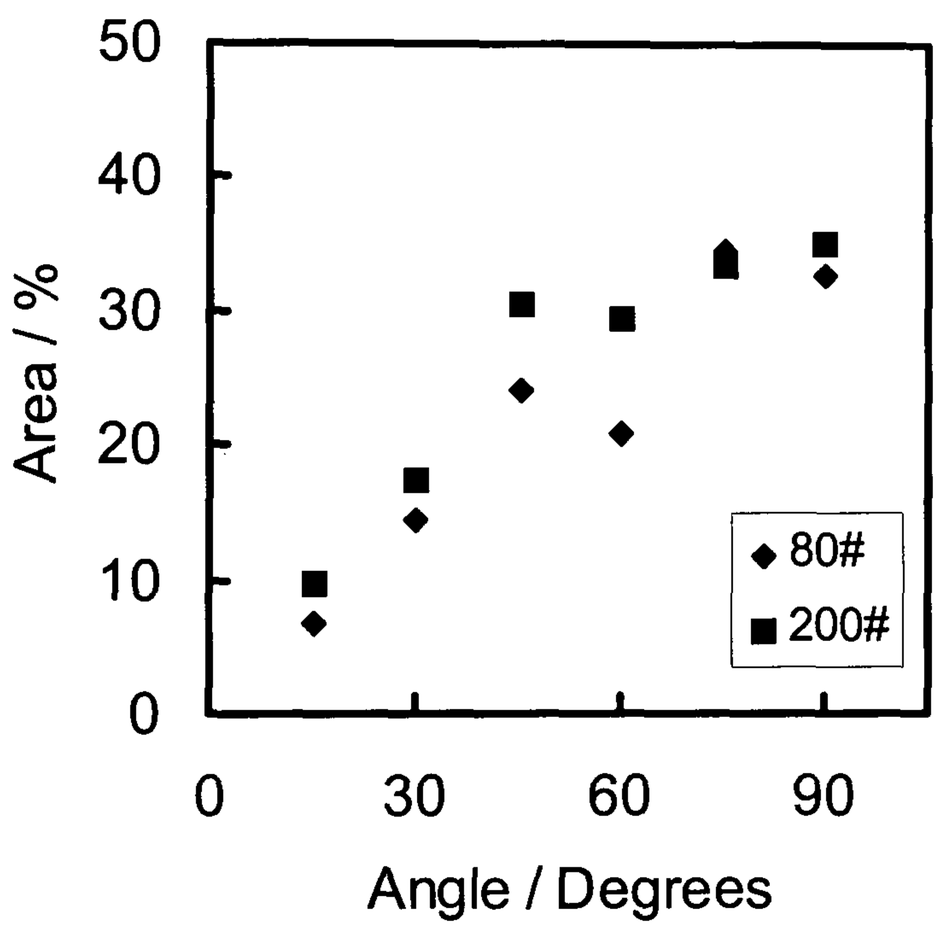

(c)

Figure 4.30 Grit embedment development during AWJ-CDM of Ti6Al4V as a function of jet impingement angle with two garnet grit sizes and in both forward and backward milling mode; water jet pressure 137.9MPa (20 000 psi), stand off distance 3mm. (a) single pass of the jet with traverse speed of 0.003 m s^{-1}; (b) single pass of the jet with traverse speed of 0.166 m s^{-1}; (c) ninety two passes of the jet with traverse speed of 5 m s^{-1}, forward milling only.

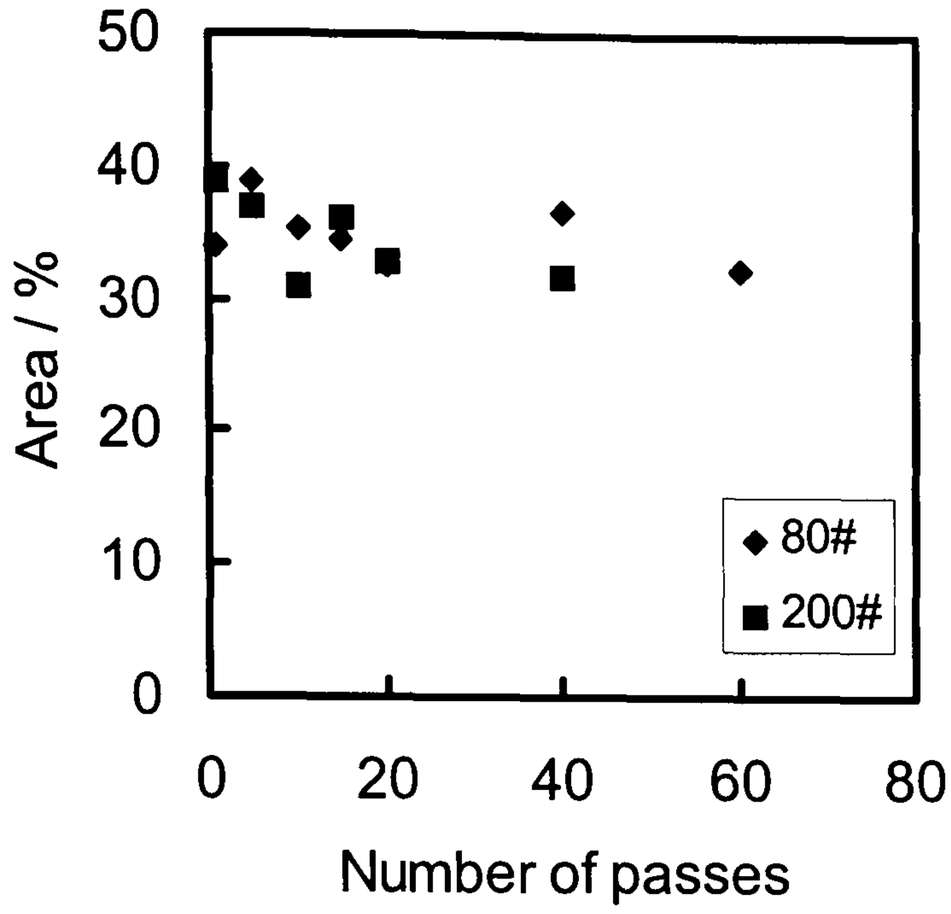

Figure 4.31 Grit embedment developed during AWJ-CDM of Ti6Al4V as function of jet passes; milling with 180 μm (80#) garnet grit; and 75 μm (200#) garnet grit; water jet pressure 137.9MPa (20 000 psi), stand off distance 3mm; high traverse speed of 0.166 m s^{-1} (10, 000 mm min^{-1}); milling at jet angle of 90°.

Fig. 4.32 shows micrographs of a forward and backward low speed milled surface with a low jet impingement angle of 15°. It can be seen that there is more grit embedment in forward milling than in backward milling. Also, although forward and backward milling at this impingement angle both result in a grooved surface morphology, the directional texture is less well defined in the case of forward milling.

Fig. 4.33 shows micrographs of a forward and backward low speed milled surface with an intermediate jet impingement angle of 45°. The differences in levels of grit embedment between forward and backward milling mode are now more pronounced, with higher levels of grit embedment in forward milling. Also, the difference in surface morphology between the different milling modes are now easily discernable with a cratered/grooved morphology in forward milling and still a primarily grooved morphology in backward milling.

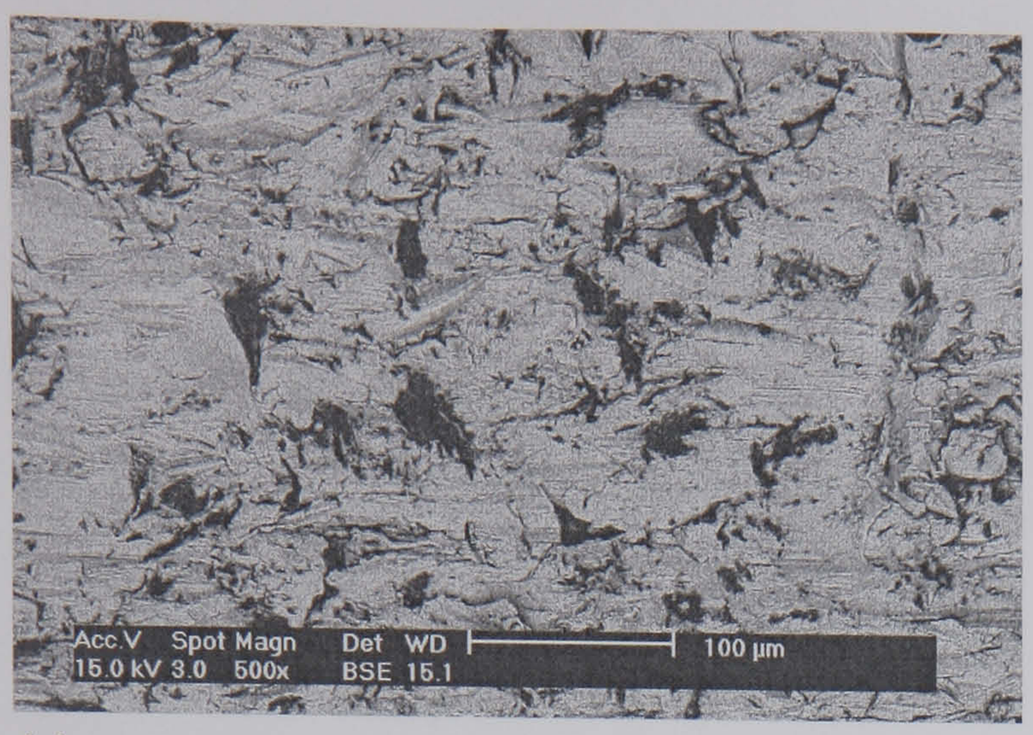

(a)

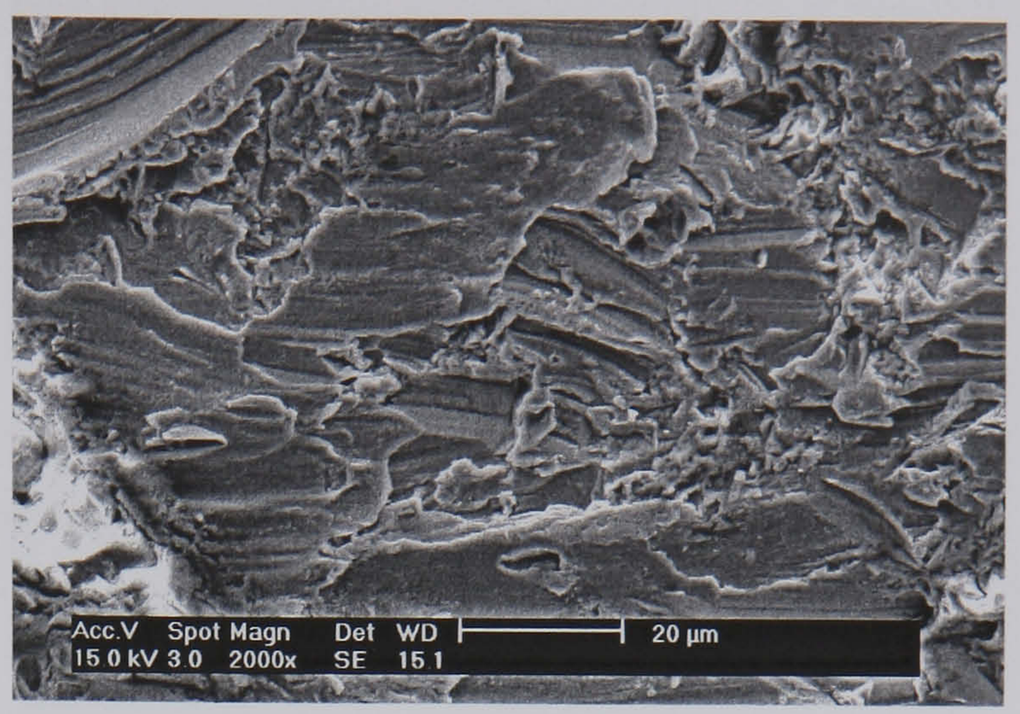

(b)

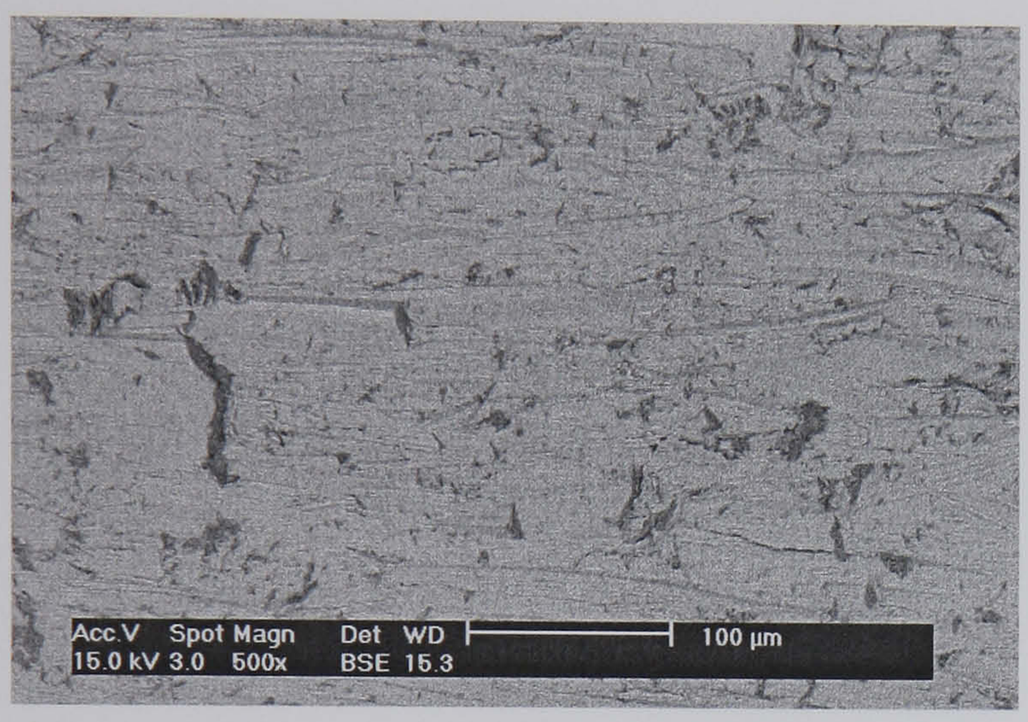

(c)

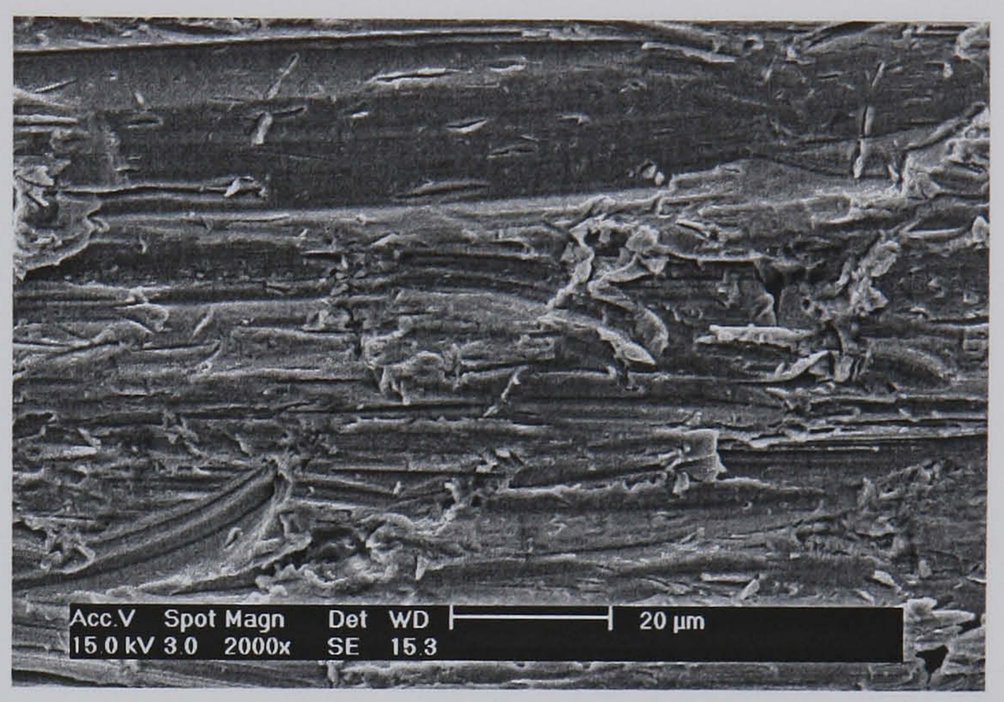

(d)

Figure 4.32 SEM micrographs of the bottom of AWJ-CDM tracks in Ti6Al4V using 180 µm (80#) garnet grit following a single pass of the jet; jet traverse speed of 0.003 m s^{-1} (200 mm min^{-1}); Jet angle $\theta = 15°$. Water jet pressure 137.9MPa (20 000 psi), stand off distance 3mm; (a) Forward milling - BSE; (b) Forward milling - SE; (c) Backward milling - BSE; (d) Backward milling - SE.

Fig. 4.34 shows micrographs of a forward and backward low speed milled surface with a still higher jet impingement angle of 75°. The difference in level of grit embedment between the two milling modes is now much less discernable, with a significant increase in the level of grit embedment in backward milling mode. Also, in forward milling mode, the surface morphology is now clearly cratered with little evidence of grooving, whereas that resulting from backward milling still exhibits a primarily grooved morphology.

Fig. 4.35 shows micrographs of a surface milled with normal jet impingement (where forward and backward milling are the same). The level of grit embedment is clearly less than for both modes of milling with a jet impingement angle of 75°. Also, the morphology shows a primarily grooved surface morphology with some evidence for cratering.

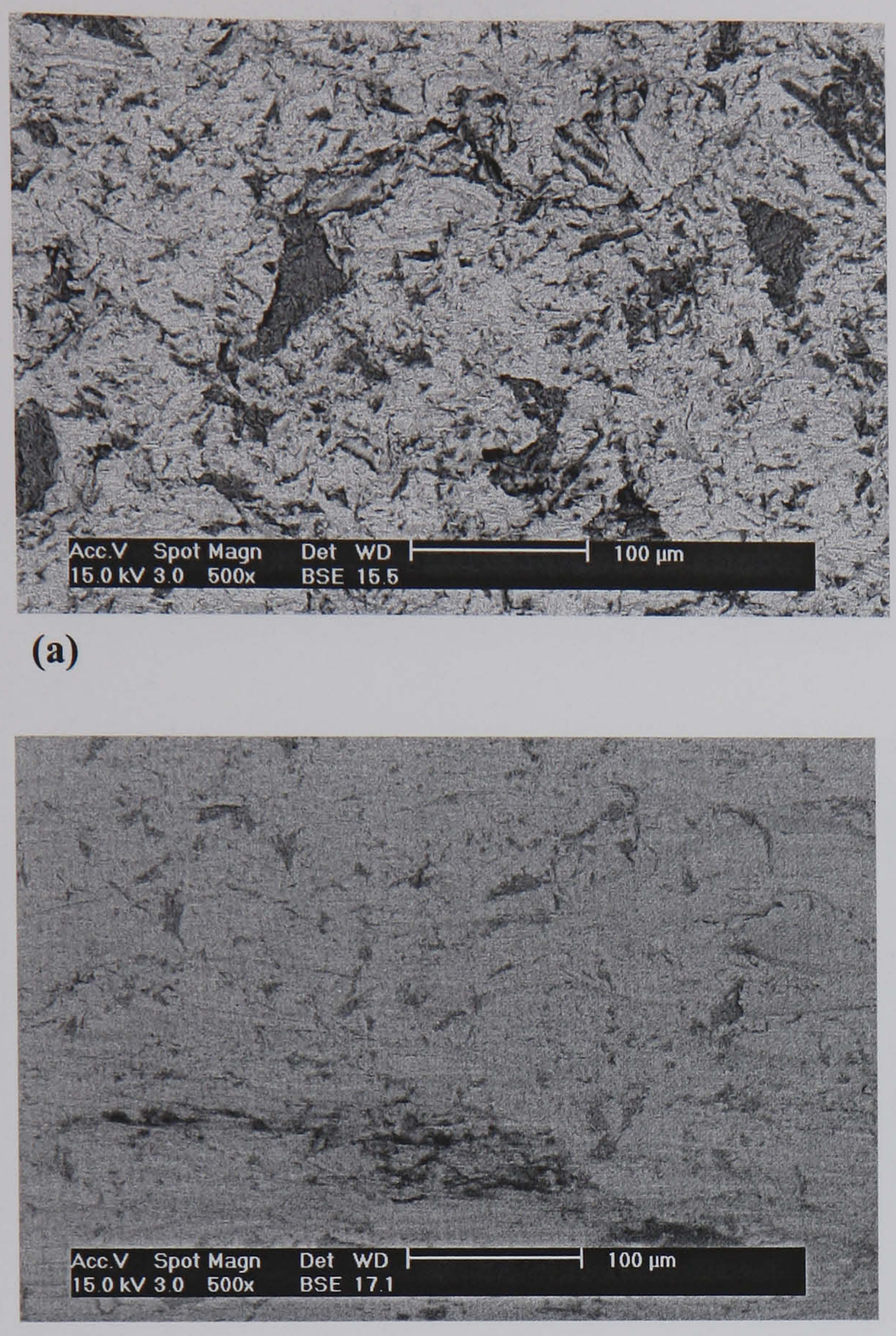

Figure 4.33 SEM micrographs of the bottom of AWJ-CDM tracks in Ti6Al4V using 180 µm (80#) garnet grit following a single pass of the jet; jet traverse speed of 0.003 m s^{-1} (200 mm min^{-1}); Jet angle $\theta = 45°$. Water jet pressure 137.9MPa (20 000 psi), stand off distance 3mm; (a) Forward milling - BSE; (b) Forward milling - SE; (c) Backward milling - BSE; (d) Backward milling - SE.

It can be seen from Fig. 4.30b and Figs. 4.27d and 4.27e that at high jet traverse speeds, the angle of jet impingement has a significant influence on the level of grit embedment and the morphology of the milled surface. However, the influence of the milling mode (forward or backward milling) is now small at these higher jet traverse speeds. Accordingly, Fig. 4.36 shows SEM micrographs of the grit embedment (using BSE) and surface morphology (using SE) in the bottom of tracks backward milled with a single jet pass using large garnet grit and a high traverse speed of 0.166 m s^{-1} only in backward milling mode. Micrographs from tracks at three jet impingement angles of 15°, 45° and 90° are presented. It can be seen that the degree of grit embedment increased significantly as the jet impingement angle was increased from 15° to 90°. Also, the two lower jet impingement angles resulted in a directional, grooved surface morphology whereas the higher impingement angle resulted in a cratered workpiece morphology. Similar effects were also observed when forward milling under the same experimental conditions.

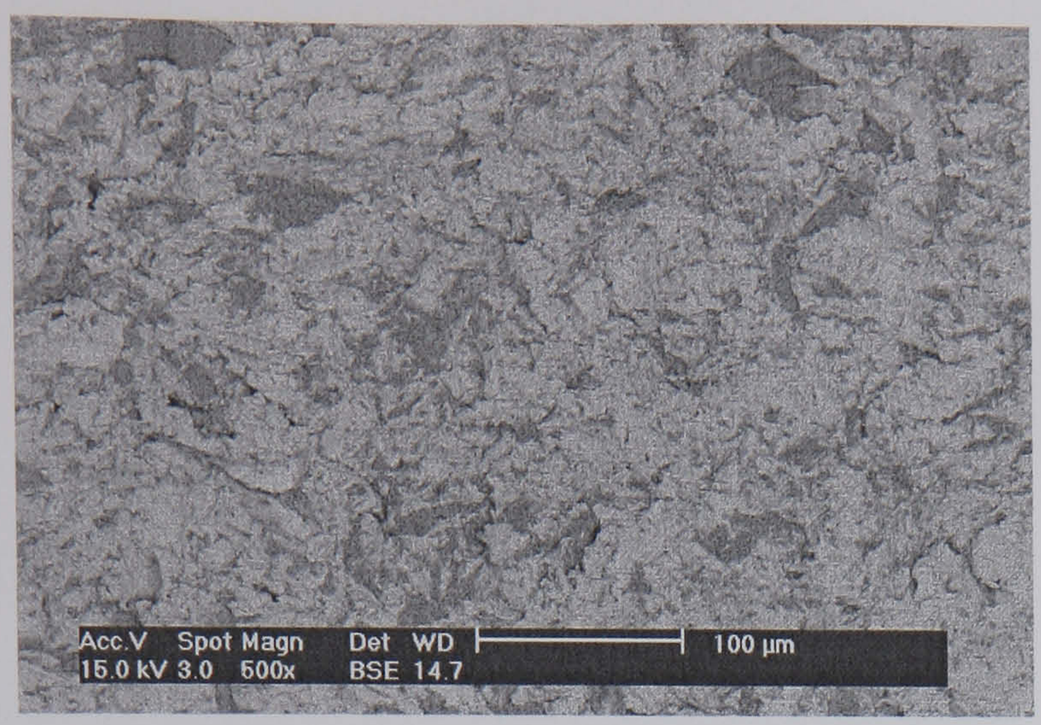

(a)

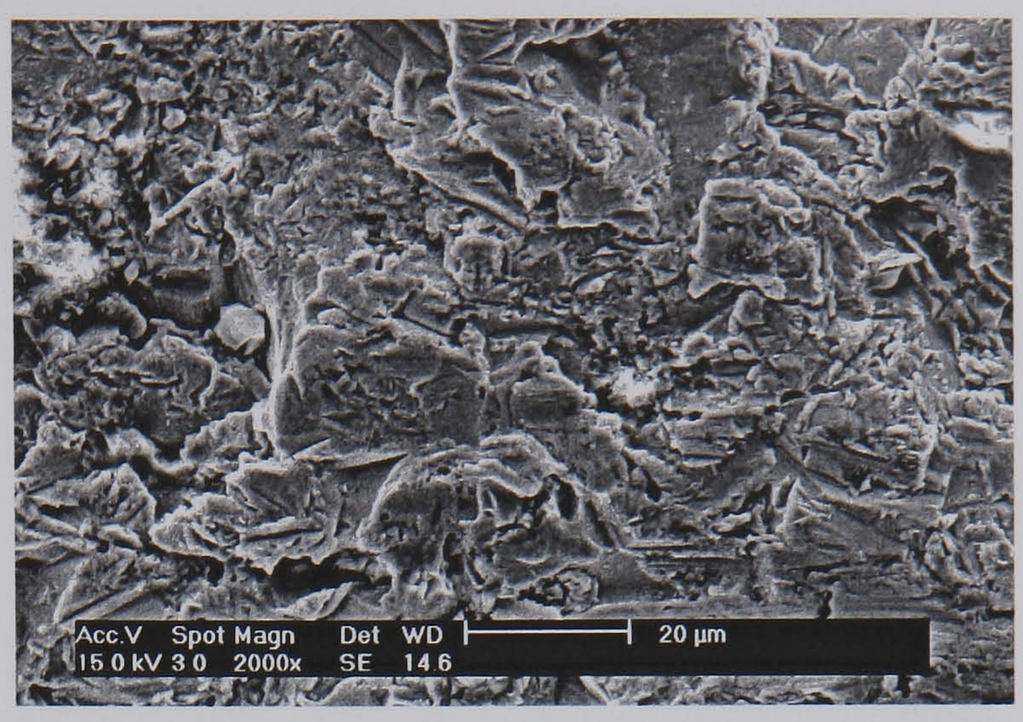

(b)

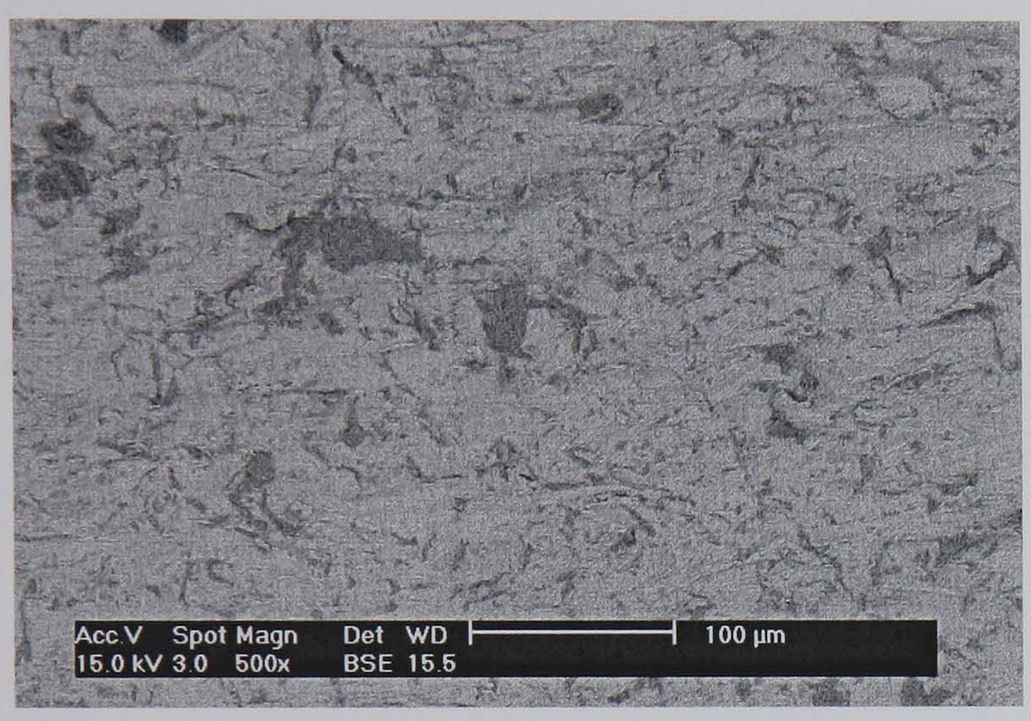

(c)

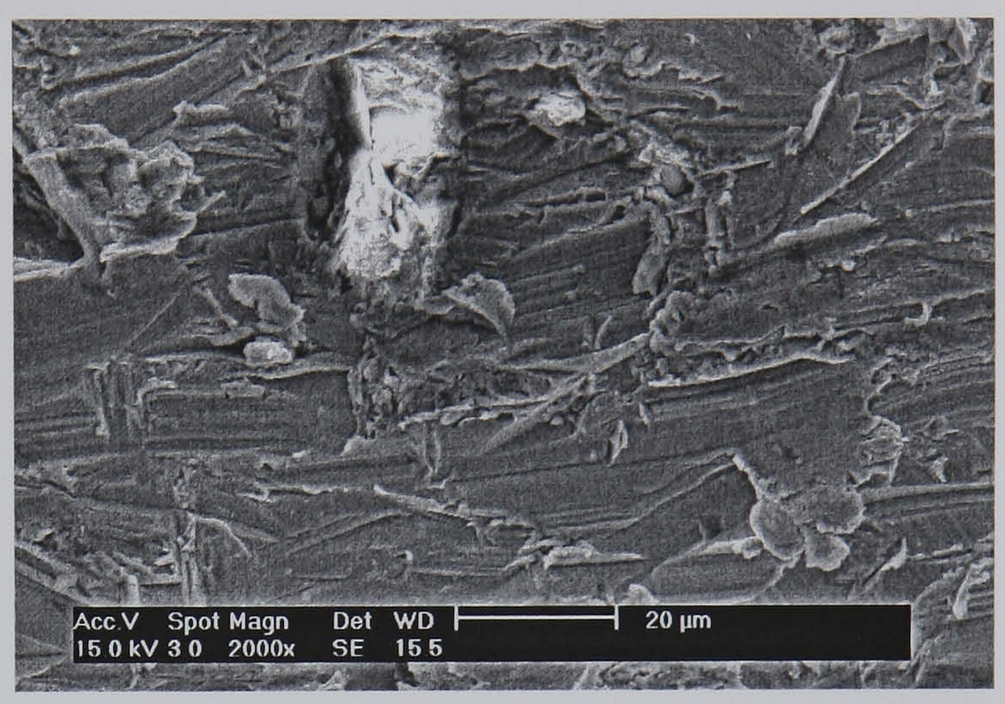

(d)

Figure 4.34 SEM micrographs of the bottom of AWJ-CDM tracks in Ti6Al4V using 180 µm (80#) garnet grit following a single pass of the jet; jet traverse speed of 0.003 m s^{-1} (200 mm min^{-1}); Jet angle $\theta = 75°$; water jet pressure 137.9 MPa (20 000 psi), stand off distance 3mm. (a) Forward milling - BSE; (b) Forward milling - SE; (c) Backward milling - BSE; (d) Backward milling - SE.

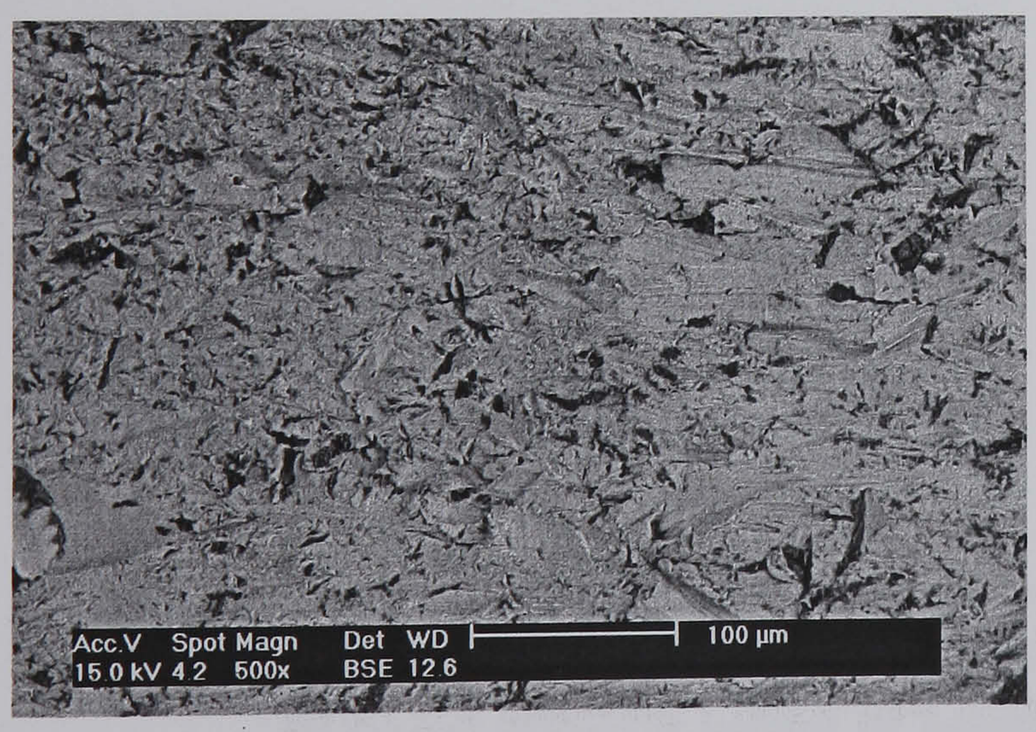

(a)

(b)

Figure 4.35 SEM micrographs of the bottom of AWJ-CDM tracks in Ti6Al4V using 180 µm (80#) garnet grit following a single pass of the jet: jet traverse speed of 0.003 m s^{-1} (200 mm min^{-1}); Jet angle $\theta = 90°$; water jet pressure 137.9 MPa (20 000 psi), stand off distance 3mm. (a) BSE showing grit embedment; (b) SE showing surface morphology.

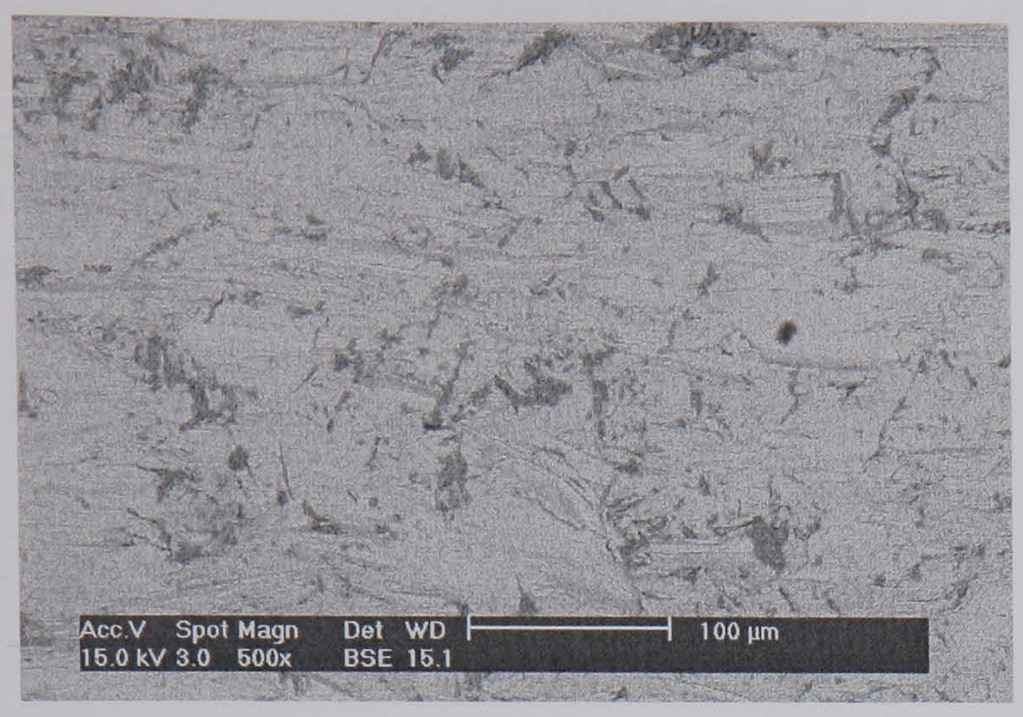

(a)

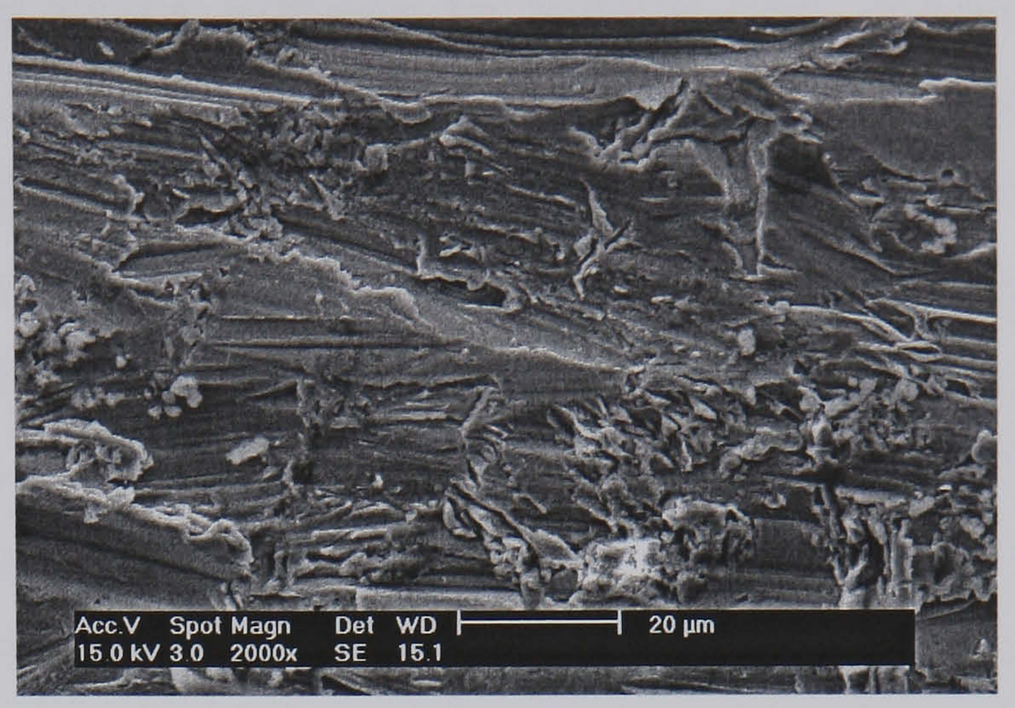

(b)

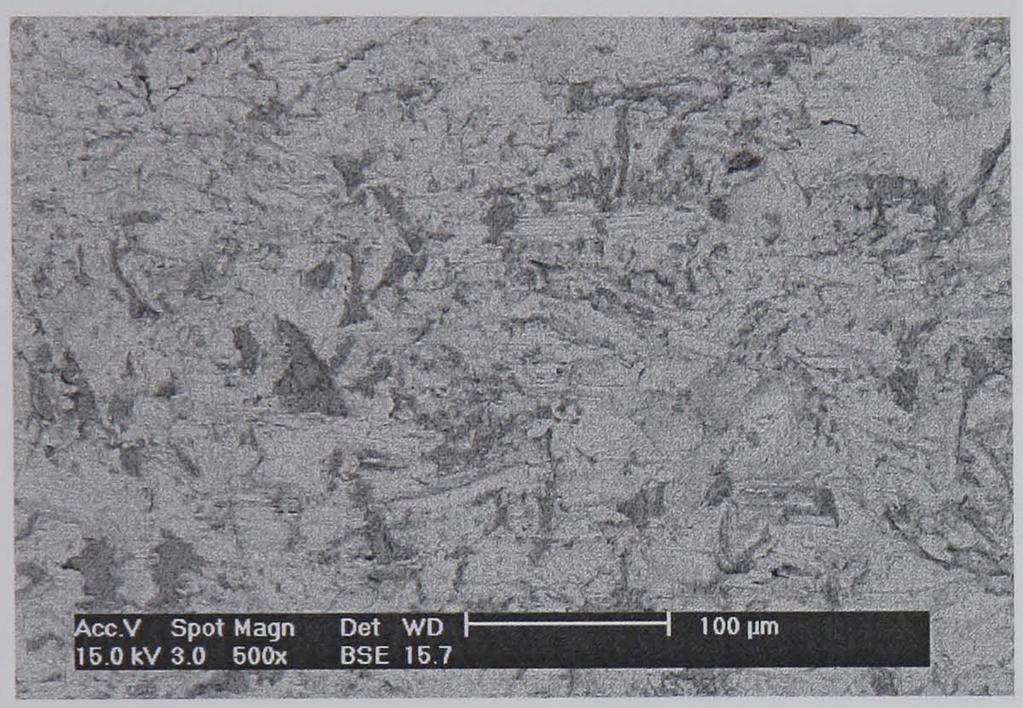

(c)

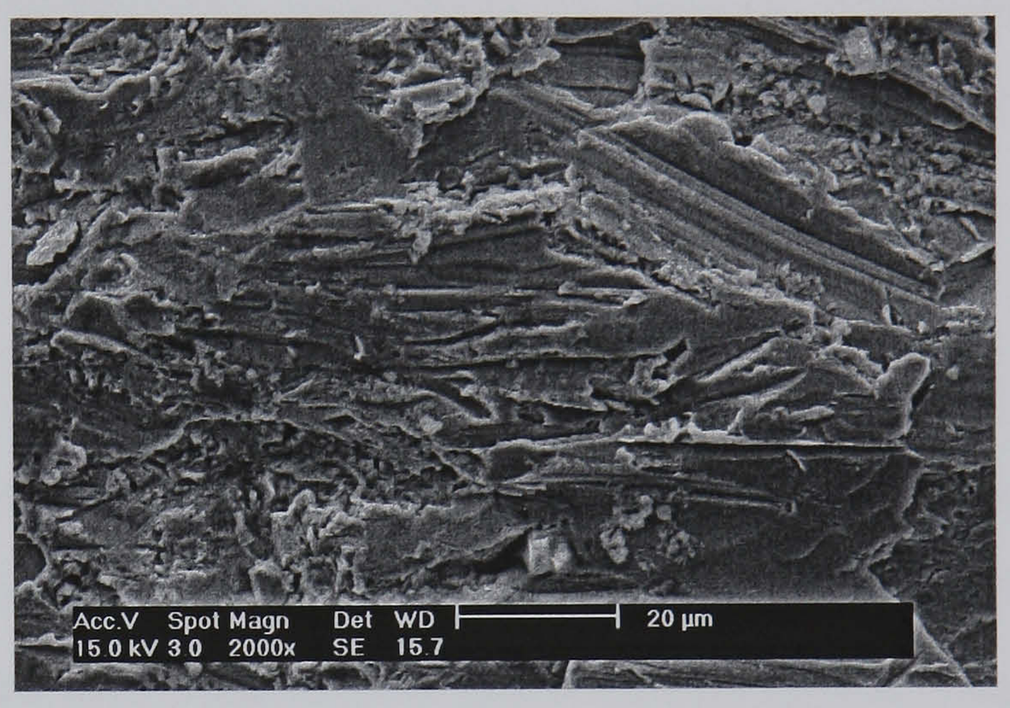

(d)

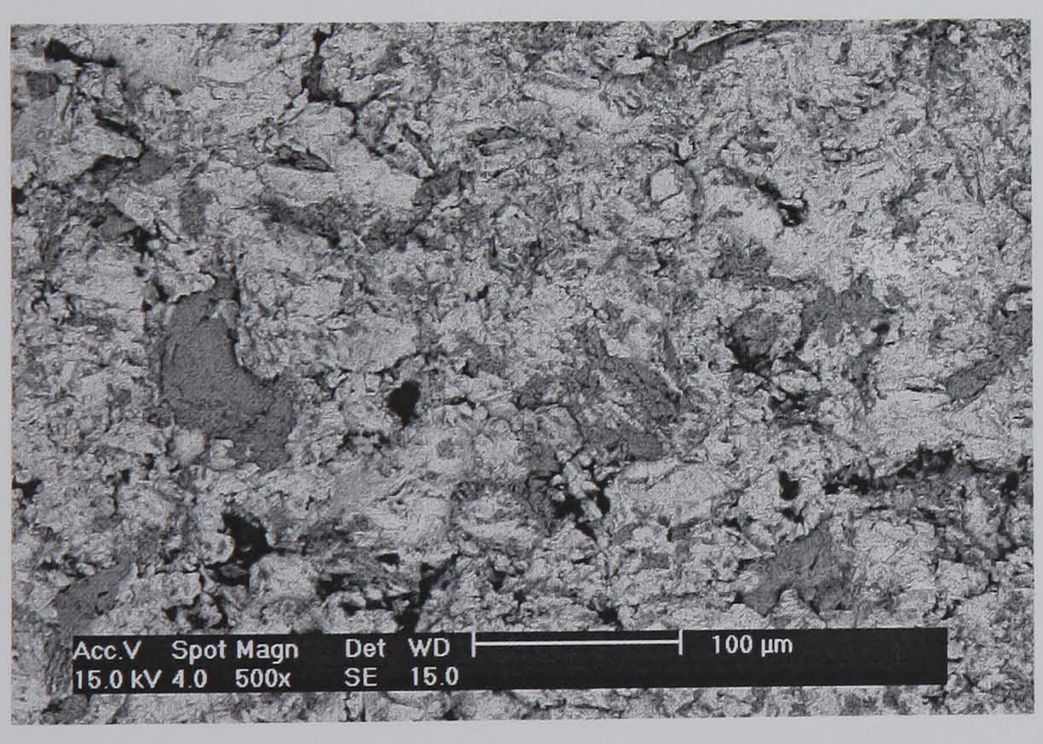

(e)

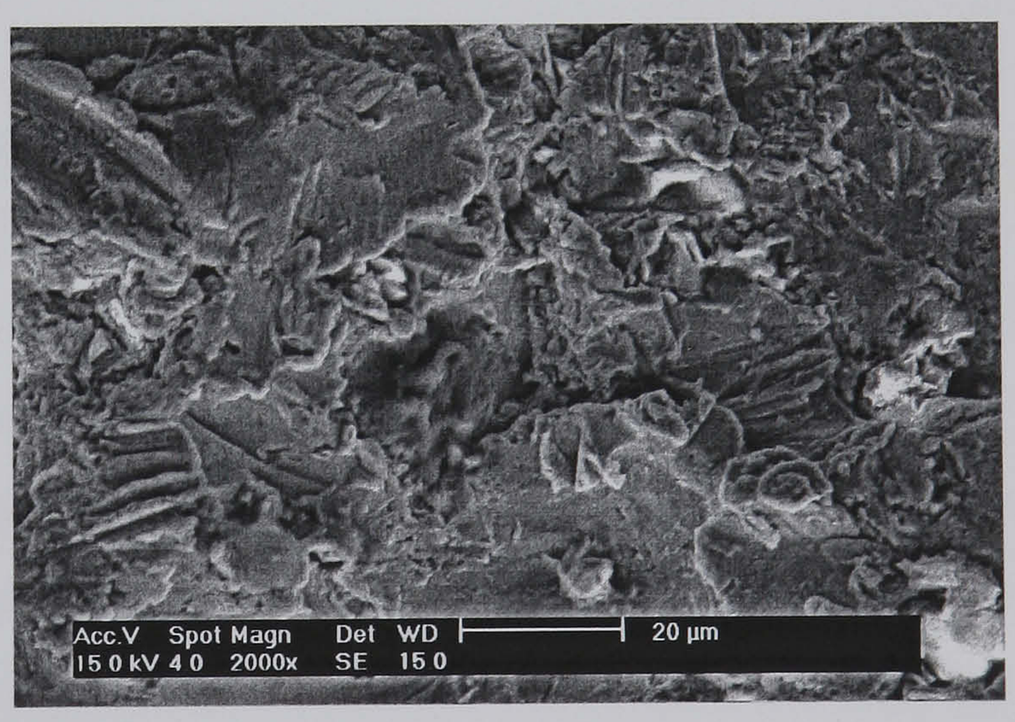

(f)

Figure 4.36 SEM micrographs of the bottom of AWJ-CDM track in Ti6Al4V using 180 µm (80#) garnet grit following a single pass of the jet with a traverse speed of 0.166 m s^{-1} (10 000 mm min^{-1}); Backward milling at various jet impingement angles, θ. Water jet pressure 137.9 MPa (20 000 psi), stand off distance 3mm. (a) θ = 15°, BSE; (b) θ =15°, SE; (c) θ = 45°, BSE; (d) θ = 45°, SE;. (e) θ = 90°, BSE; (f) θ = 90°, SE.

4.4.2 Discussion.

Table 4.2 shows that the method of using image software to analyse BSE images results in a comparable figure to that derived for Fe location maps to assess the level of embedded grit. However, it should be noted that the image analysis of the BSE images are problematic since the roughness of the surface itself results in contrast which is difficult to differentiate from embedded grit. Therefore, the selection of thresholds to distinguish these needs care. Also, rough surfaces affect the accuracy of the EDX analysis. A further limitation of the image analysis of BSE image is that only grit embedment at the surface will be seen; sub-surface grit will not be detected. Nevertheless, grit is present and was observed to be present under all the experimental conditions investigated. Fig. 4.29 shows embedded fragments of surface and sub surface grits of different sizes all of which were identified as garnet grit using EDX spot analysis.

4.4.2.1 The nature of embedded grit.

Embedded grit was observed on milled surfaces under all the experimental conditions investigated in this programme. Fig. 4.29 shows embedded fragments of grit of different sizes; some of these fragments are exposed and fragmented grit (Fig.4.29a) and may be able to be removed from the surface by methods such as the high pressure water jet technique as suggested by Hashish [1991]. The particles observed in Fig. 4.29b have been totally covered over by metal being deformed over them by subsequent impacts. The sample in Fig. 4.29b was electroplated with cobalt to aid retention of the surface during metallographic preparation. It can be seen that cobalt has plated onto the metal which surrounds the left hand buried particle, indicating that there was a route for electrolyte to enter this region which is consistent with metal being deformed over the particles to entrap them. Similar observations of particles buried below the surface have been made by Ives and Ruff [1977] in stationary low pressure particle laden fluid erosion and by Singh and Jain [1995] following a post treatment method of ball milling to polish and remove surface defects such as burrs. It can be seen in Fig. 4.29b that the particles are only present just below the surface. Further passes of the water jet will either erode away the embeded grit, or the grit will be completely covered by parent material. This suggests that the embedment model derived by Ives and Ruff [1977] (Fig. 2.25) for stationary low pressure particle laden fluid erosion may be applicable to AWJ-CDM. Fig. 4.31 also shows that the level of embedded grit observed on a workpiece surface does not increase with number of passes of the jet, implying that a steady state situation is

quickly achieved where embedded particles are removed by later passes of the jet. We may also assume, therefore, these buried particles will be removed during further milling of the metal.

Examination of Fig. 4.29 and Figs. 4.32 - 4.36 reveals that most of the particles observed are less than 50 μm in size. When this is compared to the average original particle size of 180 μm of the grit employed to mill these surfaces (Fig. 4.29c), it is clear that whole grit particles are not embedded, but only fragments. It is not clear whether particles fragment upon impact leaving just portions of the particle embedded, or whether whole particles embed, but only to a depth which is a small fraction of the particle size and the non-embedded portion of the particle is broken away by subsequent impacts. It is, however, clear that whichever mechanism operates, significant damage is inflicted on the particles themselves; embedded particles (e.g. Fig. 4.29a, Fig. 4.29b) often show a fragmented structure, which is clearly identified in used milled grit retrieved from process effluent (Fig. 4.29d). The grit retrieved from process effluent is severely fragmented comprising of many sharp irregular fragments of particles rather than the regular sub rounded 'as received grit' (Fig. 4.29d), indicating that the former explanation is most likely. Moreover, it is clear that whichever mechanism operates significant damage is inflicted on the particles themselves and the embedded particles (Fig. 4.29) often show a fragmented structure.

The sub-surface grit is a concern since it may provide an initiation source for fatigue cracks, coating delamination or a source of mechanical failure. A method for removal of surface grit may be required per pass as suggested by Hashish [1987, 1991] and Singh and Jain [1995]. Incrementation of the water jet may also result in sub-surface grit development since 75% of the jet passes over previously milled surface. Therefore, water flushing as suggested by Hashish would require a cut, flush, increment, cut flush, increment system.

4.4.2.2 The influence of particle size on grit embedment.

Fig. 4.30 and 4.31 shows that grit size has only a small influence on the level of grit embedment for all the experimental conditions investigated. It is reasonable to assume that the degree of grit embedment will be a function of both the number of particles striking unit area and the tendency for an individual particle to embed. However, the level of grit embedment does not increase linearly with particle dose (number of particles impacting per unit area) since as the dose becomes greater, some embedded particles will be removed by the later impacts. For the same abrasive mass flow rate, the dose of

particles (measured by particle number rather than mass) impacting the surface will be larger for the smaller sized grit. Whilst it is not clear exactly what parameters control grit embedment into a surface, it is reasonable to assume that particles that penetrate deeper into the workpiece will have a higher tendency to embed. Assuming that particle size does not affect particle shape, the depth of indentation will depend upon the impulse of the particle impact and thus the particle momentum. Thus, whilst the number of particle impacts increases for a smaller particle size, the momentum of each particle is reduced since there is a reduction in mass. However, Blickwedel [1990] found that during the entraining of the abrasive grit in to water jet, the particle velocity increased as the mass of the particle is reduced. The experimental data to implies that these two opposing effects cancel each other out, resulting in the insensitivity of grit embedment to particle size. However, there is no evidence presented here that such a conclusion can be extrapolated beyond the particle sizes examined.

4.4.2.3 Grit embedment behaviour at low jet traverse speeds.

The behaviour of the workpiece material (in terms of grit embedment and development of surface morphology) depends upon the traverse speed of the jet across the sample surface. Previously in Fig. 4.1, it was shown that for traverse speeds above 0.016 m s^{-1}, the material removal rate was insensitive to traverse velocity whereas below this velocity, there was a significant increase in material removal rate with decreasing traverse speed. In this work, 0.003 m s^{-1} was taken as representing a low velocity (below this threshold) whereas 0.166 m s^{-1} and 5 m s^{-1} were taken as representing behaviour above this threshold velocity. The differences in surface morphology observed in this work after milling at different speeds indicates that the mechanisms of material removal in the two cases are different. In this section, workpiece behaviour under a slow traverse speed of 0.003 m s^{-1} is discussed.

Fig. 4.30a, 4.27d and 4.27e demonstrate that there is a difference in the angular dependence of level of grit embedment and surface morphology dependent on whether forward or backward milling is employed. In broad terms, the level of grit embedment is generally lower in backward milling than in forward milling at low jet traverse speeds. The changes in surface morphology are summarised in Figs. 4.27d and 4.27e and can be seen directly in Figs. 4.32 - 4.35. The most significant differences are that at intermediate jet impingement angles of 45° and 75°, forward milling results in a more cratered morphology whereas backward milling results in a more directional grooved morphology. At the low jet impingement angle of 15°, both modes of milling result in a grooved morphology and at normal jet impingement (where forward and backward mode

are indistinguishable), a primarily grooved morphology (with some evidence for cratering) resulted.

When milling in backward mode at this low traverse speed, the grooved morphology is observed at all jet angles considered (Fig. 4.32d, 4.33d and 4.34d), except at 90° (Fig. 4.35b) where some evidence for cratering was observed. Ojmertz [1993] and Li et al. [1996a] both observed similar directional grooved morphologies following AWJ milling in backward mode. When milling at normal jet angles with a low jet traverse speed, Ojmertz [1993] observed a mixed morphology of craters due to deformation wear and scratch like grooves due to cutting wear whereas Li et al. [1996a] observed only a cratered morphology under similar conditions. In this work, there is evidence of primarily directional grooving in the sample milled under normal conditions (Fig. 4.35b). In forward milling, grooved morphologies result from milling at low impingement angles (Fig. 4.32b), with an increasingly cratered morphology as the impact angle is increased (Fig. 4.33b) until at 75° no evidence of grooving is present (Fig. 4.34b). However, at normal impingement, the primarily grooved morphology again results (Fig. 4.35b).

Such significant changes in grit embedment and surface morphology suggest changes in mechanisms of material removal, dependent upon jet impact angle and milling mode. Fig. 4.11 shows schematically the modes of material removal with a low jet traverse speed. As argued earlier, a rapid change in momentum of a particle will result in a high tendency for grit embedment. Also, impact of particles at high impact angles will result in a cratered morphology whereas impact at low angles will result in a grooved morphology. However, the local impact conditions do not depend only on the global jet impingement angles but also upon the shape developed in the material by material removal. In low speed milling, the depth of material removed per pass can be large (Fig. 4.1). Fig. 4.11a illustrates the situation for milling at a high jet impingement angle in forward mode. A deep groove is formed and much of the cutting is performed at very low angles of attack on the leading edge of the kerf face. As the particles reach the area where the kerf face and the bottom of the groove intersect, the particle momentum change is large and rapid, whatever direction the particles leave the impact zone. Some particles will leave the impact zone by flowing along the already milled groove whilst most will leave the impact zone by rebound away from the surface. Fig. 4.34b (typical of this situation) exhibits a cratered morphology on the groove base as a result of such particle interactions. As the impact angle is raised further to 90°, there is more tendency for the particle-containing fluid to run along the groove bottom and to provide evidence of directionality as this removes material by cutting. Similar evidence of grooving associated with particles striking the surface at low impact angles as the jet has flowed

along the groove has been reported by other workers [Hashish, 1998a, Bitter, 1963a, 1963b, Summers, 1995]. The increased tendency between 75° and 90° for the particle-containing fluid to flow along the groove also results in the removal of some of the embedded grit, and thus to the lower levels of embedded grit at 90° (Fig. 4.29a).

Fig. 4.11b illustrates the change in the situation as the jet impingement angle is reduced in low traverse speed forward milling. Here the zone where the particle momentum is rapidly changed (the impact zone) moves from the bottom of the groove to the kerf wall. In this region, high grit embedment is expected (due to the high particle impulse) but this region of the material is removed as the milling proceeds and thus at low impact angles, the level of grit embedment is low (Fig. 4.29a). At these low impact angles, the back edge of the jet will actually strike the groove bottom at a low impact angle, producing a grooved morphology (Fig. 4.32b) and again remove already embedded grit.

Fig. 4.11c illustrates the situation for a high jet impingement angle in backward milling mode. Here the kerf front wall exhibits a smooth transition into the groove bottom. As such, the rate of change of momentum of a particle (the impulse) is lower than in the forward milling case (Fig. 4.11a) and thus the degree of grit embedment is lower (Fig. 4.30a). The natural tendency of the fluid stream will be to be diverted and flow along the groove bottom so that even at high nominal jet impingement angles, a grooved morphology is produced (Fig. 4.34d). The impulse of particles will be reduced as the nominal jet impingement angle is reduced (Fig. 4.11d). Here, low local particle impact angles will result, giving low levels of particle embedment and a grooved morphology as the grit loses energy during ploughing and embeds at the end of a partially formed groove [Ramulu and Raju, 1993, Ives and Ruff, 1977].

In summary, it has been shown that at low jet traverse speeds, embedment is favoured by high local impact angles. In backward milling, the local impact angle increases with increasing jet impingement angle, thus resulting in an increase in particle embedment. In forward milling, the local particle impact angle is high in all cases; however, as the jet impingement angle is reduced, the zone where particle embedment occurs moves from the groove bottom to the kerf front wall. Any embedment on the kerf front wall will be removed by the removal of that material in the milling process and so is not observed in the final product. The level of embedment for a jet impingement angle of 90° is lower than expected due to removal of grit due to enhanced flow of particle-laden fluid along the groove. Also, it has been shown that the observed morphology can be influenced by local impact conditions and by flow of particle-laden fluid from later milling. In backward milling, all impacts and flow of the particle-laden fluid tend to lead to a grooved

morphology. In forward milling, high impact angles result in cratering whereas low impact angles result in grooving, primarily from the back edge of the jet.

4.4.2.4 Grit embedment behaviour at high jet traverse speeds.

At high jet traverse speeds, the situation is much less complex than for low jet traverse speeds, since in this case the effect of milling mode (forward or backward) becomes insignificant. Fig. 4.30b and Fig. 4.30c show that the milling mode does not affect the level of grit embedment, with a monotonic increase in level of grit embedment with increasing jet impingement angle. A similar trend was also observed by other researchers using a variety of erosion methods [Hashish, 1991, Hashish, 1989b, Zu et al. 1991]. The level of grit embedment observed was as high as 36% at high jet impingement angles and as low as 5% at low jet impingement angles. The grit embedment is higher than that seen by other workers [Armada et al. 1999, Griffiths et al. 1999, Zu et al. 1991], who observed about 9% grit embedment following low pressure particle laden erosion such as grit blasting at high jet angles. The higher level of grit embedment seen in the current investigation may result from the higher particle impact velocities (resulting in higher particle impulses) and the nature of the milled material.

The jet impingement angle also has a strong influence on the surface morphology of a surface milled with a high jet traverse speed. Fig. 4.36 shows that a cratered morphology is observed at high jet impingement angles and a directional grooved morphology is observed at low jet impingement angles. In the current investigation, a cratered morphology was observed when high speed milling at jet impingement angles above 45° and a directional grooved morphology at jet impingement angles below 45°. Armada et al. [1999], Griffiths et al. [1999] and Zu et al. [1991] also observed a similar change in morphology when grit blasting using stationary low pressure particle laden fluids; they observed the surface morphology changed from cratered morphology at high blasting angles to a directional grooved like morphology at blasting angles below 45°.

Fig. 4.12 illustrates the modes of material removal with high jet traverse speeds. In all cases, the depth of cut is small and the leading edge of the kerf face makes up a very small proportion of the total cutting area. The small depth of cut is the reason why forward and backward milling result in very similar behaviour. Also, the local particle impact angles are generally the same as that of the jet impingement angle. Also, since the small depth of cut of the material being milled in the current pass is very small to that of the surrounding material (not the case for low jet traverse velocities), then the tendency of the particle laden fluid to run along the groove is also reduced. Thus, the

monotonic increase in levels of grit embedment with jet impingement angle is simply associated with increasing particle impulse (related to the normal component of the velocity vector). Also, due to the lack of fluid channelling, the surface morphology is as expected, with directional grooving at low jet impingement angles and cratering at high impact angles.

Once the influence of the kerf front wall has become small, further decreases in the height of that wall (by increasing the jet traverse speed) have negligible effect. This can be clearly seen when comparing the levels of grit embedment with jet traverse speeds of 0.166 m s^{-1} and 5 m s^{-1} (Fig. 4.30b and Fig. 4.30c). Here the levels of grit embedment are identical (within the limits of experimental error) indicating that the level of grit embedment is controlled primarily by the mechanism of material removal, which is the same for these two traverse speeds (Fig. 4.1).

4.4.2.5 The effect of secondary milling.

It is interesting to compare the behaviour of the material milled with high jet traverse speed with that backward milled with low jet traverse speed, since it has been argued in both cases that the local particle impact angle is similar to that of the jet impingement angle. The morphologies are very similar at low and intermediate angles (cf. Fig. 4.32d and Fig. 4.36b; also cf. Fig. 4.33d and Fig. 4.36d). However, at normal jet impingement, there is a significant difference in morphology (cf. Fig. 4.35b and Fig. 4.36f). Under high speed conditions (Fig. 4.36f), only cratering can be observed, due to the impact of particles. The scale of the damage appears to be similar to that occurring for the other impact angles (Fig. 4.36b and Fig. 4.36d). However, under low speed conditions (Fig. 4.35b), the mechanism of material removal is dominated by grooving. In this case, the cratered surface produced during milling by particle impact has been smoothed off by the later flow of the particle laden fluid along the deep channel. This has also resulted in a decrease in grit embedment between the two conditions; Fig. 4.30 shows that under low speed conditions, grit embedment is less than 20% whereas under high speed conditions it is around 40%. Thus, the flow of the particle-laden fluid along the groove has resulted in significant removal of material, giving a grooved morphology and a significant reduction in the level of embedded grit.

Comparing Fig. 4.30a and Fig. 4.30b, it is also notable that the level of grit embedment was always higher following milling with a high jet traverse speed than following backward milling with a low jet traverse speed. At first sight, this is counterintuitive since at low traverse speed the dose of particles is much higher. However, the secondary

milling due to channelling of particle laden fluid along the groove with low traverse speeds has resulted in removal of embedded grit resulting in consistently lower values of embedded grit across the range of jet impingement angles examined.

Fig. 4.30c shows that forward milling as a function of jet impingement angle at very high traverse speeds (5 m s^{-1}) with a fixed number of jet passes, results in similar grit embedment to that seen when milling at a high traverse speed (0.166 m s^{-1}) with single passes. In order to establish whether the jet traverse speed or the number of passes of the jet has the stronger influence on the grit embedment process, an investigation was conducted at a high jet angle and a known high traverse speed with a variable number of passes. Fig. 4.30b indicates that the direction of milling has little influence when milling at high speeds. Fig. 4.30c and Fig. 4.31 show that as the number of jet passes increases, the grit embedment remains constant. Further, multiple passes of the jet at the very high traverse speed of 5 m s^{-1} had little influence on the surface morphology (Fig. 4.26b and Fig. 4.26d also cf. Fig. 4.36b and Fig. 4.36f). The morphology was observed to be similar to that observed at the lower speed of 0.166 m s^{-1} which were conducted with a single pass of the jet. Fig. 4.25c shows that the roughness also remains constant while the waviness increased (Fig. 4.25b). The grit size also has no influence on the degree of grit embedment following multiple passes of the jet. The jet impingement angle has the strongest influence on the grit embedment and surface morphology at high traverse speeds.

4.5 The role of process parameters on the milling of titanium aluminide.

4.5.1 Results.

The main body of research presented in this thesis has addressed the process characteristics of AWJ milling of Ti6Al4V, a material that is difficult to machine by conventional methods. However, there is interest in the wider applicability of the AJW-CDM process to the machining of ductile and brittle materials. Included in this group of materials is titanium aluminide which is considered to be a brittle material with an elongation to failure of 1- 4% [Stoloff and Sikka, 1996]. It is difficult to machine by any conventional methods (where as Ti6Al4V can be machined to some extent with care).

The aerospace industry has interest in titanium aluminide as a potential material for components which require enhanced creep resistance at elevated temperatures [Stoloff and Sikka, 1996]. The material is however, very difficult to machine [Stoloff and Sikka, 1996] and requires examination in how the material responds to AJW-CDM. A comparison of the AJW-CDM behaviour of titanium aluminide and Ti6Al4V is presented in this section. Tables 4.4 and 4.5 show the composition and basic mechanical property data for titanium aluminide and Ti6Al4V for comparision.

Element	**Ti6Al4V (%Wt)**	**Titanium Aluminide**
Titanium (Ti) (Wt %)	90.1*	63.6**
Aluminium (Al) (Wt %)	5.8*	30.4**
Vanadium (V) (Wt %)	4.1*	
Niobium (Nb) (Wt %)		5.0**
Manganese (Mn) (Wt %)		1%**
Boron (as TiB_2) (Wt %)		0.8% vol**

Table 4.4 Chemical Composition TiAl6V4 alloy and titanium aluminide material. [* as measured], [**as measured aerospace company].

Material Property	Ti6Al4V Alloy	Titanium Aluminide
Basic composition	Ti6Al4V	Ti30Al
Primary Formed Shape	Annealed rolled flat bar stock**	Investment casting**
Crystal Structure	α - β**	γ - α_2 – TiB_2**
Tensile Strength	960 MN m^{-2} *	685 MN m^{-2}**
Elongation to failure	13%* 8%min***	1.5%**
Fracture toughness	52 MPa $m^{1/2}$****	20 MPa $m^{1/2}$**
Youngs modulus	114 GN m^{-2}****	150 GN m^{-2}**
Vickers Hardness	331*	329*
Knoop hardness	378*	386*
Density	4.46 kg m^{-3}****	4.01 kg m^{-3}**
Grain size	52 μm*	43 μm*

Table 4.5 Material Properties of TiAl6V4 alloy and titanium aluminide material. [* as measured]. [**as measured aerospace company]. [***British Standards Institute BSI 2TA11] [****Polmear, 1995].

Fig. 4.37a shows the effect of traverse speed on material removal rate for both Ti6Al4V and titanium aluminide for two grit sizes. It can be seen that material removal rate is similar for both materials across the range of traverse speeds examined. Again, Fig. 4.37b and Fig. 4.37c show that titanium aluminide shows very similar waviness and roughness characteristics to the Ti6Al4V discussed in section 4.1.

The role of jet impingement angle on material removal rates, waviness and roughness when milling titanium aluminide is shown in Fig. 4.38. It can be seen that material removal rates are similar for both materials with the erosion rate maxima occurring at similar jet impingement angles (Fig. 4.38a). The waviness and roughness developed in titanium aluminide (Fig. 4.38b and Fig. 4.38c) also show similar characteristics to Ti6Al4V as discussed in section 4.2.

Fig. 4.39 shows the development of depth of cut, roughness and waviness with multiple passes of the nozzle across the workpiece for both Ti6Al4V and titanium aluminide. The behaviour of titanium aluminide is similar to that of Ti6Al4V in that, the depth of cut increased linearly with number of passes (Fig. 4.39a). Titanium aluminide also exhibited similar waviness (Fig. 4.39b) and roughness (Fig. 4.39c) characteristics to Ti6Al4V as discussed in section 4.2.

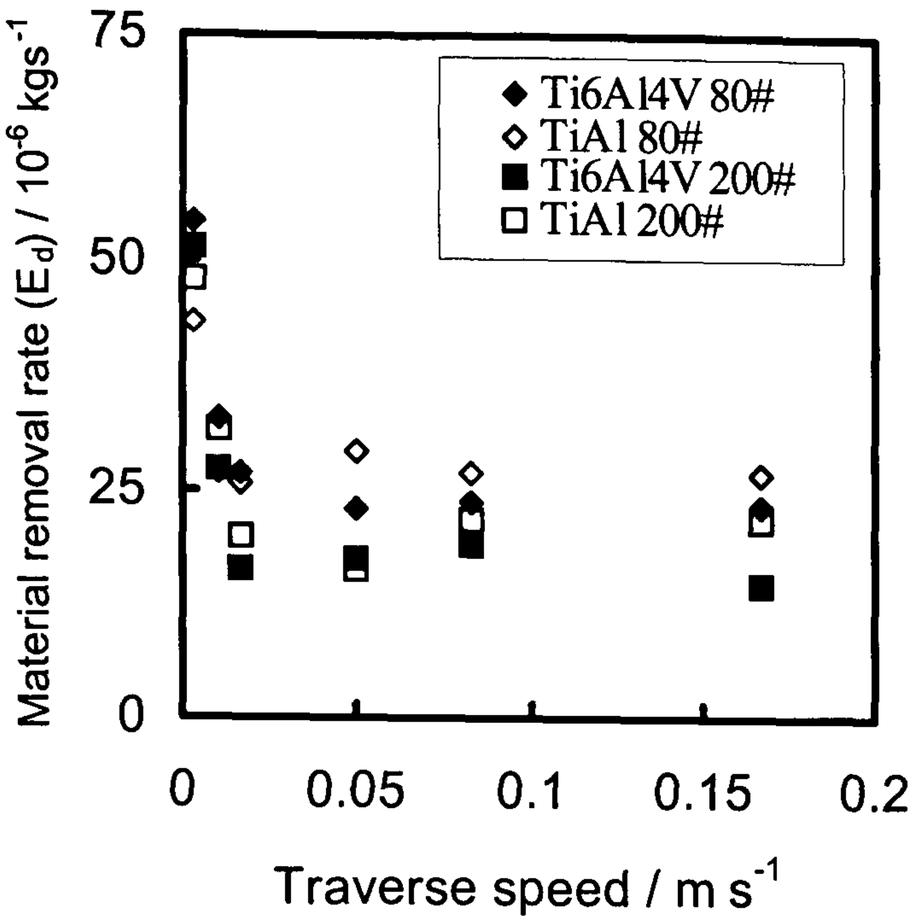

(a)

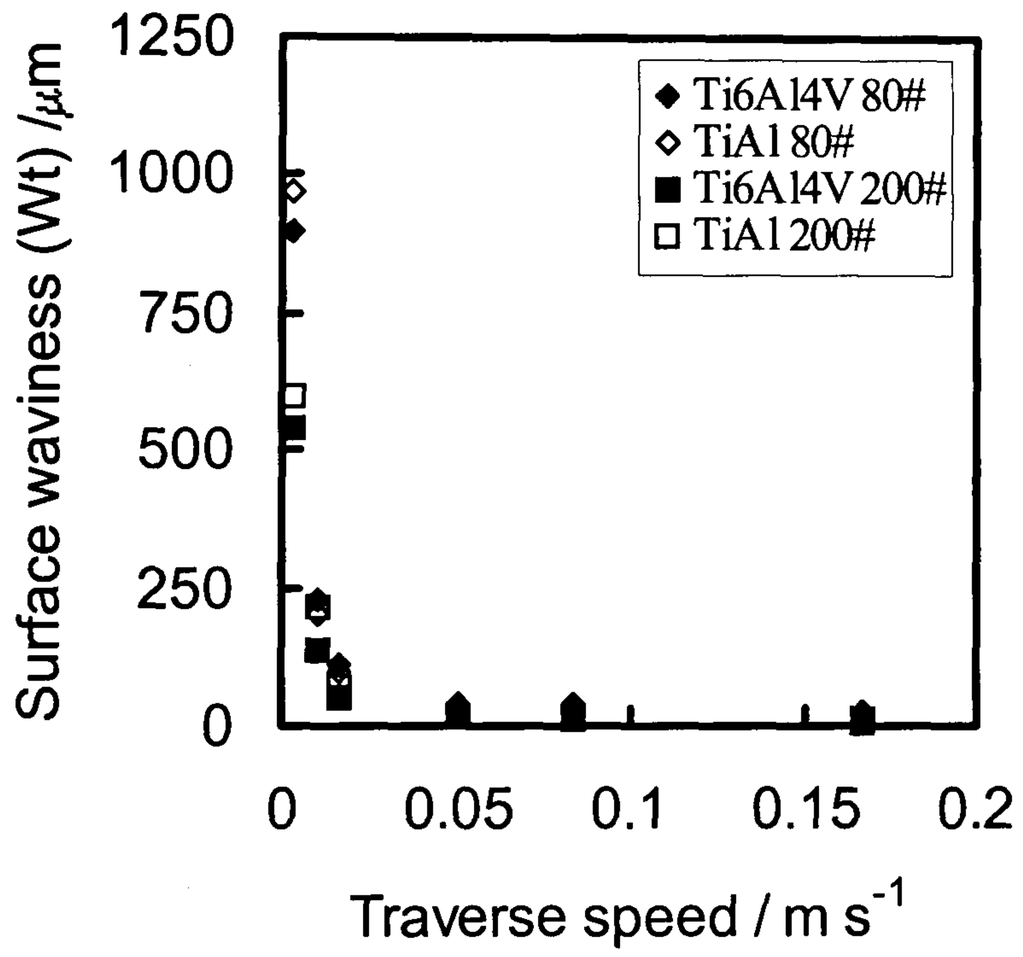

(b)

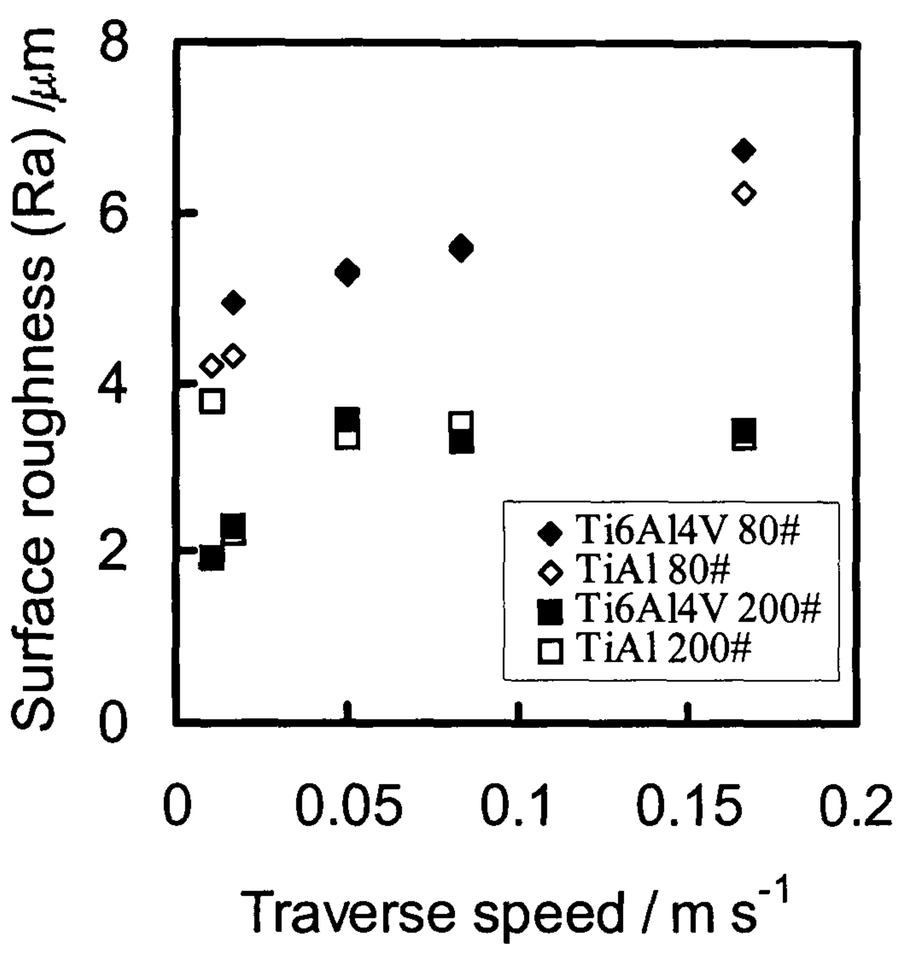

(c)

Figure 4.37 Material removal rate, surface waviness and roughness developed during AWJ-CDM of Ti6Al4V and titanium aluminde as a function of jet traverse speed; milling with 180 μm (80#) and 75 μm (200#) garnet grit; water jet pressure 137.9 MPa (20 000 psi), stand off distance 3 mm, jet impingement angle 90° (a) Material removal rate developed as a function of jet traverse speed. (b) Surface waviness developed as a function of jet traverse speed. (c) Surface roughness developed as a function of jet traverse speed.

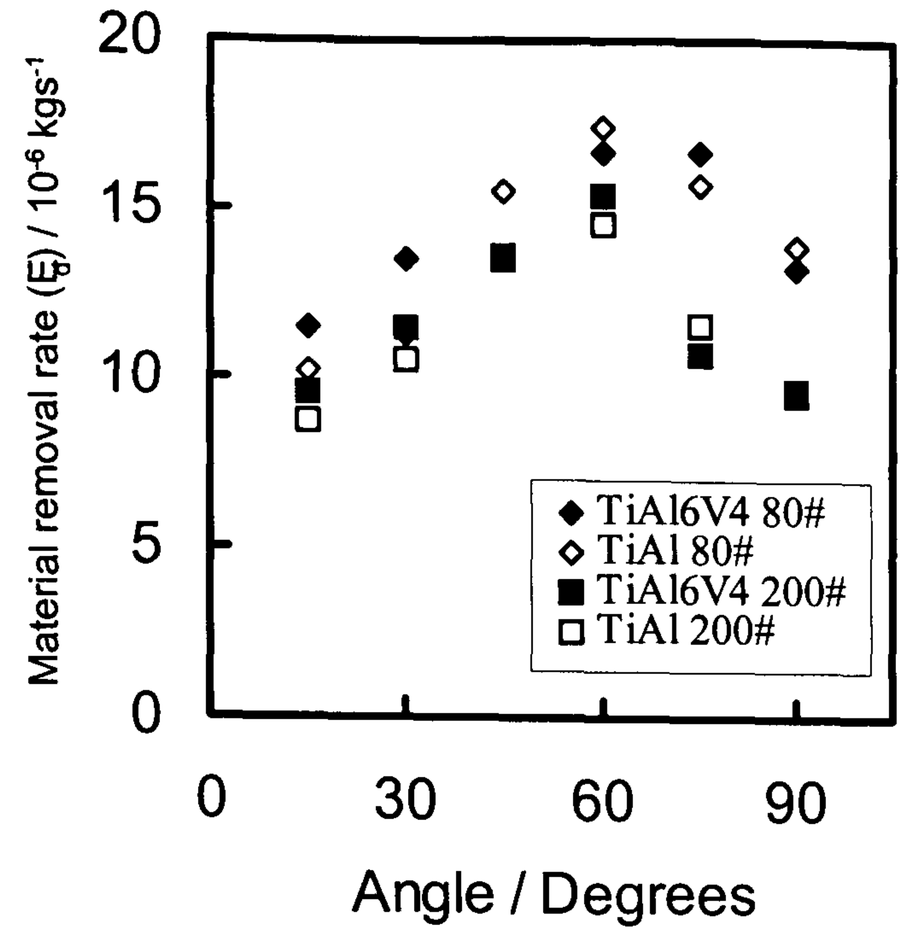

(a)

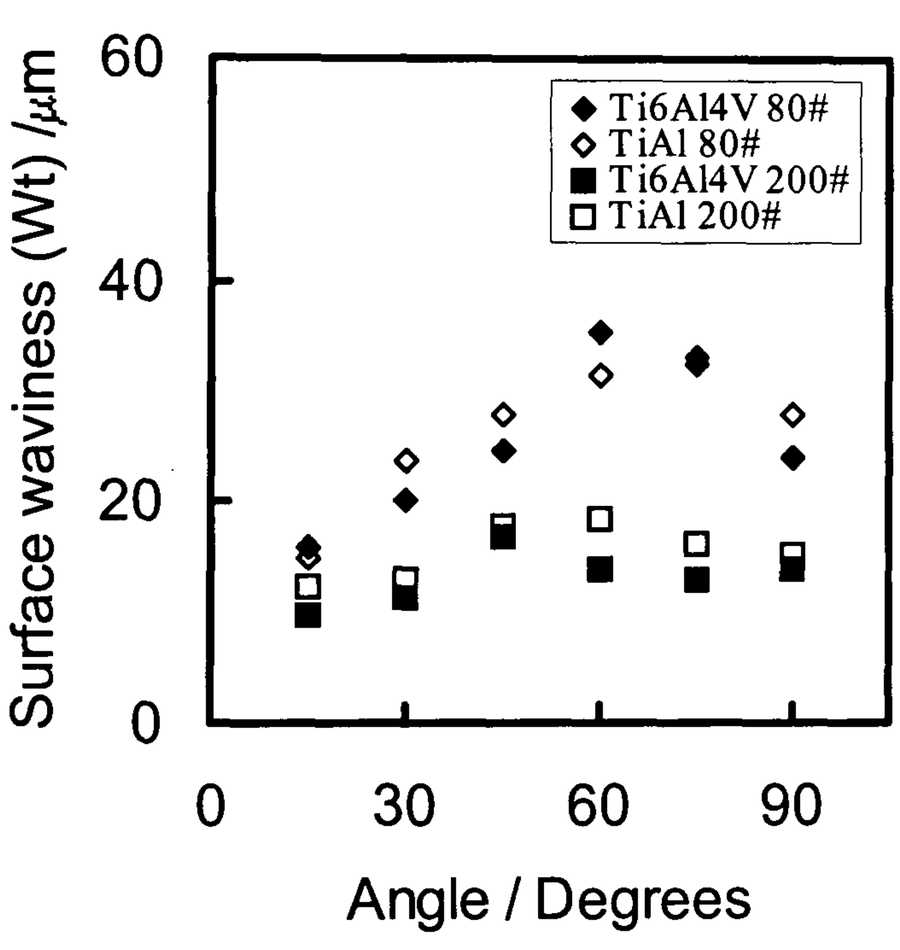

(b)

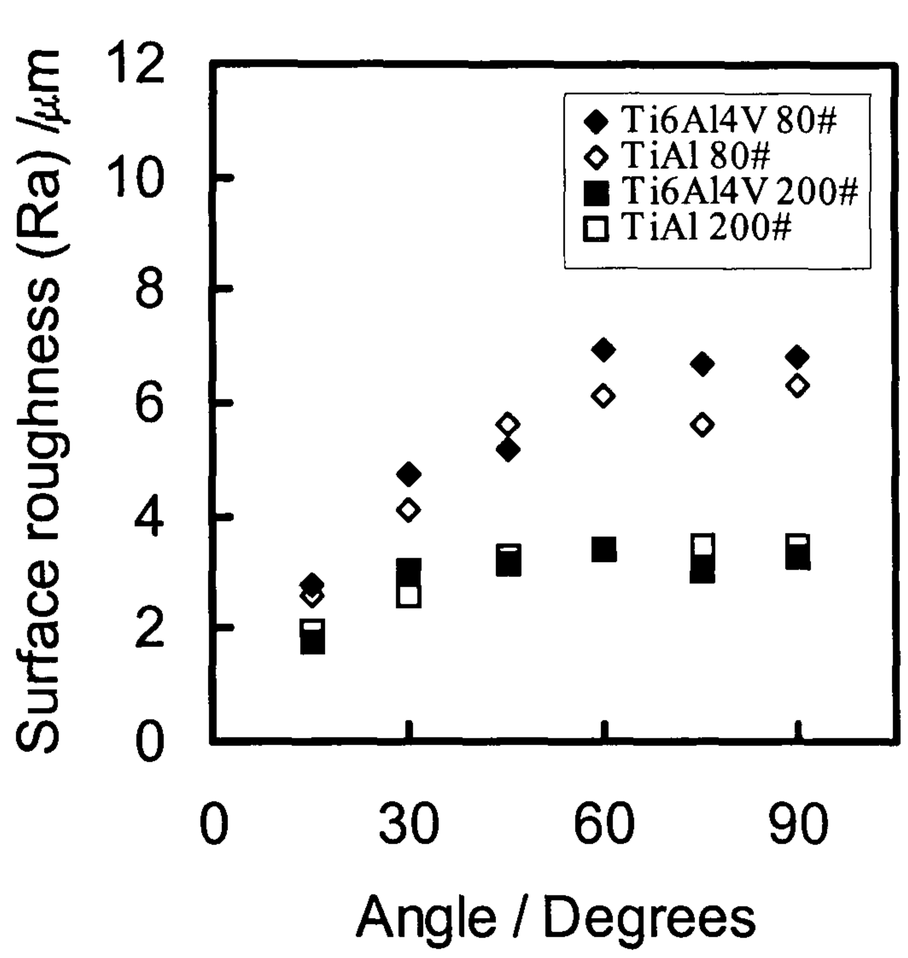

(c)

Figure 4.38 Material removal rate, Surface waviness and roughness developed during AWJ-CDM of Ti6Al4V and titanium aluminde as a function of jet impingement angle; high speed Forward milling (5 m s^{-1}) with 180 μm (80#) and 75 μm (200#) garnet grit; water jet pressure 137.9 MPa (20 000 psi), stand off distance 3mm. (a) Material removal rate developed as a function of as a function of jet impingement angle. (b) Surface waviness developed as a function of jet impingement angle. (c) Surface roughness developed as a function of jet impingement angle.

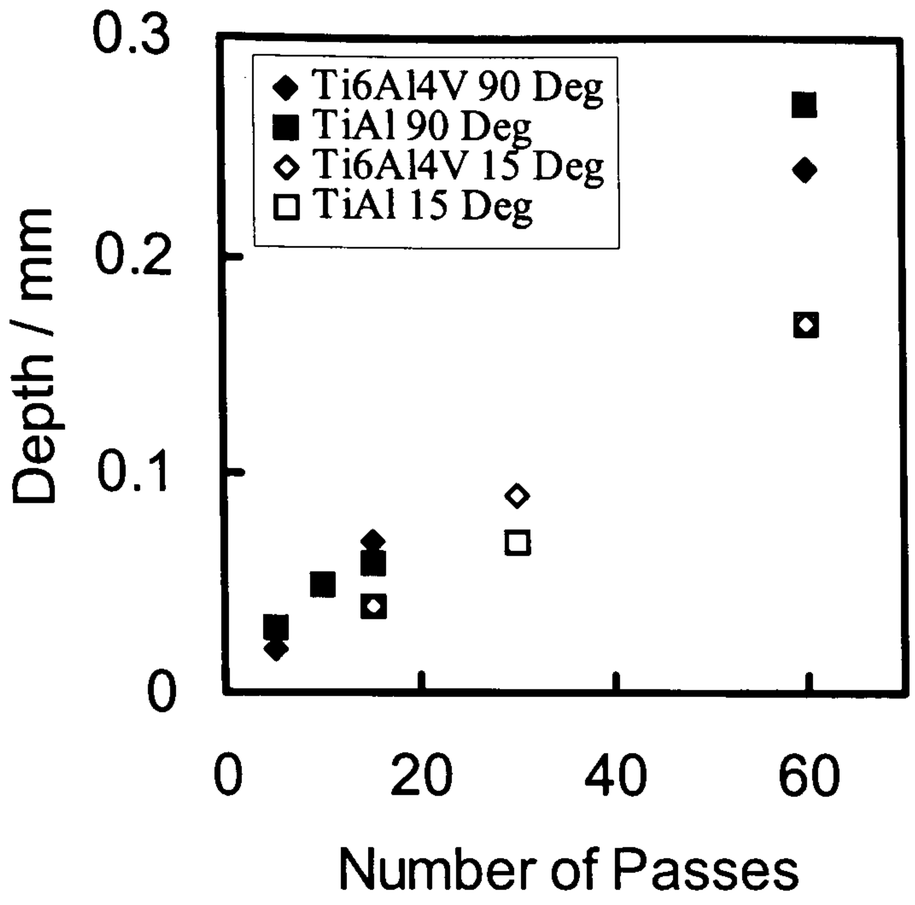

(a)

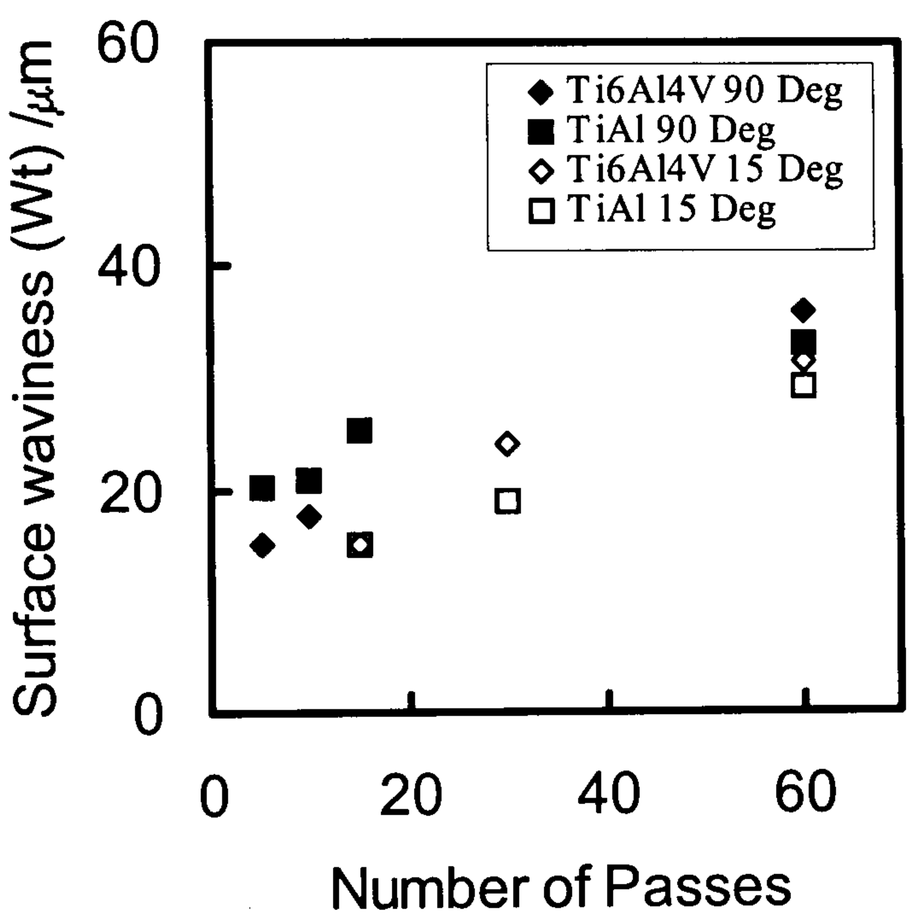

(b)

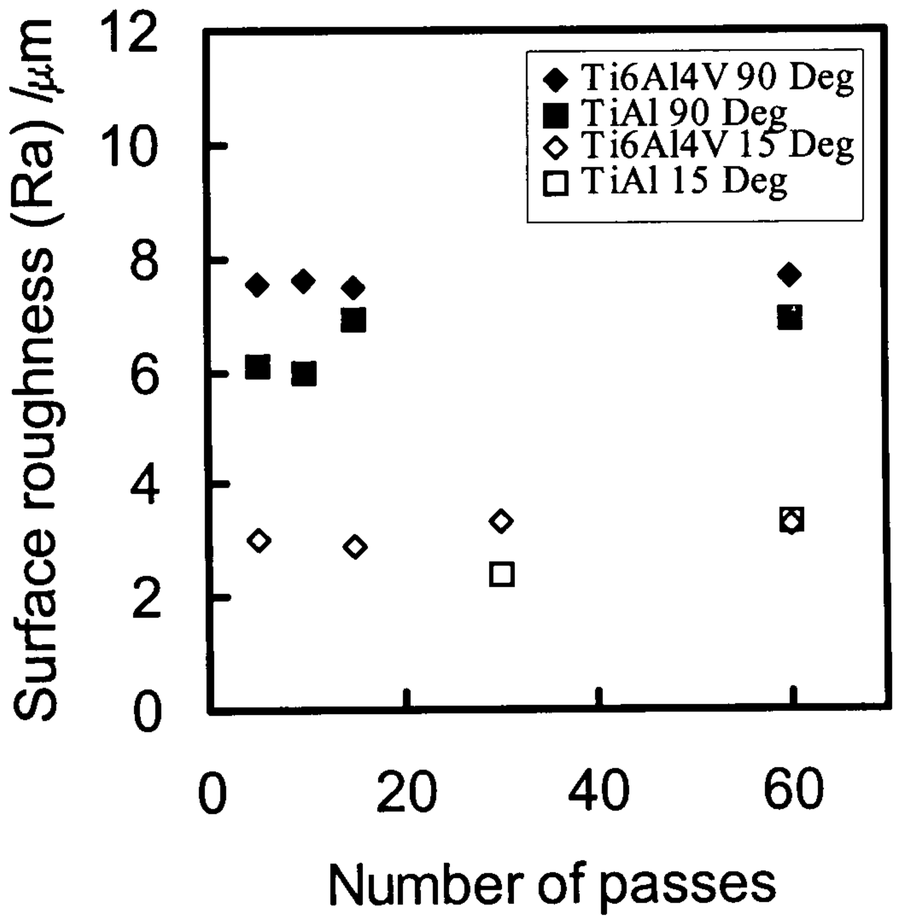

(c)

Figure 4.39 Depth, surface waviness and roughness developed during AWJ-CDM of Ti6Al4V and titanium aluminde as a function of jet passes; high speed Forward milling (5 m s^{-1}) with 180 μm (80#) garnet grit using high (90°) and low (15°) jet angles; water jet pressure 137.9 MPa (20 000 psi), stand off distance 3mm; milling at 10 mm slot with ¼ jet increment. (a) Depth developed as a function of jet passes. (b) Surface waviness developed as a function of jet passes; (c) Surface roughness developed as a function of jet passes.

(a)

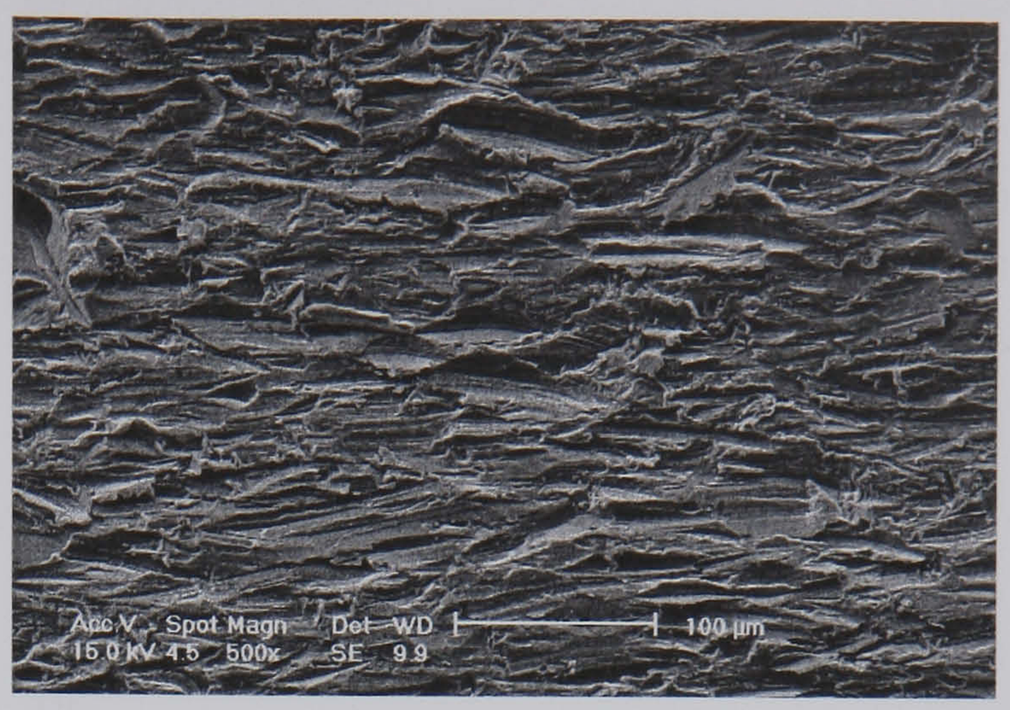

(b)

(c)

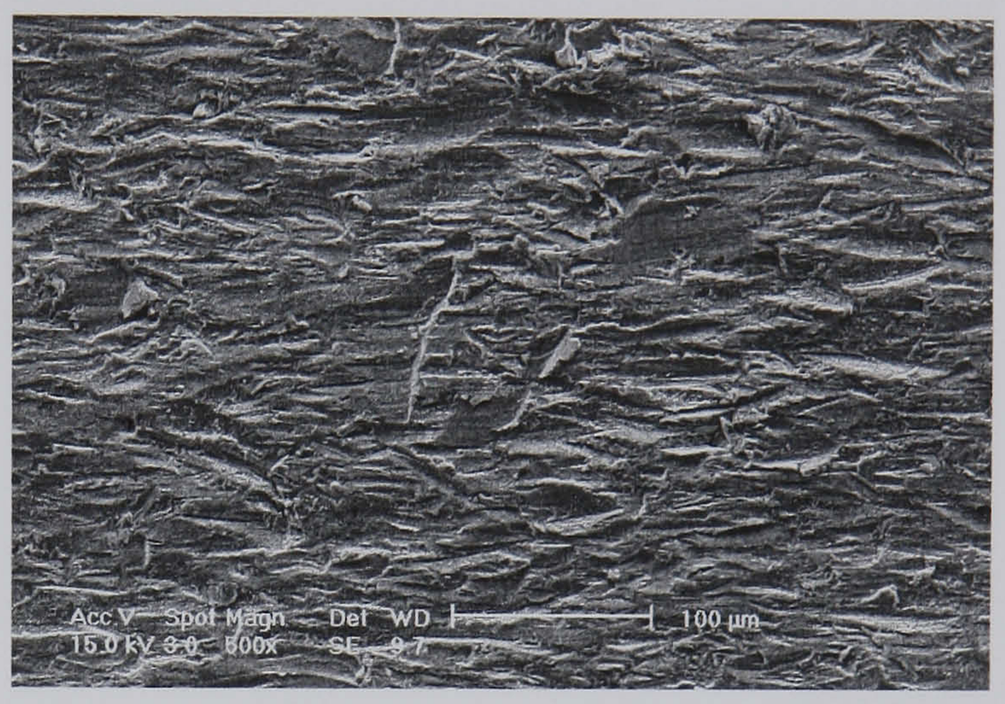

(d)

Figure 4.40 SEM micrographs of the bottom of AWJ-CDM tracks in Ti6Al4V and titanium aluminide using 75 µm (200#) garnet grit: forward milling with 92 passes of the jet: jet traverse speed of 5 m s^{-1}(300, 000 mm min^{-1}); water jet pressure 137.9 MPa (20 000 psi), stand off distance 3mm; Jet impingement angle $\theta = 15^{o}$: (a) Ti6Al4V - BSE; (b) Ti6Al4V - SE; (c) titanium aluminde - BSE; (d) titanium aluminde - SE

An examination of the grit embedment characteristic of the titanium aluminide shows similarity to that exhibited by Ti6Al4V (Fig. 4.27c) under high speed milling (5 m s^{-1}) conditions. Fig. 4.40 and Fig. 4.41 show a comparison of grit embedment and the surface morphology of Ti6Al4V and titanium aluminide when high speed forward milled with small grit, at both low (Fig. 4.40) and high (Fig. 4.41) jet impingement angles with multiple passes of the jet. It can be seen that for the two materials exhibit similar grit embedment (Fig. 4.40a and Fig.4.40c) and surface morphology characteristics. At low impact angles (Fig. 4.40), the morphology is grooved with the grit embedment being in the region of 10% (cf. Fig. 4.36a). For forward milling at high jet impingement angles (Fig. 4.41), again it can be seen that titanium aluminide exhibits similar grit embedment and morphology characteristics to Ti6Al4V. The morphology is cratered with the grit embedment being in the region of 36% (cf. Fig. 4.36f). The grit embedment and morphology characteristics of titanium aluminide are similar to Ti6Al4V discussed in section 4.4.

(a)

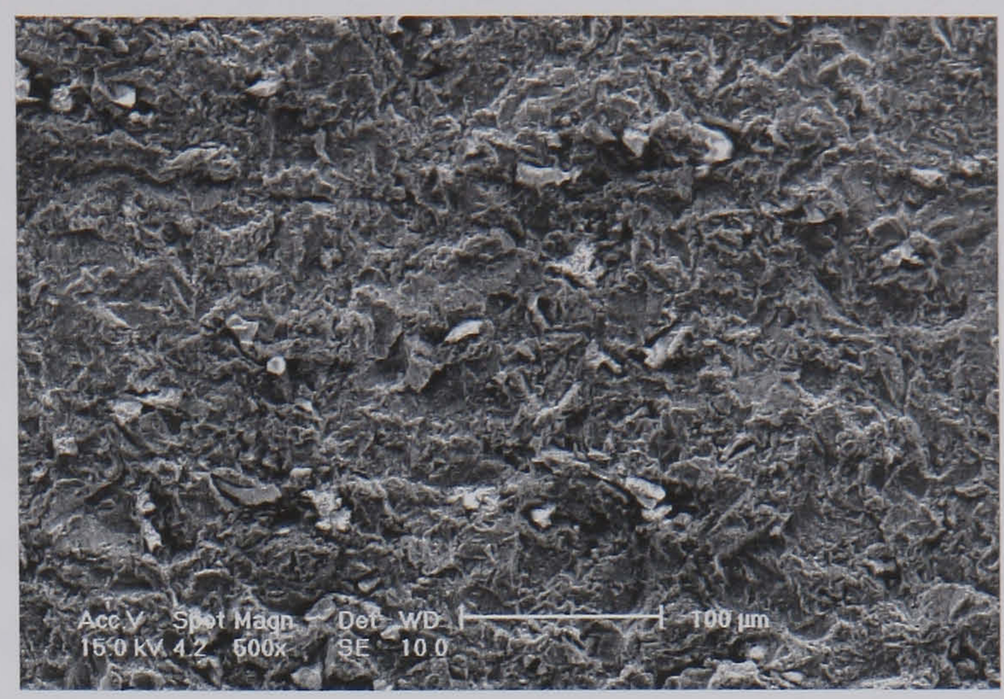

(b)

(c)

(d)

Figure 4.41 SEM micrographs of the bottom of AWJ-CDM tracks in two Ti6Al4V and titanium aluminide using 75 µm (200#) garnet grit: forward milling with 92 passes of the jet: jet traverse speed of 5 m s^{-1}(300, 000 mm min^{-1}); water jet pressure 137.9 MPa (20 000 psi), stand off distance 3mm; Jet angle $\theta = 90°$: (a) Ti6Al4V - BSE; (b) Ti6Al4V - SE; (c) titanium aluminde - BSE; (d) titanium aluminde - SE.

4.5.2 Discussion.

4.5.2.1 The behaviour of titanium aluminide.

The AJW-CDM process characteristics of Ti6Al4V (a ductile material with tensile elongation of 13%) and titanium aluminide (a brittle material with tensile elongation of about 1.5%) are somewhat similar as a function of traverse speed (Fig. 4.37a), jet impingement angle (Fig. 4.38a) and number of jet passes (Fig. 4.39a). Similarly, there is little difference in surface roughness and waviness (Fig. 4.38b, 4.38c, 4.39b and 4.39c) between the two materials when machined under a range of conditions. It should also be noted that under the high speed (5 m s^{-1}) milling conditions, grit embedment levels and surface morphologies were as those for Ti6A4V. Fig. 4.40 and Fig. 4.41 show no discernible changes and demonstrates the similarities observed. The discussion of grit

embedment and surface morphology for Ti6Al4V in chapter 4 is applicable to AJW-CDM titanium alumininde.

The similarity of the two materials under AJW-CDM was unexpected in view of the different crystal structures and properties of the titanium alloys; Ti6A4lV is an alpha-beta material with a hexagonal close packed structure in the alpha phase and a body centred cubic structure in the beta phase. Titanium aluminide is an intermetallic compound made up of two or more elements producing a new phase with it's own composition, crystal structure and properties. The titanium aluminide has a laminar grain structure consisting of gamma phase with an ordered face centred tetragonal structure and an alpha (α_2) phase with an ordered hexagonal structure with an intergranular TiB_2 phase with a body centred cubic structure [Stoloff and Sikka, 1996]. The ordered crystal structures have atoms of titanium and aluminium atoms that occupy specific locations in the atom lattice rather than being randomly located at the lattice points as in most solid solutions (Ti6Al4V). The ordered structure makes it more difficult for dislocations to move (resulting in poor ductility at low temperatures) but it also leads to high activation energy for diffusion and enhances creep resistance at elevated temperatures [Askeland, 1996]. Moreover, the composition of the Ti6Al4V is different to that of the titanium aluminide, as is the primary forming format of the supplied material. Ti6Al4V is supplied as annealed cold rolled flat bar stock and the titanium aluminide was supplied as an investment casting. The two materials possess differing crystal structures, composition and supplied primary forming shape, thus possessing different mechanical properties and would be expected to perform differently when exposed to AJW-CDM. Titanium alumininde is considered a brittle and difficult to machine since it is susceptible to cracking when being machined by conventional processes [Stoloff and Sikka, 1996] whereas Ti6Al4V is more ductile and can be machined conventionally with care. The mechanical properties in table 4.5 may help explain the similarities between the AJW-CDM process characteristics for the two materials. Tensile strength and hardness values are similar but the elongation of the two materials are dissimilar. The elongation to failure of Ti6Al4V is approximately ten times more than titanium aluminide and the fracture toughness of Ti6Al4V is approximately twice that of titanium aluminide. Bitter [1963b] and Finnie [1960] suggest that for brittle materials, maximum erosion takes place at high impingement angles while for soft ductile materials maximum erosion takes at low impingement angles. However, in AJW-CDM, both Ti6Al4V and titanium aluminide have maximum erosion rates at angles of 60° indicating that both exhibit ductile material removal.

Finnie [1960] showed that the maximum erosion rate of hardened and annealed SAE 1055 steel occurred at different impingement angles; annealed steel exhibits a maximum material removal rate at 30° whereas the maximum material removal rate for hardened steel was 90°. Sheldon and Finnie [1966] indicated that glass exhibited brittle type erosion behaviour when eroded by large particles of silicon carbide (127μm), and ductile type erosion behaviour when eroded by smaller particles of silicon carbide (9μm). Moreover, erosion with aluminium oxide exhibited brittle type erosion for all particle sizes. Therefore, the mode of erosion (ductile or brittle) may not depend of the actual ductility of the material itself, but on erosion conditions and other material properties.

4.6 Summary

Traverse speed and jet impingement angle is shown to govern the operative mechanism of material removal and thus the material removal rate. A model of the mechanism for the embedment of grit is proposed for a number of traverse speeds and jet impingement angles. It has been shown that grit embedment can be minimised either by milling with a high jet traverse speed at low impingement angles or by low speed milling at jet impingement angles up to 45° in the backward direction only. It was also demonstrated that the surface waviness can be reduced as the traverse speed is increased or as the jet impingement angle is decreased, but it should be also noted that waviness increases with an increase in number of passes of the jet over the workpiece. The surface roughness is not strongly dependent on traverse speed or water jet pressure. Although surface waviness and roughness are strongly dependent on jet impingement angle, significant reductions are possible by employing low angle milling techniques. Moreover, a reduction in particle size also leads to a reduction in waviness and roughness but also to a decrease in material removal rate. Table 4.6 summarises the affect of the parameters examined on the process characteristics of material removal rate, waviness, roughness and grit embedment. It indicates the effect of an increase in value of an AWJ parameter has on a process characteristic in AJW-CDM of Ti6Al4V.

Parameter		Material removal rate	Waviness	Roughness	Grit embedment
Water pressure	↑	↑	↑	Small Effect	×
Lateral increment	↑	↓	Small effect	Small Effect	×
Jet impingement angle	↑	↑	↑	↑	↑
Number of passes	↑	↑	↑	Small Effect	Small Effect
Traverse speed	↑	↓	↓	↑	↑
Stand off distance	↑	↓	Small effect	Small Effect	×
Abrasive characteristics -particle size	↑	↑	↑	↑	Small Effect

↑ = increasing function. ↓ = decreasing function. × = not examined.

Table 4.6 Roles of parameters showing their affect on material removal rate, roughness and waviness and grit embedment in AWJ milling of Ti6Al4V.

Chapter 5

5 Mechanisms of material removal in AJW milling.

The mechanism of material removal in AJW-CDM depends upon the processing parameters as seen in chapter 4. Indeed a model which sought to explain the changes was proposed in Fig. 4.11 and 4.12. In this chapter, further critical experiments are presented which add to the understanding of the mechanism of material removal in AWJ-CDM. An investigation was conducted into the material removal mechanism of Ti6Al4V (a ductile material). Whilst the material removal mechanism during AWJ cutting of PMMA and glass (brittle materials) at low jet traverse speeds has been conducted [Hashish, 1987, 1989a], no published research on the material removal mechanism of ductile materials during AJW-CDM was available.

5.1 Method.

Single passes of the water jet were traversed across a Ti6Al4V alloy sample and at the selected point the water pressure was switched off, the water pressure and the abrasive grit flow being instantly reduced to zero. The cutting front is thus captured in an instant of time.

The track so formed was sectioned for SEM analysis as shown in Fig. 5.1. SEM BSE and SE imaging was conducted on the complete track in the direction of arrow A (Fig. 5.1b) to establish the material removal mechanism at the bottom of the eroded track. The sample was then sectioned B - B to allow, by SEM BSE and SE imaging in the direction of arrow B (Fig. 5.1a), the material removal mechanism at the kerf side wall to be identified.

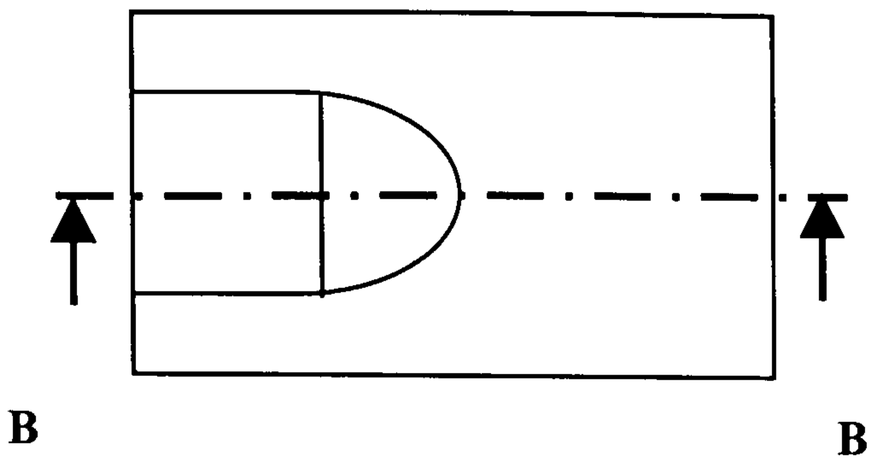

Figure 5.1 Illustration of the AJW single pass tracks sectioned for SEM analysis: (a) Plan view; (b) Vertical sectional view B - B; (c) Angled sectional view C - C.

The profiles of the track that were milled with high jet traverse speeds are very different from those machined at low traverse speeds resulting in differing points of interest for the SEM analysis. Fig. 5.2 illustrates the differing track profiles and the locations of SEM examination. Low speed milling (Fig. 5.2c) which results in deep undulating kerfs requires a high number of analysis points while the shallower, less undulating medium (Fig. 5.2b) and high speed (Fig. 5.2a) milled kerfs require fewer examination points. The points examined in the plan view are maintained to the same position in the cross sectional views.

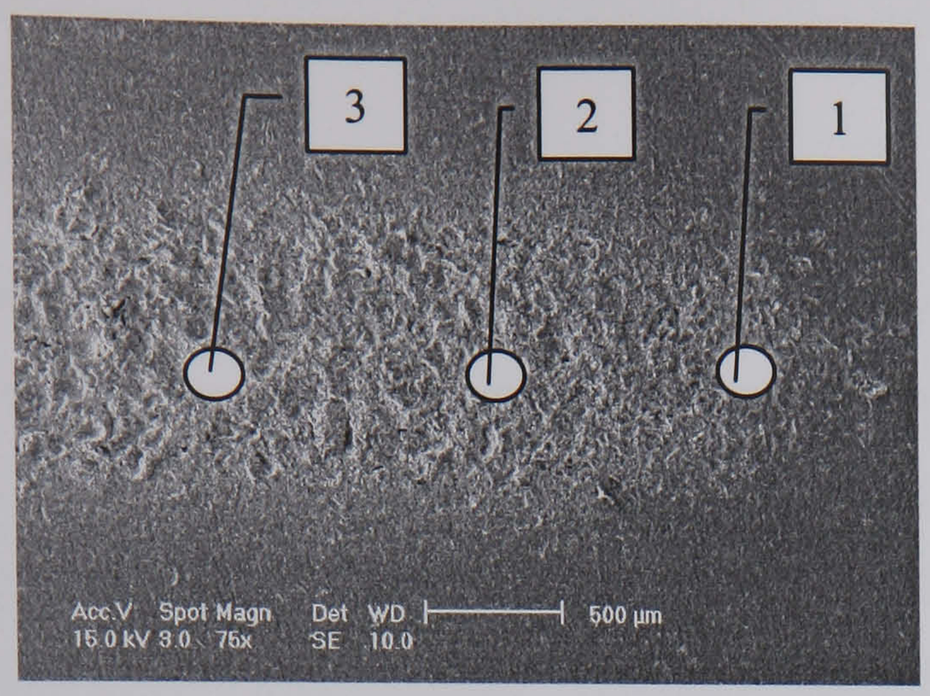

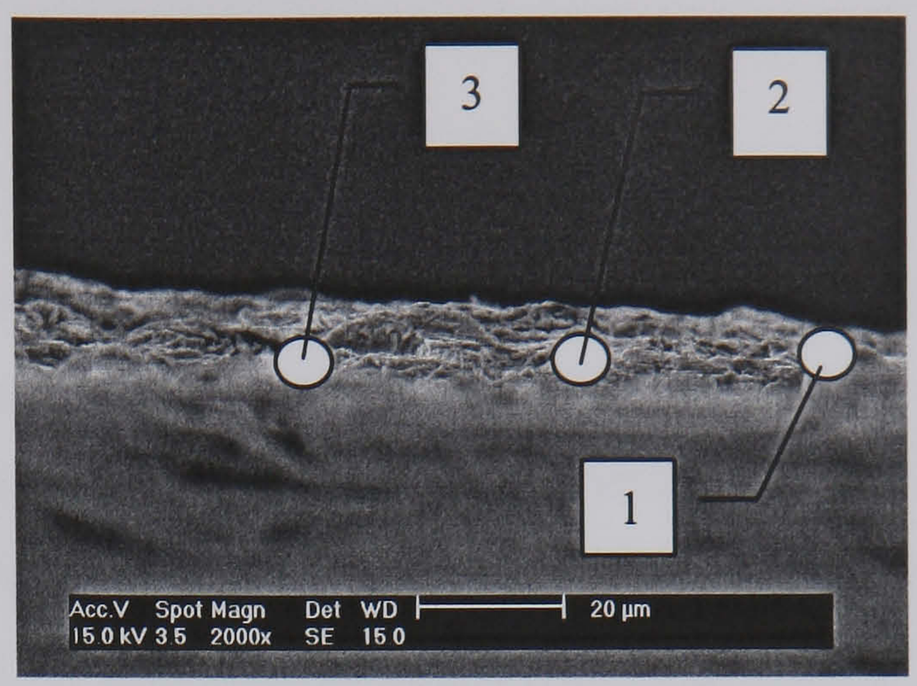

(a)

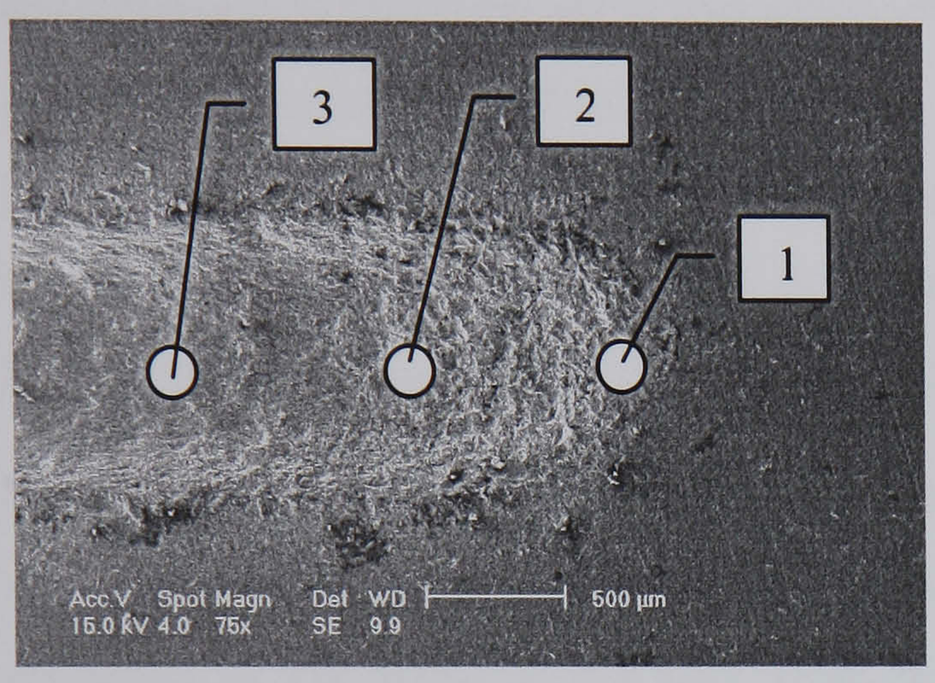

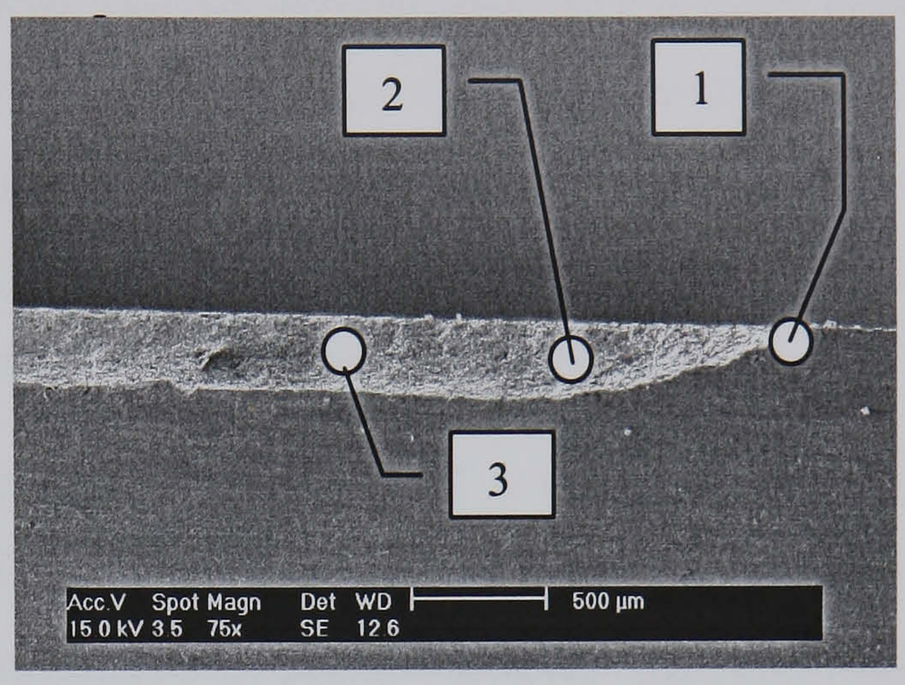

(b)

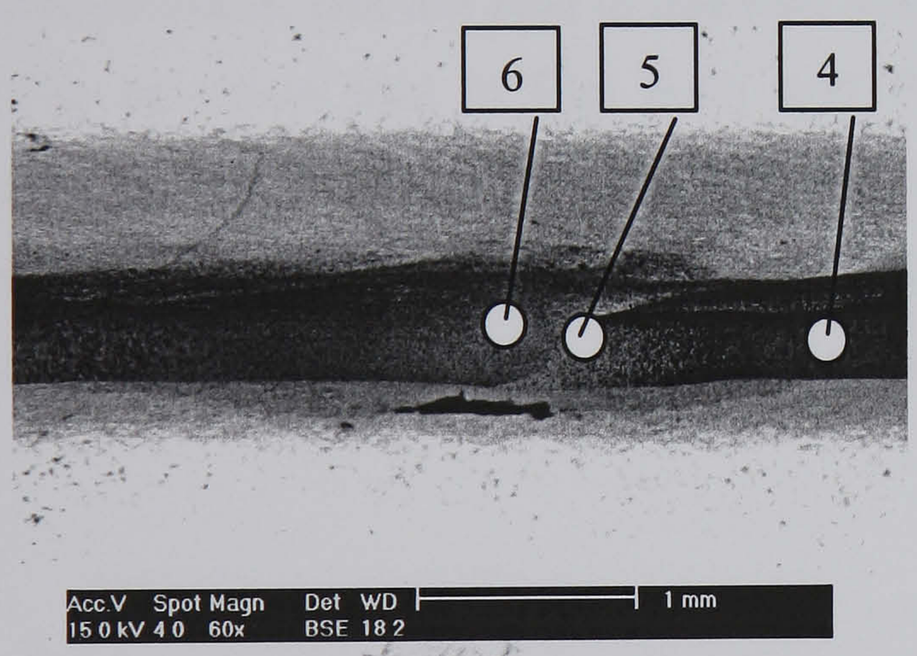

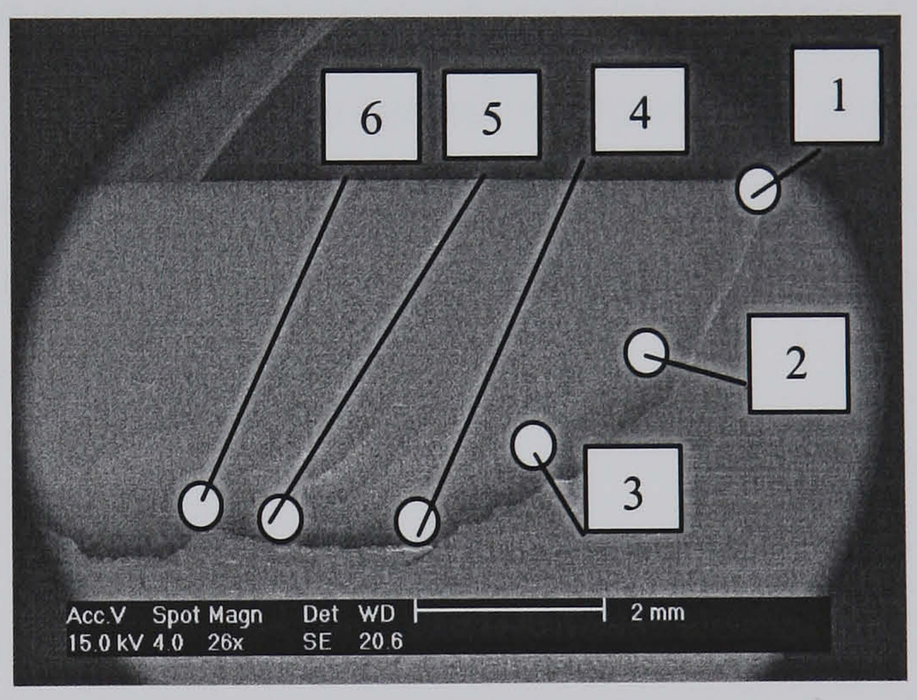

(c)

Figure 5.2 Illustration of SEM analysis points of the sectioned AJW single pass tracks: AJW-CDM with various traverse speeds with a water jet pressure of 137.9 MPa (20 000 psi), stand off distance 3mm using 180 µm (80#) garnet grit. (a) High speed milling (0.166 m s^{-1}): Plan (left); Section (right); (b) medium speed milling (0.016 m s^{-1}): Plan (left); Section (right); (c) low speed milling (0.003 m s^{-1}): Plan (left); Section (right). Position number 1 to 6 indicate the position of the SEM examination point that corresponds to the micrographs observed in Figs. 5.3 to 5.7. E.g. Fig. 5.3a is plan view micrograph and Fig. 5.4a is the section micrograph seen at the examination point, position 1 in Fig. 5.2c.

5.2 Results.

Fig. 5.3 shows plan view SEM micrographs of the surface morphology of AJW milled single pass tracks, milled at low traverse speeds of 0.003 m s^{-1} (200 mm min^{-1}) with large grit. It can be seen that the morphology has a cratered morphology on the very edges of the cutting front of the water jet (Fig. 5.3a). As it approaches the bottom of the kerf, the morphology changes quickly to a grooved morphology (Fig. 5.3c). The morphology of the bottom of the track undulates, but as can be seen in Fig 5.3e and Fig. 5.3f, the undulation exhibits truncation as the water jet has deflected and eroded the undulation. A cratered morphology can also been at the back of the undulation, (indicated by the arrow in Fig. 5.3d and Fig. 5.3e) where normal impact of the particles has occurred. A similar effect was also observed when milling with small grit.

Fig. 5.4 shows SEM micrographs of the surface morphology of a cross section of the same track as examined in Fig. 5.3. Again, it can be seen that the morphology is initially cratered at the edge of the kerf, (Fig. 5.4a) indicative of predominantly normal impact of the particles, but the rest of the kerf wall exhibits predominately directional cutting. It can also be seen that in Fig. 5.4b and Fig. 5.4c that the grooved morphology changes direction flowing from the vertical to the horizontal. The grooved morphology changes direction as seen in Fig. 5.4e and Fig. 5.4f when the water jet encounters the undulation. A similar effect was also observed when milling with small grit.

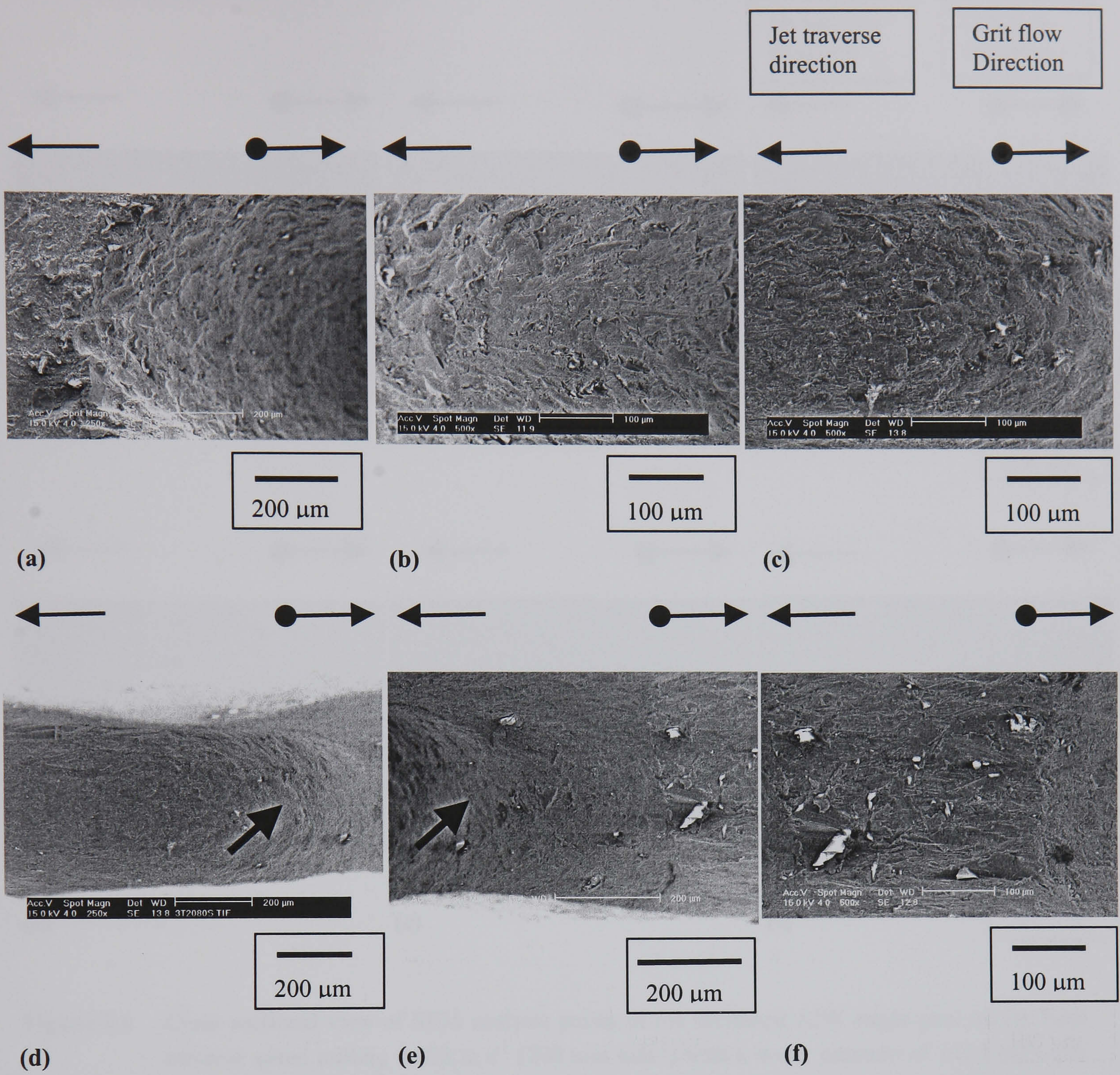

Figure 5.3 Plan view of SEM analysis points of the sectioned AJW single pass tracks. Low traverse speed milling 0.003 m s^{-1} (200 mm min^{-1}) with a water pressure of 137.9 MPa (20 000 psi), stand off distance 3mm using 180 µm (80#): (a) Position 1; (b) Position 2; (c) Position 3; (d) Position 4; (e) Position 5; (f) Position 6.

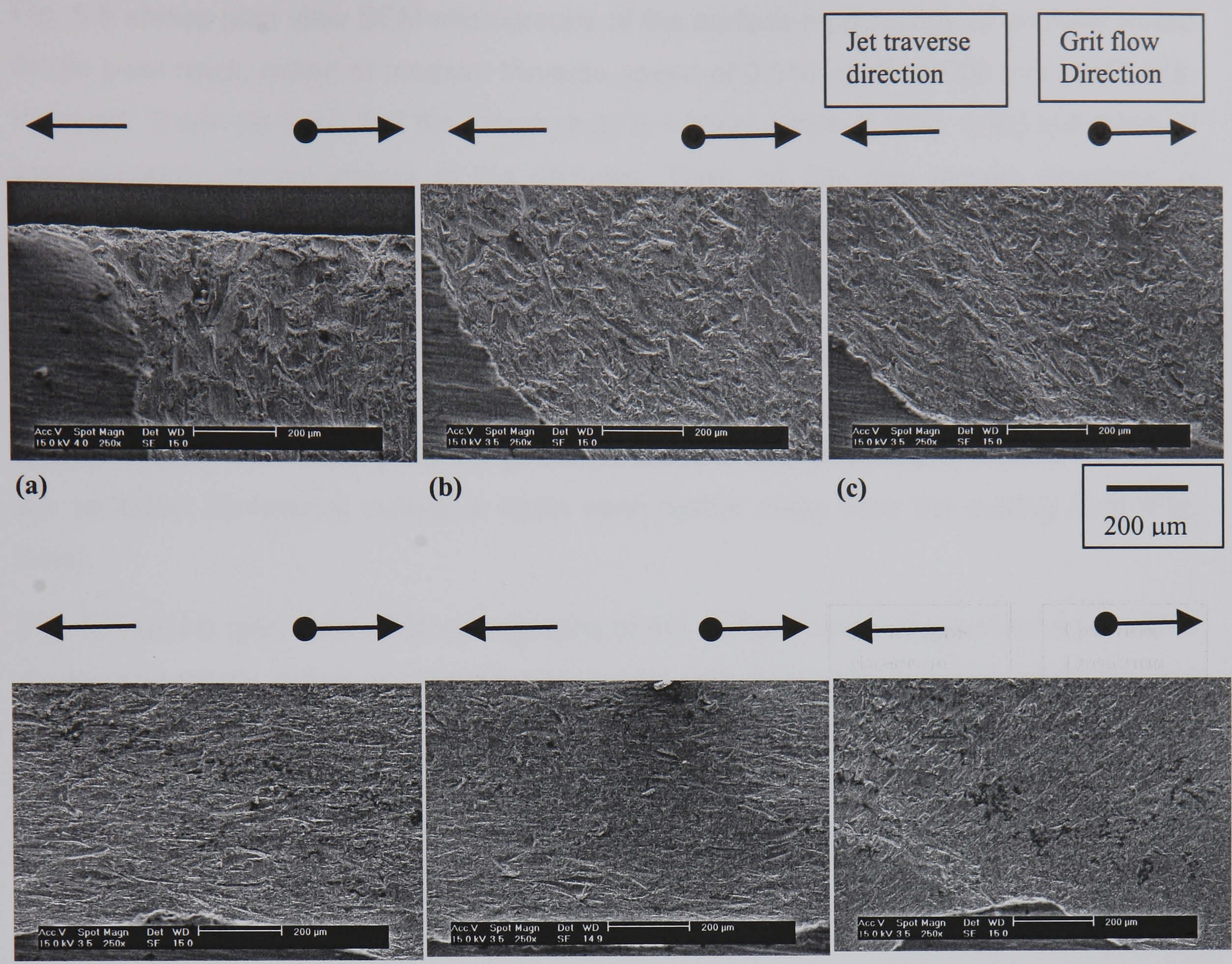

Figure 5.4 Cross sectional view of SEM analysis points of the sectioned AJW single pass tracks. Low traverse speed milling 0.003 m s^{-1} (200 mm min^{-1}) with a water pressure of 137.9 MPa (20 000 psi), stand off distance 3mm using 180 µm (80#): (a) Position 1; (b) Position 2; (c) Position 3; (d) Position 4; (e) Position 5; (f) Position 6.

Fig. 5.5 shows plan view SEM micrographs of the surface morphology of an AJW milled single pass track, milled at medium traverse speed of 0.016 m s^{-1} (1 000 mm min^{-1}) with large grit. It can be seen that the morphology is initially cratered, (Fig. 5.5c) indicative of predominantly normal impact of the particles. Then, as the fluid stream develops, a grooved morphology with clear directionality is observed indicative of abrasive impinging at a low angle (Fig. 5.5a). A similar effect was also observed when milling with small grit.

Fig. 5.6 shows SEM micrographs of the surface morphology of a cross section of the same track as examined in Fig. 5.5. Again, it can be seen that the morphology is initially cratered close to the cutting front (Fig. 5.6c) indicative of predominantly normal impact of the particles. Directional cutting is again seen further away from the cutting front (Fig. 5.6a).

Fig. 5.7 shows plan view SEM micrographs of the surface morphology of an AJW milled single pass track, milled at high traverse speed with large grit. It can be seen that the morphology at all positions is cratered indicative of predominantly normal impact of the particles. This effect was observed when milling at traverse speeds above 0.033 m s^{-1} (2 000 mm min^{-1}). A similar effect was also observed when milling with small grit.

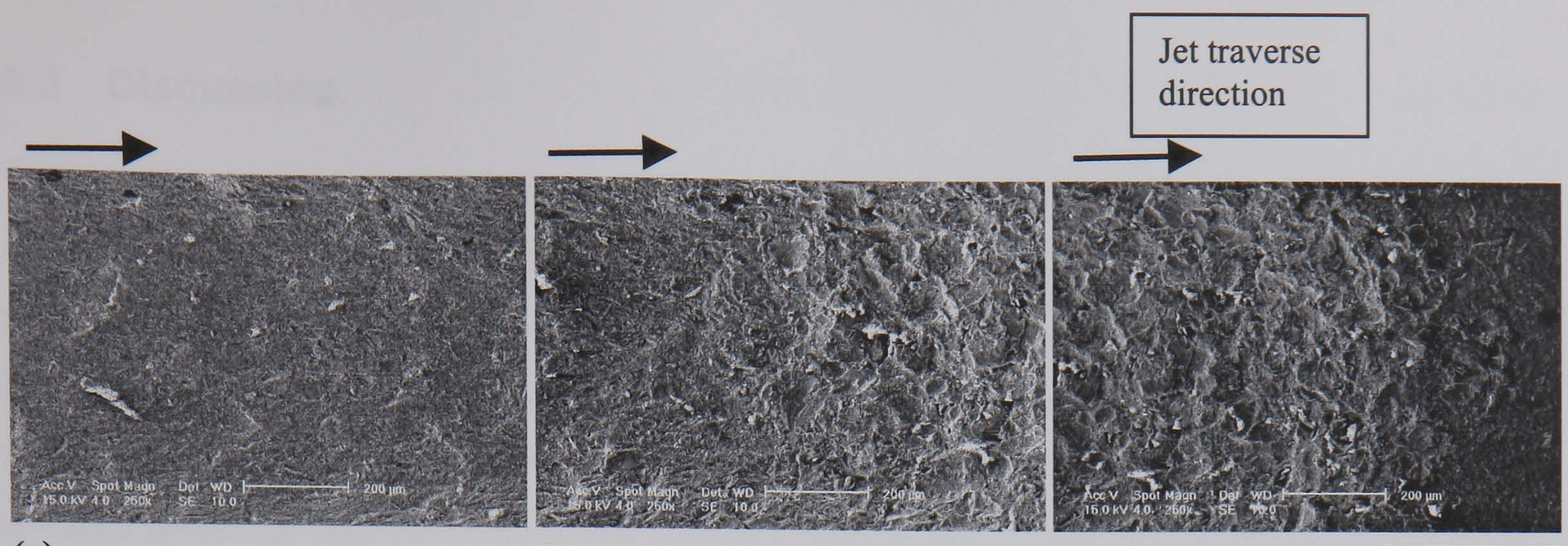

Figure 5.5 Plan view of SEM analysis points of the sectioned AJW single pass tracks. Medium traverse speed milling 0.0166 m s^{-1} (1 000 mm min^{-1}) with a water pressure of 137.9 MPa (20 000 psi), stand off distance 3mm using 180 µm (80#): (a) Position 3; (b) Position 2; (c) Position 1.

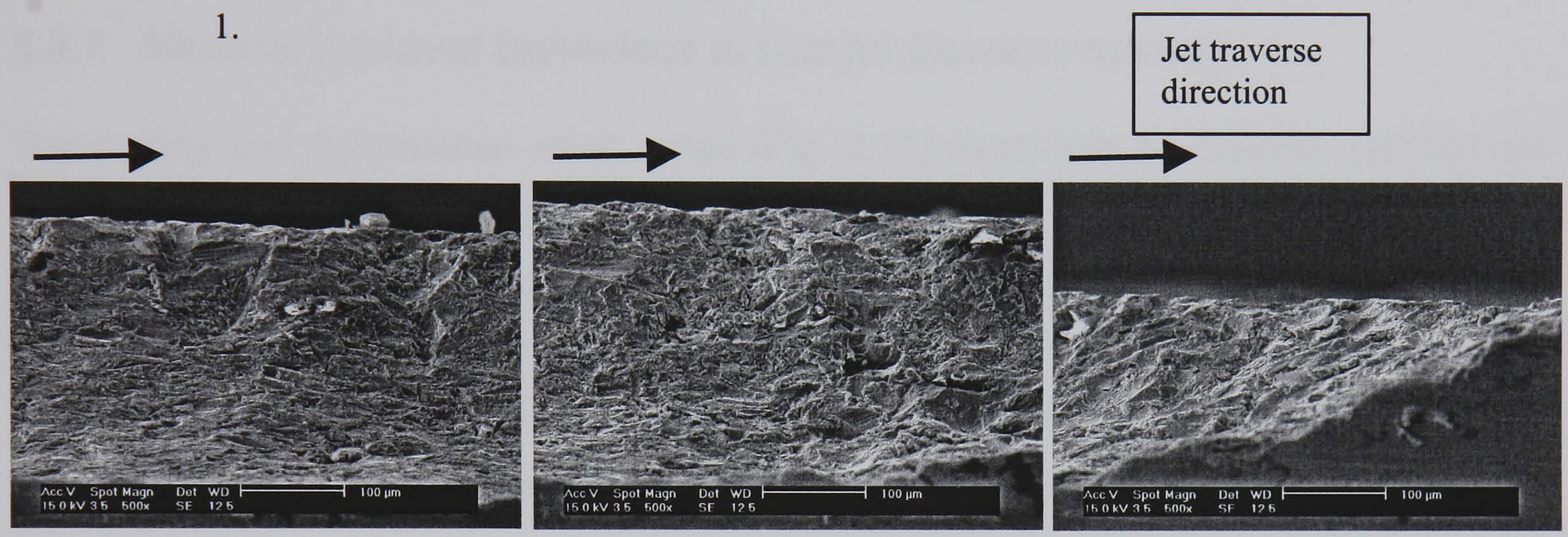

Figure 5.6 Cross sectional view of SEM analysis points of the sectioned AJW single pass tracks. Medium traverse speed milling 0.0166 m s^{-1} (1 000 mm min^{-1}) with a water pressure of 137.9 MPa (20 000 psi), stand off distance 3mm using 180 µm (80#): (a) Position 3; (b) Position 2; (c) Position 1.

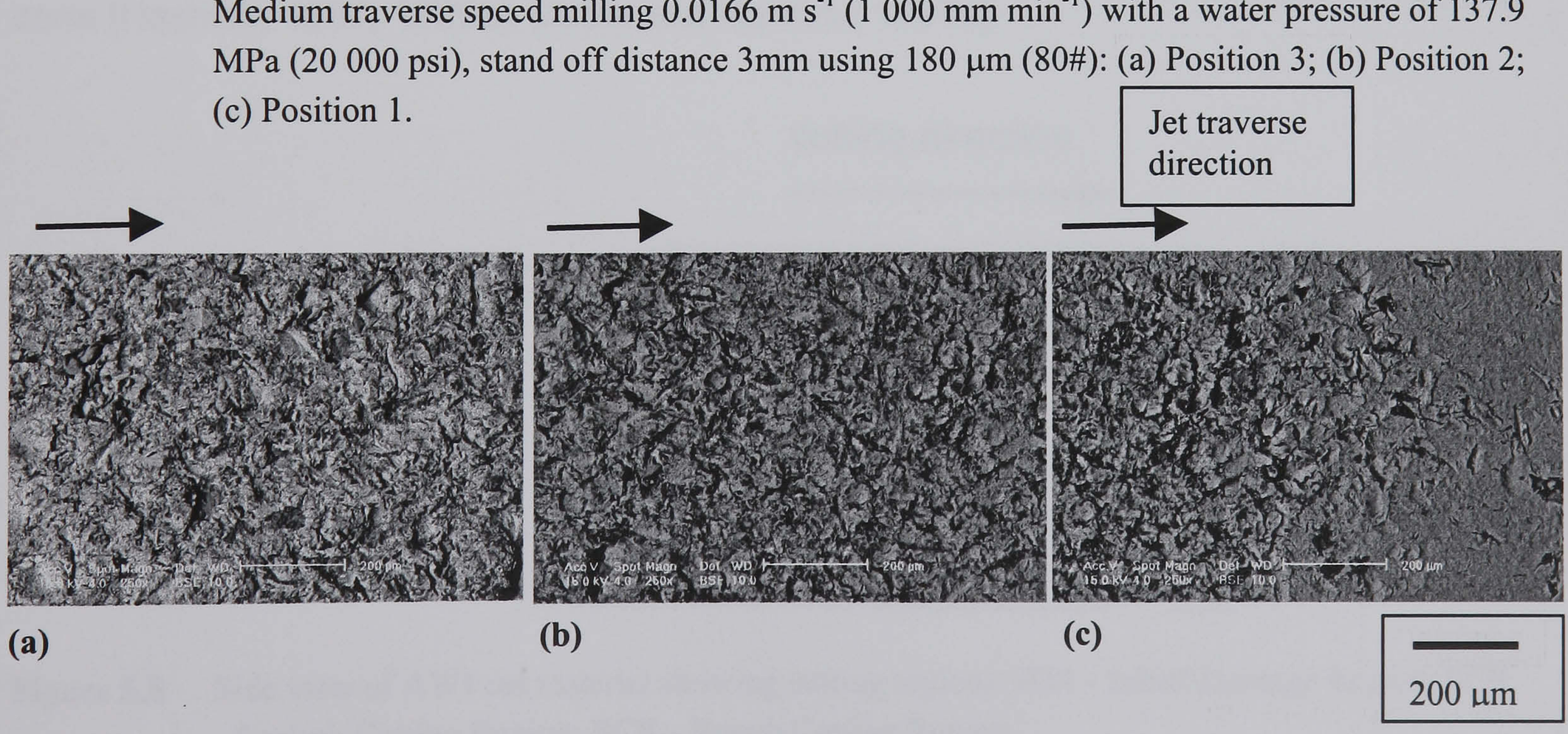

Figure 5.7 Plan view of SEM analysis points of the sectioned AJW single pass tracks. High traverse speed milling 0.166 m s^{-1} (10 000 mm min^{-1}) with a water pressure of 137.9 MPa (20 000 psi), stand off distance 3mm using 180µm (80#); (a) Position 3; (b) Position 2; (c) Position 1.

5.3 Discussion.

The mechanism of material removal from workpiece depends upon the traverse speed of the jet across the sample surface. In chapter 4, (Fig. 4.1) it was shown that for traverse speeds above 0.016 m s^{-1}, the material removal rate was insensitive to further increase in the traverse velocity whereas below this velocity, there was a significant increase in material removal rate with decreasing traverse speed. In this work, 0.003 m s^{-1} was taken as representing a low velocity (below this threshold) whereas 0.166 m s^{-1} and 5 m s^{-1} were taken as representing behaviour above this threshold velocity. In section 5.3.1, workpiece behaviour under a slow traverse speed of 0.003 m s^{-1} is discussed.

5.3.1 Material removal behaviour at low jet traverse speeds.

The cutting and deformation wear zones (Fig. 2.22) described by Hashish [1992a] are clearly observed (Fig. 5.2c and Fig. 5.4). However, Arola and Ramulu [1993, 1997a] argue that there are three distinct material removal regions (Fig. 5.8): (i) The initial Damage Region (IDR) where particle entrance damage occurs. This region is not identified by many researchers including Hashish; (ii) Smooth Cutting Region (SCR) where the surface texture is smooth with limited damage phenomena and referred to as the cutting wear region Hashish [1987, 1989a] (Fig. 2.22); (iii) Rough Cutting Region (RCR) where the region from the SCR to jet exit edge exists and is characterised by a rough surface texture and waviness patterns and commonly known as the deformation zone [Hashish, 1987, 1989a], [Arola and Ramulu, 1997a].

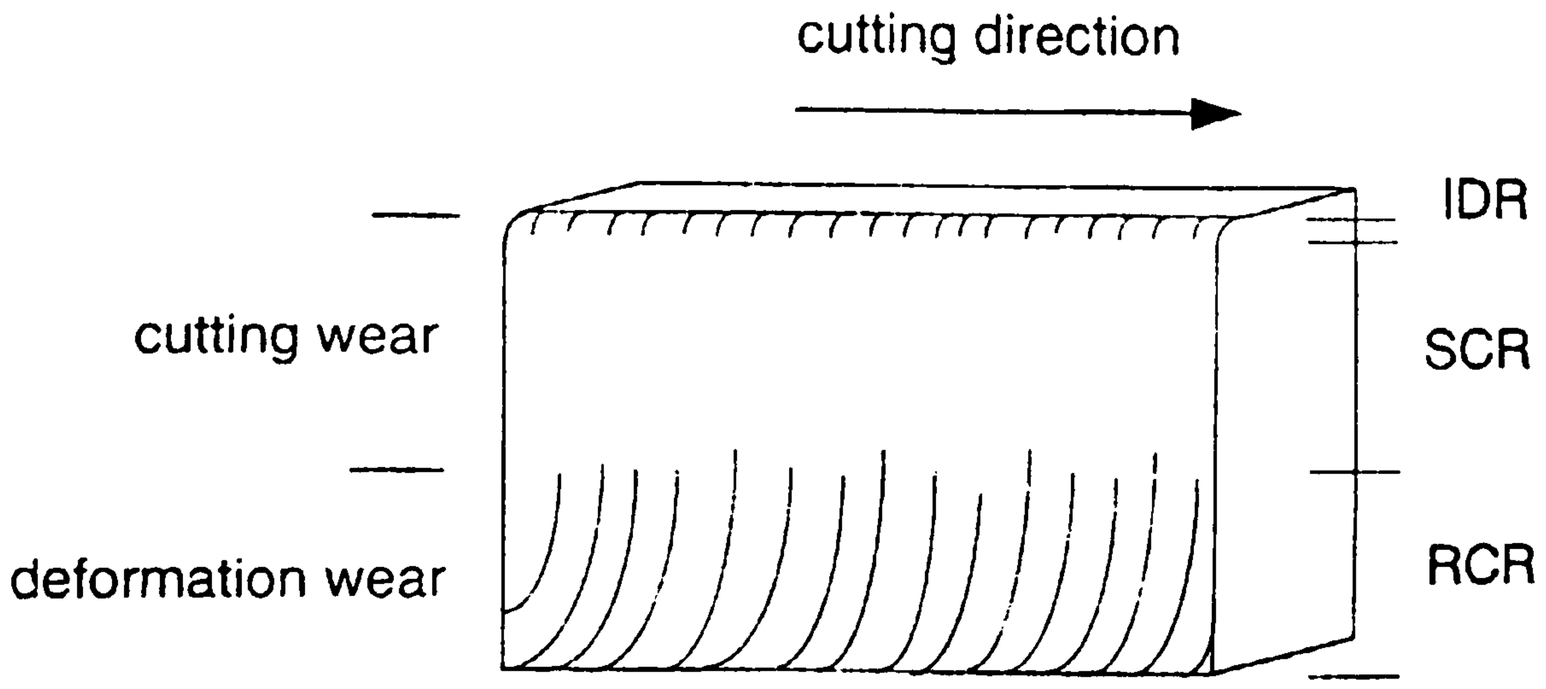

Figure 5.8 Side view of AWJ cut material showing cutting regions: IDR - Initial Damage Region; SCR - Smooth Cutting Region; RCR - Rough Cutting Region.

When low speed milling, areas close to the cut front, (Fig. 5.3a and Fig. 5.4a) show a cratered morphology, which is prevalent along the top edge along the whole length of

the kerf (Fig. 5.4a). The depth of the IDR is about 100 μm [Arola and Ramulu, 1993, 1997a]. Arola and Ramulu [1993] observed a mix of cratering and directional grooves in this region, to a depth of 200 - 300 μm in aluminium.

Below this is the smooth cutting or cutting wear zone. In this region a grooved morphology is prevalent indicating material being removed at low angles of attack due to microcutting [Chen and Siores, 2003]. Arola and Ramulu [1993] observed a similar morphology following cutting of 7075 T6 aluminium and suggested ductile shearing mechanisms were responsible for this morphology.

Microcutting is also observed along the cutting front of the water jet (Fig. 5.4) and the kerf side walls. The data here supports the hypotheses of Hashish [1987, 1989a] in that the material removal is by microcutting at low angles of attack. Further, the step changes in the cut front observed by Hashish during AWJ cutting have also been observed (close to position 3 Fig. 5.2c). Such steps, that form as the cutting front develops, are responsible according to Hashish [1989a, 1991,1995b] for the inducement of the waviness observed in the bottom of the kerf. The step results in instabilities in the flow which in turn result in the waviness forming. Hashish argues that these steps occur in the deformation wear region (see Fig. 2.22). Arola and Ramulu [1993] suggest that waviness formation is a result of a reduction in the jet energy. It is unclear whether this reduction in energy is the physical initiator of the step or the initiator in a change of the local attack angle of the eroding grit. The deformation zone can be identified in Fig.5.2c at position 3 where striations on the kerf wall can be seen. Although this region has been termed the deformation zone, the micro-morphology is one of directional grooves associated with microcutting and not cratered as associated with deformation morphology (Fig. 5.4d, Fig. 5.4e and Fig. 5.4f). Arola and Ramulu [1993] and Chen and Siores [2003] also reported that the rough cutting region or deformation wear zone of through-cut 7075 T6 aluminium also exhibited a grooved morphology.

It is clear that the material removal mechanism is complex, and the terminology employed for the macro level does not represent processes occurring at the micro level and should be employed with care.

5.3.2 *Material removal behaviour at high jet traverse speeds.*

At high jet traverse speeds, the situation is much less complex than for low jet traverse speeds, since in all cases, the depth of cut is small and the leading edge of the kerf face makes up a very small proportion of the total cutting area. As a result, the local particle impact angles are generally the same as that of the jet impingement angle (as argued in chapter 4). Also, since the local height of the material being milled in the current pass is very similar to that of the surrounding material (not the case for low jet traverse velocities), then the tendency of the particle laden fluid to run along the groove is also reduced.

At the medium traverse speeds of 0.016 m s^{-1}, the material removal mechanism is one of deformation as seen in Fig. 5.5c and Fig. 5.6c. The deformation is also evident at the top of the side walls along the length of the track as seen in Fig. 5.6a and Fig. 5.6b. However, it is also evident that secondary milling has occurred since the morphology changes from a cratered morphology to one exhibiting directional grooving (Fig. 5.5a and Fig. 5.5b) (Fig. 5.6a and Fig. 5.6b).

At still higher traverse speeds the secondary milling is replaced by a pure deformation material removal mechanism indicated by the presence of a cratered surface both close to the cutting front and far away (Fig. 5.7). Plastic deformation beyond the strain to failure results in material removal from the surface.

5.3.3 *Secondary milling.*

At normal jet impingement, there is a significant difference in morphology between low speed and high speed milling. Under high speed conditions (Fig. 5.7), only cratering is observed, due to the impact of particles. However, as the traverse speed is reduced to 0.016 m s^{-1} (1 000 mm min^{-1}) the mechanism of material removal is dominated by cratering at the cutting front (Fig. 5.5c) but is replaced down stream by grooving. As the water jet loses energy and turns through 90° it continues to remove material as the grit runs along the bottom the kerf by microcutting at low attack angles indicated by the directional grooves observed in Fig. 5.5a and Fig. 5.5b. In this case, the cratered surface produced during milling by particle impact has been smoothed off by the later flow of the particle laden fluid along the deep channel. It is argued that the flow of the particle-laden fluid along the groove is the cause of the significant reduction in the level of embedded grit under these conditions (see section 4.4).

At low traverse speeds, 0.003 m s^{-1} (200 mm min^{-1}) the effect of secondary milling on the macro scale of the material removal mechanism is more complex. Secondary milling

by the flow of the particle-laden fluid along the groove (Fig. 5.3d and Fig. 5.3f) has resulted in a grooved morphology. However, the flow of the particle-laden fluid along the groove has been disturbed by coarse undulations; the water jet has struck the near vertical wall of the undulation with normal attack angles. The water jet is deflected over the undulation, as observed in Fig. 5.4f where a change in the direction of the grooving is observed.

5.4 Summary.

At low jet traverse speeds, the material removal mechanism is microcutting irrespective of depth, apart from the small IDR region where deformation occurs At jet traverse speeds of 0.016 m s^{-1} (1 000 mm min^{-1}) and above, the material removal mechanisms changes to deformation (cratering) with the effect of secondary machining being much reduced. The commonly employed terminology of the micro and macro material removal mechanism has to be used with some caution or clarification.

Chapter 6

6 A manufacturing solution: AWJ Milling for Component Manufacture.

The process parameters investigated in chapter 4, were applied to the manufacture of a thin walled component discussed in the Experimental method, namely, an 'Engine cowling structural support rib' (see Fig. 3.2) for an aerospace company, normally manufactured by chemical milling.

6.1 Problems of Manufacture.

The geometric feature of the component selected for manufacture by AWJ-CDM as an alternative to chemical milling is that of a slot like feature 465 mm x 127 mm by 1 mm deep. The manufacture of the feature may be performed by linear milling the slot, by traversing back and forth, with lateral passing and depth passing to depth or by milling a rectangular pocket and removing the unwanted sides of the rectangle.

The trials for the two selected manufacturing methods resulted in the following geometric features seen in Fig. 6.1.

Fig. 6.1 illustrates the problems of machining slots without masks on a two axis machine. The front and back edges seen at position 1 and 2 in Fig. 6.1 are rounded, and not square; this feature shall be termed as 'edge bevel'. At position 3 the side wall geometry or draft angle can be seen where the edge is not perpendicular to the top surface. The mechanism that is responsible for edge bevel geometry is the lead and trailing edge deflections of the water jet as the water jet hits the workpiece [Hashish, 1991,1995b].

A number of solutions to circumnavigate formation of these features can be seen in Fig. 6.2. Non-masking techniques use the machine tool movements of the jet nozzle to correct any draft angle or edge bevel geometry anomalies, and eliminate the need for masks. Masking solutions may be used to reduce draft angle and edge bevel anomalies, and four ways of employing masks are discussed. One solution to resolve edge bevel is to extend the parent material of the work piece to move the position of the anomaly away from the required workpiece dimensions. Through-cutting to the required component dimensions removes waste material on which the anomaly is now present. Alternatively, the work piece can be extended artificially by placing sacrificial masks on

the front and back edge of the work piece which will result in the rounded edges appearing on the mask and not the work piece (Fig. 6.3). A non-masking solution to remove edge bevel is to machine a pocket to the required rectangular dimensions on over sized material, and through-cut the component to the required dimensions and removing the unwanted sides of the rectangle. Although this solution would remove edge bevel, it will result in other problems since any dwell or acceleration and deceleration of the jet will result in significant material removal where the jet is stationary or changes speed [Ojmertz, 1997a] (Fig. 2.19). Fig. 6.4 illustrates the problems of machining pockets without masks using a circular traverse (Fig. 6.4a) and a spiral traverse (Fig. 6.4b) on a two axis machine. Fig. 6.4a has cruciform slots arising from the dwell time initiated by the machine as it reconciles its x and y position. This dwell time is not contained in the CNC program but is caused by the CNC controller waiting to process information to perform the CNC program requirements. The water jet, when stationary, removes a significant material at that point. The slot is made up of a number of holes where the water jet has stopped. The two axis machine does not have automatic pressure control to increase or decrease pressure (termed pressure ramping) or automatic abrasive flow cut off to compensate for such anomalies. Fig. 6.4b shows a spiral traverse to try to overcome the anomaly seen in Fig. 6.4a. The slow movement in the centre results in a deep cut, whilst at the outer edge of the circle the jet is moving much faster and so a shallower cut results. Moreover, the side walls of non-masked milling of pockets and slots result in significant draft angles (Fig. 6.1 and Fig. 6.4). In Fig. 6.1 the angle of the side walls of the slot are not perpendicular to the base but instead make an angle of approximately 75 °. This deviation of the side wall angle is a result of the water jet deflecting into the slot as the depth of the slot develops, and that the water jet cuts a vee shaped profile at normal jet angles. (see Fig. 2.15) This vee shape is exaggerated by following jet passes. The elimination of this draft angle geometry may be achieved by changing the jet impingement angle of the water jet at each jet pass as the water jet approaches the edge of the slot (or pocket Fig. 6.4). Such a change in jet angle can be performed automatically on a five axis machine but this is not possible on a two axis machine.

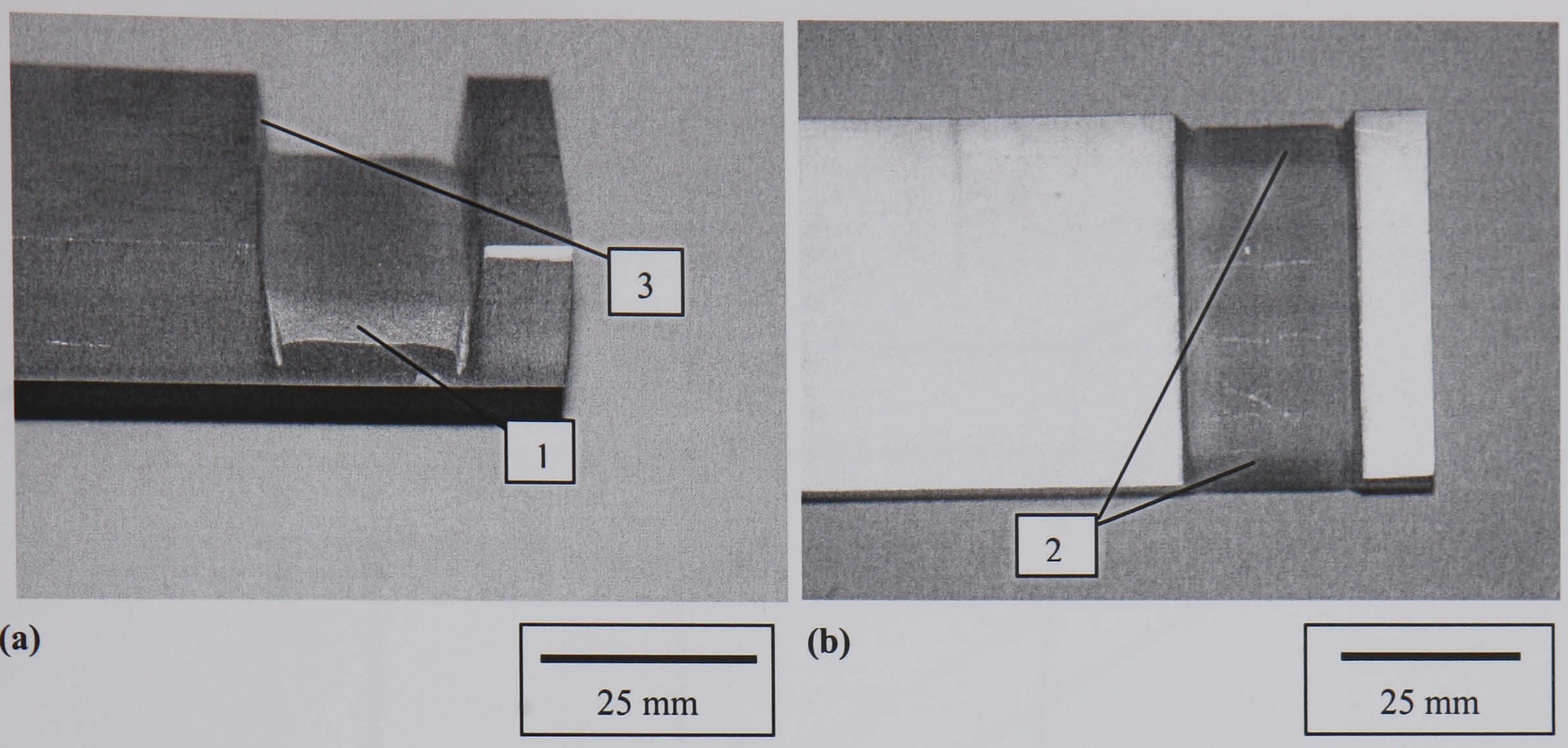

Figure 6.1 Illustration of the AJW-CDM slots milled without the use of masking using a traverse speed of 0.166 m s^{-1} (10 000 mm min^{-1}); water jet pressure 137.9 MPa (20 000 psi); stand off distance 3 mm; ¼ jet increment; 180 μm (80#) garnet grit. (a) Front elevation. (b) Plan view.

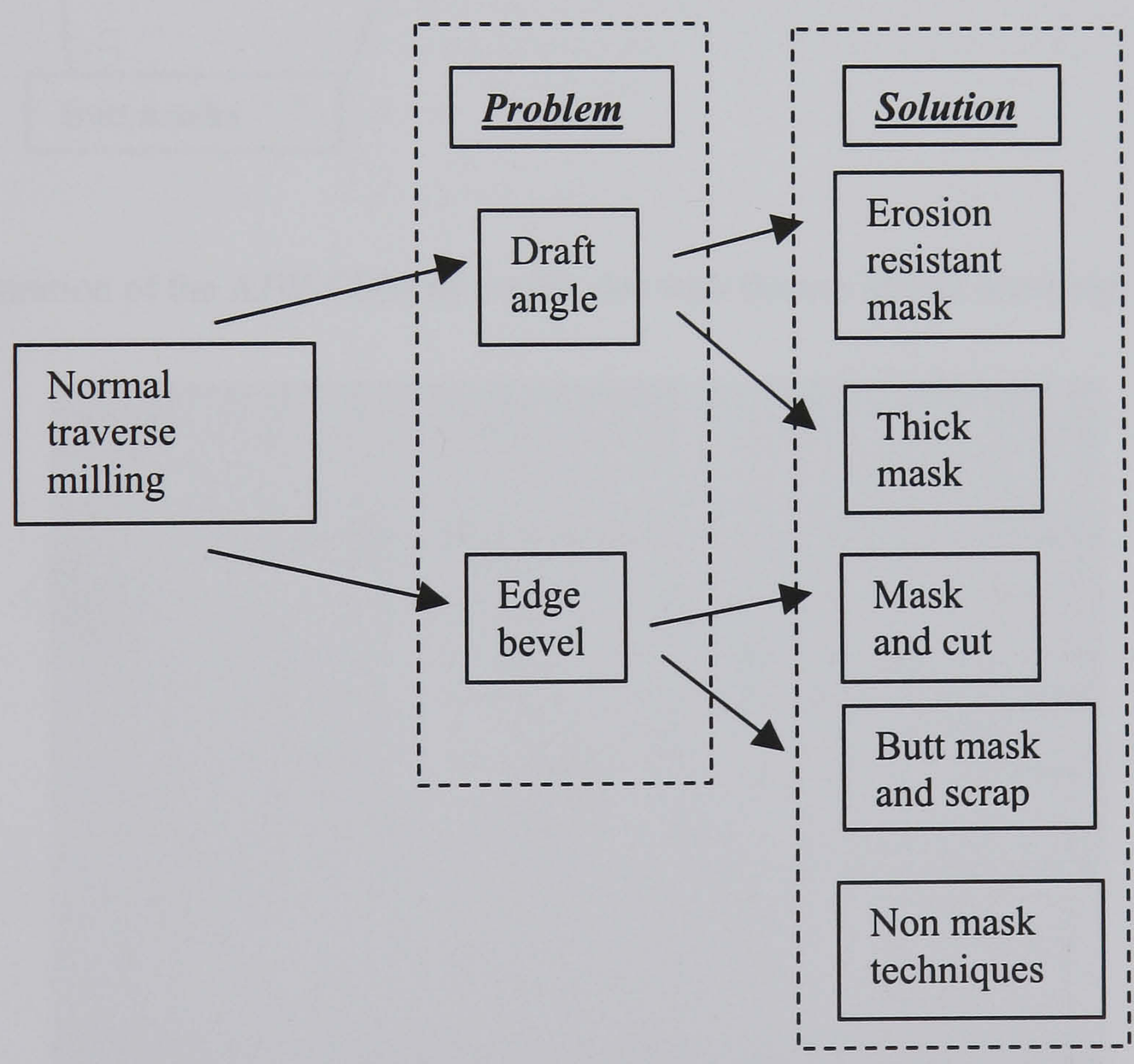

Figure 6.2 Solution tree for the AJW-CDM of a wide slot.

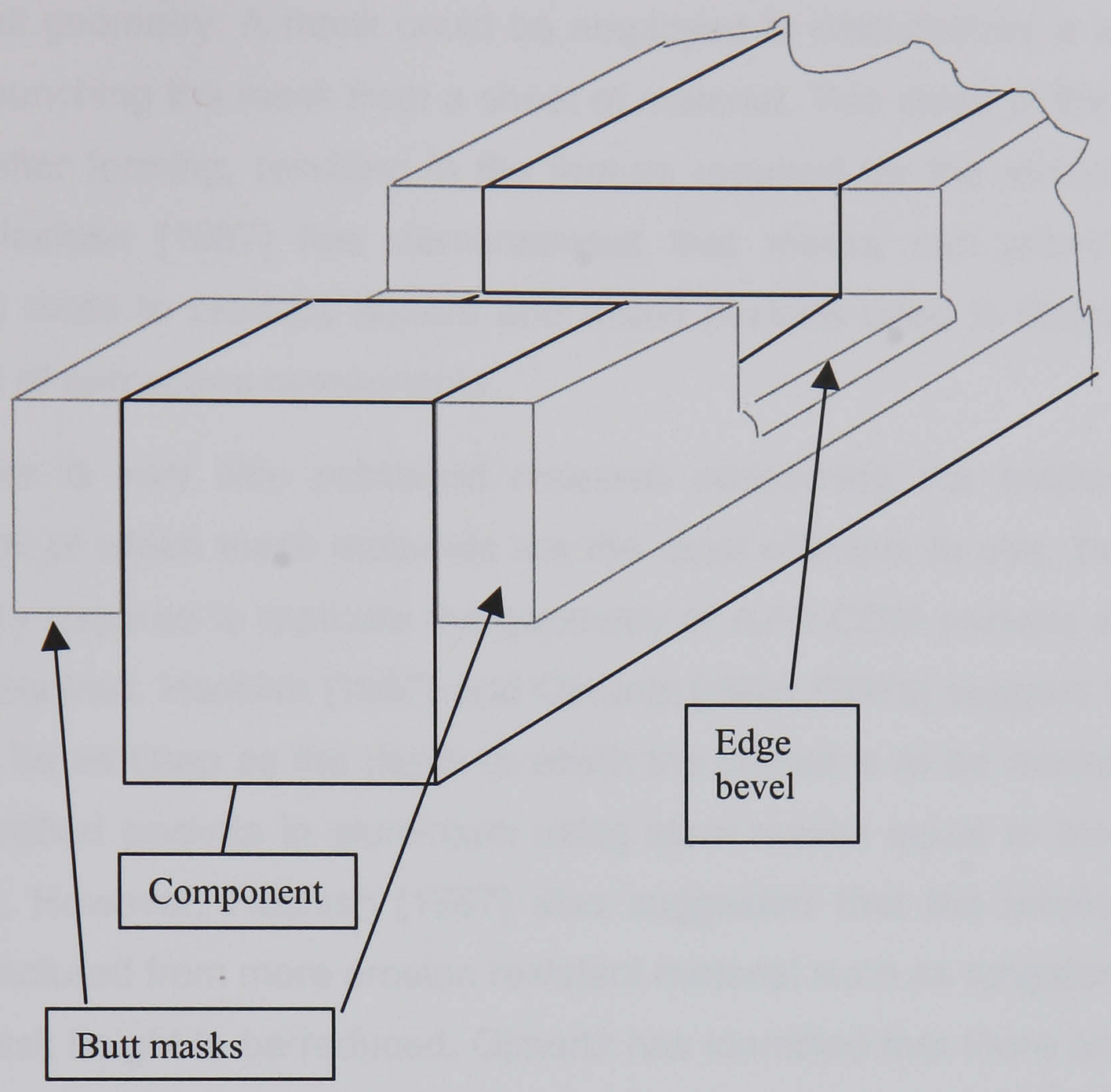

Figure 6.3 Illustration of the AJW-CDM of a wide slot with the use of butt masking.

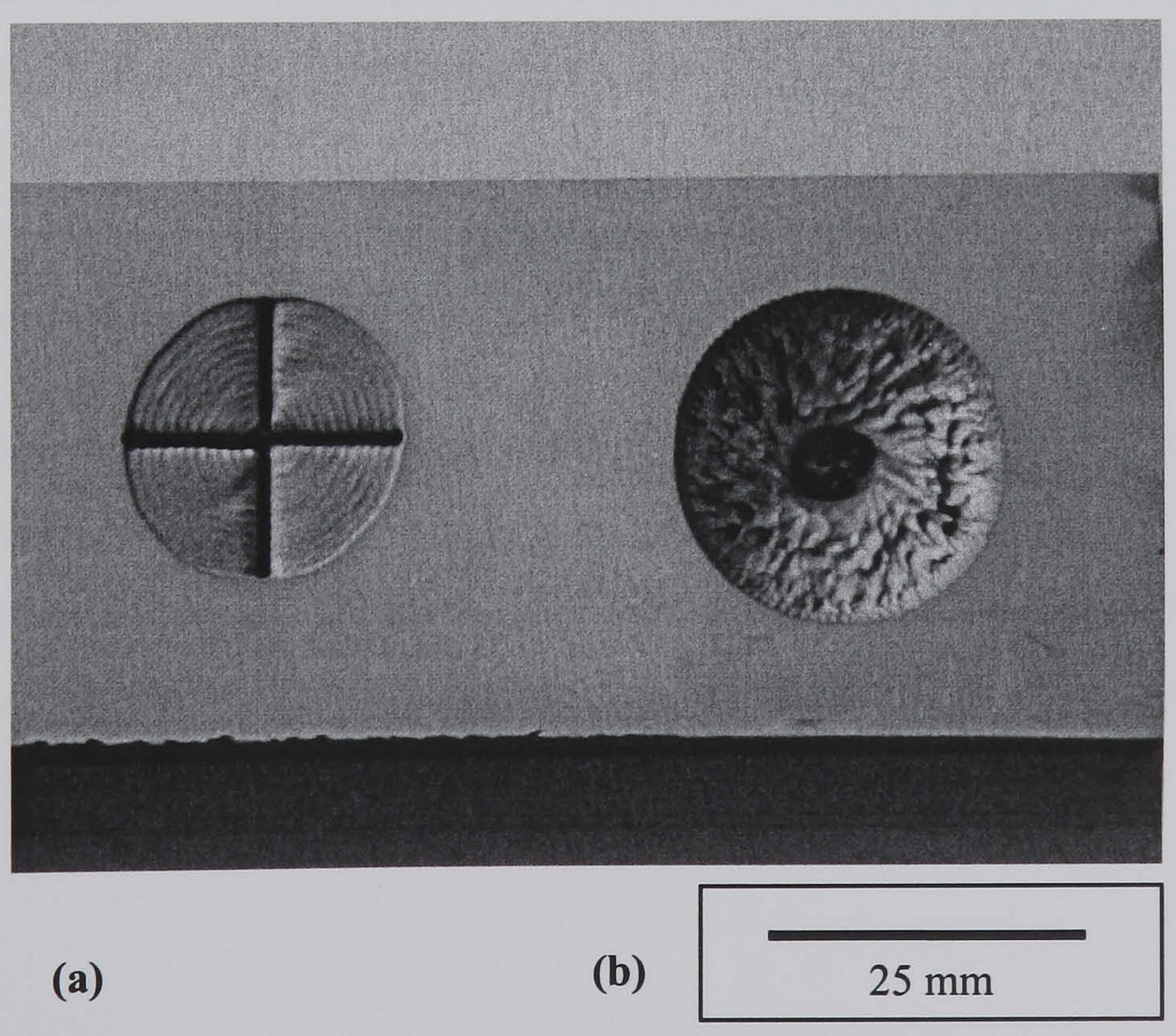

Figure 6.4 AJW-CDM pockets milled without the use of masking using a traverse speed 0.166 m s^{-1} (10 000 mm min^{-1}); water jet pressure 137.9 MPa (20 000 psi); stand off distance 3 mm; ¼ jet increment; 180 μm (80#) garnet grit. (a) Circular CNC interpolation. (b) Spiral CNC Program.

6.2 Manufacturing solution.

The employment of cut masks may provide a solution to control the geometric deviations in the side wall geometry. A mask could be employed to manufacture a square pocket by cutting or punching the mask from a sheet of material. Two sides of the pocket could be removed after forming, resulting in the feature required for the manufacture of the engine rib. Hashish [1987] has demonstrated that masks can provide a suitable manufacturing route to produce square and round pockets used in isogrid patterns to reduce weight of aerospace components.

However, there is very little published research concerning the employment of cut masks in terms of which mask materials are the most effective to use, the accuracy of mask geometry required to replicate the geometry of AJW-CDM pockets and the height of the mask required. Hashish [1987] and Ojmertz [1996,1997a] suggest that the mask height should be as deep as the depth to which the pocket is to be machined. Hashish and Ojmertz milled pockets in aluminium using steel masks equal to the depth of the milled pocket. However, Hashish [1987] also suggested that the employment of cut masks manufactured from more erosion resistant material such as tungsten carbide may enable the mask height to be reduced. Ojmertz has identified that there are problems of secondary machining when employing masks but gives no indication as to the magnitude of the effects of secondary machining. Therefore, the effect of mask height, material and dimensions on the geometry of the milled pocket was investigated to provide a solution to enable the engine rib component to be manufactured by AJW-CDM.

6.2.1 Masking materials.

Table 6.1 shows erosion rates (in terms of depth loss per pass under fixed AWJ conditions) of possible mask materials that were evaluated. Boron carbide has the lowest material removal rate, followed by alumina while Nimonic alloy and the steel based masks have similar material removal rates. Ti6Al4V was the worst mask material, with the highest depth of cut per pass.

Material	Depth (μm/pass)
Steel	75
Stainless Steel	100
Nimonic Alloy	70
Titanium	111
Alumina	73
Boron Carbide	2.5

Table 6.1 Table to show comparison of mask material erosion rates. Milling with a high traverse speed 0.166 m s^{-1} (10 000 mm min^{-1}); water jet pressure 137.9 MPa (20 000 psi); stand off distance 3 mm; ¼ jet increment; 180 μm (80#) garnet grit.

6.2.2 Pocket Geometry.

6.2.2.1 Mask Height.

Fig. 6.5 shows the effect of increasing mask height on the AJW-CDM pocket geometry. In Fig. 6.5a position 1 shows edge bevel as a result of low mask height, position 2 shows small undercuts and position 3 shows a miss-cut radius as a result of a miss-cut in the cut mask replicated in the workpiece, which was exaggerated since the mask height was low.

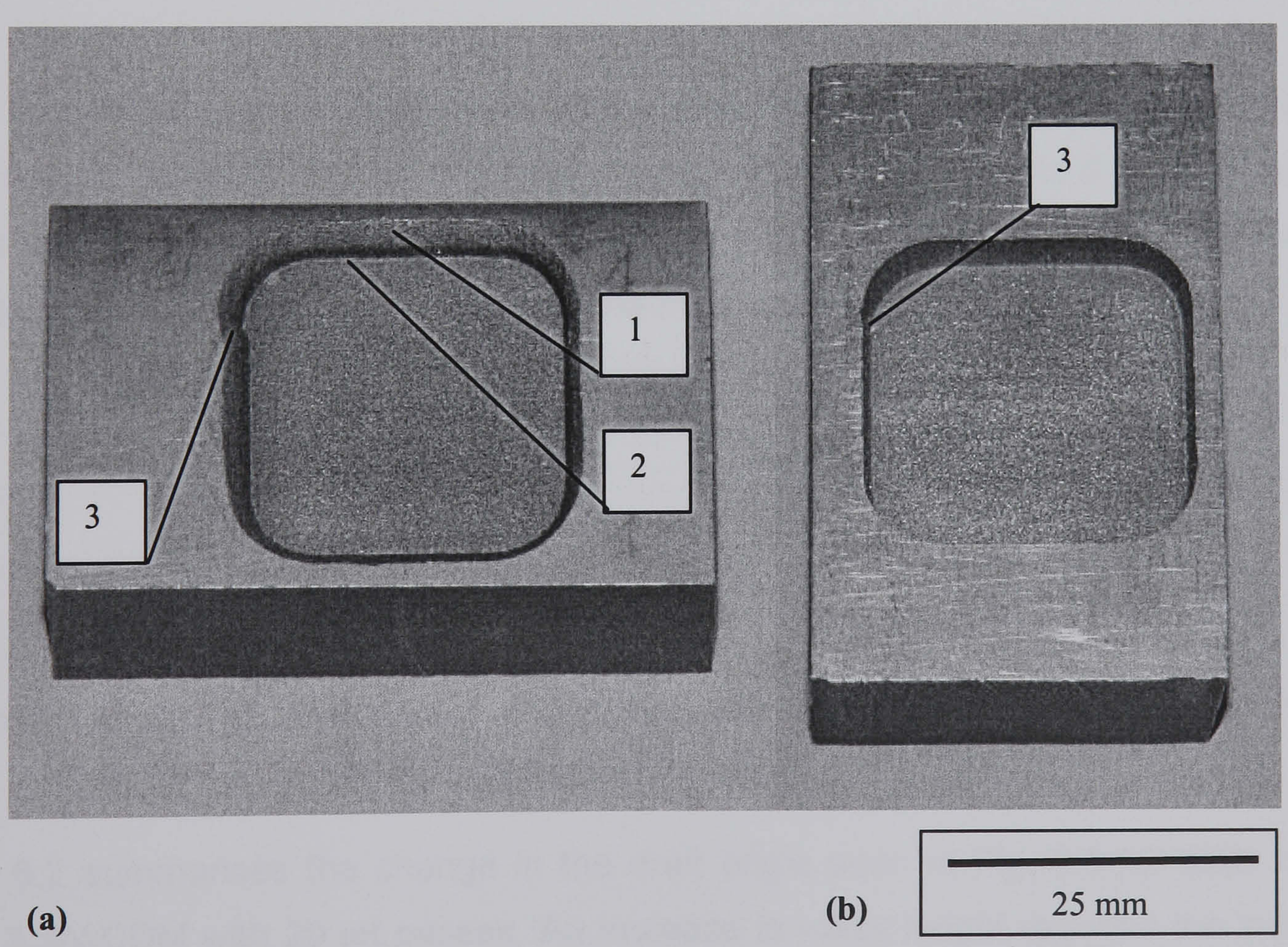

Figure 6.5 Illustration of the AJW-CDM of square pockets with radius corner, milled with masks using a traverse speed 0.166 m s^{-1} (10 000 mm min^{-1}); water jet pressure 137.9 MPa (20 000 psi); stand off distance 3mm; ¼ jet increment; number of passes of the jet 20; 180 μm (80#) garnet grit (a) Milled with mask height of 2 mm; (b) milled with mask height of 4mm. (All samples made from Ti6Al4V).

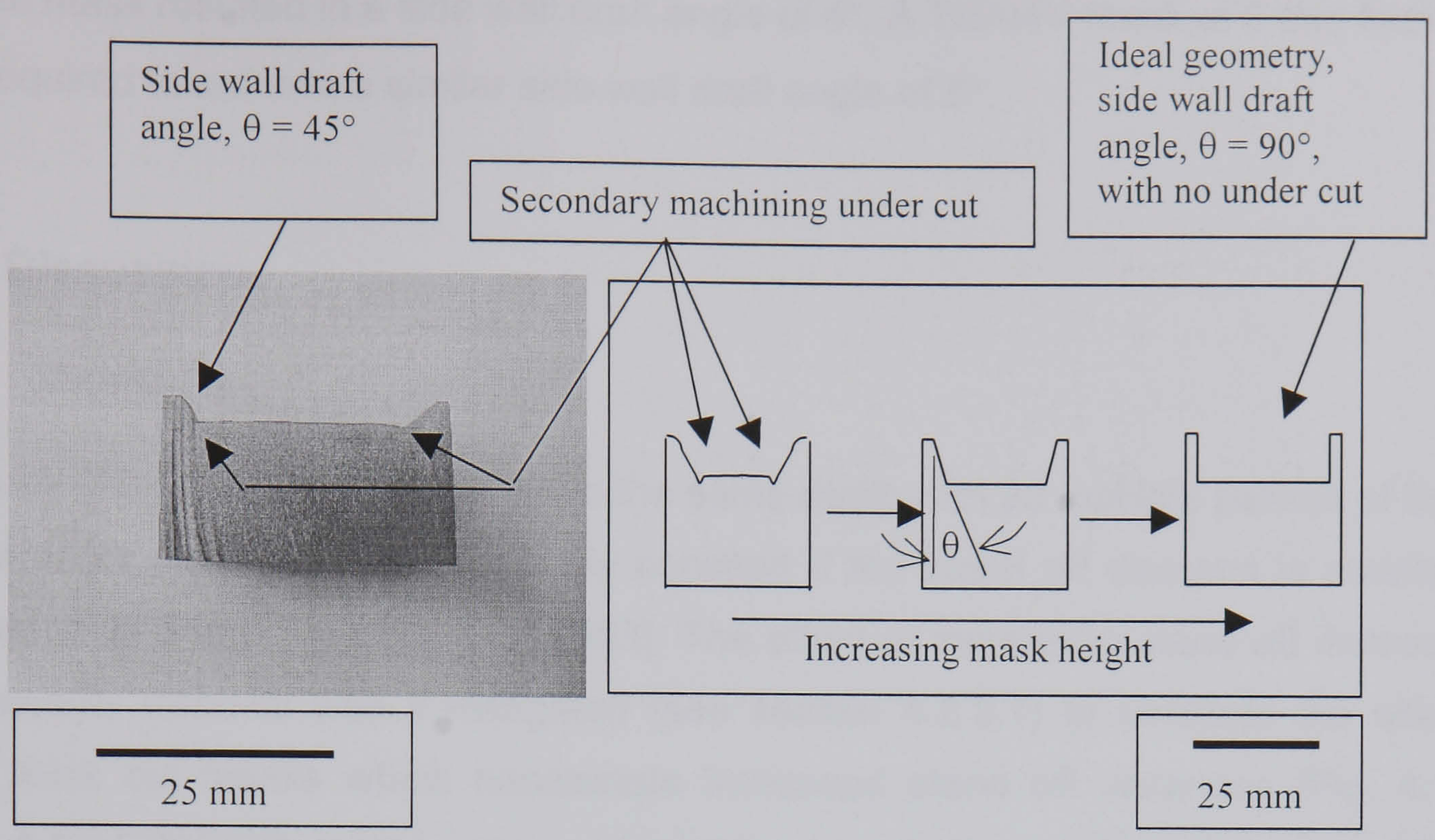

Figure 6.6 Cross sectional illustrations of AJW-CDM pockets; (a) Cross section of a pocket produced by AWJ milling with 2 mm mask using a traverse speed 0.166 m s^{-1} (10 000 mm min^{-1}); water jet pressure 137.9 MPa (20 000 psi); 20 passes of the jet; stand off distance 3 mm; ¼ jet increment; 180 μm (80#) garnet grit. (b) Schematic diagram of changes in the cross section of a pocket when increasing the height of mask. (The draft angle θ, is the angle subtended between the normal and the actual angle of the side wall of the pocket).

Fig. 6.6 shows the undercut in more detail, where a milled pocket has been sectioned. The undercut is about 0.3 mm at a mask height of 2 mm, reducing to 0.1 mm at a mask height of 6 mm. The draft angle θ is defined in Fig. 6.6b. It can also be seen that the draft angle of the side wall is reduced as the mask height increases.

Mask Height (mm)	Draft Angle (Degrees)
2	24.10
4	10.65
6	8.87

Table 6.2 Draft angle as a function of increasing mask height. Mask material: Mild steel. AJW conditions as specified in Fig. 6.6.

Table 6.2 summarises the change in the draft angle seen in Fig. 6.6 for steel masks when AJW-CDM with 20 jet passes. An increase in mask height reduced the side wall draft angle to 9° for mild steel masks. Ti6Al4V, Nimonic alloy and other steel based masks resulted in similar geometries. However, AJW-CDM pockets with an alumina mask of 4 mm in height resulted in a side wall draft angle of 5° and a 5 mm thick boron

carbide mask resulted in a side wall draft angle of 4°. A Ti6Al4V mask of 8 mm thickness was required to achieve a similar side wall draft angle of 5°.

6.3 Discussion.

6.3.1 Masks.

The AJW-CDM pockets were milled to the same depth with 20 multiple passes of the jet. The material removal rate is relatively constant if the stand off distance is maintained between 2 to 5 mm [Laurinat et al.1993]. The effect of increasing stand off distance on the material removal was investigated (see section 4.2.2.1) to evaluate the effect of using thick cut masks which necessitate increased stand off distances (Fig. 4.15a). Thus, AJW-CDM with masks may require an increase in the number of passes of the jet to compensate for the reduction in material removal rate. Any required increase in stand off distance as a result of increased mask height will have no significant effect on waviness or roughness on the bottom of the milled pocket (see section 4.2.2.2).

The depth of the pocket was maintained within a tolerance of ± 0.1 mm and the average depth of the pocket was 2.9 mm. For a mask to be effective it is expected to last the whole of the machining operation and to maintain pocket geometry. Whilst all the materials examined will satisfy this criterion, boron carbide was the by far the most resistant mask material. The depth of material removal from the mask cut for boron carbide was only 0.0025 mm per pass, losing 0.05 mm in depth during the machining of a 3 mm deep pocket milled in Ti6Al4V. Thus, employing a mask manufactured from such a material would enable much deeper pockets to be milled, or to be employed many times. The cost of boron carbide itself is however expensive; moreover it is a difficult material to process, complicating the manufacture of masks and increasing mask manufacturing costs. The exceptional erosion resistance of boron carbide is due to the fact that the material has a hardness value of H_v 3200 whilst the hardness of garnet grit is H_v 600 – 1 000 (table 2.1 and table 3.2). Hardness influences the erosion rate of a material; material with hardness very much higher than that of the abrading particle exhibit very low erosion rates. If particles are harder than the surface that is being eroded, then the influence of hardness is low and erosion rate increases. It should be noted that the mask depth loss per pass for alumina was similar to steel based materials. The alumina erodes in a brittle manner and is unable to suppress lateral cracking due to the similarity in its hardness as that of garnet abrasive.

Although the masks resisted erosion for the time span of the milling operation, the mask is sacrificial by nature and is in essence a consumable (it must economical to replace and easy to obtain). The choice of mask material will be based on economics, availability and the lowest material removal rate for the pocket geometry and depth required.

The erosion of the mask affects the length, *l* over which enhanced depth removal due to particle rebound from the mask is observed (defined in Fig. 6.7d). It is reduced to the point where it blends into the bottom of the milled pocket when the mask height reaches 6mm. This type of undercutting is also seen in chemical etching [Harris, 1976 (pp 39 & 97)] arising from gas bubble entrapment, etchent type, masking errors, and incorrect use of knife tools when masking.

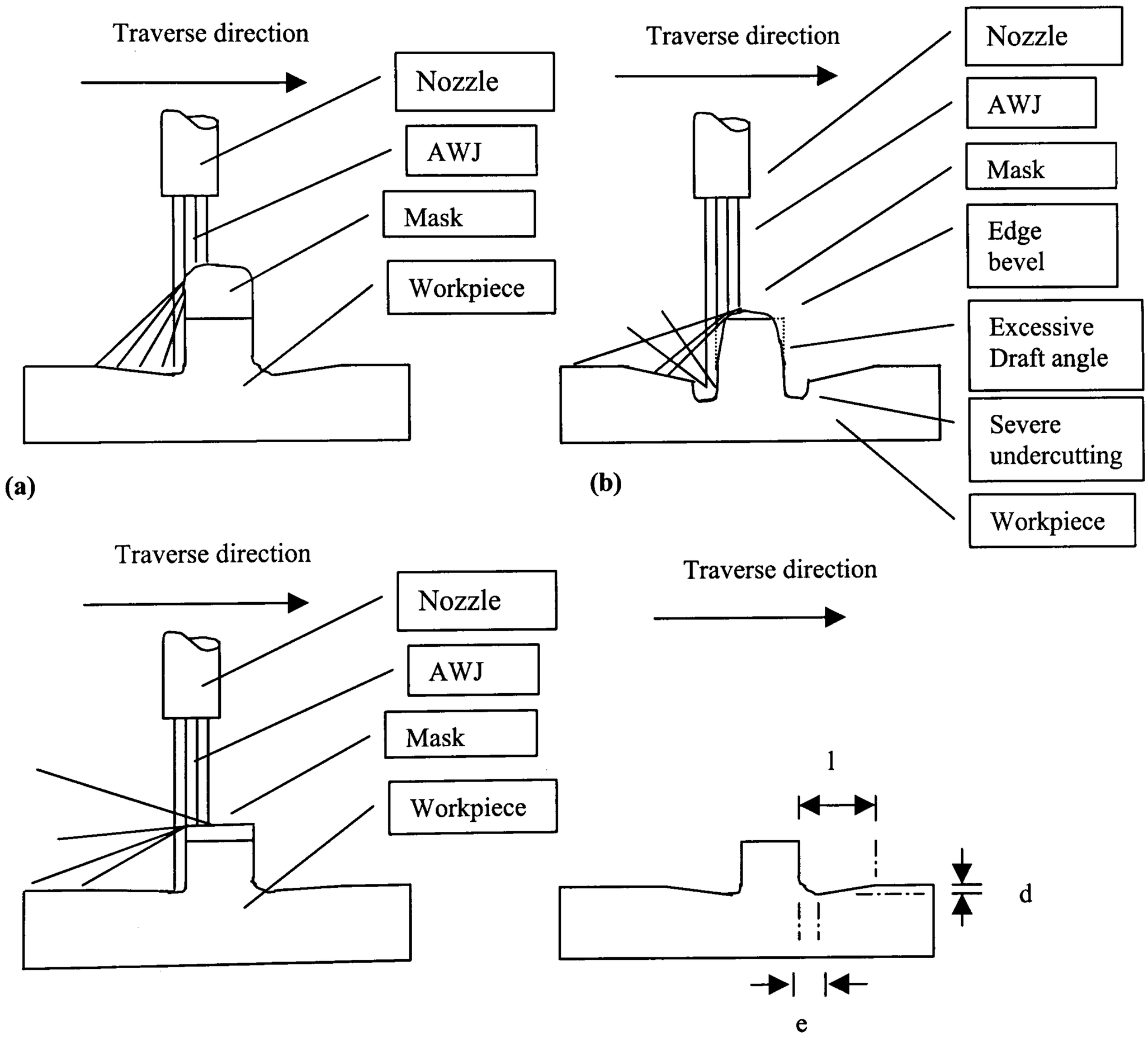

Figure 6.7 Secondary machining effects when AJW-CDM with masks. (a) High mask height. (b) Low mask height. (c) Low height erosion resistant mask. (d) l, d, and e, indicate dimensions of form errors caused by secondary machining due to jet deflections.

Square and round pockets milled with masks made from all the materials examined exhibited similar changes in side wall draft angles as the mask height increased. The pocket geometry was also similar when measured in the direction of traverse and perpendicular to the traverse direction of the water jet. The largest side wall draft angle was observed with the lowest mask height. The draft angle decreased as the mask height increased. It should be noted that the difference in the draft angle between a mask height of 4 mm and a mask height of 6 mm (for mild steel masks) is only 1.82° (Table 6.2). The height of the mask will depend on the customer requirements for the side wall geometry. For a side wall draft angle less than 10°, a rule of thumb for milling Ti6Al4V would be to use a metallic mask height twice the depth of the pocket to be milled. For milling a 6 mm deep pocket in aluminium, Ojmertz [1996, 1997a] and Hashish [1987] suggested a steel mask with height at least the depth of the pocket to be milled; they recommended that if a tungsten carbide mask is employed, the mask height could be reduced to 1.5 mm. The draft angle variation is a result of secondary machining as observed by Ojmertz [1996,1997a] and trailing and leading jet movement as described by Hashish [1987]. Fig. 6.7 shows the effect of mask height and erosion resistant masks on workpiece geometry. Masks made of low erosion resistance material erode quickly with the formation of edge bevels. Low mask height (Fig. 6.7b) exposes the workpiece to the water jet much earlier in the milling process than higher masks as the mask height reduces under eroding conditions. The edge bevel is transferred to the workpiece as the mask erodes, and the water jet erodes the work piece directly resulting an excessive draft angle. Both the draft angle and the edge bevel deflect the water jet at reduced angles promotes an increase in secondary machining, resulting in increased undercut, depth *d*. Moreover, at reduced deflection angles, the vertical fluid streamlines of the water jet are less likely to be deflected leading to increased erosion of the undercut, *e*. The draft angle increases and severe undercutting results. As the mask height is increased sufficiently to delay the erosion of the workpiece, much of the edge bevel remains on the mask high above the workpiece (Fig. 6.7a). Jet deflections are at higher angles and so reduce direct contact of the water jet with the side wall of the workpiece. The draft angle and undercutting depth d is reduced as a result of reduced secondary machining. Fig. 6.7c shows the employment of a low height mask made from erosion resistant material. In this case, the erosion resistance of the material is sufficient to significantly reduce edge bevel formation. Water jet deflections are very much larger than the two previous cases. Larger deflections result in less erosion since they are more likely to hit the workpiece much further away from the side wall of the pocket or miss the workpiece completely. Thus, increasing the undercut length *l* and also reduces

the undercut depth *d*. Moreover, large deflections also deflect the water jet away from the side wall of the pocket further reducing the undercut depth *d* and the radius length *e*, resulting in a sharp cornered pocket with a reduced draft angle observed as in Fig. 6.5b.

The relationship between mask material and target material erosion rate is not clearly defined. Tables 6.1 and 6.2 show that alumina has a similar erosion rate to steel but requires 2 mm less height to achieve a similar side wall geometry. The hardness relationship between target, grit and material will play a role in mask material and height selection.

Analysis of the corner radii developed in the AJW-CDM pockets (Fig. 6.5) indicates that the size of the radius machined follows the radius machined in the mask. However, the height of the mask is a key parameter to the control of the size of the corner radii. The variation in the size of the radius, at the top of the milled pocket and the size of the radius in the bottom of the milled pocket results in the same draft angle that develops on the pocket wall.

The width of the milled pocket is 0.1mm bigger than the width of the pre-machined aperture of the mask when a mask height of 6 mm is employed for all the mask materials examined apart from that of the boron carbide where the width increase was reduced to 0.05 mm. This dimensional difference is a result of mask side wall erosion; the more erosion resistant the mask material, the smaller the dimensional difference between mask and pocket geometry. Therefore, the mask aperture dimensions will require adjustment to achieve the required pocket size; the amount of adjustment will depend on the height of masks selected.

It should be noted that 2 mm plate was selected to enable fast, economic prototyping of the masks and enable a change in mask height to be achieved quickly, with the possibility to assess the benefits of changing partially worn masks. Changing partially worn masks resulted in no benefit to the geometry of the milled pocket. This may be due to insufficient mask height at the point of changeover. A concern in the employment of thin masks manufactured from rolled plate is that as the material is removed from the mask, the mask begins to bow and affect the geometry of the milled pocket. This may be a result of peening or the residual stress release from rolling process as the material becomes thinner. The masks may need to be firmly clamped to the work by glue as suggested by Hashish [1987] or some other means of clamping. Other solutions would be to employ a thicker mask, exchange masks as they wear near the bowing point or employ masks manufactured from stiffer materials such as alumina.

6.3.2 A manufacturing solution.

The manufacture of the engine rib on a two axis machine would require a masking operation as depicted in Fig. 6.8. The slot required is 1 mm deep; a cut mask of steel 2 mm would be clamped to a material blank larger than the finished component. The pocket could be AJW-CDM to depth, using the following process variable settings depending on customer requirements: water pressure of 137.9 MPa or 258.6 MPa, high traverse speed of 0.166 m s^{-1} (10 000 mm min^{-1}), a grit size of 180 μm (80#) or 75 μm (200#), a ¼ jet increment, with 5 depth passes, at normal angles to the required depth. These settings are analysed in the economics section of this discussion. The mask can be removed (if desired) and the component through-cut to size. The circular hole would be pierced and through-cut, followed by a profile through-cut to form the elongated hole, and the outside edge profile of the finished component, thus forming the 465 mm x 127mm x 1 mm deep slot.

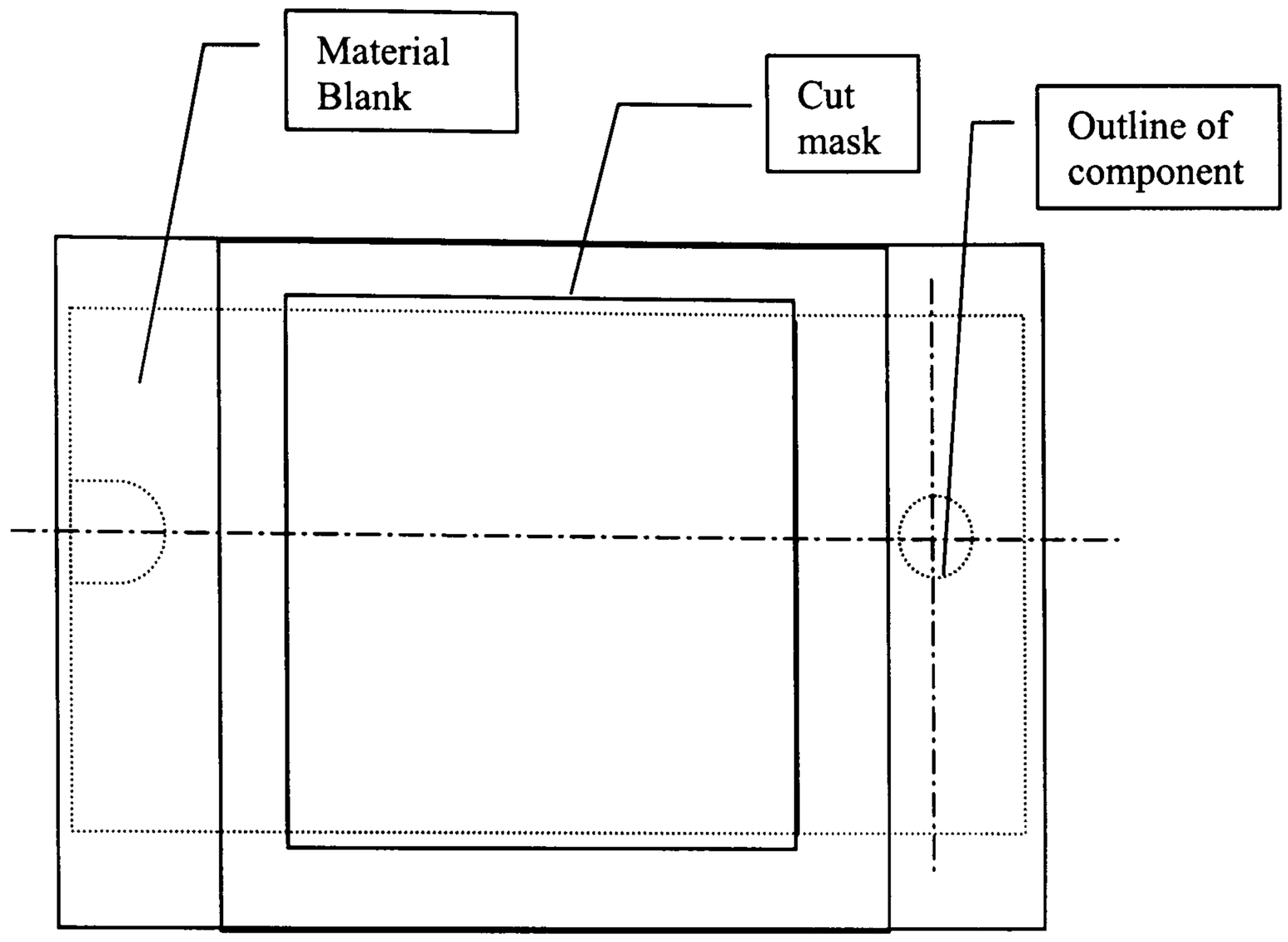

(a)

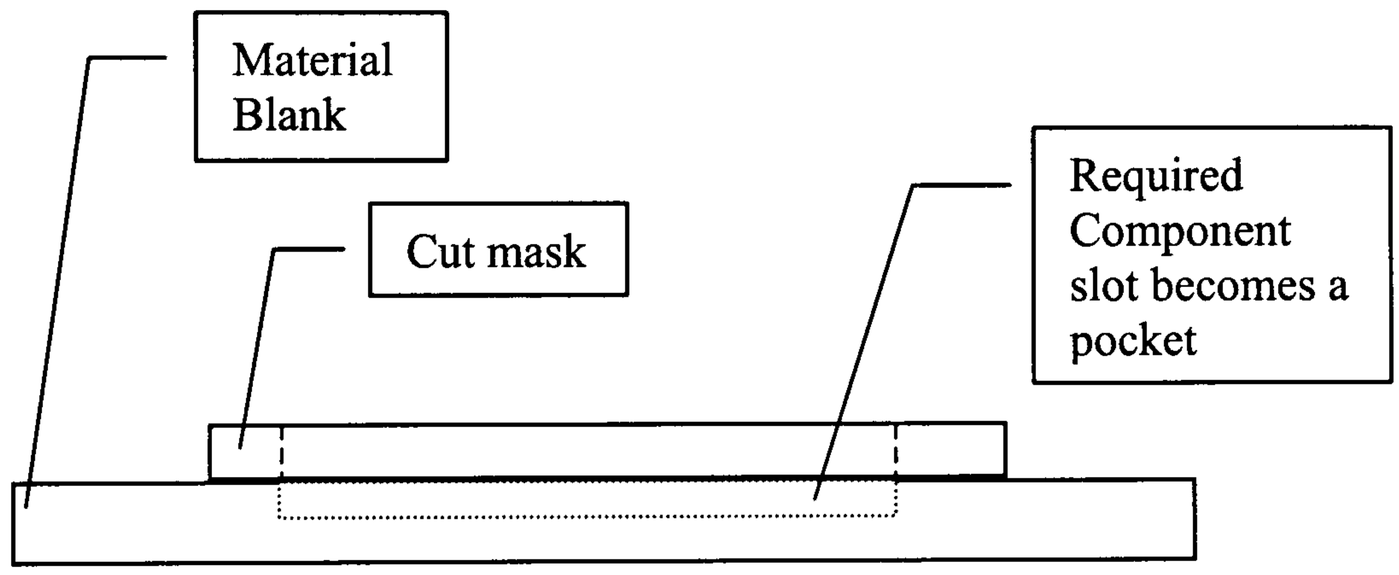

(b)

Figure 7.8 (a) Plan View of cut mask operation to manufacture slot in the Engine rib component. (b) Front elevation of the cut operation to manufacture slot in the Engine rib component.

6.3.3 Manufacturing Strategy.

The manufacturing strategy of employing AWJ-CDM as a opposed to some other process to machine a component is dependent on whether the process is considered to be a roughing or a finishing process. In the context of machining, the roughing process is a manufacturing process employed to remove material quickly with little regard for surface roughness or component geometry, whereas a finishing process is one that is employed to meet drawing or customer requirements with no additional machining requirement. The roughing process is a precursor to finishing with either a different manufacturing process or the same manufacturing process but a different set of parameters compared to those for roughing, with more emphasis placed on obtaining the required roughness and component geometry.

The AWJ-CDM process based on roughness values of 2 - 6.5 μm observed in this investigation are similar to those roughness generated by the manufacturing process of conventional turning and milling, electrodischarge, electrochemical, electron and laser beam machining. However, the material removal rates of AWJ-CDM are much higher than those of electrodischarge, electrochemical, electron and laser beam machining, but much less than conventional turning and milling [Hashish, 1987]. Moreover, limited research on the polishing of titanium aluminide with low impingement angles of 3° using 200 - 400# (75 μm - 17 μm) grit resulted in roughness values of 0.6 - 1.0 μm, which are comparable with those of grinding, honing and lapping [Rank Taylor Hobson, 1985a].

The choice of AWJ-CDM as a roughing or finishing process will depend on drawing requirements, material machinability, process economics and structural integrity. Thus, e.g. conventional milling can be used as a roughing process as a precursor to another manufacturing process or as a finishing process itself, then so too can AWJ-CDM.

6.3.4 *Economics.*

An analysis of the technical and economic requirements for AJW-CDM as a suitable replacement for chemical milling of the engine rib (see Fig. 3.2) has been conducted as indicated in Table 6.3.

	Chemical milling	**AJW-CDM**
Depth control	± 0.05 mm**	± 0.05 mm*
Surface waviness (*Wt*)	0.1 mm**	0.1 mm*
Surface roughness (Ra)	0.3 - 0.8 μm milling sheet material and 1.5 μm milling forgings**	2.5 – 6.5 μm*
Time to Mill Volume (465 mm long x 127 mm wide to depth of 1 mm)	3 hours.***	2.25 - 4.5 hours.*
Overhead Recovery Rate	£2.14X per hour ***	£X per hour***
Process force	Low force***	Low force***
Masking	Long masking times, skilled mask scribing with pre mask and post mask cleaning/environmental disposal problems***	Low masking times using low cost recyclable materials, requiring conventional machining skill with minimal pre mask and post mask cleaning and disposal operations. *
Limitations	Surface defects exaggerated by etching process. Quality of pre- milled surface important**	Surface defects exaggerated by milling process. Quality of pre-milled surface important*
Fatigue Life	Little or no effect**	Unknown
Environmental Disposal Costs	High***	Low***
Health & Safety	Toxic chemicals & Fumes***	Dust*
Capital Equipment Costs	High £750 000*	Low £200 000*

Table 6.3 Comparison of AJW-CDM and Chemical milling of Engine cowling rib; milling at normal jet angles, at high traverse speed 0.166 m s^{-1} (10 000 mm min^{-1}), a high water pressure of 258.6 MPa (37 500 psi) and 137.9 MPa (20 000 psi) using 180 μm (80#) and 75 μm (200#) garnet grit. X is an commercially sensitive value for the overhead recovery rate. [* as measured], [**Harrris, 1976], [*** aerospace company].

Table 6.3 illustrates the comparison of chemical milling and AJW milling technologies that can be applied to a mill a large area of thin walled component. Depth can be controlled to ± 0.05 mm, with a roughness value of 6.5 μm, milling time was 2 hrs 15 minutes. However, using a smaller grit of 75 μm (200#), roughness can be reduced to 2.5 μm but milling time is increased to 4 hours. Chemical milling takes 3 hours [data supplied by aerospace company] to mill to the same depth of 1mm. The times for mask/demask, and cleaning operations have been omitted for clarity. The machining conditions were selected, to show the best and worst roughness, when milling to achieve the least waviness in light of the aerospace companies requirement to achieve an unquoted roughness and waviness for the maximum material removal rate. The machining conditions being based of the results of the research, and do not include any polishing techniques that may result in improved waviness and roughness values.

Chemical milling can achieve a roughness of 0.3 - 0.8 μm [Harris 1976], however, the roughness actually achieved by aerospace company chemical milling methodology was undeclared. In order to achieve such a roughness (Ra) of 0.8 μm when using AJW-CDM, a smaller sized grit of 17 μm (400#) can be employed or milling at a low jet impingement angle of 3° as the depth approaches 1 mm, but the material removal rates drop significantly. Therefore, a few depth passes as a part of the finishing/polishing process with small grit or lower jet impingement angle to achieve the chemi-milled roughness quoted by Harris would further increase the manufacturing times quoted. AJW-CDM and chemical milling are both low force processes reducing distortion effects [Li et al. 1996b, Harris 1976]. However they both suffer from the disadvantage of exaggerating previously machined surface defects.

Chemical milling has little or no effect on the fatigue life of components [Harris, 1976, Koster, 1973] whilst the fatigue life of manufacturing a component using AJW-CDM is unknown with little published research on the effect of grit embedment on the fatigue life of AJW-CDM components.

The overhead recovery rates assume full recovery of the cost of capital equipment, disposal costs, maskants and other consumables. The overhead recovery rates for manufacturing the same component using chemical milling is about 2.14 times more than the cost of manufacturing AJW-CDM. The increase in overhead recovery rates for chemical milling is a result of the increased cost of pre and post masking, cleaning operations and the disposal of chemical contaminated masking materials. Long manufacturing times are also involved in mask manufacture via scribing which is

considered to be highly skilled. [Harrris, 1976]. Masks for AJW-CDM can be manufactured using low cost recyclable materials such as steel, which can be manufactured using conventional machining techniques. The capital equipment cost requirement for chemical milling is much higher than that required for AJW-CDM. The chemicals employed in the chemical milling of titanium alloys are corrosive, requiring capital equipment to be manufactured from highly corrosion resistant materials. Also they require more stringent control of liquid and fume emissions under the health, safety and environmental disposal legislation. AWJ is a low cost method with cost similar to conventional machine tools but requiring additional dust control equipment.

The cost analysis for the conditions stipulated show that a reduction in manufacturing costs of 30 to 65% may be possible by changing from chemical milling to AJW milling.

In chemical milling, etching times are related to depth and not area. Therefore, AJW-CDM could be even more cost competitive for milling of smaller areas.

6.4 Conclusions.

- Increased mask height and erosion resistant masks reduce draft angle, undercutting and edge bevels leading to improved pocket geometry.
- The accuracy of the mask geometry and erosion resistance affect the accuracy of AJW-CDM pocket.
- Masks are sacrificial and must last the required machining time. Material selection must be based on economics; the relationship between mask and workpiece must be carefully chosen to ensure correct mask height.
- Masking is a possible solution for the manufacture of the engine rib.
- AJW-CDM is a low cost method that can provide a possible alternative to chemical milling.
- The employment of AWJ-CDM as a roughing process as the precursor to another manufacturing process or as a finishing process itself will depend on drawing requirements, material machinability, process economics and structural integrity.

Chapter 7

7 Conclusions.

This study aimed to characterise and evaluate the AJW-CDM process as a replacement manufacturing technique for the process of chemical milling.

The research established the effects of process characteristics on material removal rate, roughness and waviness, grit embedment and surface morphology. Table 8.1 is an updated version of table 2.3 in chapter 2 showing the contribution of this investigation to the field of AJW-CDM in the form of new research and an expansion to existing published research in the AJW-CDM of titanium alloys in particular.

Parameter	Material removal rate	Waviness	Roughness	Grit embedment
Water pressure	●[section 4.2] ✓[Hashish,1989b]	●[section 4.2] ✓ [Ojmertz, 1993]	●[section 4.2]	✘
Lateral increment	●[section 4.2] ✓[Ojmertz, 1993]	●[section 4.2] ✓[Ojmertz, 1993]	●[section 4.2]	✘
Jet impingement angle	●[section 4.3] ✓[Hashish,1989c]	●[section 4.3]	●[section 4.3] ✓[Li, 1996b]	●[section 4.4]
Number of passes	●[section 4.1, 4.2, 4.3] ✓ Hashish,1998a]	●[section 4.1, 4.2, 4.3] ✓ [Hashish,1987]	●[section 4.1, 4.2, 4.3]	●[section 4.4]
Traverse speed	●[section 4.1] ✓ Hashish,1998a]	●[section 4.1] ✓ [Hashish,1987]	●[section 4.1]	●[section 4.4]
Stand off distance	●[section 4.2] ✓ [Hashish,1987]	●[section 4.2]	●[section 4.2]	✘
Nozzle design	✓[Momber and Kovacevic, 1998]	✘	✘	✘
Abrasive characteristics -particle size	●[section 4.1,4.2] ✓[Hashish,1998a]	●[section 4.1,4.2]	●[section 4.1, 4.2] ✓ [Li, 1996b]	●[section 4.4]
Abrasive flow rate	✓[Kulekci, 2002]	✘	✘	✘
Masks	● [section 6.2] ✓ Hashish,1998a]	●[section 6.2]	●[section 6.2]	✘

✓ = information available. ✘ = information not available.

● = contribution made to research as a result of this investigation. (AJW-CDM of Ti6Al4V and titanium aluminide). Note: e.g. [section 4.1] indicates where in this work the contribution to knowledge may be found.

Table 8.1 Roles of parameters known to affect material removal rate, roughness and waviness and grit embedment in AWJ milling.

Within the bounds of the experimental programme, the following conclusions were made with respect to Ti6Al4V:

- The process variables of traverse speed, grit size, water jet pressure, jet increment (lateral passing), jet impingement angle all influence the way that the material is removed in AJW milling.
- At low jet traverse speeds (0.003 m s^{-1}), the jet cuts primarily on the leading edge of the kerf and is then channelled along the slot to produce a directional morphology on the bottom of the kerf. Whilst this leads to high material removal rates, the flow of the particle laden fluid along the kerf bottom results in high waviness. The roughness is low due to this secondary machining effect. Surface waviness is observed to increase significantly with number of passes of the jet at lower traverse speeds.
- High jet traverse speeds (5 m s^{-1}) result in lower material removal rates as material is removed primarily by high angle impingement. Little directionality in the surface morphology is observed on the bottom of the kerf. High jet traverse speeds lead to lower values of surface waviness, but higher values of surface roughness than lower jet traverse speeds.
- For the two grit sizes examined, 180 μm (80#) and 75 μm (200#) the material removal rate is lower for the smaller grit. Surface waviness is also generally lower for the smaller grit size. However, when cuts were made to the same depth with the two grit sizes, the differences in waviness for the two sizes was seen to be less dramatic at the higher traverse speeds (0.166 m s^{-1}) than at the lower traverse speeds (0.003 m s^{-1}). The surface roughness developed is generally larger for the larger grit size, due to the increased size of individual impact craters as the particle size increases, and the possibility of the smaller grit to more closely follow the flow of the fluid within the kerf during secondary machining.
- The cumulative depth of cut is shown to vary linearly with number of passes of the jet in the specific cases examined. Surface waviness increases as the number of passes of the jet increased, but roughness remained almost constant.
- Water jet pressure strongly influences material removal rates, and surface waviness, at all traverse speeds but has a less strong influence on roughness at high speeds (5 m s^{-1}) and little influence on roughness at low speeds (0.003 m s^{-1}). Increased water jet pressure increases the velocity and energy available to enhance erosion and aberrations thereby increasing material removal rate and waviness.

- Stand off distance has a strong influence on the material removal rate and little influence on the surface waviness and roughness. The material removal rate decreased as the stand off distance increased due to reducing impact velocity at the target surface.

- Lateral passing has no strong influence on material removal rate, waviness or roughness; the material removal rate was approximately constant for all process variables considered.

- Jet step increment has an influence on material removal rate, but not on waviness and roughness. Milling with small jet increments increases material removal rate due to the water jet passing over previously machined areas. Waviness is reduced when milling with small jet increments when milling with multiple passes of the jet, since small jet increments reduce the production of lay marks which are exaggerated by subsequent multiple passes of the jet.

- The material removal rate depends upon the angle of jet impingement; however, since the impact angle of the abrasive particles with the material surface is not necessarily the same as the jet impingement angle, the dependence is more complex than that observed in the gas-blast erosion literature.

- At high jet traverse speeds (5 m s^{-1}), the impact angle of the abrasive particles with the material surface is closer to the jet impingement angle, resulting in a maximum material removal rate for a jet impingement angle close to 60^{o}.

- Surface waviness and surface roughness is generally lower for lower jet impingement angles.

- Milling direction had little effect on the roughness, waviness and material removal characteristics when milling at high (5 m s^{-1}) or low (0.003 m s^{-1}) speeds. However, at intermediate speeds (0.0166 m s^{-1}), an effect was seen on the material removal rate and roughness developed.

- To achieve the low waviness required for an industrial process, a high jet traverse speed must be employed. Even then, the waviness increases with depth of material removed. Under these conditions, the waviness and material removal rate are not strong functions of jet impingement angle; however, the surface roughness can be reduced by the use of low jet impingement angle with this reduction being most significant for larger grit sizes. Thus, optimum conditions can be identified depending upon the constraints of the application.

- Grit embedment was observed under all the experimental conditions considered with embedded grit making up between 5% and 40% of a milled surface area.
- For the two grit sizes examined, grit embedment levels were similar.
- Increasing the dose of particles by multiple passing of the jet over the workpiece had no significant effect on the surface morphology or on the level of grit embedment.
- Two regimes of grit embedment behaviour have been identified, and are characterised by the traverse speed of the jet across the workpiece. With low jet traverse speeds (0.003 m s^{-1}), there is a significant effect of milling direction on the characteristic of grit embedment. Forward milling results in high levels of grit embedment and a higher tendency for cratering whilst backward milling results in lower levels of grit embedment and a more grooved surface morphology. There is a significant difference in the angular dependence of the level of grit embedment with the two modes of milling.
- With high jet traverse speeds (5 m s^{-1}), milling direction has no strong influence on grit embedment or surface morphology. A monotonic increase in the level of grit embedment with jet impingement angle is observed under these conditions.
- Abrasive water jet parameters suitable for milling TiAl6V4 alloy can be transferred to milling titanium aluminide resulting in similar characteristics of depth of cut, material removal rate, surface roughness, waviness, morphology and grit embedment. Titanium aluminide although considered somewhat brittle in an engineering context, erodes in a ductile manner as does Ti6Al4V. Erosion profiles observed in AJW-CDM for these two materials were similar.
- Mask height and material type are the controlling factors when AJW-CDM pockets. Increased mask height reduces secondary machining thus reducing draft angle of the side wall of the milled pocket geometry.
- The employment of AWJ-CDM as a roughing process as the precursor to another manufacturing process or as a finishing process itself will depend on drawing requirements, material machinability, process economics and structural integrity.
- AJW-CDM is a suitable economic replacement for the chemical milling process provided any arising fatigue debit satisfies customer requirements.

Chapter 8

8 Future work.

Recommendations for future work are as follows:

- Manufacture previously chemical milled components using the AJW-CDM process to the established process characteristics, and conduct fatigue life testing research. The research should also establish whether any residual stress is induced by the established process and determine its effect on fatigue life. Further, since post manufacturing processes may be conducted on AJW-CDM components, the research should also investigate the effect of the process characteristics on the adhesion of any coating materials and its inhibition of the mechanical strength of welded features.
- Further techniques to remove embedded grit need to be investigated.
- Instrumentation of the machine tool and work piece is recommended to expand the knowledge of the material removal mechanism in AJW-CDM. Force and pressure transducers should be employed to measure impact forces and water pressures on the workpiece. Accelerometers should also be used to measure the velocity time profiles of the traversing water jet and machine tools vibrations that may effect the milling process. The simultaneous measurement of these parameters during the milling process may provide more detailed knowledge on the formation of the process characteristics of AJW-CDM and may allow for online process monitoring.
- Establish if automatic abrasive flow rate and automatic pressure ramping can eliminate the need for masks; Machine tool design may also need to be addressed, current five and two axis machines tools are developed for through-cutting and not specifically for milling.
- A study into the benefits of employing more accurate consistent grit characteristics of shape, size, material composition and hardness to increase the consistency of process characteristics should also be conducted.

References.

Armada S, Hirose T, Senda T, 1999, "Quantitative evaluation of residual grits under angled blasting." Surface and Coatings Techn., 111, 1 - 9.

Arola D, Ramulu M, 1993, "Micro-mechanisms of material removal in abrasive water jet machining." Processing of Advanced Mater., 4, 37 - 47.

Arola D, Ramulu M, 1996, "A residual stress analysis of metals machined with the abrasive water jet." In: Gee C, (ed) Proc. 13th Int. Conf. Jet Cutting Techn., Mechan. Engng Publishers, Bury St Edmunds, 269 - 290.

Arola D, Ramulu M, 1997a, "Material removal abrasive water jet machining of metals: surface integrity and texture.", Wear, 210, 50 - 58.

Arola D, Ramulu M, 1997b, "Material removal abrasive water jet machining of metals: a residual stress analysis.", Wear, 211, 302 - 310.

Arola D, Williams C L, 2002a, "Estimating the fatigue stress concentration factor of machined surfaces.", Int. J. Fatigue, 24, 923 - 930.

Arola D, McCain M L, Kunaporn S, Ramulu M, 2002b, "Water jet and abrasive water jet surface treatment of titanium: A comparison of surface texture and residual stress.", Wear, 249, 943 - 950.

Askeland D R, 1996, "The science and engineering of materials." Chapham and Hall, London.

Badwi K, Bielle J, Castex L, 1986, "Influence of sand blasting parameters on the geometrical and mechanical characteristics of 1010 steel sand blasted surfaces." Advances in Surface Treatment Technology Applications., 3, 229 - 241.

Bennett A J, 1996, "A comprehensive analysis for the use in water jet cutting." In: Gee C, (ed) Proc. 13th Int. Conf. Jet Cutting Techn., Mechan. Engng Publishers, Bury St Edmunds, 583 - 594.

Bitter J G A, 1963a, “A study of erosion phenomena, Part 1”., Wear, 6, 5 - 21.

Bitter J G A, 1963b, “A study of erosion phenomena, Part 2”., Wear, 6, 169 - 190.

Blickwedel H, 1990, “Erzeugung und Wirkung von Hochdruck - Abrasivstrahlen.” VDI Fortschritt – Berichte, Reihe 2, Nr 206.

Cappelo E, Polini W, Semeraro Q, 1996, “Abrasive water jet cutting of MMC: Analysis of the quality of the generated surfaces.” A.S.M.E., Petroleum Div. 75, 63 - 68.

Carter G, Nobes M J, Arshak K I, 1980, “The mechanism of ripple generation on sand blasted ductile solids.”., Wear, 65, 151 - 174.

Chao J, Geskin E S, Chung Y, 1992, “Investigation of the dynamics of the surface topography formation during abrasive water jet machining.”. In: Lichtarowicz A (ed) Proc.11th Int. Conf Jet Cutting Techn., Kluwer, Dordrecht, 593 - 603.

Chao J, Zhou G, Leu M C, 1995, “Characteristics of abrasive water jet generated surfaces and effects of cutting parameters and structure vibration.”, J. Eng. Industry, Trans. A.S.M.E., 117, 516 - 525.

Chen F L, Siores E, Patel K, Momber A W, 2002 “Minimising particle contamination at abrasive water jet machined surfaces by a nozzle oscillation technique.” Int. J. Machine Tools and Manuf., 42, 1385 - 1390.

Chen F L, Siores E, 2003 “The effect of cutting jet variation on striation formation in abrasive water jet cutting.”, J. Mater. Processing Techn., 135, 1 - 5.

Colosimo B M, Monno M, Semeraro Q, 2000, “Process parameter control in water jet peening.” Int. J. of Materials and Product Techn., 15, 10 - 19.

Daniewicz S R, Cummings S D, 1999, “Characterization of a water jet peening process.” J. Eng. Mater. and Techn., 121, 336 - 340.

Dickinson W, Wilkes R D, Dickinson R W, 1987, “Conical water jet cutting.” In: Hood M, Dornfeld D (eds). Proc. 4th US Water Jet Conference. A.S.M.E. New York, 89 - 96

Dunsky C W, Hashish M, 1996, "Observations on cutting with abrasive cryogenic jets." In: Gee C, (ed) Proc.13th Int. Conf. Jet Cutting Techn., Mechan. Engng Publishers, Bury St Edmunds, 679 - 690.

Faber K, Oweinah H, 1991, "Influence of process parameters on blasting performance with the abrasive jet.". In: Saunders D. (ed) Proc.10th Int. Conf. Jet Cutting Techn., Elsevier, London, 365 - 382.

Finnie I, 1960, "An experimental study of erosion."., Proc. of Soc. of Experimental Stress Analysis., 17, 65 - 70.

Finnie I, Kabil Y H, 1965, "On the formation of surface ripples during erosion."., Wear, 8, 60 - 69.

Fordham J D, Pilkington R, Tang C C, 1997, "The effect of different profiling techniques on the fatigue performance of metallic membranes of AISI 301 and Inconel 718." Int. J. Fatigue., 19, 487 - 501.

GMA Garnet technical data sheet 2001, GMA Garnet P.O box 9, Middlewich, Cheshire, CW10 9FD.

Goodhew P J, Humphreys J, Beanland R, 2001, "Electron microscopy and analysis." Taylor & Francis, London.

Griffiths B J, Gawne D T, Dong G, 1999, "A definition of the topography of grit blasted surfaces for plasma sprayed alumina coatings." J. Manufacturing Sci. and Eng., 121, 49 - 53.

Groppetti R, Bolzern P, Pellegrini R, 1996, "A contribution to the implementation of an adaptive controller for hydro abrasive jet machining based on the generalised minimum variance method.", In: Gee C, (ed) Proc. 13th Int. Conf. Jet Cutting Techn., Mechan. Engng Publishers, Bury St Edmunds, 125 - 136.

Guilemany J M, Llorca N, Szabo P J, 1996, "Residual stress characterisation of grit blasted steel surfaces." Surface Engineering., 12, 77 - 79.

Harris W T, 1976, Chemical Milling, Oxford University Press, Oxford, 0-19-859115-2.

Hashish M, 1987, "Milling with abrasive water jets: A preliminary investigation." In: Hood M, Dornfeld D, (eds) Proc. 4th US Water Jet Conf., A.S.M.E., New York, 1 - 10.

Hashish M, 1989a, "A model for abrasive water jet machining", J. Eng. Mater. and Techn., 111, 154 - 162.

Hashish M, 1989b, "Pressure effects in abrasive water jet machining." J. Eng. Mater. and Techn., 111, 221 - 228.

Hashish M, 1989c, "The effect of beam angle in abrasive water jet machining." Symp. High Energy Beam Machining Technologies." A.S.M.E, Winter Annual Meeting, 41, 23 - 29.

Hashish M, 1991, "Characteristics of surfaces machined with abrasive water jets." J. Eng. Mater. and Techn., 113, 354 - 362.

Hashish M, 1992a, "On the modelling of surface waviness produced by abrasive water jets." In: Lichtarowicz A (ed) Proc.11th Int. Conf. Jet Cutting Techn., Kluwer, Dordrecht, 17 - 35.

Hashish M, 1992b, "Three dimensional machining with abrasive water jets." In: Lichtarowicz A (ed) Proc.11th Int. Conf. Jet Cutting Techn., Kluwer, Dordrecht, 605 - 620.

Hashish M, Monserud D O, Bondurant P D, 1993. "A new abrasive water jet nozzle for automated and intelligent machining." In: Hashish M (ed), Proc 7th US Water Jet Conf. Water Jet Techn. Ass., St Louis, 829 - 842.

Hashish M, 1994a, "Drilling of small diameter holes in sensitive materials." In: Allen N G (ed) Jet Cutting Techn., Mechan. Engng Publishers, Bury St Edmunds, 409 - 424.

Hashish M, 1994b, "Controlled Depth milling techniques using abrasive water jets." In: Allen N G (ed) Jet Cutting Techn., Mechan. Engng Publishers, Bury St Edmunds, 449 - 461.

Hashish M, 1995a, "Erosion modes during abrasive water jet lathe slotting." J. Manuf. Sci. and Eng., 3, 1263 - 1269.

Hashish M, 1995b, "Material properties of abrasive water jet machining." Trans. A.S.M.E., 117, 578 - 583.

Hashish M, 1996a, "Towards agile abrasive water jet machining." In: Gee C, (ed) Proc. 13th Int. Conf. Jet Cutting Techn., Mechan. Engng Publishers, Bury St Edmunds, 549 - 561.

Hashish M, 1996b, "Deep hole drilling in metals using abrasive water jets." In: Gee C, (ed) Proc. 13th Int. Conf. Jet Cutting Techn., Mechan. Engng Publishers, Bury St Edmunds, 691 - 707.

Hashish M, 1996c, "Method and apparatus for abrasive water jet milling." Patent Application US5704824, USA, 1996.

Hashish M, 1998a, "Controlled depth milling of isogrid structures with AWJS." J. Manuf. Sci. and Eng., 120, 21 - 27.

Hashish M, Dunsky C M, 1998b, "The formation of cryogenic and abrasive - cryogenic jets." In: Louis H. (ed) 14th Int. Conf. Jet Cutting Techn., Professional Engng. Publishing, Bury St Edmunds, 329 - 343.

Hashish M, 1999, "Cutting with water jets at 690 MPa pressure." A.S.M.E., Pressure Vessels and piping., 384, 33 - 39.

Hashish M, Stewart J, 2000, "Observations on precision turning with AWJ." In: Ciccu R (ed) Proc. 15th Int. Conf. Jetting Techn., Professional Engng Publishing, Bury St Edmunds, 367 - 380.

Hirano K, Enomoto K C, Oyamada O, Hirano E, Shimizu S, 1997, "Stress corrosion cracking mitigation by water peening." A.S.M.E., Pipe, Pressure Vessels Div., 349, 89 - 93.

Hocheng H, Tsai H Y, Shiue J J, 1997, "Feasibility study of abrasive water jet milling of fibre reinforced plastics" J. Sci. and Eng., 119, 133 - 142.

Horri K, Murata M, 1987 "Method and apparatus for the generation and utilisation of a spiral gas stream in a pipe line." Patent Application: US 4684296, Japan.

Horri K, 1990, "Cutting method and Apparatus" Patent Application: EP 0383556, Japan.

Horri K, Matsumme Y, Cheng X.M, 1991a, "A newly developed spiral nozzle for abrasive acceleration in jet cutting applications." In: Labus T J (ed) Proc.6th Amer. Water Jet Conf. Water jet Techn. Ass., St Louis, 457 - 471.

Horri K, Matsumme Y, Cheng X M, 1991b, "Development of a new mixing nozzle assembly for high pressure abrasive water jet applications." In: Saunders D. (ed) Proc.10th Int. Conf. Jet Cutting Techn., Elsevier, London, 193 - 206.

Horri K, Takei M, Hashimoto B, 1992, "Performance evaluation of a spiral water jet cutting system." In: Lichtarowicz A (ed) Proc.11th Int. Conf. Jet Cutting Techn., Kluwer , Dordrecht, 621 - 636.

Hunt D C, Reuber M, Kim T J, 1988 "Surface Finish optimisation for abrasive jet cutting.", In: Woods P. A. (ed) 9th Int. Conf. Jet cutting Techn., BHRA, Fluid Engng. Cranfield, 99 - 112.

Hutchings I M, 1992, "Tribology: Friction and wear of engineering materials." Edward Arnold, London, UK, ISBN 034056184-X

Hydro Technologies Technical Maintenance Manual. January 1998.

Ives L K, Ruff A W, 1977, "Electron microscopy study of erosion damage in copper." Amer. Soc. for Testing and Mater. Special Techn. Publication STP 664, USA.

Kishkat R, 1996, "Process control for high pressure water jet cutting systems." In: Gee C, (ed) Proc. 13th Int. Conf. Jet Cutting Techn., Mechan. Engng Publishers, Bury St Edmunds, 595 - 610.

Koster W P, Field M, 1973, "Effect of machining variables on the surface and structural integrity of Titanium." Proc. N. Am. Metal work Res. Conf. McMaster Univ, Hamilton, Ontario, 67 - 87.

Kovacevic R, 1992, "Monitoring the depth of abrasive water jet penetration." Int. J. Machine Tools and Manuf., 32, 725 - 736.

Kovacevic R, Wang L, Zhang Y M, 1993, "Detection of abrasive water jet nozzle wear using acoustic signature analysis In: Hashish M (ed), Proc 7th US Water Jet Conf. Water Jet Techn. Ass., St Louis, 217 - 231.

Kovacevic R, Mohan R, Zhang Y M, 1995, "Cutting force dynamics as a tool for surface profile monitoring in AWJ." J. Eng. Industry, Trans. A.S.M.E., 117, 340 - 350.

Kovacevic R, Yong Z, 1996, "Modelling of 3D abrasive water jet machining. Part 1: Theoretical basis." In: Gee C, (ed) Proc.13th Int. Conf. Jet Cutting Techn., Mechan. Engng Publishers, Bury St Edmunds, 73 - 82.

Kovacevic R, Hashish M, Mohan R,1997, "State of the art research and development in abrasive water jet machining." J. Eng. Industry, Trans. A.S.M.E., 119, 776 - 785.

Kulekci M K, 2002, "Processes and apparatus developments in industrial water jet applications." Int. J. Machine Tools and Manuf., 42, 1297 - 1306.

Kwak H, Kovacevic R, Mohan R S, 1996, "Monitoring of AWJ drilling of Ceramics using AE sensing technique" In: Gee C, (ed) Proc. 13th Int. Conf. Jet Cutting Techn., Mechan. Engng Publishers, Bury St Edmunds, 137 - 152.

Laurinat A, Louis H, Meier – Wiechert G, 1993, "A model for milling with abrasive water jets." In: Hashish M (ed), Proc 7th US Water Jet Conf. Water Jet Techn. Ass., St Louis, 119 - 139.

Leidheiser H, Music S, McIntyre J F, 1984, "The improved corrosion resistance of steel in water after abrasive blasting with alumina." Corrosion Science, 24, 197 - 208.

Leverant G R, Langer B S, Yuen A, 1979, "Surface residual stresses, surface topography, and the fatigue behaviour of Ti6Al4V." Amer. Soc. Metals Metallurgical. Trans. A., 10, 251 - 257.

Li F, Geskin E S, Tismenetskiy L, 1996a, "Development of ice jet machining technology." In: Gee C, (ed) Proc.13th Int. Conf. Jet Cutting Techn., Mechan. Engng Publishers, Bury St Edmunds, 725 - 734.

Li F, Geskin E S, Tismenetskiy L, 1996b, "Feasibility study of abrasive water jet polishing." In: Gee C, (ed) Proc.13th Int. Conf. Jet Cutting Techn., Mechan. Engng Publishers, Bury St Edmunds, 709 - 723.

Li H Y, Geskin E S, Chen W L, 1989. "Investigation of forces exerted by an abrasive water jet on a workpiece." In: Vijay M M, Savanwick G, (ed) Proc. 5th Amer. Water Jet Conf. Water Jet Techn. Ass., St Louis, 69 - 77.

Liu H T,1998, "Near net shaping of optical surfaces with UHP abrasive suspension jets." In: Louis H. (ed) 14th Int. Conf. Jet Cutting Techn., Professional Engng. Publishing, Bury St Edmunds, 285 - 294.

Neilson J H, Gilchrist A, 1968 "Erosion by stream of solid particles", Wear 11, 111 - 122.

Mohan R S, Momber A W, Kovacevic R, 1995, "Detection of energy absorption during abrasive water jet machining using acoustic emission technique." Proc. A.S.M.E., Manuf. Eng. Div., 2, 69 - 85.

Mohan R S, Kovacevic R, Beardsley H, 1996, "Heat flux determination at the AWJ cutting zone using IR techniques and inverse heat conduction problem.". Proc. A.S.M.E., Heat transfer Div., 332, 245 - 254.

Momber A W, Kovacevic R, 1998, "Principles of abrasive water jet machining." Springer, London, UK, ISBN 3540762396.

Ojmertz K M C, 1993, "Abrasive water jet milling: An experimental investigation." In: Hashish M (ed), Proc 7th US Water Jet Conf. Water Jet Techn. Ass., St Louis, 777 - 791.

Ojmertz K M C, 1996, "Analysis of surfaces produced by abrasive water jet milling techniques." In: Gee C, (ed) Proc. 13th Int. Conf. Jet Cutting Techn., Mechan. Engng Publishers, Bury St Edmunds, 753 - 768.

Ojmertz K M C, 1997a, "A study on abrasive water jet milling." PhD, Chalmers University of technology, Gotenborg, Sweden,

Ojmertz K M C, 1997b, "AWJ slot milling: A preliminary test for industrial application." PhD paper 5, external report: PTE 97:02, Chalmers University of technology, Gotenborg, Sweden, 1 - 16.

Ojmertz K M C, Amini N, 1997c, "A Discrete approach to the abrasive Water jet milling process" Dokorsavhandlingar vidchalmers Tekniska Hogskola Sweden., 425 - 434.

Paul S, Hoogstrate A M, Van Luttervelt C A, 1998, "An experimental investigation of rectangular pocket milling with abrasive water jet." J. Mater. Processing., 73, 179 -188.

Philips XL30 Scanning Electron Microscope Operating Instructions 1998.

Polmear I J, 1995, "Light Alloys. Metallurgy of the light metals." Arnold, London, Third edition.

Preece C M, 1979, "Erosion. treatise on materials science and technology. Volume 16." Academic Press, London, UK, ISBN 01234186-X.

Ramulu M, Raju S P, 1993, "Hydro - abrasive erosion characteristics of 30vol. %SiC_p /606-T6 Al composite at shallow impact angles.", Wear, 166, 55 - 63.

Ramulu M, Kunaporn S, Arola D, 2000, "Water jet machining and peening of metals." J. Pressure Techn., 122, 90 – 95.

Rank Taylor Hobson, 1985a, "Surftronic 3P Operating Instructions" Company Publication, 221-57/685, P O Box 36, New Star Road, Leicester, UK.

Rank Taylor Hobson, 1985b "Surface Analysis Software for Talysurf 10,3 or 3P", Company Publication, P O Box 36, New Star Road, Leicester, UK.

Rank Taylor Hobson, 1994 "Surface Texture Parameters", company Publication 800-302694, P O Box 36, New Star Road, Leicester, UK.

Ruff, A.W. and Wiederhorn, S.M.1979, "Erosion by solid particle impact" In: Preece, C.M. (Ed) Treatise on Materials Science and Technology, Academic Press, New York, 16, 69 - 126.

Savanick G A, Ricketts T E, Lohn P D, 1975 "Cutting experiments using a rotating water jet in a bore hole." USA Bureau of Mines Report Investigations, RI 8095.

Savanick G A, Krawza W G, 1989, "Abrasive enhanced water jet drill for hardrocks" USA Bureau of Mines Report Investigations, RI9261.

Sheldon G L, Finnie I, 1968 "On the ductile behaviour of nominally brittle materials during erosive cutting" J. Eng. for Industry., 88, 387 - 393.

Shuford D M, 1970, "Chemical milling close tolerance Titanium tank segments." J. Plating., 56, 605 - 609.

Singh J, Jain S C, 1995, "Mechanical issues in laser and abrasive water jet cutting." J. Metals., 28 - 30.

Souffrant P E, 1972, "Usinage chimique d'alliages de titane (titanium alloy chemical machining)." Corros. Trait. Prot. Finition, 20, 406 - 415.

Stachowiak G B, Stachowiak G W, 2000, "The effects of particle characteristics on three body abrasive wear.", Wear, 249, 201 - 207.

Stoloff N S, Sikka V K, 1996 "Physical metallurgy and processing of intermetallic compounds." Chapman & Hall, London.

Struck D, 1990, "Titan - und Aluminiumbleche im Flugzeugbau mit Abrasiv - Hochdruckwasserstrahl schneiden" Werstatt und Betrieb., 123, 861 - 864.

Summers D A, 1995, "Water jetting technology", Alden Press, Oxford, UK, ISBN 0419196609.

Tonshoff H K, 1993, "Surface bonding by water peening." Surface Engng., 385 - 390.

Tonshoff H K, Kroos F, Hartmann M, 1995. "Water peening - An advanced application of water jet technology." In: Labus T.J (ed) Proc 8th Amer. Water Jet Conf. Water Jet Techn. Ass., St Louis, 473 - 486.

Ye J, Kovacevic R, 1999, "Turbulent solid liquid flow through the nozzle of premixed abrasive water jet cutting systems." J.Eng. Manuf., 213, 59 - 67.

Yerramareddy S, Bahadur S, 1993 "Effect of operational variables, microstructure and mechanical properties on the erosion of Ti-6Al-4V.", Wear, 142, 253 - 263

Yong Z, Kovacevic R, 1996, "Modelling of 3D abrasive water jet machining. Part 2: simulation of Machining. " In: Gee C, (ed) Proc. 13th Int. Conf. Jet Cutting Techn., Mechan. Engng Publishers, Bury St Edmunds, 83 - 89.

Wagner L, Gerdes C, Luetjering G, 1984, "Influence of surface treatment on fatigue Strength of Ti6Al4V." Titanium Sci. Tech., 4, 2147 - 2154.

Westkamper E, Gottwald B, Henning A, 1998, "Intelligent means of process control during the high pressure water cutting." In: Proc. 24th Annual conf. I.E.E.E. Indust. Electronics Society: I.E.E.E, York., 4, 2631 - 2365.

Wiederhorn S M, Hockey B J, 1983, "Effect of material parameters on the erosion resistance of brittle materials." J. Mater. Sci.,18, 766 - 780.

Zu J B, Burstein G T, Hutchings I M, 1991, "A comparative study of the slurry erosion and Free Fall Particle Erosion of Aluminium.", Wear, 149, 73 - 84.